ACCSCIENCE PUBLISHING

Tumor Discovery

ISSN: 3060-8597 (Print)
ISSN: 2810-9775 (Online)
Volume 3 • Issue 4
December 2024

NUT carcinoma occurs systemically, with BRD4::NUTM1 driving progression and serving as a diagnostic and therapeutic target for BET inhibitors.

ACCSCIENCE PUBLISHING

Tumor Discovery

Print ISSN: 3060-8597
Online ISSN: 2810-9775

Tumor Discovery is a peer-reviewed and open-access journal that aims to present new cancer research with strong emphasis on fundamental and translational studies. *Tumor Discovery* covers topics such as etiology and pathogenesis of cancer, mechanisms and molecular pathways underlying cancer initiation and progression, tumor metastasis, etc.

Scan to access website:

Scan to submit papers:

About the Publisher

AccScience Publishing is a publishing company based in Singapore. We publish a range of high-quality, open-access, peer-reviewed journals and books from a broad spectrum of disciplines.

Contact Us

Managing Editor
td.office@accscience.sg

AccScience Publishing
8 Burn Road, #15-03 Trivex, Singapore 369977.

Volume 3 • Issue 4 • December 2024
ISSN 3060-8597 (print) ISSN 2810-9775 (online)

TUMOR DISCOVERY

ACCSCIENCE PUBLISHING

Access Science Without Barriers

TUMOR DISCOVERY

ISSN: 3060-8597 (print)
ISSN: 2810-9775 (online)

Editorial and Production Credits

Publisher: AccScience Publishing
Managing Editor: Daisy Zhao
Production Editor: Sharmila Velapasamy
Article Layout and Typeset: Sinjore Technologies (India)

For all advertising queries, contact td.office@accscience.sg.

Supplementary file

Supplementary files of articles can be obtained at https://accscience.com/journal/TD/3/4.

Disclaimer

AccScience Publishing is not liable to the statements, perspectives, and opinions contained in the publications. The appearance of advertisements in the journal shall not be construed as a warranty, endorsement, or approval of the products or services advertised and/or the safety thereof. AccScience Publishing disclaims responsibility for any injury to persons or property resulting from any ideas or products referred to in the publications or advertisements. AccScience Publishing remains neutral with regard to jurisdictional claims in published maps and institutional affiliations.

Tumor Discovery

Editorial Board

Youth Editorial Board Members

*Editorial Board Members as of December 26, 2024

ACCSCIENCE PUBLISHING

Volume 3 | Issue 4 | December 2024 |

Tumor Discovery

https://accscience.com/journal/TD

CONTENTS

ACCSCIENCE PUBLISHING

Tumor Discovery

EXPERT CONSENSUS

Expert consensus and current landscape of NUT carcinoma: A comprehensive strategy from diagnosis to treatment

Zhuomiao Ye[1,2†], Xin Li[1,2†], Fei Xie[3], Chao Deng[3], Dan Yang[1], Hongle Li[4], Yuanzhi Lu[5], Zhenbin Mao[6], Qingwei Meng[7], Lidong Wang[8], Zhe Wang[9], Jinliang Xing[10], Chong Bai[11], Zhimin Bian[12], Paolo Boffano[13], Steven Brower[14], Rui Chen[15], Wantao Chen[16], Jinhai Deng[17], Xinpei Deng[18], Chunming Ding[19], Jianchun Duan[20], Song Duan[21], Nejat Duzgunes[22], Pierfrancesco Franco[23], Guobin Fu[24], Longmei Guo[25], Ye Guo[26], Ruiqin Han[27], Ling Hao[28], Lang He[29], Yayi He[30], Xiaotong Hu[31], Junmei Jia[32], Yanfang Jiang[33], Weilin Jin[34], Kalevi Kairemo[35], Mohamed Kamal[36,37], Evan T. Keller[38], Rensheng Lai[1],

Abstract

Nuclear protein of the testis (NUT) carcinoma is a rare and highly aggressive malignancy characterized by the rearrangement of the NUT midline carcinoma family member 1 (*NUTM1*) gene. Nevertheless, standardized strategies for its diagnosis and treatment remain unavailable, underscoring the need for expert consensus. To address this gap, we conducted a systematic review to gather comprehensive information on NUT carcinoma from five databases: PubMed, Web of Science, Embase, Cochrane Library, and Ovid Medline. This expert consensus was collaboratively developed by a team of international multidisciplinary experts, in partnership with the NUT Carcinoma Diagnosis Working Group of the Chinese Anti-Cancer Association's Oncogene Diagnosis Professional Committee. This working group comprises medical oncologists, radiation oncologists, surgical oncologists, pathologists, nurses, molecular biologists, statisticians, and bioinformatics specialists. A systematic review, based on data from 526 patients across 199 articles, was conducted to comprehensively explore various characteristics, including demographic features (e.g., patient gender, distribution regions, and age), tumor-node-metastasis (TNM) classification stage, clinical symptoms, tumor size, metastatic patterns, immunohistochemical (IHC) findings, treatment modalities, prognosis-related information, and *NUTM1* fusion partners. We have developed an expert consensus on diagnosing and treating NUT carcinoma using a multidisciplinary approach. The guideline provides eight recommendations, addressing epidemiological characteristics, clinical and imaging manifestations, pathological findings, IHC features, molecular mechanisms and subtypes, prognosis, diagnosis, and treatment strategies for NUT carcinoma. Furthermore, an international platform has been established to disseminate NUT carcinoma knowledge and patient recruitment, providing patients and healthcare providers access to NUT carcinoma-related information and updates on clinical trial recruitment.

Keywords: Nuclear protein of the testis carcinoma; Expert consensus; Diagnosis; Treatment

[†]These authors contributed equally to this work.

***Corresponding authors:**
Mingzhu Yin (yinmingzhu@cqu.edu.cn);
Minghui Zhang (zhmhui@cqu.edu.cn)

Citation: Ye Z, Li X, Xie F, *et al.* Expert consensus and current landscape of NUT carcinoma: A comprehensive strategy from diagnosis to treatment. *Tumor Discov.* 2024;3(4):4904. doi: 10.36922/td.4904

Received: September 22, 2024

Accepted: November 14, 2024

Published Online: December 24, 2024

Chao Li[39], Jun Li[40], Lifeng Li[41], Qingxia Li[42], Wenbin Li[43], Xuening Li[44], Yang Li[45], Yongsheng Li[46], Yu Li[47], Mikael S. Lindström[48], Xiaodong Liu[49], Yan Liu[50], Yanqing Liu[51], Zengjun Liu[52], Jose Manuel Lopes[53], Hongyang Lu[54], Xiangwen Luo[1,2], Wenping Ma[55], Hongxue Meng[56], Anjie Min[57], Amancio Carnero Moya[58], Athanasios G. Papavassiliou[59], Xi Pan[60], Min Peng[61], Helmut H. Popper[62], Lixin Qiu[63], Di Qu[64], Axel H. Schönthal[65], Vishal Shelat[66], Yi Shi[67], Alexander Shtil[68], Hifzur R Siddique[69], Yang Song[70], Haichuan Su[70], Min Tang[71], Mengyuan Wang[3], Qiming Wang[72], Shubin Wang[73], Bing Wei[74], Dawei Wu[75], Longxiang Wu[76], Liangbi Xu[77], Yubo Yan[78], Nong Yang[79], Zihuan Yang[80], Zongbi Yi[81], Songtao Yu[82], Heng Zhang[83], Hongmei Zhang[84], Lijuan Zhang[85], Jianfu Zhao[86], Zheng Zhao[87], Shaoquan Zheng[88], Chengzhi Zhou[89], Pu Zhou[90], Qin Zhou[91], Guodong Zhu[92], Qin Yan[93], Minghui Zhang[1,2*], and Mingzhu Yin[1,2*]

[1]Clinical Research Center, Medical Pathology Center, Cancer Early Detection and Treatment Center and Translational Medicine Research Center, Chongqing University Three Gorges Hospital, Chongqing University, Wanzhou, Chongqing, China

[2]School of Medicine Chongqing University, Chongqing University, Shapingba, Chongqing, China

[3]Department of Breast Surgery, Chongqing University Three Gorges Hospital, Chongqing University, Wanzhou, Chongqing, China

[4]The Affiliated Cancer Hospital of Zhengzhou University and Henan Cancer Hospital, Zhengzhou, Henan, China

[5]Department of Clinical Pathology, The First Affiliated Hospital of Jinan University, Guangzhou, Guangdong, China

[6]The China Food and Drug Corporation Quality and Safety Promotion Association, China

[7]Department of Medical Oncology, Harbin Medical University Cancer Hospital, Harbin, Heilongjiang, China

[8]State Key Laboratory of Esophageal Cancer Prevention & Treatment and Henan Key Laboratory for Esophageal Cancer Research of the First Affiliated Hospital, Zhengzhou University, Zhengzhou, Henan, China

[9]Department of Thyroid, Breast, and Vascular Surgery, Xijing Hospital, The Air Force Medical University, Xi'an, Shaanxi, China

[10]State Key Laboratory of Cancer Biology and Department of Physiology and Pathophysiology, Air Force Medical University, Xi'an, Shaanxi, China

[11]Department of Respiratory and Critical Care Medicine, Shanghai Changhai Hospital, the First Affiliated Hospital of Second Military Medical University, Shanghai, China

[12]Department of Comprehensive, National Cancer Center/National Clinical Research Center for Cancer/Cancer Hospital, Chinese Academy of Medical Sciences and Peking Union Medical College, Beijing, China

[13]Division of Dentistry, Vercelli Hospital, Vercelli, Piemonte, Italy

[14]The Lefcourt Family Cancer Treatment and Wellness Center, Englewood Health, Englewood, New Jersey, United States of America; Icahn School of Medicine at Mount Sinai, New York City, New York, United States of America; Hackensack Meridian School of Medicine, Nutley, New Jersey, United States of America

[15]Department of Pathology, Chongqing University Cancer Hospital, Shapingba, Chongqing, China

[16]Department of Oral and Maxillofacial-Head and Neck Oncology, Shanghai Ninth People's Hospital, Shanghai Jiao Tong University School of Medicine, Shanghai, China

[17]Richard Dimbleby Laboratory of Cancer Research, School of Cancer & Pharmaceutical Sciences, King's College London, London, Greater London, United Kingdom

[18]Sun Yat-sen University Cancer Center, Collaborative Innovation Center for Cancer Medicine, Guangzhou, Guangdong, China

[19]Department of Pathology, Fudan University Shanghai Cancer Center, Shanghai, China

[20]State Key Laboratory of Molecular Oncology, Department of Medical Oncology, National Cancer Center/National Clinical Research Center for Cancer/Cancer Hospital, Chinese Academy of Medical Sciences and Peking Union Medical College, Beijing, China

[21]Department of Pathology, Chongqing University Three Gorges Hospital, Wanzhou, Chongqing, China

[22]Department of Biomedical Sciences, Arthur A Dugoni School of Dentistry, University of the Paci□c, San Francisco, California, United States of America

[23]Department of Translational Medicine (DIMET), University of Eastern Piedmont, Department of Radiation Oncology, 'Maggiore della Carità' University Hospital, Novara, Piedmont, Italy

[24]The Second Clinical Medical College, Shandong University of Traditional Chinese Medicine, Jinan, Shandong, China; Department of Oncology, Shandong Provincial Hospital Affiliated to Shandong First Medical University, Jinan, Shandong, China; The Third Affiliated Hospital of Shandong First Medical University, Jinan, Shandong, China

[25]Department of Otolaryngology, The Fourth Hospital of Harbin Medical University, Nangang, Harbin, Heilongjiang, China

[26]Department of Oncology, Shanghai East Hospital, School of Medicine, Tongji University, Shanghai, China

[27]State Key Laboratory of Medical Molecular Biology, Department of Biochemistry and Molecular Biology, Institute of Basic Medical Sciences, Chinese Academy of Medical Sciences and Peking Union Medical College, Beijing, China

[28]Department of Oncology, The Fourth Hospital of Harbin Medical University, Harbin, Heilongjiang, China

[29]Department of Oncology, Cancer Prevention and Treatment Institute of Chengdu, Chengdu Fifth People's Hospital (The Second Clinical

Medical College Affiliated Fifth People's Hospital of Chengdu University of Traditional Chinese Medicine), Chengdu, Sichuan, China

[30]Department of Medical Oncology, Shanghai Pulmonary Hospital, Tongji University Medical School Cancer Institute, Tongji University School of Medicine, Shanghai, 200433, China

[31]Department of Pathology, Sir Run Run Shaw Hospital of Zhejiang University College of Medicine & Sir Run Run Shaw Institute of Clinical Medicine of Zhejiang University, Hangzhou, Zhejiang, China

[32]Department of Oncology, The First Hospital of Shanxi Medical University, Yingze, Taiyuan, Shanxi, China

[33]Key Laboratory of Organ Regeneration and Transplantation of the Ministry of Education, Genetic Diagnosis Center, the First Hospital of Jilin University, Changchun, Jilin, China

[34]Institute of Cancer Neuroscience, Medical Frontier Innovation Research Center, The First Hospital of Lanzhou University, The First Clinical Medical College of Lanzhou University, Lanzhou, Gansu, China

[35]Department of Nuclear Medicine, University of Texas MD Anderson Cancer Center, Houston, Texas, United States of America

[36]USC Michelson Center Convergent Science Institute in Cancer, Los Angeles, California, United States of America

[37]Department of Zoology, University of Benha, Benha, Egypt

[38]Departments of Urology and Pathology and the Biointerfaces Institute, University of Michigan, Ann Arbor, Michigan, United States of America

[39]Department of Pathology, College of Clinical Medicine for Oncology, Fujian Medical University, Fuzhou, Fujian, China

[40]Department of Molecular Pathology, Clinical Pathology Center, Affiliated Cancer Hospital of Zhengzhou University and Henan Cancer Hospital, Zhengzhou, Henan, China

[41]Henan International Joint Laboratory of Children's Infectious Diseases, Children's Hospital Affiliated to Zhengzhou University, Henan Children's Hospital, Zhengzhou Children's Hospital, Zhengzhou, Henan, China

[42]Departments of Oncology & Immunotherapy, Hebei General Hospital, Shijiazhuang, Hebei, China

[43]Department of Pathology, National Cancer Center, National Clinical Research Center for Cancer/Cancer Hospital, Chinese Academy of Medical Sciences and Peking Union Medical College, Beijing, China

[44]Department of Clinical Pharmacology, Zhongshan Hospital, Fudan University, Shanghai, China

[45]Department of Neurosurgery, The Second Affiliated Hospital of Harbin Medical University, Harbin, Heilongjiang, China

[46]Department of Medical Oncology, Chongqing University Cancer Hospital, Shapingba, Chongqing, China

[47]Department of Pathology, Chongqing University Cancer Hospital & Chongqing Cancer Institute & Chongqing Cancer Hospital, Shapingba, Chongqing, China

[48]Division of Genome Biology, Department of Medical Biochemistry and Biophysics, Karolinska Institutet, Box 1031, 171 21, Stockholm, Sweden

[49]Department of Trauma and Emergency Surgeon, The Second Affiliated Hospital, Harbin Medical University, Harbin, Heilongjiang, China

[50]Department of Medical Oncology, The Fourth Affiliated Hospital of Harbin Medical University, Harbin, Heilongjiang, China

[51]Herbert Irving Comprehensive Cancer Center, Columbia University, New York City, New York, United States of America

[52]Department of Rare Tumors, Shandong Cancer Hospital and Institute, Shandong First Medical University and Shandong Academy of Medical Sciences, Taian, Shandong, China

[53]Department of Pathology, São João Local Health Unit, Faculty of Medicine, Institute for Research and Innovation in Health, Institute of Molecular Pathology and Immunology of University of Porto, Portugal

[54]Zhejiang Key Laboratory of Diagnosis & Treatment Technology on Thoracic Oncology (Lung and Esophagus), Zhejiang Cancer Hospital, Institute of Basic Medicine and Cancer, Department of Thoracic Medical Oncology, Zhejiang Cancer Hospital, Institute of Basic Medicine and Cancer, Chinese Academy of Sciences, Hangzhou, Zhejiang, China

[55]Department of Neurosurgery, Beijing Children's Hospital, Capital Medical University, National Center for Children's Health, Beijing, China

[56]Department of Pathology, Harbin Medical University Cancer Hospital, Harbin, Heilongjiang, China

[57]Department of Oral and Maxillofacial Surgery, Xiangya Hospital, Central South University, Changsha, Hunan, China

[58]Institute of Biomedicine of Seville (Instituto de Biomedicina de Sevilla), Spanish National Research Council (Consejo Superior de Investigaciones Cientí□cas), Seville, Spain

[59]Department of Biological Chemistry, Medical School, National and Kapodistrian University of Athens, Athens, Greece

[60]Department of Oncology, the third Xiangya Hospital, Central South University, Changsha, Hunan, China

[61]Department of Oncology, Renmin Hospital of Wuhan University, Wuhan, Hubei, China

[62]Department of Pathology, Medical University of Graz, Graz, Styria, Austria

[63]Department of Medical Oncology, Fudan University Shanghai Cancer Center, Shanghai, China

[64]Department of Oncology, The Second Affiliated Hospital of Harbin Medical University, Harbin, Heilongjiang, China

[65]Department of Molecular Microbiology & Immunology, Keck School of Medicine, University of Southern California (USC), Los Angeles, CA 90089, USA

[66]Surgical Science Training Center, Tan Tock Seng Hospital, 11 Jalan Tan Tock Seng, Singapore 308433, Singapore

[67]Department of Pathology, Fujian Cancer Hospital Affiliated to Fujian Medical University, Fuzhou, Fujian, China

[68]Blokhin National Medical Research Center of Oncology, Ministry of Health, Moscow, Russia

[69]Molecular Cancer Genetics and Translational Research Lab, Section of Genetics, Aligarh Muslim University, Aligarh, Uttar Pradesh, India

[70]Department of Oncology, Tangdu Hospital, Air Force Medical University, Xi'an, Shaanxi, China

[71]Department of Oncology, Chongqing General Hospital, Chongqing University, Shapingba, Chongqing, China

[72]Department of Internal Medicine, The Affiliated Cancer Hospital of Zhengzhou University, Henan Cancer Hospital, Zhengzhou, Henan, China

[73]Department of Medical Oncology, Peking University Shenzhen Hospital, Beijing University, Shenzhen, Guangdong, China

[74]Department of Molecular Pathology, Henan Key Laboratory of Molecular Pathology, The Affiliated Cancer Hospital of Zhengzhou University & Henan Cancer Hospital, Zhengzhou, Henan, China

[75]National Cancer Center/National Clinical Research Center for Cancer/Cancer Hospital, Chinese Academy of Medical Sciences and Peking Union Medical College, Beijing, China

[76]Department of Gastrointestinal Surgery, Affiliated Tumor Hospital of Nantong University, Nantong Tumor Hospital, Nantong, Jiangsu, China

[77]Endoscopy Center of the Affiliated Hospital of Guizhou Medical University, Guiyang, Guizhou, China

[78]Department of Thoracic Surgery, Harbin Medical University Cancer Hospital, Harbin, Heilongjiang, China

[79]Department of Pulmonary Gastroenterology, Hunan Cancer Hospital, Changsha, Hunan, China

[80]Guangdong Provincial Key Laboratory of Colorectal and Pelvic Floor Diseases, Guangdong Institute of Gastroenterology; Department of Clinical Laboratory, The Sixth Affiliated Hospital of Sun Yat-sen University, Guangzhou, Guangdong, China

[81]Department of Radiation and Medical Oncology, Zhongnan Hospital of Wuhan University, Hubei Key Laboratory of Tumor Biological Behaviors Hubei Cancer Clinical Study Center, Wuhan, Hubei, China

[82]Department of Oncology, Southwest Hospital, Third Military Medical University (Army Medical University), Shapingba, Chongqing, China

[83]Department of General Thoracic Surgery, Xiangya Hospital, Central South University, Changsha, Hunan, China

[84]Department of Oncology, Xijing Hospital, Air Force Medical University, Xincheng, Xi'an, Shaanxi, China

[85]Department of Respiratory and Critical Care Medicine, The First Affiliated Hospital of Harbin Medical University, Harbin, Heilongjiang, China

[86]Research Center of Cancer Diagnosis and Therapy, Department of Oncology, The First Affiliated Hospital of Jinan University, Guangzhou, Guangdong, China

[87]Department of Oncology, Shaanxi Cancer Hospital, Xi'an, Shaanxi, China

[88]Breast Disease Center, The First Affiliated Hospital, Sun Yat-sen University, Guangzhou, Guangdong, China

[89]State Key Laboratory of Respiratory Diseases, National Clinical Research Center for Respiratory Diseases, Guangzhou Institute of Respiratory Health, The First Affiliated Hospital of Guangzhou Medical University, Guangzhou, Guangdong, China

[90]Department of Oncology, People's Hospital of Shapingba, Shapingba, Chongqing, China

[91]Department of Oncology, Xiangya Hospital, Central South University, No. 87, Changsha, Hunan, China

[92]Guangdong-Hong Kong-Macau Great Bay Area Geroscience Joint Laboratory, School of Medicine, Jinan University, Guangzhou, China

[93]Department of Pathology, Yale Center for Immuno-Oncology, Yale Cancer Center, Yale University, New Haven, Connecticut, United States of America

1. Introduction

Nuclear protein of the testis (NUT) carcinoma, also known as midline carcinoma resulting from the rearrangement of the NUT gene, is a rare and highly aggressive malignant tumor. It is associated with rearranging the NUT midline carcinoma family member 1 (*NUTM1*) gene on chromosome 15q14. First described in 1991, subsequent cases of NUT carcinoma have primarily been reported in the midline structures of the human body, including the head, neck, and thoracic/mediastinal regions, which is why it was initially termed "midline carcinoma."[1-4] However, NUT carcinoma can also occur in various organs, including the lungs, bones, nasal cavity, salivary glands, central nervous system (CNS), and soft tissues. As a result, the World Health Organization renamed the condition "NUT carcinoma" to better reflect its broader clinical presentation.[5-15] The rearrangement of the *NUTM1* gene was initially considered a hallmark molecular alteration in NUT carcinoma. In recent years, *NUTM1* rearrangements have also been identified in tumor types, such as round-cell sarcoma, acute leukemia, hidradenoma, and hidradenocarcinoma, broadening the spectrum of diseases associated with this genetic change. Multiple partner genes that can fuse with *NUTM1* have now been identified, including members of the bromodomain protein family, the myelocytomatosis-

associated factor X (MAX) dimerization family, Capicua (CIC) transcription factor, and the transcriptional enhancer structural domain activation factor. This fusion results in the formation of the X: NUTM1 fusion protein.[2] The carboxy-terminal portion of the fusion protein retains nearly intact NUT protein, indicating the critical role of NUT in the epigenetic regulation of histone acetylation and its significance in the pathogenesis of these tumors. The pathological characteristics of NUT carcinoma exhibit low specificity,[16] which complicates clinical diagnosis. At present, the most commonly used diagnostic methods involve immunohistochemical (IHC) detection of NUT overexpression in the nucleus or identification of *NUTM1* gene (15q14) copy number variations or fusion events with common partner genes, often using fluorescence *in situ* hybridization (FISH) or next-generation sequencing (NGS).

The NUT carcinoma predominantly affects young individuals, although it can occur at any age.[17] The disease is highly invasive, often diagnosed at an advanced stage with distant metastasis, resulting in a poor prognosis.[18] Furthermore, the prognosis is closely linked to the specific fusion partners involved with *NUTM1*.[19] Radiation therapy and chemotherapy have limited efficacy, with rapid tumor progression typically occurring within months.[1,18,20] Recent studies indicate that bromodomain and extra-terminal domain (BET) inhibitors and histone deacetylase (HDAC) inhibitors may offer promising new treatment options for NUT carcinoma.[21,22]

The NUT Carcinoma Diagnosis Working Group of the Chinese Anti-Cancer Association's Oncogene Diagnosis Professional Committee was formally established in June 2023. This paper aims to provide more precise and standardized diagnostic and therapeutic guidelines for clinicians by summarizing and analyzing the general characteristics, clinical features, imaging, pathology, treatment, and prognosis of 526 cases of NUT carcinoma from 199 published articles. An expert consensus was developed through consultations with experts and scholars in relevant domestic and international research fields, and it has been periodically revised to incorporate the latest developments in the field to meet current clinical needs.

2. Methods

We followed the methodology recommended by the World Health Organization (WHO) handbook for guideline development[23] and utilized the Appraisal of Guidelines for Research and Evaluation (AGREE II) for assessment.[24] The draft of the final guideline was developed following the Reporting Items for Practice Guidelines in Healthcare (RIGHT).[25] An overview of the entire development process is provided in Figure S1.

2.1. Sponsor and supporters

This work was initiated and supported by the NUT Carcinoma Diagnosis Working Group of the Chinese Anti-Cancer Association's Oncogene Diagnosis Professional Committee, the Tumor Biomarker Professional Committee of the Chinese Anti-Cancer Association, and the China Food and Drug Corporation Quality and Safety Promotion Association.

2.2. Registration

This guideline has been registered on the International Practice Guideline Registry Platform under the registration number PREPARE-2023CN767 (http://www.guidelines-registry.cn).[26]

2.3. Scope

This guideline focuses on the diagnosis and treatment of NUT carcinoma. The primary target audience includes medical oncologists, radiation oncologists, surgical oncologists, pathologists, nurses, and the general public. Other healthcare professionals and decision-makers in cancer management may also benefit from this guideline.

2.4. Guideline working group

We established the following four groups to direct the development of the guidelines (Table S1):

(i) The steering committee comprised 10 chief oncologists and pathologists. They were responsible for guiding the overall design of the guidelines, making final decisions at each stage, and overseeing the entire process. They also wrote the guidelines.

(ii) The consensus panel consisted of 65 multidisciplinary experts, including 23 comprehensive oncology specialists, 12 pulmonary oncology specialists, six head and neck oncology specialists, five surgical oncology specialists, five pathology specialists, four gastrointestinal oncology specialists, two laboratory medicine specialists, two bone oncology specialists, two rare oncology specialists, along with experts in hematologic oncology, clinical pharmacology, pediatric oncology, and biochemistry and molecular biology. This group was responsible for clinical issues, voting on recommendations, and establishing consensus.

(iii) The evidence synthesis group, composed of four members, was responsible for gathering clinical issues, conducting literature searches, evaluating, synthesizing, and grading evidence, performing systematic reviews,

and creating summary tables of findings and decision tables for recommendations.

(iv) An external review group comprising 21 first-line healthcare professionals was responsible for providing external review and feedback on the guideline.

2.5. Ethical considerations

All steering committee and consensus panel members completed a conflict-of-interest disclosure form before participating in the guideline development process.[27] No relevant financial conflicts of interest were identified.

2.6. Systematic review and grading

To enhance an early and comprehensive understanding of NUT carcinoma and provide potentially effective treatment options for patients, we conducted a systematic review to collect detailed information on the key characteristics and treatment scenarios associated with this malignancy.

The protocol for this systematic review was registered with PROSPERO (CRD42021277083) on November 10, 2023. The review methodology followed the Preferred Reporting Items for Systematic Reviews and Meta-Analyses (PRISMA) guideline. Given the highly heterogeneous patient populations and differences in study designs, a meta-analysis was deemed inappropriate.

We searched for relevant studies in the following databases: PubMed, Web of Science, Embase, Cochrane Library, and Ovid Medline, without language restrictions. The search strategy was based on the following terms: "NUT Carcinoma," "NUT midline carcinoma," "nuclear protein in testis carcinoma," "NUTM1," and "nuclear protein of the testis midline carcinoma." Further, details on the search terms are provided in Table S2. Each study was reviewed to confirm the presence of *NUTM1* gene rearrangement in the included patients, with diagnoses verified using pathological tissues and techniques such as IHC, FISH, or NGS. The final search was conducted on January 20, 2024. No restrictions were applied based on age, gender, country, or tumor stage. Some of the authors on our team were trained in the purpose and methodology of the review. The selection process was conducted independently by two reviewers (XL and ZMY), with disagreements resolved through discussion or by consulting a third reviewer (JZ). A PRISMA flow diagram illustrating the study selection procedure is provided in Figure S2.

Data extracted from each study included the following variables: author, year of publication, country, sample size, gender, region, age, smoking status, symptoms at first diagnosis, tumor location, metastatic lesions, tumor staging, maximum tumor diameter, type of treatment received, treatment sequence, IHC results, overall survival (OS), and *NUTM1* fusion partner (if known). The methodological quality of the studies was assessed using the Agency for Healthcare Research and Quality (Table S3). Two reviewers (LL and ZY) independently performed the quality rating, and a third reviewer (JZ) was consulted if disagreements occurred. Given that the most published studies on NUT carcinoma are observational, such as case reports, case series, and small retrospective cohort studies, they carry a higher risk of bias.

2.7. Data analysis and survival analysis

Based on the data extracted from the literature, we conducted a descriptive statistical analysis of NUT carcinoma's general characteristics, features, and current treatment strategies. In addition, we performed both univariate and multivariate analyses of OS. We ensured that each subgroup in the survival analysis cohort contained more than 10 individuals. Survival analyses were conducted for various factors, including patient gender, region of origin, age, site of metastasis, tumor-node-metastasis (TNM) classification stage, tumor diameter, antigen Kile 67 (Ki-67) index, *NUTM1* fusion partner, treatment type, and chemotherapy regimen. It is important to note that due to the rarity of NUT carcinoma and the lack of large-scale cohort data, the vast majority of data in this study comes from case reports, making the data non-continuous with significant heterogeneity. These data results are for clinical reference only, and the results of analyses and statistics based on these data should be interpreted and treated with caution.

2.8. Formulation of recommendations

After reviewing the literature and integrating clinical experience, we initially drafted a set of recommendations. The evidence levels and definitions of evidence-based medicine in this expert consensus are based on the Oxford Centre for Evidence-Based Medicine levels (Table S4). The initial recommendations underwent expert consultation, with three voting options: "agree," "uncertain," or "disagree." Experts were invited to provide suggestions for modification of each recommendation. After each round of consultation, the recommendations were revised or supplemented based on expert feedback. The recommendations were categorized as "strong recommendation," "recommendation," or "no consensus" based on expert votes. If the agreement rate (i.e., the proportion of experts selecting "agree") was ≥ 70%, the recommendation was considered to have reached a consensus. An agreement rate > 90% was classified as a "strong recommendation," 70 – 90% as a "recommendation," and anything less as "no consensus." The consensus draft was then submitted to the External Review Group for additional external review.

3. Results

3.1. Patient characteristics

As compiled from the literature, the distribution and general characteristics of NUT carcinoma patients are summarized in Figure 1. Additional patient details are provided in Table S5.

3.1.1. Patient gender

This study evaluated 526 patients from 199 articles; no significant difference was observed in the gender ratio among patients with known gender. The overall male-to-female ratio was 1.18 (276 males and 232 females). In the thoracic group, the male-to-female ratio was 1.52 (144 males and 95 females), while in the head and neck group, the ratio was 0.97 (81 males and 83 females).

3.1.2. Patient distribution by region and age

Most patients were in the Americas (51.52%), followed by Asia (34.6%). The average age of all patients was 38 years. Thoracic NUT carcinoma patients had a slightly higher average age of 40.02 years (range: 6 – 86 years) than head-and-neck NUT carcinoma patients, whose average age was 33.82 years (range: 1 – 82 years).

3.1.3. Patient TNM classification of malignant tumors staging

Among NUT carcinoma patients with a known TNM stage, 50.9% (56/110) were at stage IV, and 33.6% (37/110) were at stage III. In thoracic NUT carcinoma patients, the proportion of those at stage III (36.36%, 24/66) and stage IV (53.03%, 35/66) was higher than in head-neck NUT carcinoma patients, whereas 26.32% (10/38) were at stage III and 47.37% (18/38) were at stage IV.

3.1.4. Clinical symptoms at initial diagnosis of NUT carcinoma in patients

A total of 24 clinical symptoms were identified by combining data from the literature. Patients with thoracic NUT carcinoma frequently present with non-specific symptoms. Common clinical symptoms at the initial diagnosis of thoracic NUT carcinoma include cough (56.45%, 70/124), pain (40.32%, 50/124), and dyspnea (30.65%, 38/124). In contrast, patients with head-and-neck NUT carcinoma primarily exhibited compression symptoms due to tumor enlargement (53.01%, 44/83), pain (37.35%, 31/83), nasal congestion (14.46%, 12/83),

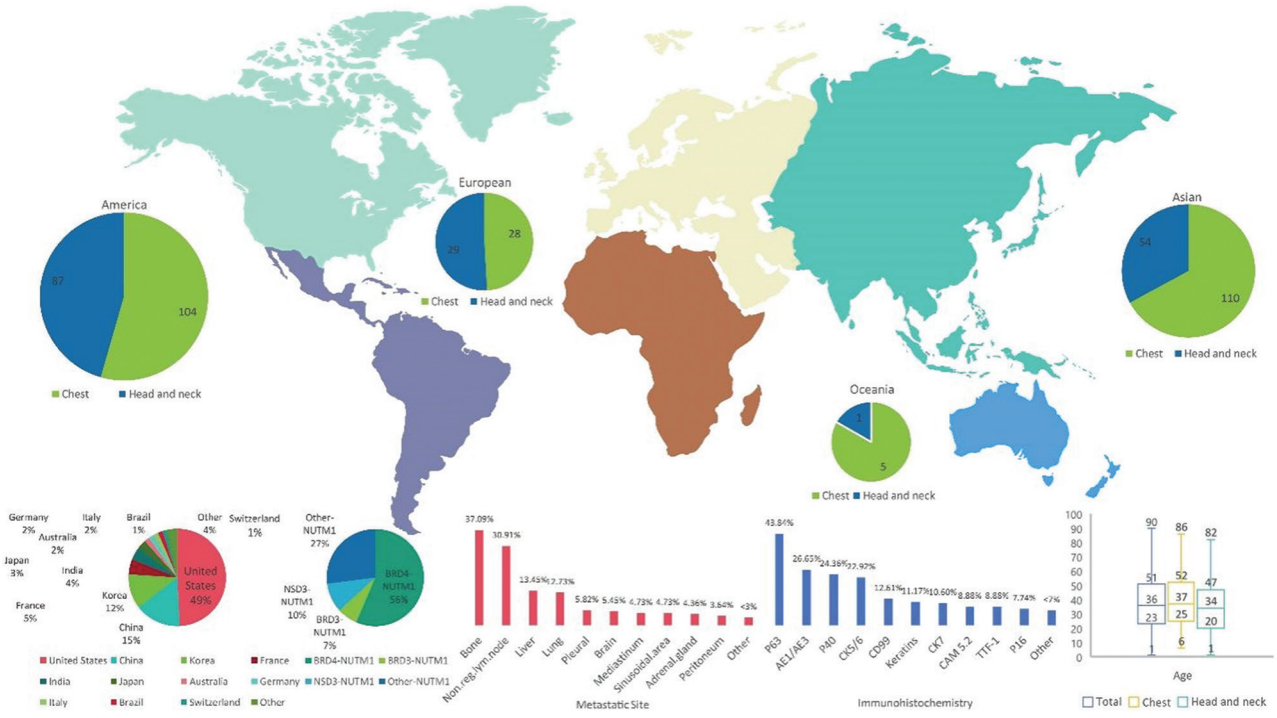

Figure 1. The distribution and general characteristics of nuclear protein of the testis carcinoma patients.
Note: The X-axis represents the specific indicators under each category, while the Y-axis indicates the percentage (%) of these indicators within the corresponding category.
Abbreviations: BRD3: Bromodomain-containing protein 3; BRD4: Bromodomain-containing protein 4; Non.reg.lym.node: Non-regional lymph node; NSD3: Nuclear receptor binding SET domain protein 3; NUTM1: Nuclear protein of the testis midline carcinoma family member 1.

and hemorrhage (13.25%, 11/83), resulting from local tumor compression and invasion of surrounding tissues.

3.2. Tumor characteristics

Tumor diameter: The average tumor diameter of NUT carcinoma patients was 6.04 cm. The average diameter in thoracic NUT carcinoma (6.86 cm) was larger than that of head-and-neck NUT carcinoma (4.08 cm).

3.2.1. NUT carcinoma fusion partners

Among patients with known specific *NUTM1* fusion partners, bromodomain-containing protein 4 (*BRD4*)::*NUTM1* was the most common (56.4%, 167/296), followed by nuclear receptor binding SET domain protein 3 (*NSD3*)::*NUTM1 (*9.80%, 29/296), *and* bromodomain-containing protein 3 (*BRD3*)::*NUTM1 (*6.76%, 20/296).

3.2.2. NUT carcinoma metastasis

A total of 29 metastatic sites were identified. About 52.28% (275/526) of all patients had distant metastasis. Among thoracic NUT carcinoma patients, 60.25% (144/239) had distant metastasis, while 40.85% (67/164) of head-and-neck NUT carcinoma patients had distant metastasis. These findings suggest that thoracic NUT carcinoma may be more prone to distant metastasis than head-and-neck NUT carcinoma. Based on the available data, the bones were the most common site of distant metastasis (37.09%, 102/275). The likelihood of bone metastasis in thoracic NUT carcinoma patients (48.61%, 70/144) was higher than in head-and-neck NUT carcinoma patients (35.82%, 24/67). In addition, NUT carcinoma, found in both thoracic and head/neck regions, was prone to metastasize to the liver (13.45%, 37/275).

3.2.3. NUT carcinoma histopathology and immunohistochemistry

Based on our comprehensive analysis of the available literature, the histopathology of NUT carcinoma predominantly demonstrates poor differentiation (81.90%) and undifferentiation (3.02%). Notably, 72 studies reported partial or focal squamous differentiation, while 32 studies indicated the absence of squamous differentiation. The remaining studies did not specifically address this aspect. Among the literature reporting tumor cell morphology of NUT carcinoma, tumor cells primarily present with three morphological patterns: round cell morphology (approximately 40%), spindle cell features (30%), and epithelioid characteristics (30%). The cells typically exhibit monomorphic growth patterns characterized by vesicular nuclei, prominent nucleoli, and varying amounts of cytoplasm. Microscopic examination frequently reveals sheet-like growth patterns accompanied by extensive necrosis. Regarding specific differentiation, 25% of cases demonstrated neuroendocrine differentiation, 15% exhibited myoepithelial features, and 60% showed no specific differentiation. Many cases presented with numerous mitotic figures and were often associated with geographic necrosis. The stromal component varies from minimal to fibrotic, with occasional infiltration of inflammatory cells. The most prevalent IHC findings for NUT carcinoma included tumor protein p63 (43.84%, 153/349), cytokeratin AE1/AE3 (26.65%, 93/349), ribonucleic acid-binding protein p40 (24.36%, 85/349), and cytokeratin 5/6 (CK5/6; 22.92%, 80/349). The average Ki-67 index expression was approximately 55.16% (15 – 95%).

3.3. Treatment strategy

We identified 17 primary treatment modalities for current NUT carcinoma patients based on the patient's previous treatment histories. NUT carcinoma is generally insensitive to chemotherapy and radiotherapy.[1,18,28] Evidence suggests that surgery, BET inhibitors, HDAC inhibitors, and immunotherapy may be potentially effective against NUT carcinoma.[1,18,28] However, the sample sizes for BET inhibitors, HDAC inhibitors, and immunotherapy are generally limited. When combined with chemotherapy and radiotherapy, the sample size for each group was insufficient (<10 patients). Therefore, we grouped patients who received surgery, BET inhibitors, HDAC inhibitors, and immunotherapy into a category labeled "include surgery/BET/immunotherapy." For example, patients treated with BET inhibitors in combination with chemotherapy or radiotherapy were collectively assigned to the "include BET" group.

3.3.1. Current treatment modalities

Approximately 59.32% (312/526) of patients have relatively comprehensive treatment data. Among the various therapeutic approaches, patients received chemotherapy (18.59%, 58/312), chemotherapy combined with radiotherapy (11.54%, 36/312), chemotherapy combined with surgery and radiotherapy (9.94%, 31/312), and surgery combined with immunotherapy (9.62%, 30/312). In thoracic NUT carcinoma patients, chemotherapy (28.28%, 41/145) and chemotherapy combined with radiotherapy (14.48%, 21/145) were the most common approaches, with 10.34% (30/312) of patients receiving chemotherapy combined with surgery. Conversely, head-and-neck NUT carcinoma patients more commonly received treatment plans based on surgery, including chemotherapy/radiotherapy/surgery (20.34%, 24/118), radiotherapy/surgery (19.49%, 23/118), and surgery combined with immunotherapy (16.95%, 20/118).

3.3.2. Treatment sequence

(a) Treatment sequence 1

We analyzed the treatment sequences of various therapeutic approaches based on the timing when patients initially received each treatment regimen. In the literature dataset, approximately 51.92% (81/156) of thoracic NUT carcinoma patients received chemotherapy first, while 12.18% (19/156) underwent surgery. In head-and-neck NUT carcinoma patients, the majority initially underwent surgery (41.27%, 52/126), with some receiving chemotherapy first (29.37%, 37/126).

(b) Treatment sequence 2

After initial treatment, many thoracic NUT carcinoma patients continued to receive further treatment or, due to the failure of previous treatments, underwent radiation therapy (14.1%, 22/156), chemotherapy (7.69%, 12/156), or BET inhibitors (8.97%,14/156). In contrast, head-and-neck NUT carcinoma patients had a higher proportion receiving subsequent radiation therapy (31.75%, 40/126), followed by chemotherapy (23.02%, 29/126), and surgery (9.52%, 12/126).

(c) Treatment sequence 3 – 4

The number of patients receiving third-line or later treatment was relatively small. Maintenance treatment was primarily based on radiotherapy (7.96%, 27/339) and immunotherapy (2.95%, 10/339) among these patients. Due to the generally poor prognosis of NUT carcinoma patients, the number of patients who received third-line and subsequent treatments remained low. In our data, the proportion of patients receiving immunotherapy (1.47%) was slightly higher than those receiving other treatments.

3.4. Univariate and multivariate analyses

Both multivariate and univariate analyses revealed that the risk ratio for *BRD3::NUTM1* and *BRD4::NUTM1* fusion partners was higher than that for other *NUTM1* fusion partners, such as MAX gene-associated protein (MGA). The risk ratio for NUT carcinoma originating in the thoracic region was higher than that for carcinoma originating in the head and neck. Patients with bone metastasis had a worse prognosis. Conversely, having undergone radiotherapy, immunotherapy, or surgery was identified as a protective factor for patient survival. In addition, receiving radiation therapy as part of salvage treatment prolonged the survival of NUT carcinoma patients. Specific results are available in Figure S3.

3.5. Survival analysis

Further, details on survival data are provided in Table S6.

3.5.1. Patient characteristics

There were no statistically significant differences in prognosis based on patient gender. Asian patients with thoracic NUT carcinoma had better prognoses compared to those from America (overall median survival [mOS]: 5 months) and Europe (mOS: 5 months), with an mOS of 11.4 months. No significant association between age and prognosis in NUT carcinoma was observed. TNM stage, however, was statistically associated with prognosis: patients in stages I–II had the best prognosis (mOS: 54 months), followed by stage III (mOS: 14.9 months), and stage IV had the poorest prognosis (mOS: 6 months). Among thoracic NUT carcinoma patients, a statistically significant difference ($P < 0.05$) in prognosis was observed between stage III (mOS: 12.9 months) and stage IV (mOS: 3 months).

3.5.2. Tumor characteristics

As with other malignancies, tumor size can reflect prognosis to some extent. NUT carcinoma tumors larger than 7 cm had the worst prognosis (mOS: 5 months), followed by tumors between 5 cm and 7 cm (mOS: 8 months). The best prognosis was observed in patients with tumors smaller than 5 cm (mOS: 12 months). However, in thoracic NUT carcinoma, different tumor sizes showed statistically significant differences in prognosis, with a dividing point at a diameter of 5 cm (mOS: 11.6 months). The prognosis of patients with thoracic NUT carcinoma and tumors between 5 – 7 cm (mOS: 4 months) was not significantly different from those with tumors larger than 7 cm (mOS: 4 months). The prognosis for patients with *BRD4::NUTM1* (mOS: 7 months) was significantly worse than that for patients with *NSD3::NUTM1* (mOS: 21 months), with similar findings observed in head and neck carcinoma patients. Prognosis also varied with different metastatic sites. The prognosis for patients with bone metastasis (mOS: 6 months) and lung metastasis (mOS: 6 months) was similar. There were no statistically significant differences in survival analysis across different subgroups of the Ki-67 index (p=0.084). Minimal difference in prognosis was observed between the Ki-67 40–70% and >70% groups (mOS: 8 months [3.6, not available {NA}] versus 8 months [5.7, NA]).

3.5.3. Treatment strategy

We conducted survival analyses separately for patients who received surgery and immunotherapy, comparing them to those who did not. The results demonstrated that patients who underwent surgical treatment achieved a median survival time of 18.7 months (12.2-29), while patients without surgical intervention had a median survival time

of 6 months (5-7.93). Regarding immunotherapy, patients who received immunotherapy treatment reached a median survival time of 19.5 months (12-NA), while those without immunotherapy treatment had a median survival time of 7.93 months (6-10.6).

Although surgery and immunotherapy demonstrated significant survival benefits ($p<0.05$) in the thoracic NUT carcinoma group, immunotherapy had the most pronounced effect. In thoracic NUT carcinoma patients, those who received immunotherapy in combination with other therapeutic modalities achieved a median overall survival (mOS) of 19.5 months. For patients who did not receive immunotherapy, the median overall survival was 6 months. Regarding surgical intervention, patients who underwent surgery demonstrated a median overall survival of 18.7 months (12.2 – 24.6), while those who did not receive surgical treatment had a median overall survival of 10 months (8.4 – 26). In head-and-neck NUT carcinoma patients, those who underwent surgical treatment achieved a median overall survival of 16.5 months, while patients who did not receive surgery had a median overall survival of 7.46 months. Regarding immunotherapy, patients who received combined immunotherapy demonstrated a median overall survival of 31.4 months, whereas those who did not receive immunotherapy had a median overall survival of 11 months.

Patients who received combined immunotherapy during treatment (mOS: 19.5 months [: 12, NA]) showed better survival outcomes compared to those who did not receive immunotherapy (mOS: 7.93 months [6,10.6]), particularly among patients undergoing combined surgery and immunotherapy (mOS: 31.43 [10, NA]). Unfortunately, our study recorded a low incidence of PD-L1/programmed cell death protein 1 (PD-1) positivity, making it challenging to assess the efficacy of immunotherapy in NUT carcinoma patients with negative PD-L1/PD-1 expression. Thus, validation through large-scale cohort studies is necessary.

A survival analysis was conducted on 339 patients, with survival data categorized by treatment type. The treatments were ranked by median survival time as follows (Figure 2): include surgery + immunotherapy (mOS: 31.43 months), radiotherapy + surgery (mOS: 24 months), chemotherapy + radiotherapy + surgery (mOS: 14 months), chemotherapy + surgery (mOS: 12 months), include immunotherapy (mOS: 12 months), chemotherapy + radiotherapy (mOS: 7.93 months), surgery (mOS: 7 months), include BET (mOS: 6 months), radiotherapy (mOS: 5.95 months), include HDAC (mOS: 5.8 months), and chemotherapy (mOS: 4 months). For thoracic NUT carcinoma patients, treatment types were ranked by median survival time as follows: chemotherapy + surgery (mOS: 19 months), including immunotherapy (mOS: 12 months), chemotherapy + radiotherapy (mOS: 6 months), and chemotherapy (mOS: 4 months).

Due to the limited analyzable data, we only evaluated the first and second treatment regimens. The benefit of surgery was most pronounced regardless of whether it was the first or second treatment (sequence 1 mOS: 15 months, sequence 2 mOS: 16.5 months).

Among patients unable to undergo surgery as the first-line treatment, the median survival times were ranked as follows: chemotherapy (mOS: 8 months), radiotherapy (mOS: 7.46 months), and BET (mOS: 6 months). In thoracic NUT carcinoma patients, those receiving radiotherapy (mOS: 6.95 months) had a slightly higher median survival time compared to those receiving chemotherapy (mOS: 6 months). However, this trend was reversed in head-and-neck NUT carcinoma patients, where chemotherapy [mOS: 10 months (8.4,28)] showed a better outcome than radiotherapy [mOS: 7.46 months (5.5,NA)]. No statistically significant differences were observed between the second-line treatment or after surgery.

We also analyzed treatment regimens and specific chemotherapy drugs for NUT carcinoma patients who received chemotherapy exclusively. No significant statistical difference in survival was found between ifosfamide (IFO; mOS: 8 months) alone and platinum-containing chemotherapy regimens without IFO (mOS: 8 months). However, chemotherapy regimens containing IFO had higher OS times compared to other drugs, including Abraxane, docetaxel, paclitaxel, cisplatin, carboplatin, doxorubicin, cyclophosphamide, and etoposide. However, the difference between IFO and platinum-based drugs was not statistically significant.

In thoracic NUT carcinoma patients, chemotherapy regimens containing IFO still provided slightly better survival outcomes than other drugs. Conversely, in head-and-neck NUT carcinoma patients, regimens including platinum-based drugs showed better outcomes than other drugs (Table S6).

Finally, we conducted a separate comparison of regimens containing multiple chemotherapy drugs. The IFO+etoposide+platinum (IEP) regimen provided the best survival benefits (mOS: 10 months) compared to regimens containing only platinum (Taxanes +platinum [TP]: 8.4 months [6,16], etoposide+platinum [EP]: 7 months [4, NA]), or only IFO (IFO+etoposide: 8 months [4.5, NA]). However, no statistically significant difference was found

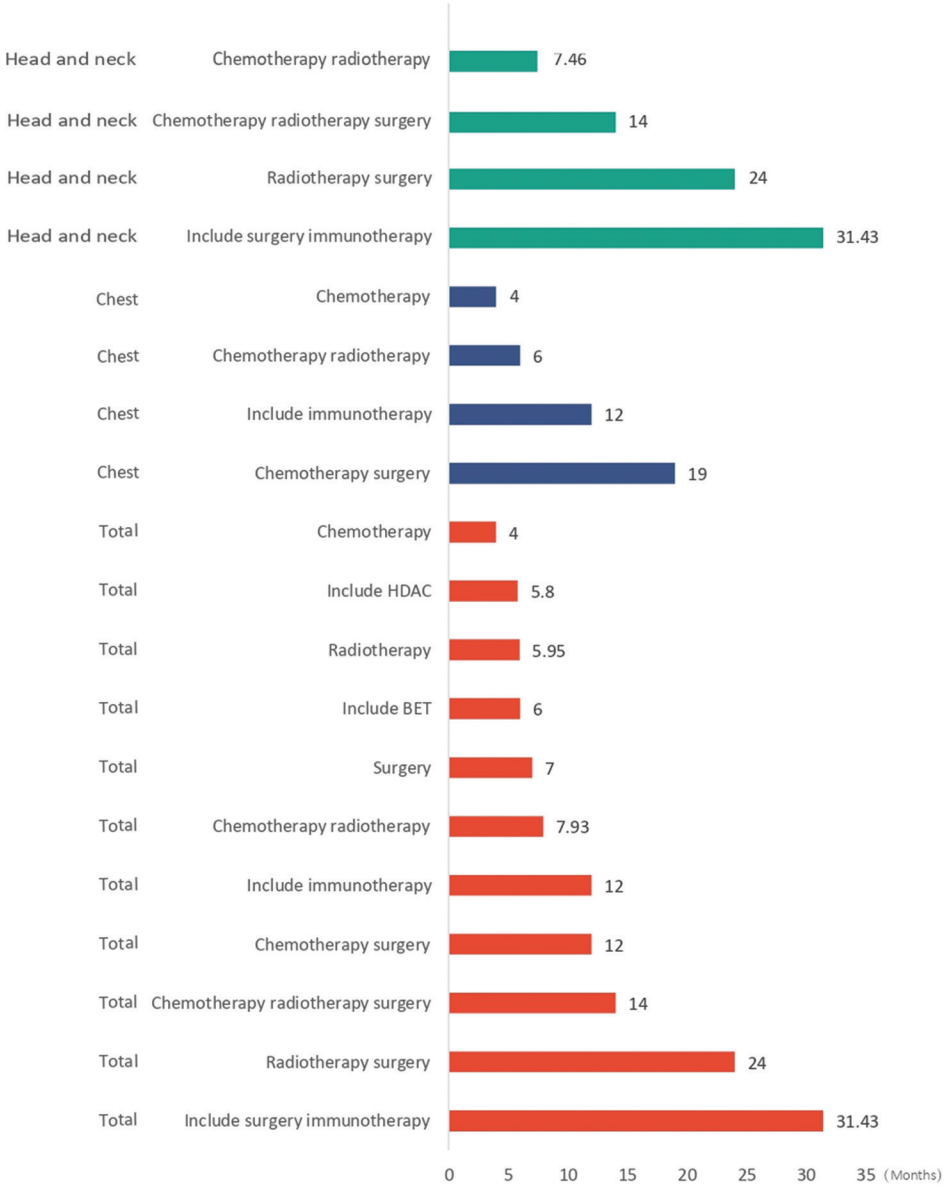

Figure 2. Treatment types ranked by median survival time
Abbreviations: BET: Bromodomain and extra-terminal domain; HDAC: Histone deacetylase.

between these regimens.

4. Expert consensus

Eight recommendations were formulated covering the entire process of diagnosing and treating NUT carcinoma (Table S7). These recommendations address key aspects such as epidemiological characteristics, clinical manifestations, imaging findings, pathological histology and IHC characteristics, molecular mechanisms and subtypes, prognosis, diagnosis, and treatment.

4.1. Epidemiological characteristics

The NUT carcinoma can occur at any age, with varying median ages of onset reported across different studies. More than 80% of NUT carcinoma patients belong to the adolescent and young adult age groups, with onset ranging from newborns to 81 years of age.[15,18,29]

4.2. Clinical manifestations

The clinical symptoms and laboratory test results of NUT carcinoma lack specificity,[28] and the disease typically

presents as rapidly growing masses, often associated with pain and low-grade fever. Between 60% and 77% of cases exhibit distant metastasis at the initial diagnosis,[17,18,30-32] with approximately 50.9% of patients in our dataset classified as stage IV. The most common sites of distant metastasis include the bones, lungs, pleura, liver, brain, adrenal glands, kidneys, and skin. In addition, 68% of cases show involvement of regional lymph nodes.[31] NUT carcinoma typically originates along the midline, with approximately 51% of cases occurring in the thoracic/mediastinal region.[33] In our data, 45.4% of cases were of thoracic origin, and 31.2% were of head-and-neck origin. Clinical manifestations of thoracic NUT carcinoma are often dominated by a persistent cough, with other common symptoms including wheezing, chest tightness, dyspnea, thoracic pain, shoulder pain, back pain, hemoptysis or bloody sputum, and fever.[34,35] Beyond the thoracic region, NUT carcinoma frequently involves the head and neck, particularly the sinonasal area.[31] Most head-and-neck NUT carcinoma cases originate in the nasal cavity, with 30.2% involving the paranasal sinuses and 14.3% affecting the salivary glands. Clinical manifestations of head-and-neck NUT carcinoma include pain at the lesion site, firm swelling of the skin, difficulty opening the mouth, nasal congestion, and other symptoms. At the time of diagnosis, 56.7% of head-and-neck NUT carcinoma patients show invasion of surrounding tissues, with 26.7% exhibiting regional lymph node involvement.[12] Patients with head-and-neck NUT carcinoma may also exhibit pain, swelling, decreased vision, diplopia, facial numbness, choking on liquids, epistaxis, and other symptoms due to tumor invasion of adjacent tissues.

4.3. Imaging manifestations

Computed tomography (CT), magnetic resonance imaging (MRI), ultrasound, positron emission tomography (PET)-CT, and other imaging modalities are crucial for the diagnosis, clinical staging, treatment response assessment, and follow-up monitoring of NUT carcinoma. Endoscopic examinations may also be performed when appropriate, depending on the anatomical sites involved. Contrast-enhanced CT or MRI is recommended for anatomical regions affected by NUT carcinoma. Due to the high malignancy of NUT carcinoma, distant metastasis can occur early, with metastases commonly observed in multiple organs. The skeleton is the most frequent metastatic site, although metastases can occur in other locations, including the brain, liver, adrenal glands, and kidneys.[31] Approximately 75% of bone metastases in NUT carcinoma are osteolytic lesions.[31] Patients with NUT carcinoma often present with single or widespread bone metastases at initial diagnosis (Figure 3). Some patients may exhibit early, moderate osteolytic metastases without obvious clinical symptoms. Metastases may not be present initially but can develop during treatment. It is recommended that a comprehensive, whole-body contrast-enhanced CT scan of the chest, abdomen, pelvis, and brain MRI is performed at the initial visit. If feasible, PET-CT or a whole-body bone scan should be performed to establish baseline data for subsequent treatment planning and efficacy assessment.

Imaging findings in NUT carcinoma are typically nonspecific, resembling those of other common malignant solid tumors in the same anatomical location. These findings are characterized by non-uniform enhancement of low-density masses with significant invasiveness.[36] Primary lung NUT carcinoma typically presents as centrally located masses with invasive, infiltrative growth patterns, and irregular shapes. About 36.8% of cases exhibit pleural effusion, and 57.9% are associated with obstructive atelectasis or obstructive pneumonia.[37] Head-and-neck NUT carcinoma typically manifests as large, poorly defined, and space-occupying masses with internal necrosis and hemorrhage. These tumors often

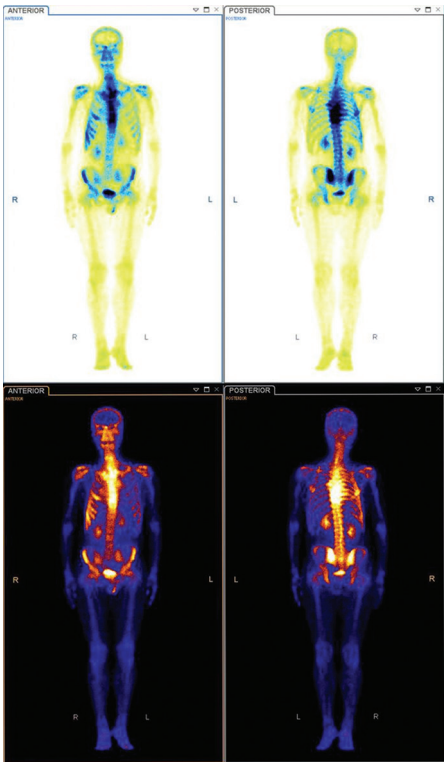

Figure 3. Whole-body bone scan of a 30-year-old male patient with thoracic nuclear protein of the testis carcinoma. The patient, with no history of smoking or alcohol consumption, presented with the right-sided chest pain for 1 month. Bone scan images reveal abnormal radionuclide shadows in multiple right-sided ribs, vertebral bodies in the thoracic spine and the left iliac bone, suggesting bone metastasis.

invade adjacent tissues, such as the sinus walls, muscles, and nerves, and may involve cervical lymph nodes.[12] On CT imaging, head-and-neck NUT carcinoma typically appears as low-density masses with internal necrosis and hemorrhage.

In contrast, MRI findings of NUT carcinoma typically show low-signal intensity on T1-weighted images and high-signal intensity on T2-weighted images, along with heterogeneous enhancement.[36] Both primary and metastatic lesions in thoracic and head-and-neck NUT carcinoma exhibit high fluorodeoxyglucose uptake on PET-CT imaging.[31] Lung NUT carcinoma tumors typically have a maximum standardized uptake value (SUV) exceeding 10, with an average SUV of 12, ranging from 5 to 40. Extra-pulmonary NUT carcinoma tumors have an average SUV of 13.8, ranging from 4.5 to 64.1.[38,39] Imaging features of NUT carcinoma in other locations typically include primary masses accompanied by metastatic lymph node enlargement and widespread distant metastases. These features resemble those of advanced tumors in the respective sites, posing challenges in distinguishing from other malignancies.[38,39] While bone metastases can be evaluated using bone scintigraphy or PET-CT, current data suggest that NUT carcinoma bone metastases are predominantly osteolytic. Since bone scintigraphy relies on enhanced sodium phosphate metabolism driven by osteoblastic activity,[40] PET-CT is recommended for a more accurate assessment.

4.3.1. Recommendation 1

NUT carcinoma frequently presents as large masses, often accompanied by regional lymph node metastases and distant metastases. Due to its lack of specificity, its imaging features closely resemble those of advanced tumors in the corresponding anatomical regions. Bone metastases are commonly observed in NUT carcinoma, and clinicians should be particularly vigilant when patients present with extensive bone metastases at the time of initial diagnosis. Enhanced CT/MRI examinations of the relevant anatomical sites and bone scans or PET-CT (more recommended) are beneficial for staging and treatment evaluation (level of evidence: Grade 4; recommendation level: Strong recommendation).

4.4. Pathological histology and IHC features

4.4.1. Sampling of pathological specimens

Suitable pathological samples for analysis include surgical specimens, biopsy tissues, sputum, fiberoptic bronchoscope brushings, and shed cells from pleural or peritoneal fluid. These samples can be used for various tests, such as hematoxylin and eosin staining, IHC, FISH, NGS, and liquid biopsy for molecular testing. However, samples for molecular testing must undergo enrichment and quality control to ensure reliability. It is essential to note that tissue samples obtained through endoscopy, fine-needle aspiration, or core-needle biopsy may not fully represent the morphology and structure of the tumor. This limitation could hinder the identification of typical histological features, such as abrupt keratinization in NUT carcinoma, thereby increasing the diagnostic challenge.[41] Since NUT carcinoma is frequently diagnosed in advanced stages when tumor samples cannot be obtained through surgery, liquid biopsy samples such as circulating-tumor DNA (ctDNA) and high-throughput sequencing can be considered supplementary diagnostic tools. In addition, endoscopy, fine-needle aspiration, or core-needle biopsy may still be helpful in these cases.

4.4.2. Pathological histological features

Due to its rarity and nonspecific manifestations, NUT carcinoma is often misdiagnosed during the initial pathological examination. In most cases, NUT carcinoma lacks specific histological features, with cancer cells typically showing poorly differentiated morphology.[42] Approximately 33% to 40% of NUT carcinomas may exhibit focal squamous differentiation with abrupt keratinization (Figure 4). In such cases, squamous cells can abruptly form small, round cell clusters with abundant keratinized cytoplasm and nuclear shrinkage, lacking stratification, and gradual differentiation processes.[43] The stroma may show

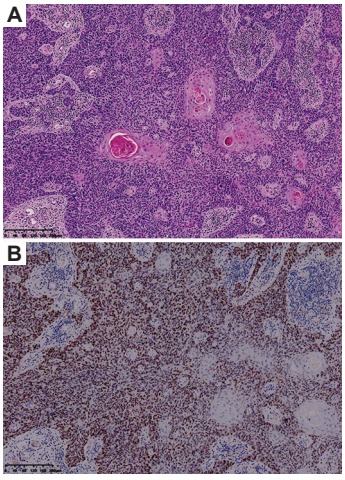

Figure 4. Immunohistochemical (IHC) characteristics of nuclear protein of the testis carcinoma tumor tissue. (A) Hematoxylin and eosin stain (magnification = 10×; scale bar = 200 μm) of a head-and-neck nuclear protein of the testis carcinoma biopsy, revealing areas of sudden keratinization surrounded by primitive, undifferentiated, or poorly differentiated small round cells, with minimal lymphocytic infiltration in the stroma. (B) Nuclear protein of the testis IHC staining (magnification = 10×; scale bar = 200 μm) of the same biopsy, showing diffuse nuclear staining.

edema, mucinous appearance, and fibrous changes, often accompanied by varying connective tissue proliferation. Neutrophil infiltration may also be observed, occasionally with intraepithelial and stromal lymphocyte infiltration.[42]

4.4.3. IHC markers

Immunohistochemistry in NUT carcinoma can reveal a range of epithelial markers to varying extents, including AE1/AE3, epithelial membrane antigen p63, p40, as well as sex-determining region Y-box 2 (SOX2), thyroid transcription factor-1, paired box 8, and MYC. In addition, other relevant markers such as neuroendocrine markers (e.g., synaptophysin, chromogranin, cluster of differentiation [CD] 56), lymphocyte markers (e.g., CD56, CD30, CD34, CD43, CD138, and CD45), germ cell tumor markers (e.g., CD30, placental alkaline phosphatase, and split-like protein 4), vascular markers (e.g., friend leukemia integration 1 transcription factor [FLI1] and CD34), and Ewing's sarcoma markers (e.g., FLI1 and CD99) can also be expressed in NUT carcinoma.[2] In our analysis, the top positive IHC markers were p63 (43.84%), AE1/AE3 (26.65%), p40 (24.36%), CK5/6 (22.92%), and CD99 (12.61%). With few exceptions, the NUT protein was expressed in nearly all cases of NUT carcinomas;[44] however, it was also widely expressed in other solid tumors. The characteristic diagnostic feature of NUT carcinoma is the diffuse nuclear dot-like pattern of NUT staining positivity.[45]

(a) Recommendation 2

Apart from surgical specimens, NUT carcinoma tissue samples can be obtained through endoscopy, aspiration, and core-needle biopsy. The histology of NUT carcinoma is often nonspecific, with some cases showing focal squamous differentiation accompanied by sudden keratinization and neutrophil infiltration. IHC staining for NUT typically reveals diffuse nuclear dot-like patterns. While NUT positivity is a key feature, other IHC markers in NUT carcinoma do not exhibit specificity (level of evidence: grade 4; recommendation level: strong recommendation). If the diagnosis remains inconclusive through these methods, supplementary diagnostic approaches, such such as high-throughput sequencing via blood ctDNA, can be considered (level of evidence: grade 5; recommendation level: strong recommendation).

4.5. Molecular mechanisms and molecular subtypes of NUT carcinoma

The *NUTM1* gene on chromosome 15 encodes the NUT protein, which is usually expressed in testicular and ovarian germ cells. Chromosomal translocations or rearrangements lead to fusion with various partner genes.[42] In over 70% of NUT carcinoma patients, *NUMT1* fuses with *BRD4*, a gene commonly expressed in the cell nucleus. Comparative genomic analyses suggest that the classification, clinical behavior, and treatment strategies for NUT carcinoma are best defined by the fusion partner of *NUTM1* rather than by tumor morphology or IHC profile.[46] Evidence indicates that NUT carcinoma is driven by the NUT fusion oncoprotein, with BRD4 being the most common fusion partner. Less common fusion partners include *BRD3::NUTM1* t(15;19)(q14;p34.2), *NSD3::NUTM1*, t(8;15)(p12;q15), and zinc finger protein (*ZNF*) *532,* among others.

The survival rate of NUT carcinoma patients is closely related to the tumor site and the specific fusion partners of NUTM1, with BRD4 fusion generally associated with the poorest prognosis.[18] BRD4 is a member of the BET protein family, which includes two bromodomains that bind to acetylated histones and an additional C-terminal protein interaction domain.[47] Bromodomain-containing proteins 2 (BRD2), BRD3, and BRD4 share sequence homology and participate in the transcriptional regulation of numerous genes involved in cell growth, proliferation, survival, and inflammation. Among these, BRD4 acts as a coactivator in the transcription of genes involved in the G1 phase of the cell cycle (such as MYC, B-cell lymphoma 2 [BCL2], and cyclin-dependent kinase 9 [CDK9]).[48] Fusion of NUTM1 with BRD2, BRD3, or BRD4 generates chimeric genes that encode BRDX-NUTM1 fusion proteins; fusions with other partner genes (such as *NSD3*) are collectively referred to as NUT variants.[49] *BRD4::NUTM1* typically inhibits cellular differentiation and supports the growth of NUT carcinoma cells by binding to acetylated chromatin through its dual bromodomains. It recruits histone acetyltransferase p300 to enhance wild-type BRD4 activity, markedly increasing the transcription of target genes, thereby activating oncogenes such as MYC and SOX2.[50] MYC and SOX2 maintain cells in a relatively undifferentiated, stem-like state, similar to cells in NUT carcinomas. Overexpression of oncogenes such as MYC activates cyclin D1 and cyclin D2, driving the cell cycle[51] while simultaneously inhibiting p53 activation, which blocks apoptosis[52] and facilitates tumor progression. A genetically engineered mouse model of NUT carcinoma based on the *BRD4::NUTM1* fusion gene closely mirrors human NUT carcinoma. This model provides strong evidence that BRD4-NUT alone drives squamous progenitor cells into a cancerous stage, with BET inhibitors inducing differentiation and extending survival.[53]

In addition, it is important to note that NUT carcinoma is generally considered a rare, undifferentiated squamous cell carcinoma, typically characterized by fusion partners such as BRD4, BRD3, NSD3, ZNF532, or ZNF592, predominantly affecting the mediastinum or head and

neck regions. As next-generation sequencing technologies have expanded, more NUTM1 fusion partners have been identified. Consequently, NUT carcinoma is now recognized as a subtype of NUTM1-rearranged neoplasms (NRNs), which also include skin tumors, sarcomas, CNS tumors, and hematologic malignancies.[29]

Skin tumors associated with NUTM1 rearrangements include classic poroma, hidradenoma simplex, dermal duct tumor, poroid hidradenoma, porocarcinoma, and malignant poroid hidradenoma/poroid hidradenocarcinoma. The fusion transcripts in these tumors primarily include yes1 associated transcriptional regulator (*YAP1*)::*NUTM1*, WW domain containing transcription regulator 1 (*WWTR1*):*NUTM1*, and endoplasmic reticulum membrane protein complex subunit 7 (*EMC7*)::*NUTM1*. Sarcomas with NUTM1 rearrangements can originate in soft tissues, dura mater, thoracic structures, ovaries, or the colon. The relevant fusion transcripts include MAX dimerization protein 1 (*MXD1*)::*NUTM1*, MAX interactor 1 (*MXI1*)::*NUTM1*, MAX dimerization protein MGA (*MGA*)::*NUTM1*, MAX dimerization protein 4 (*MXD4*)::*NUTM1*, B-cell lymphoma 6 corepressor like 1 (*BCORL1*)::*NUTM1*, and *CIC*::*NUTM1*, among others. These sarcomas can present with fibrosarcoma, epithelioid, and rhabdomyoblastic morphology. CNS tumors linked to NUTM1 rearrangements include fusion transcripts such as *CIC*::*NUTM1*, ataxin 1 (*ATXN1*)::*NUTM1*, par-3 family cell polarity regulator beta (*PARD3B*)::*NUTM1*, and spectrin beta, non-erythrocytic 4 (*SPTBN4*)::*NUTM1*. Hematologic malignancies associated with NUTM1 rearrangements can occur in B-cell acute lymphoblastic leukemia (B-ALL), T-cell acute lymphoblastic leukemia (T-ALL), and acute myeloid leukemia (AML). The fusion transcripts in B-ALL typically include apoptotic chromatin condensation inducer 1 (*ACIN1*)::*NUTM1*, cut-like homeobox 1 (*CUX1*)::*NUTM1*, *ZNF618*::*NUTM1*, solute carrier family 12 member 6 (*SLC12A6*)::*NUTM1*, chromodomain helicase DNA binding protein 4 (*CHD4*)::*NUTM1*, bromodomain containing 9 (*BRD9*)::*NUTM1*, AF4/FMR2 family member 1 (*AFF1*)::*NUTM1*, ATPase family AAA domain containing 5 (*ATAD5*)::*NUTM1*, Runt-related transcription factor 1 (*RUNX1*)::*NUTM1*, Ikaros family zinc finger 1 (*IKZF1*)::*NUTM1*, nucleosome assembly protein 1 like 4 (*NAP1L4*)::*NUTM1*, and apoptosis and caspase activation inhibitor (*AVEN*)::*NUTM1*. Meanwhile, T-ALL shows fusion transcripts such as bromodomain PHD finger transcription factor (*BPTF*)::*NUTM1*, and AML demonstrates fusion transcripts such as zinc finger and BTB domain containing 7A (*ZBTB7A*)::*NUTM1*, adenylate cyclase 7 (*ADCY7*)::*NUTM1*, and apoptosis and caspase activation inhibitor (*AVEN*)::*NUTM1*. Myeloid neoplasms associated with NUTM1 mainly involve the nucleosome assembly protein 1 like 4 (*NAP1L4*)::*NUTM1* fusion transcript.[2,29]

The distinction between NUT carcinoma and other non-NUT carcinoma is not entirely clear and is mainly based on fusion partners, tumor origin, and pathology. The oncogenic mechanisms of NUT carcinoma and other non-NUT carcinoma may differ.[2,29,42,54] Moreover, non-NUT carcinoma tends to respond more favorably to standard therapies, exhibit lower malignancy and invasiveness, and show better overall prognoses than NUT carcinoma.[29,55]

4.6. Prognosis

NUT carcinoma is associated with a poor prognosis and rapid progression, with a median survival period of 6.7 – 9.5 months. Many patients lose the opportunity for surgery due to local progression and distant metastasis.[2,15,17,30,56,57] For NUT carcinoma patients aged 7 – 16 years, the median survival is 8 months (ranging from 4.5 months to 2.4 years), with 60% of cases originating in the thoracic region (median survival of 4.5 – 15 months) and 40% in the head, neck, or adjacent to the spine (median survival of 10 months – 2.4 years).[58] In a study by Chau *et al.*[18] involving 124 patients, it was reported that the prognosis for primary NUT carcinoma originating in the thorax is worse compared to other locations, with a higher likelihood of distant metastasis, larger tumors (>6 cm) that are difficult to remove completely, and a mOS of only 4.4 months, resulting in a 2-year survival rate of 5%. Patients with thoracic NUT carcinoma carrying the *BRD4*::*NUTM1* fusion gene have the worst prognosis.[18,59] In contrast, those without this fusion (such as *BRD3*::*NUTM1* and *NSD3*::*NUTM1*) exhibit the best prognosis among non-thoracic NUT carcinoma patients, with a 2-year survival rate of 64% and a mOS of 36.5 months.[18] The mOS for non-thoracic NUT carcinoma tumors with the *BRD4*::*NUTM1* fusion is 10 months.[29] Patients with head and neck NUT carcinoma tend to have a better prognosis compared to those with tumors in the lungs and other locations (OS: 16 months vs. 6 months).[31]

4.7. Diagnosis

Diagnosing NUT carcinoma is challenging due to its nonspecific clinical manifestations and histopathological features, which require differentiation from other small round cell tumors such as Ewing sarcoma, primitive neuroectodermal tumor (PNET), rhabdomyosarcoma, synovial sarcoma, undifferentiated carcinoma (including nasopharyngeal or salivary gland undifferentiated carcinoma), proliferative fasciitis-like low-grade fibromyxoid sarcoma, and other poorly differentiated or undifferentiated tumors.[1] Similar to hematologic malignancies, NUT carcinoma can also present with

diffuse bone infiltration and express CD34, which can lead to misdiagnosis as acute leukemia or other hematologic diseases.[60] NUT carcinoma lacks specific diagnostic morphological features; it is a poorly differentiated or undifferentiated tumor, with some cases exhibiting sudden keratinized foci, leukocyte infiltration, and extensive necrosis. At present, NUTM1 rearrangement can be confirmed using IHC staining for NUT positivity or FISH (with over 20% of tumor cells showing the t(15;19)(q14;p13.1) separation probe-positive), along with other molecular techniques such as cell cytogenetics, reverse transcription polymerase chain reaction, and second-generation sequencing, all of which assist in diagnosing NUT carcinoma.[18] In the 2021 edition of the WHO classification of lung cancer, NUT carcinoma is categorized under "other epithelial tumors of the lung."

The 2024 National Comprehensive Cancer Network clinical practice guidelines for non-small-cell lung cancer recommend testing for NUT rearrangement in all poorly differentiated lung cancers that lack glandular differentiation or specific causes, especially in nonsmokers or young patients. However, this recommendation is not widely followed due to the rarity of NUT carcinoma. Moreover, when NUT carcinoma masses are detected in non-midline anatomical structures (e.g., head/neck/thorax) or in elderly patients with limited tumor samples that lack typical NUT carcinoma morphology, NUT IHC staining may not be performed, potentially leading to misdiagnosis.[61] According to the 2023 Chinese Society of Clinical Oncology guidelines for head-and-neck tumors, NUT IHC testing is recommended as a level II diagnostic tool. It is advised for patients with poorly differentiated carcinoma, regardless of age or medical history. According to the WHO recommendations, NUT antibody IHC staining with a cutoff value of ≥50% positivity for the C52B1 clone has 100% specificity and 87% sensitivity for diagnosing NUT carcinoma.[45] Although transcriptome sequencing has higher sensitivity in NGS than DNA-based NGS, false negatives are still possible. Therefore, NGS results should be validated using other molecular detection methods to ensure diagnostic accuracy.

Fluorescence *in situ* hybridization with a NUTM1 breakpoint 15q14 probe is considered one of the essential methods for diagnosing NUT carcinoma.[2] However, FISH has low resolution and may miss potential breakpoints. Therefore, when cases are IHC NUT-positive, full-length NUTM1 probe FISH or second-generation sequencing (preferably transcriptome sequencing) is recommended to confirm the diagnosis.[2]

At present, NUT carcinoma can be diagnosed using NUTM1 IHC or FISH. While NUT carcinoma shows high IHC specificity, molecular testing can identify various fusion partners of NUTM1, which helps predict patient prognosis. BET inhibitors may have suboptimal efficacy for patients with gene fusions not dependent on BRD4. Therefore, identifying NUTM1 fusion partners and available drug targets through second-generation sequencing can validate the pathological diagnosis, predict disease prognosis, and inform treatment options, including later-stage drug therapies and combination treatments.[41,62]

4.7.1. Recommendation 3

The clinical presentation, histopathology, and conventional IHC features of NUT carcinoma lack specificity, highlighting the importance of using specific NUT antibodies for IHC staining in its diagnosis. For patients with an initial diagnosis accompanied by rapid progression or distant metastasis, especially those with poorly differentiated carcinomas or small round cell tumors, it is strongly recommended to consider NUT IHC examination (evidence level: grade 4; recommendation level: strong recommendation). In addition, FISH or high-throughput sequencing should be considered to identify the type of NUTM1 fusion partner (such as BRD4, BRD3, and NSD3) (evidence level: grade 5; recommendation level: strong recommendation).

4.8. Treatment

Given the highly invasive nature and poor prognosis of NUT carcinoma, it is essential to emphasize the importance of multidisciplinary team (MDT) consultations, including the involvement of a Molecular Tumor Board (MTB). In the MTB, experts from various disciplines collaboratively analyzed the patients' clinical manifestations, imaging, pathology, and molecular biology/genetic data to comprehensively assess the patient's general condition, disease diagnosis, extent of invasion, and prognosis. Based on existing treatment standards and evidence-based medicine, combined with available treatment methods, treatment plans should be adjusted in real time according to changes in the patient's condition to develop the most appropriate treatment strategy.

NUT carcinoma can occur in various organs, and currently, there is no specific staging system exists for this cancer. Therefore, the staging system from the American Joint Committee on Cancer for tumors in corresponding locations may be applied to NUT carcinoma.

A study of 124 patients with NUT carcinoma showed an objective remission rate of 49% for treatments involving surgery, radiotherapy, and chemotherapy.[18] New treatment possibilities may emerge from targeting

fusion partners, including inhibiting DNA binding with BET inhibitors or modifying downstream histones with HDAC inhibitors to disrupt the function of fusion partners. NUT carcinoma is a newly classified tumor by the WHO, and awareness of it remains limited globally. At present, most treatment evidence for NUT carcinoma comes from retrospective analyses and case reports, with relatively less evidence from treatment-related studies in NUT carcinoma patients. Moreover, given that NUT carcinoma can arise in various organs, treatment guidelines for other tumors in affected locations may be adopted for NUT carcinoma. Based on relevant literature, clinical experience with NUT carcinoma, and expert opinions, this consensus refers to guidelines for other tumors in the specific locations affected by NUT carcinoma. It summarizes the principles for treating NUT carcinoma (Figure 5). Patients with NUT carcinoma who are candidates for surgery should undergo the procedure.

For patients unsuitable for surgery or require adjuvant therapy post-surgery, other treatment modalities, such as radiotherapy and systemic therapies (e.g., chemotherapy and targeted therapy), can be considered based on the patient's condition. Considering the rapid progression and high malignancy of NUT carcinoma, particularly in cases with poor prognosis, such as those carrying the *BRD4::NUTM1* fusion gene, participation in clinical trials is strongly recommended. Maintenance therapy based on prior treatments can continue if lesions stabilize following initial treatment. In cases of disease progression, potential drugs should be selected based on high-throughput sequencing results, with treatment plans tailored to the patient's previous treatment history. If necessary, MDT consultations can guide further diagnosis and treatment. We encourage patients to participate in prospective clinical trials and explore potential new treatment options.

4.8.1. Surgery

Surgery plays a pivotal role in the comprehensive management of NUT carcinoma. Surgical strategies should be developed based on the patient's overall health, the extent of tumor invasion, tumor staging, and the feasibility of resection, which can be assessed through enhanced CT or MRI evaluation. Surgery is the primary curative method for NUT carcinoma, with surgical techniques often adapted from protocols used for similar cancers in specific anatomical sites. Before surgery, a specialized medical team should evaluate or discuss in an MDT meeting whether NUT carcinoma patients should undergo neoadjuvant therapy. Patients eligible for direct surgical excision should be assessed based on pre-operative and post-operative TNM staging, pathological findings, surgical resection margins (R0, R1, and R2), and post-operative lymph node involvement to determine the need for post-operative adjuvant therapy. Surgical treatment remains a viable option for patients with localized tumor recurrence, which provided that they are still deemed suitable for surgery. For patients unsuitable for surgery, alternative treatment modalities such as radiotherapy and systemic treatment (e.g., chemotherapy and targeted therapy) may be considered.

Relying solely on chemotherapy is unlikely to result in a favorable prognosis. In cases where NUT carcinoma lesions are localized without distant metastasis, comprehensive surgical resection should be actively considered, as it can lead to a better prognosis when followed by radiotherapy and chemotherapy. Some studies on head and neck NUT carcinoma suggest that prophylactic cervical lymph node dissection should be considered even in the absence of lymph node metastasis (N0).[1] Patients with head-and-neck NUT carcinoma who undergo surgical resection followed by radiotherapy tend to experience longer OS and progression-free survival (PFS). In head-and-neck NUT carcinoma, the extent of surgical resection, the achievement of negative margins, and the response to initial treatment are all significantly associated with better PFS and OS. For instance, patients who underwent surgery had a 2-year OS rate of 50%, compared to just 7% for those who did not (p=0.003). The degree of surgical resection also correlated with PFS and OS in a graded manner: patients with negative margins had a 2-year OS of 80%, those with gross total resection but positive margins had a 2-year OS of 44%, and those who underwent debulking had a 2-year OS of 37%.[30,56] However, these findings require further validation through prospective research.[56] Palliative surgical debulking may also be an option to improve quality of life.[63]

In addition, collaboration among multidisciplinary surgical teams may be crucial due to the aggressive nature of NUT carcinoma, mainly when it affects multiple anatomical regions. Following surgery, proactive planning should include radiotherapy for the primary tumor site and affected lymph nodes, along with timely systemic treatment.[12,56]

(a) Recommendation 4

Patients with resectable NUT carcinoma should undergo curative surgery as the primary treatment as early as possible. Post-operative adjuvant therapy should be determined based on pre-operative and post-operative TNM staging, pathological conditions, surgical margins (R0, R1, and R2), and post-operative lymph node status (level of evidence: level 3; recommendation grade: strongly

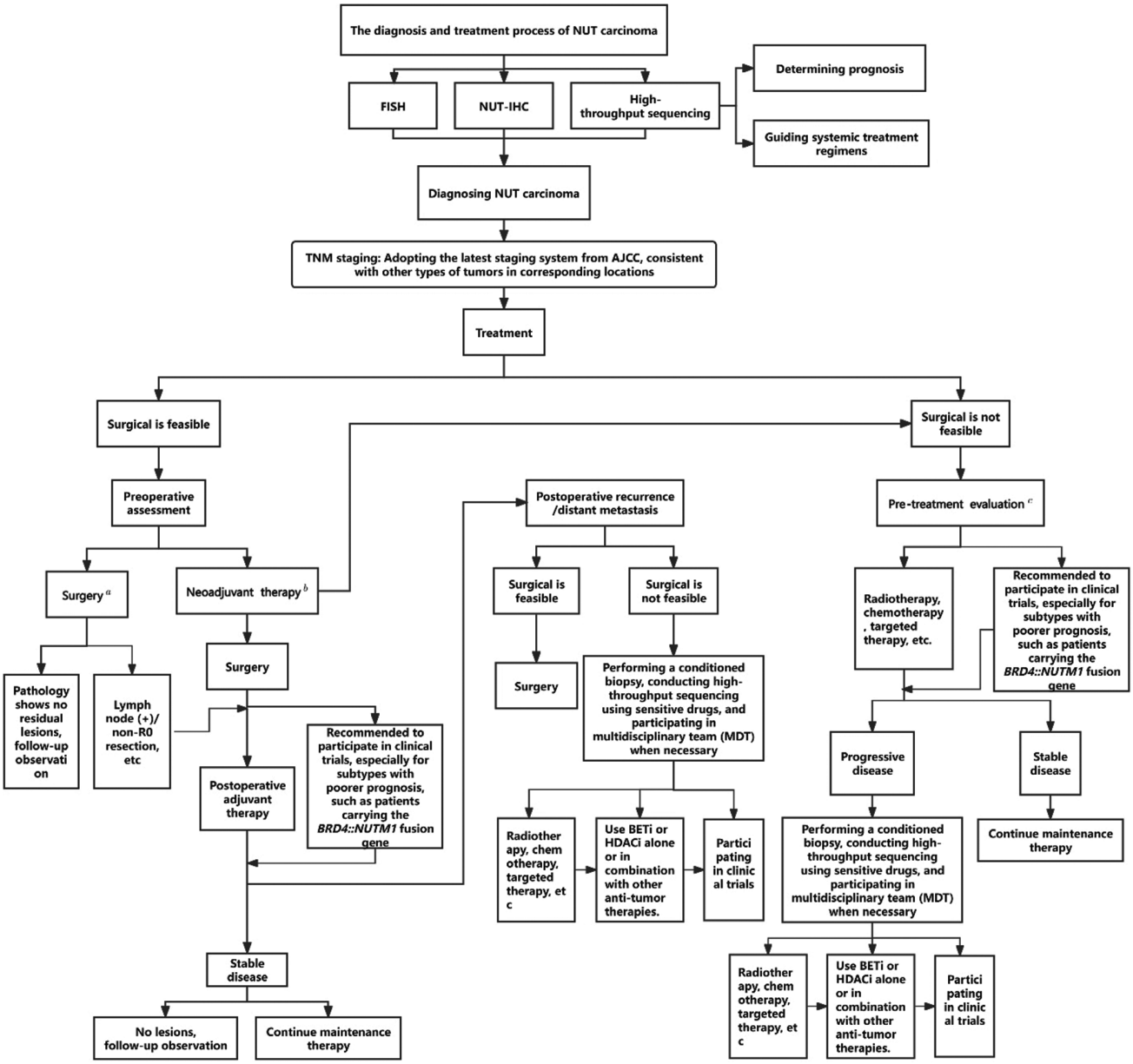

Figure 5. Flowchart of diagnosis and treatment for the nuclear protein of the testis carcinoma

Notes: [a]Prior to surgery, assessment by specialists or a multidisciplinary team can determine whether direct surgery is feasible. Postoperatively, decisions on whether to undergo adjuvant therapy are based on factors such as the patient's pre-operative TNM staging, pathological findings, surgical margin status (R0, R1, R2), and lymph node positivity. [b]Prior to surgery, evaluation by specialists or a multidisciplinary team can assess the feasibility of neoadjuvant therapy for potentially resectable nuclear protein of the testis carcinoma. Specific neoadjuvant treatment modalities are recommended based on guidelines for other tumor types at the specific site of NUT carcinoma. [c]Non-surgical patients with nuclear protein of the testis carcinoma should undergo evaluation by specialists or a multidisciplinary team before treatment. Treatment decisions should be based on guidelines for other tumor types at the specific site of nuclear protein of the testis carcinoma, as well as the patient's overall condition.

Abbreviations: AJCC: American Joint Committee on Cancer; BRD4: Bromodomain-containing protein 4; FISH: Fluorescence *in situ* hybridization; IHC: Immunohistochemistry; NUT: Nuclear protein of the testis; NUTM1: Nuclear protein of the testis midline carcinoma family member 1; TNM: TNM classification of malignant tumors.

recommended). Pre-operative assessment by specialized physicians or an MDT can help determine the feasibility and approach of neoadjuvant therapy (level of evidence: level 4; recommendation grade: strongly recommended).

4.8.2. Radiotherapy

Considering the high malignancy and aggressive invasiveness of NUT carcinoma, along with its propensity for recurrence, it is recommended that post-operative

NUT carcinoma patients who have undergone non-R0 resections, exhibit lymph node positivity, and receive post-operative adjuvant treatments. Many NUT carcinoma patients are not candidates for surgery at the time of diagnosis; for such patients, concurrent chemoradiotherapy becomes a viable treatment option for inoperable tumors. Standardization of radiation doses for NUT carcinoma remains elusive. Radiation plans should incorporate at least three-dimensional conformal techniques, with a preference for intensity-modulated radiotherapy. The radiation dose and target area should be tailored to the patient's overall health, tumor site involvement, and tumor staging. These parameters should be informed by radiation doses and target areas used for advanced malignancies in similar tumor types.

Radiation therapy generally employs curative doses, although palliative doses may be used if the tumor is located near critical organs or if the patient has limited tolerance for treatment. Radiation doses typically range from 50 Gy to 70 Gy, with studies showing that NUT carcinoma patients who received doses exceeding 50 Gy have a higher survival rate.[56,64] Before radiation therapy, a comprehensive evaluation of the patient's overall health, dietary habits, speech, and any organs that may be irradiated within the target area is required. It is recommended that the primary tumor area is irradiated with 65 – 70 Gy and the affected regional lymph nodes with 50 – 54 Gy" to: "In cases where radiotherapy is used exclusively, it is recommended to deliver a dose of 65 – 70 Gy to the primary tumor and lymph node lesions, and 50 – 54 Gy to elective lymph node regions.[1] The radiation dose should be adjusted based on the lesions and the extent of local disease involvement, including tumor margins and neurovascular invasion. The target area should encompass as many microlesions as possible, with recommendations to irradiate the expanded primary tumor site and any involved lymph node regions.

Chemotherapy drugs used during concurrent chemoradiotherapy for NUT carcinoma patients are typically based on those used for other malignancies at the same anatomical sites, with platinum-based agents being the most common. In one case of head and neck NUT carcinoma with primary lesions in the ethmoid and sphenoid sinuses, the lesions involved both optic nerves and the skull base 1.5 months postoperatively. After 11 sessions of concurrent chemoradiotherapy and hyperthermia (total radiation dose: 69.96 Gy, 2.12 Gy × 33F; cisplatin, temozolomide 75 mg/m^2), the lesions shrank significantly. However, due to side effects from radiotherapy, the patient was unable to complete the treatment, which led to an increase in the dose of temozolomide (200 mg/m^2), but the tumor continued to progress. Eventually, adding lapatinib led to further shrinkage of the lesions, but this effect lasted only 2 months, resulting in an OS of 17 months.[65] In another case, a 22-year-old patient with supraglottic NUT carcinoma (stage cT3N2bM0) achieved a complete response after concurrent chemoradiotherapy (total radiation dose: 70 Gy, 2 Gy × 35F; cisplatin 80 mg/m^2 every 3 weeks), although ovarian metastasis occurred 3 weeks after completing radiotherapy.[66] In the case of pulmonary NUT carcinoma, combined radiotherapy and anlotinib resulted in a 78% reduction in tumor size within 2 months.[67] A patient with locally advanced head-and-neck NUT carcinoma achieved complete remission after concurrent chemoradiotherapy and alternating regimens of vincristine, doxorubicin, and cyclophosphamide, with IFO and etoposide.[68] Adolescent patients tend to have a poor prognosis, with a median survival of 8 months (range: 4.5 – 28.8 months) for five NUT carcinoma patients aged 7 – 16 years who received radiotherapy and chemotherapy.[58]

Before radiotherapy, it is necessary to assess the patient's general condition, diet, speech, and any organs affected by irradiation. For NUT carcinoma patients with high-risk factors such as positive lymph nodes or non-R0 resection and those who are unsuitable for surgery, an MDT evaluation should be conducted before treatment to determine the most appropriate comprehensive treatment, which should primarily involve concurrent or sequential chemoradiotherapy. The radiation target area and dose can be based on those used for other malignancies at corresponding sites.

(a) Recommendation 5

Patients with high-risk factors, such as lymph node positivity or non-R0 resection, especially those with inoperable NUT carcinoma, particularly in the head-and-neck region, should undergo evaluation by specialized physicians or an MDT before treatment, aiming to select comprehensive therapy, primarily based on concurrent chemoradiotherapy. The radiotherapy protocol and dosage can be guided by delineating target areas and radiation doses for other corresponding malignant tumors (level of evidence: grade 3; recommendation level: strongly recommended).

4.8.3. Chemotherapy

The response rate of NUT carcinoma to chemotherapy is approximately 40%, but it tends to develop resistance regardless of the type of chemotherapy regimen used.[20,64] Anthracyclines, cisplatin, alkylating agents, etoposide, gemcitabine, irinotecan, and taxanes have been reported as part of chemotherapy combinations for NUT carcinoma. However, almost all chemotherapy regimens demonstrate only temporary efficacy or no therapeutic response.[1,20,56,64,69]

Some studies suggest an association between chemotherapy and improved survival rates,[56] but consensus has not been reached on the optimal chemotherapy regimen and timing. Relying solely on chemotherapy is often ineffective in controlling the progression of NUT carcinoma.

At present, the effective chemotherapy regimens used for achieving some degree of relief in multimodal treatments – combined with surgery, radiotherapy, and targeted therapy – are primarily based on anthracyclines, alkylating agents, and platinum compounds.[69,70] In a cohort study of 118 NUT carcinoma patients, the objective response rate with chemotherapy, including IFO, was 75%, compared to only 31% with platinum compounds; however, both regimens showed no difference in OS and PFS.[71] Some reported cases suggest that patients achieved favorable outcomes using high-dose etoposide+doxorubicin+IFO (VAI) and cisplatin+doxorubicin+IFO (PAI) as part of the Scandinavian Sarcoma Group IX (SSG IX) protocol for sarcoma.[72,73] For example, a patient with *BRD3::NUT* head-and-neck NUT carcinoma (stage T4bN0M0) achieved partial response (PR) after alternating treatment with VAI and PAI, followed by radiotherapy and a total of 4 cycles of chemotherapy. On resection, no residual cancer was found, indicating a pathological complete response.[72] Another patient with a vast mediastinal mass showed tumor shrinkage after one cycle of EP and the SSG IX regimen, but the tumor progressed again after 1 month.

Despite subsequent treatments with radiotherapy, anlotinib, bevacizumab, paclitaxel chemotherapy, and pembrolizumab immunotherapy, the patient passed away 4.7 months after diagnosis. Among these treatments, only radiotherapy, the EP regimen, and the SSG IX chemotherapy regimen alleviated the patient's pain and temporarily controlled tumor progression.[74] Two pediatric patients with head-and-neck NUT carcinoma maintained tumor remission for at least 6 years and 8 months, respectively, after receiving three cycles of SSG IX chemotherapy regimen, along with surgical resection and radiotherapy.[70] At present, the most effective chemotherapy regimens reported for NUT carcinoma are those related to sarcoma treatment protocols. However, there are relatively few documented cases of effective chemotherapy specifically for NUT carcinoma, warranting further exploration. It is recommended that chemotherapy drugs be selected based on anthracyclines, alkylating agents, and platinum compounds in combination with chemotherapy regimens for other types of malignancies in corresponding anatomical sites of NUT carcinoma. In addition, patients should actively consider high-throughput sequencing to help identify potentially sensitive personalized drug therapy regimens.

At present, no prospective randomized controlled trials demonstrate induction chemotherapy's effectiveness in improving survival outcomes for NUT carcinoma. For operable NUT carcinoma patients undergoing induction chemotherapy, close monitoring of tumor size is necessary to prevent rapid progression and loss of surgical opportunities. For inoperable NUT carcinoma, a comprehensive treatment model combining induction chemotherapy with radiotherapy may be considered. However, no prospective randomized controlled trials have demonstrated that adjuvant chemotherapy improves survival in NUT carcinoma after radiotherapy. Given the high recurrence rate of NUT carcinoma, traditional treatment (surgery, radiotherapy, and chemotherapy) generally only temporarily controls disease progression. It is, therefore, recommended to consider appropriate systemic treatments after concurrent chemoradiotherapy or radiotherapy, depending on factors such as the patient's overall condition. Considering chemotherapy's toxicity, a pre-chemotherapy assessment and consideration of the cumulative chemotherapy dose is necessary to reduce both acute and long-term side effects. Effective chemotherapy regimens for NUT carcinoma remain limited, and clinical trials for rare disease chemotherapy regimens should be prioritized to identify potentially effective first-line treatments.

(a) Recommendation 6

Clinicians may consider selecting chemotherapy drugs primarily based on IFO or platinum-based agents or combining them with chemotherapy regimens used for other types of malignancies in corresponding anatomical sites of NUT carcinoma (level of evidence: level 4; recommendation grade: strongly recommended). High-throughput sequencing can be considered to identify potentially sensitive personalized drug regimens (level of evidence: level 5; recommendation grade: recommended). For inoperable NUT carcinoma, a comprehensive treatment model combining induction chemotherapy with radiotherapy should be considered (level of evidence: level 4; recommendation grade: strongly recommended). Specific chemotherapy regimens should be evaluated based on the patient's condition after concurrent chemoradiotherapy (level of evidence: level 4; recommendation grade: strongly recommended).

4.8.4. Immunotherapy

The NUT carcinoma is driven by the fusion of the NUT oncogenic protein, which is typically associated with a low tumor mutation burden, and the tumor is often insensitive to immunotherapy.[75] Only a subset of NUT carcinoma patients expresses programmed cell death ligand 1 (PD-L1). Aside from a few reported cases, there

are currently no prospective randomized controlled trials that demonstrate the effectiveness of immunotherapy in improving the survival of NUT carcinoma patients. A case report of primary thyroid NUT carcinoma revealed a PD-L1 combined positive score of ≥30, with the patient surviving for 10 months following a combination of chemotherapy and immunotherapy.[57] Some studies have reported cases of thoracic NUT carcinoma patients with high PD-L1 expression who were treated with immunotherapy, leading to significantly prolonged survival. These patients, who also received combined surgery, chemotherapy, and other treatments, survived for over 7.5 years.[76] In contrast, other studies suggest that PD-L1-negative NUT carcinoma patients can experience tumor shrinkage after receiving immune checkpoint inhibitors. While a few patients have shown partial or complete remission, these responses have generally been short-lived, with lesions rapidly relapsing or metastasizing.[77] Moreover, there are cases in which a combination of immunotherapy and oncolytic viruses has relieved both primary and metastatic lesions in patients.[78]

(a) Recommendation 7

For NUT carcinoma patients who are PD-L1/PD-1 positive, it is strongly recommended to consider combined immunotherapy as part of standard anti-tumor treatment. For patients who are PD-L1/PD-1 negative, the decision to use combined therapy should be made based on individual patient preference and circumstances (level of evidence: level 4; recommendation grade: strongly recommended).

4.8.5. Targeted therapy

Early research suggests that BET inhibitors or HDAC inhibitors can induce epithelial differentiation of NUT carcinoma cells and inhibit cell proliferation.[78] This event, along with a deeper understanding of NUT carcinoma's pathogenesis, has spurred the development of targeted therapies, particularly given the limited long-term efficacy of conventional treatments.

Histone deacetylase inhibitors, such as vorinostat, can induce histone acetylation, squamous differentiation, and growth arrest. For example, an 11-year-old patient with *BRD4::NUTM1* fusion salivary gland NUT carcinoma experienced partial remission of both primary and metastatic lesions after undergoing four cycles of chemotherapy (IFO+etoposide) combined with the HDAC inhibitor vorinostat as part of multimodal therapy.[79] While some cases with favorable prognoses have been reported, the evidence on using HDAC inhibitors for NUT carcinoma treatment remains insufficient and requires further investigation.[80,81]

Bromodomain and extra-terminal domain inhibitors work by competing with acetylated histones at bromodomain-chromatin interaction sites and histone tails, disrupting the binding of BRD4 protein to chromatin. This inhibition affects gene transcription during the M and G1 phases, impairs mitosis, induces squamous differentiation, and exerts antiproliferative effects. Non-*BRD4::NUTM1* fusion NUT carcinomas, such as those with *BRD3::NUTM1*, *NSD3::NUTM1*, or *ZNF532::NUTM1* fusions, also rely on BRD4 for oncogenicity, as the NUT fusion partners interact with BRD2, BRD3, and BRD4.[50] This dependency makes BET inhibitors a promising therapeutic option. A statistical analysis of clinical trials involving BET inhibitors revealed tumor control rates ranging from 75% to 87.5%, with the highest control rate observed at 87.5%, notably surpassing the efficacy of chemotherapy.[82-84] In a Phase I study of birabresib (OTX015/MK-8628), the recommended dose of BET inhibitors was 80 mg once daily orally. The response durations ranged from 1.4 to 8.4 months. Among nine NUT carcinoma patients, three showed PRs, three had stable disease (SD), two experienced disease progression (PD), and one was not evaluated (NE). Dose-limiting toxicities included thrombocytopenia and hyperbilirubinemia.[84] In a Phase I clinical trial of RO6870810, administered subcutaneously, eight NUT carcinoma patients showed two PRs, five SDs, and one PD, yielding an objective response rate of 25%. Treatment-related adverse events included fatigue (42%), decreased appetite (35%), and injection site erythema (35%).[82] The Phase I trial of molibresib, which enrolled the largest cohort of NUT carcinoma patients (*N*=19), showed primary adverse events, including thrombocytopenia (51%), gastrointestinal discomfort (e.g., diarrhea, vomiting, nausea, anorexia, and taste disturbances; 22 – 42%), anemia (22%), and fatigue (20%). The recommended dose was 80 mg, and the efficacy assessment revealed 4 PRs (21.1%), 8 SDs (42.1%), 4 PDs (21.1%), and 3 NEs (15.8%).[83] Several clinical trials related to BET inhibitors (e.g., NCT02516553 and NCT03936465) are ongoing, though formal data specific to NUT carcinoma have not been reported. NUT carcinoma has been observed in children and an ongoing Phase I clinical trial is recruiting pediatric patients with solid tumors, brain tumors, and lymphomas to assess the therapeutic effects of BET inhibitors (BMS-986158 and BMS-986378) on pediatric NUT carcinoma.[84] Given the poor prognosis associated with conventional treatments, BET inhibitors are poised to become a crucial option for first-line therapy. However, it is important to note that the blood-brain barrier may impede the entry of BET inhibitors into the brain, which could affect their efficacy in treating brain metastases.[85,86]

Given the poor prognosis of NUT carcinoma and its propensity for recurrence and metastasis, targeted therapies like BET inhibitors demonstrate superior control

rates compared to conventional treatments, offering a new promising therapeutic avenue. Considering the poor prognosis of NUT carcinoma, where most patients have short survival times and are unsuitable for repeat surgery, post-operative recurrent or metastatic patients should prioritize refining high-throughput sequencing to identify sensitive drugs. Given that there are currently no approved targeted therapeutic agents specifically for NUT carcinoma, it is recommended that patients either directly participate in clinical trials involving BET inhibitors, HDAC inhibitors, and other novel therapies, or on disease progression following conventional anti-tumor treatments, patients are encouraged to actively participate in clinical trials involving BET inhibitors, HDAC inhibitors, and other novel therapies.

(a) Recommendation 8

For patients with post-operative recurrence or distant metastasis who are unsuitable for further surgery, apart from optimizing high-throughput sequencing to select sensitive drugs. It is recommended that patients either directly participate in clinical trials involving BET inhibitors, HDAC inhibitors, and other novel therapies, or on disease progression following conventional anti-tumor treatments, patients are encouraged to actively participate in clinical trials involving BET inhibitors, HDAC inhibitors, and other novel therapies (evidence level: grade 3; recommendation level: strongly recommended). In cases of treatment progression, high-throughput sequencing should be refined, suitable drugs should be selected based on the results, and participation in relevant clinical trials should be actively considered (evidence level: grade 5; recommendation level: strongly recommended).

5. Limitations

This study has several limitations. First, high-quality data were not available for some of the topics discussed. Observational studies inherently carry a high risk of incomplete outcome data and selective outcome reporting. Publication bias may also influence researchers to prioritize reporting positive results over negative ones. In case series, selective reporting may lead to an emphasis on successful surgical outcomes. Other potential sources of bias include baseline imbalances, such as population selection in observational studies.

In addition, some relevant articles may have been overlooked. Second, due to the extreme rarity and poor prognosis of NUT carcinoma, physicians often lack sufficient awareness of the disease. Consequently, we aimed to include all available data on NUT carcinoma, but large-scale studies remain scarce. Much of the data analyzed in this review derived from case reports, leading to gaps and non-continuous data. The 199 reviewed papers did not uniformly or comprehensively study and report all relevant indicators, resulting in potential discrepancies in IHC and fusion gene results. These findings must be interpreted within the clinical context. Future large-scale, multi-center studies are required for a more precise investigation.

6. Conclusion

Based on the existing literature and insights from multidisciplinary experts, we have developed an expert consensus on the diagnosis and treatment of NUT carcinoma. This consensus provides comprehensive and practical recommendations for healthcare providers managing NUT carcinoma throughout patient care.

Given the poor prognosis and high invasiveness of NUT carcinoma as a rare tumor, its non-specific features complicate diagnosis, and the overall effectiveness of existing conventional treatment methods remains insufficient. Although the prospects for targeted agents such as BET and HDAC inhibitors are promising, overcoming drug resistance to these agents and selecting the most appropriate treatment combinations still require further exploration. Therefore, focused research on NUT carcinoma patients is essential to enhance our understanding of the disease and improve diagnostic and treatment strategies in the future. Specialized committees have recently been established in various countries.[87-89] For example, the International NUT Carcinoma Registry was established in the United States to record the clinical, genetic, and pathological characteristics and outcomes of NUT carcinoma patients diagnosed since 1993.[18] However, the patients included are predominantly from the American and European populations.

According to the most recent data on population and vital statistics from the United Nations (April 2024),[90] the United States and Europe account for 4.16% (331,449,281/7,975,105,000) and 9.32% (743,556,000/7,975,105,000) of the global population, respectively. In contrast, China and the other Asian countries account for 17.8% (1,419,873,864/7,975,105,000) and 59.2% (4,722,635,000/7,975,105,000) of the total population, respectively. These demographic data indicate a significant potential number of NUT carcinoma cases in China and Asia. In response to these statistics, we established the first specialized center for NUT carcinoma in China in January 2023. In June 2023, the NUT Carcinoma Gene Diagnosis Working Group was established under the Tumor Gene Diagnosis Special Committee of the Chinese Anti-Cancer Association. We initiated a real-world cohort study (NCT06073938) investigating the efficacy of the BET inhibitor (NHWD 870 HCl) for solid

tumors with NUT rearrangement, which began in 2022. From June 2023 to April 2024, we diagnosed and treated 80 cases of NUT carcinoma. However, due to insufficient awareness among most physicians and the high rate of misdiagnoses, the actual number of NUT carcinoma cases could be much higher. To address these issues, we collaborated with multidisciplinary experts from various countries to establish an international platform to increase public awareness and improve the understanding of NUT carcinoma among medical professionals. This platform (http://resource.yin-lab.com/NUT/) provides scientific information about NUT carcinoma and continuously updates all published cases and available cohort data, facilitating better research on this rare disease. Furthermore, it will support the publication of relevant clinical trials on NUT carcinoma in different countries, making it easier for patients to access appropriate clinical trials. With growing awareness and a broader understanding of NUT carcinoma among clinicians, pathologists, radiologists, and cancer researchers, we believe that the diagnosis and treatment of NUT carcinoma can improve, ultimately benefiting more patients in the future.

Acknowledgments

We extend our sincere gratitude to all the experts who contributed to the development of the Expert Consensus on the Diagnosis and Treatment of NUT Cancer and the members who participated in the retrieval, screening, and summarization of clinical evidence. We thank all the guideline development group members for their valuable contributions, particularly the external reviewers who provided insightful comments on the draft guidelines.

Funding

This work was supported in part by the Chongqing Wanzhou Municipal Science and Health Joint Medical Research Project Key Program (grant no. wzstc-kw2023001), the Chongqing Wanzhou PhD "Through Train" Research Project (grant no. Wzstc20230402), and the Chongqing Natural Science Foundation (grant no. CSTB2023NSCQ-MSX0658).

Conflict of interest

Mingzhu Yin and Helmut H. Popper are the Editors-in-Chief and Xin Li, Paolo Boffano, Steven Brower, Xinpei Deng, Nejat Duzgunes, Pierfrancesco Franco, Weilin Jin, Kalevi Kairemo, Mohamed Kamal, Evan T. Keller, Mikael S. Lindström, Yanqing Liu, Jose Manuel Lopes, Wenping Ma, Amancio Carnero Moya, Athanasios G. Papavassiliou, Axel Schonthal, Vishal Shelat, Alexander Shtil, Hifzur R Siddique, Shaoquan Zheng, and Qin Yan are Editorial Board Member of this journal. However, none of these individuals were involved in this paper's editorial or peer-review process, either directly or indirectly. In addition, the other authors declare that they have no known competing financial interests or personal relationships that could have influenced the work reported in this paper.

Author contributions

Conceptualization: Zhuomiao Ye, Xin Li
Writing – original draft: Zhuomiao Ye, Xiangwen Luo, Xin Li, Minghui Zhang
Writing – review & editing: All authors

Ethics approval and consent to participate

Not applicable.

Consent for publication

Not applicable.

Availability of data

The data supporting the findings of this study are available from the corresponding author on reasonable request. Some data may not be made available due to privacy or ethical restrictions.

References

1. Lemelle L, Flaadt T, Fresneau B, *et al*. NUT carcinoma in children and adolescents: The expert European standard clinical practice harmonized recommendations. *J Pediatr Hematol Oncol*. 2023;45(4):165-173.

   doi: 10.1097/MPH.0000000000002568

2. Luo W, Stevens TM, Stafford P, Miettinen M, Gatalica Z, Vranic S. NUTM1-rearranged neoplasms-a heterogeneous group of primitive tumors with expanding spectrum of histology and molecular alterations-an updated review. *Curr Oncol*. 2021;28(6):4485-4503.

   doi: 10.3390/curroncol28060381

3. Kees UR, Mulcahy MT, Willoughby ML. Intrathoracic carcinoma in an 11-year-old girl showing a translocation t(15;19). *Am J Pediatr Hematol Oncol*. 1991;13(4):459-464.

   doi: 10.1097/00043426-199124000-00011

4. Kubonishi I, Takehara N, Iwata J, *et al*. Novel t(15;19)(q15;p13) chromosome abnormality in a thymic carcinoma. *Cancer Res*. 1991;51(12):3327-3328.

5. Travis WD, Brambilla E, Nicholson AG, *et al*. The 2015 World Health Organization classification of lung tumors: Impact of genetic, clinical and radiologic advances since the 2004 classification. *J Thorac Oncol*. 2015;10(9):1243-1260.

   doi: 10.1097/JTO.0000000000000630

6. French CA, Kutok JL, Faquin WC, *et al*. Midline carcinoma

of children and young adults with NUT rearrangement. *J Clin Oncol*. 2004;22(20):4135-4139.

doi: 10.1200/JCO.2004.02.107

7. Shehata BM, Steelman CK, Abramowsky CR, *et al*. NUT midline carcinoma in a newborn with multiorgan disseminated tumor and a 2-year-old with a pancreatic/hepatic primary. *Pediatr Dev Pathol*. 2010;13(6):481-485.

doi: 10.2350/09-10-0727-CR.1

8. Dickson BC, Sung YS, Rosenblum MK, *et al*. NUTM1 gene fusions characterize a subset of undifferentiated soft tissue and visceral tumors. *Am J Surg Pathol*. 2018;42(5):636-645.

doi: 10.1097/PAS.0000000000001021

9. Mertens F, Wiebe T, Adlercreutz C, Mandahl N, French CA. Successful treatment of a child with t(15;19)-positive tumor. *Pediatr Blood Cancer*. 2007;49(7):1015-1017.

doi: 10.1002/pbc.20755

10. Yuan J, Xu Z, Guo Y. Diagnosis, treatment and prognosis of primary pulmonary NUT carcinoma: A literature review. *Curr Oncol*. 2022;29(10):6807-6815.

doi: 10.3390/curroncol29100536

11. Ribeiro da Costa AEA, Santos IL, Pereira Soares MJA, Reis de Paula ID, da Silva Júnior RG, Coelho de Sá CE. A case of metastatic NUT carcinoma of the nasal cavity. *Oral Oncol*. 2023;142:106432.

doi: 10.1016/j.oraloncology.2023.106432

12. Jimenez C, Stanton E, Kondra K, *et al*. NUT carcinoma of the mandible in a child: Case report and systematic review. *Int J Oral Maxillofac Surg*. 2023;52(3):304-312.

doi: 10.1016/j.ijom.2022.07.002

13. Ribeiro JA, Sousa J, Jesus F, *et al*. NUT carcinoma - An aggressive thoracic tumor. *Am J Med Sci*. 2023;366(1):64-70.

doi: 10.1016/j.amjms.2023.03.028

14. Saiki A, Sakamoto K, Bee Y, Izumo T. Nuclear protein of the testis midline carcinoma of the thorax. *Jpn J Clin Oncol*. 2022;52(6):531-538.

doi: 10.1093/jjco/hyac033

15. Lemelle L, Pierron G, Freneaux P, *et al*. NUT carcinoma in children and adults: A multicenter retrospective study. *Pediatr Blood Cancer*. 2017;64(12):e26693.

doi: 10.1002/pbc.26693

16. Yang SM, Zhang B. The research advances of neoplasm with NUTM1 gene rearrangement. *Zhonghua Bing Li Xue Za Zhi*. 2022;51(3):271-275.

doi: 10.3760/cma.j.cn112151-20211123-00853

17. French CA. Pathogenesis of NUT midline carcinoma. *Annu Rev Pathol*. 2012;7:247-265.

doi: 10.1146/annurev-pathol-011811-132438

18. Chau NG, Ma C, Danga K, *et al*. An anatomical site and genetic-based prognostic model for patients with Nuclear Protein in Testis (NUT) midline carcinoma: Analysis of 124 patients. *JNCI Cancer Spectr*. 2020;4(2):pkz94.

doi: 10.1093/jncics/pkz094

19. Scherman N, Wassermann J, Tlemsani C, *et al*. Possible primary thyroid nuclear protein in testis carcinomas with NSD3:NUTM1 translocation revealed by RNA sequencing: A report of two cases. *Thyroid*. 2022;32(10):1271-1276.

doi: 10.1089/thy.2022.0136

20. Napolitano M, Venturelli M, Molinaro E, Toss A. NUT midline carcinoma of the head and neck: Current perspectives. *Onco Targets Ther*. 2019;12:3235-3244.

doi: 10.2147/OTT.S173056

21. Tontsch-Grunt U, Traexler PE, Baum A, *et al*. Therapeutic impact of BET inhibitor BI 894999 treatment: Backtranslation from the clinic. *Br J Cancer*. 2022;127(3):577-586.

doi: 10.1038/s41416-022-01815-5

22. Yu D, Liang Y, Kim C, *et al*. Structural mechanism of BRD4-NUT and p300 bipartite interaction in propagating aberrant gene transcription in chromatin in NUT carcinoma. *Nat Commun*. 2023;14(1):378.

doi: 10.1038/s41467-023-36063-5

23. World Health Organization. *WHO Handbook for Guideline Development* [*EB/OL*]. 2nd ed. Geneva, Switzerland: World Health Organization. Available from: https://www.who.int/groups/guidelines-reviewcommittee [Last accessed on 2024 Apr 03].

24. Brouwers MC, Kho ME, Browman GP, *et al*. AGREE II: Advancing guideline development, reporting and evaluation in health care. *CMAJ*. 2010;182(18):E839-E842.

doi: 10.1503/cmaj.090449

25. Chen Y, Yang K, Marusic A, *et al*. A reporting tool for practice guidelines in health care: The RIGHT statement. *Ann Intern Med*. 2017;166(2):128-132.

doi: 10.7326/M16-1565

26. World Health Organization. *International Practice Guideline Registry Platform* [*EB/OL*]. Geneva, Switzerland: World Health Organization. Available from: https://www.guidelines-registry.cn/guid/2939 [Last accessed on 2024 Apr 01].

27. Wang X, Chen Y, Yao L, *et al*. Reporting of declarations and conflicts of interest in WHO guidelines can be further improved. *J Clin Epidemiol*. 2018;98:1-8.

doi: 10.1016/j.jclinepi.2017.12.021

28. Lemelle L, Moya-Plana A, Dumont B, *et al*. NUT carcinoma in children, adolescents and young adults. *Bull Cancer*. 2022;109(4):491-504.

doi: 10.1016/j.bulcan.2022.01.015

29. Charlab R, Racz R. The expanding universe of $NUTM_1$ fusions in pediatric cancer. *Clin Transl Sci*. 2023;16(8):1331-1339.

doi: 10.1111/cts.13535

30. Bauer DE, Mitchell CM, Strait KM, *et al*. Clinicopathologic features and long-term outcomes of NUT midline carcinoma. *Clin Cancer Res*. 2012;18(20):5773-5779.

doi: 10.1158/1078-0432.CCR-12-1153

31. Virarkar M, Mallery M, Saleh M, Ramani NS, Morani AC, Bhosale P. Clinical, radiographic, pathologic characterization and survival outcomes of nuclear protein of the testis carcinoma. *J Comput Assist Tomogr*. 2021;45(3):431-441.

doi: 10.1097/RCT.0000000000001163

32. Polsani A, Braithwaite KA, Alazraki AL, Abramowsky C, Shehata BM. NUT midline carcinoma: An imaging case series and review of literature. *Pediatr Radiol*. 2012;42(2):205-210.

doi: 10.1007/s00247-011-2272-3

33. Lantuejoul S, Pissaloux D, Ferretti GR, McLeer A. NUT carcinoma of the lung. *Semin Diagn Pathol*. 2021;38(5):72-82.

doi: 10.1053/j.semdp.2021.06.005

34. Nelson BA, Lee EY, French CA, Bauer DE, Vargas SO. BRD4-NUT carcinoma of the mediastinum in a pediatric patient: Multidetector computed tomography imaging findings. *J Thorac Imaging*. 2010;25(3):W93-W96.

doi: 10.1097/RTI.0b013e3181b5d84d

35. Teo M, Crotty P, O'Sullivan M, French CA, Walshe JM. NUT midline carcinoma in a young woman. *J Clin Oncol*. 2011;29(12):e336-e339.

doi: 10.1200/JCO.2010.32.7486

36. Orman G, Masand P, Hicks J, Huisman TAGM, Guillerman RP. Pediatric thoracic mass lesions: Beyond the common. *Eur J Radiol Open*. 2020;7:100240.

doi: 10.1016/j.ejro.2020.100240

37. Chen J, Li M, Lu H. Nuclear protein in testis carcinoma of the lung. *Transl Oncol*. 2023;30:101640.

doi: 10.1016/j.tranon.2023.101640

38. Chang AI, Kim TS, Han J, Kim TJ, Choi JY. NUT midline carcinoma of the lung: Computed tomography findings in 10 patients. *J Comput Assist Tomogr*. 2021;45(2):330-336.

doi: 10.1097/RCT.0000000000001133

39. Huang W, Zhang Y, Yang Q, *et al*. Clinical imaging of primary pulmonary nucleoprotein of the testis carcinoma. *Front Med* (*Lausanne*). 2022;9:1083206.

doi: 10.3389/fmed.2022.1083206

40. Davila D, Antoniou A, Chaudhry MA. Evaluation of osseous metastasis in bone scintigraphy. *Semin Nucl Med*. 2015;45(1):3-15.

doi: 10.1053/j.semnuclmed.2014.07.004

41. Gasljevic G, Matter MS, Blatnik O, Unk M, Dirnhofer S. NUT carcinoma: A clinical, morphological and immunohistochemical mimicker-the role of RNA sequencing in the diagnostic procedure. *Int J Surg Pathol*. 2022;30(3):273-277.

doi: 10.1177/10668969211047981

42. Moreno V, Saluja K, Pina-Oviedo S. NUT carcinoma: Clinicopathologic features, molecular genetics and epigenetics. *Front Oncol*. 2022;12:860830.

doi: 10.3389/fonc.2022.860830

43. French CA. NUT carcinoma: Clinicopathologic features, pathogenesis, and treatment. *Pathol Int*. 2018;68(11):583-595.

doi: 10.1111/pin.12727

44. Allison DB, Rueckert J, Cornea V, Lee CY, Dueber J, Bocklage T. Thyroid carcinoma with NSD3::NUTM1 fusion: A Case with thyrocyte differentiation and colloid production. *Endocr Pathol*. 2022;33(2):315-326.

doi: 10.1007/s12022-021-09700-2

45. Haack H, Johnson LA, Fry CJ, *et al*. Diagnosis of NUT midline carcinoma using a NUT-specific monoclonal antibody. *Am J Surg Pathol*. 2009;33(7):984-991.

doi: 10.1097/PAS.0b013e318198d666

46. McEvoy CR, Fox SB, Prall O. Emerging entities in NUTM1-rearranged neoplasms. *Genes Chromosomes Cancer*. 2020;59(6):375-385.

doi: 10.1002/gcc.22838

47. French CA, Cheng ML, Hanna GJ, *et al*. Report of the first international symposium on NUT carcinoma. *Clin Cancer Res*. 2022;28(12):2493-2505.

doi: 10.1158/1078-0432.CCR-22-0591

48. Huang Y, Durall RT, Luong NM, *et al*. EZH2 synergizes with BRD4-NUT to drive NUT carcinoma growth through silencing of key tumor suppressor genes. bioRxiv [Preprint]. 2023.

doi: 10.1101/2023.08.15.553204

49. Barletta JA, Gilday SD, Afkhami M, *et al*. NUTM1 -rearranged carcinoma of the thyroid: A distinct subset of NUT carcinoma characterized by frequent NSD3 - NUTM1 fusions. *Am J Surg Pathol*. 2022;46(12):1706-1715.

doi: 10.1097/PAS.0000000000001967

50. Alekseyenko AA, Walsh EM, Zee BM, *et al*. Ectopic protein interactions within BRD_4-chromatin complexes drive oncogenic megadomain formation in NUT midline carcinoma. *Proc Natl Acad Sci U S A*. 2017;114(21):E4184-E4192.

doi: 10.1073/pnas.1702086114

51. Bouchard C, Dittrich O, Kiermaier A, *et al*. Regulation of cyclin D2 gene expression by the Myc/Max/Mad network: Myc-dependent TRRAP recruitment and histone acetylation at the cyclin D2 promoter. *Genes Dev*. 2001;15(16):2042-2047.

doi: 10.1101/gad.907901

52. Yang A, Kaghad M, Wang Y, *et al*. p63, a p53 homolog at 3q27-29, encodes multiple products with transactivating, death-inducing, and dominant-negative activities. *Mol Cell*. 1998;2(3):305-316.

doi: 10.1016/s1097-2765(00)80275-0

53. Durall RT, Huang J, Wojenski L, *et al*. The BRD4-NUT fusion alone drives malignant transformation of NUT carcinoma. *Cancer Res*. 2023;83(23):3846-3860.

doi: 10.1158/0008-5472.CAN-23-2545

54. McEvoy CR, Holliday H, Thio N, *et al*. A MXI1-NUTM1 fusion protein with MYC-like activity suggests a novel oncogenic mechanism in a subset of NUTM1-rearranged tumors. *Lab Invest*. 2021;101(1):26-37.

doi: 10.1038/s41374-020-00484-3

55. Boer JM, Valsecchi MG, Hormann FM, et al. Favorable outcome of $NUTM_1$-rearranged infant and pediatric B cell precursor acute lymphoblastic leukemia in a collaborative international study. *Leukemia*. 2021;35(10):2978-2982.

doi: 10.1038/s41375-021-01333-y

56. Chau NG, Hurwitz S, Mitchell CM, *et al*. Intensive treatment and survival outcomes in NUT midline carcinoma of the head and neck. *Cancer*. 2016;122(23):3632-3640.

doi: 10.1002/cncr.30242

57. Zhou J, Duan M, Jiao Q, *et al*. Primary thyroid NUT carcinoma with high PD-L1 expression and novel massive IGKV gene fusions: A case report with treatment implications and literature review. *Front Oncol*. 2021;11:778296.

doi: 10.3389/fonc.2021.778296

58. Carter T, Crook M, Murch A, *et al*. Incidence of NUT carcinoma in Western Australia from 1989 to 2014: A review of pediatric and adolescent cases from perth children's hospital. *BMC Cancer*. 2021;21(1):740.

doi: 10.1186/s12885-021-08432-0

59. Costa BA, Maraveyas A, Wilkoff MH, *et al*. Primary pulmonary NUT carcinoma: Case illustration and updated review of literature. *Clin Lung Cancer*. 2022;23(4):e296-e300.

doi: 10.1016/j.cllc.2022.03.001

60. Li W, Chastain K. NUT midline carcinoma with leukemic presentation mimicking CD34-positive acute leukemia. *Blood*. 2018;132(4):456.

doi: 10.1182/blood-2017-07-796268

61. Prall O, Thio N, Yerneni S, Kumar B, McEvoy CR. A NUT carcinoma lacking squamous differentiation and expressing TTF1. *Pathology*. 2021;53(5):663-666.

doi: 10.1016/j.pathol.2020.09.027

62. Yang F, Shen D, Shi J. Primary renal NUT carcinoma identified by next-generation sequencing: A case report and literature review. *Int J Clin Exp Pathol*. 2021;14(5):662-669.

63. Alcasid NJ, Banks KC, Sun A, Velotta JB. Case report on the role of aggressive palliative surgery in lung NUT carcinoma after induction chemoimmunotherapy. *Int J Surg Case Rep*. 2023;105:108015.

doi: 10.1016/j.ijscr.2023.108015

64. Giridhar P, Mallick S, Kashyap L, Rath GK. Patterns of care and impact of prognostic factors in the outcome of NUT midline carcinoma: A systematic review and individual patient data analysis of 119 cases. *Eur Arch Otorhinolaryngol*. 2018;275(3):815-821.

doi: 10.1007/s00405-018-4882-y

65. Huang WP, Gao G, Qiu YK, *et al*. Multimodality imaging and treatment of paranasal sinuses nuclear protein in testis carcinoma: A case report. *World J Clin Cases*. 2022;10(33):12395-12403.

doi: 10.12998/wjcc.v10.i33.12395

66. Higashino M, Kinoshita I, Kurisu Y, *et al*. Supraglottic NUT carcinoma: A case report and literature review. *Case Rep Oncol*. 2022;15(3):980-987.

doi: 10.1159/000526815

67. Jiang J, Ren Y, Xu C, Liu X. NUT midline carcinoma as a primary lung tumor treated with anlotinib combined with palliative radiotherapy: A case report. *Diagn Pathol*. 2022;17(1):4.

doi: 10.1186/s13000-021-01188-y

68. Muramatsu J, Takada K, Sugita S, *et al*. Complete response induced by concurrent chemoradiotherapy in a patient with NUT carcinoma. *Intern Med*. 2022;61(8):1299-1304.

doi: 10.2169/internalmedicine.7741-21

69. Sopfe J, Greffe B, Treece AL. Metastatic NUT midline carcinoma treated with aggressive neoadjuvant chemotherapy, radiation, and resection: A case report and review of the literature. *J Pediatr Hematol Oncol*. 2021;43(1):e73-e75.

doi: 10.1097/MPH.0000000000001860

70. Vulsteke C, Lurquin E, Debiec-Rychter M, *et al*. First evidence of treatment efficacy in metastatic carcinoma of the parotid gland with BRD_4/NUT translocation. *J Chemother*. 2016;28(3):242-246.

doi: 10.1179/1973947815Y.0000000046

71. Luo J, Sanchez M, Lee E, *et al*. Initial chemotherapy for locally advanced and metastatic NUT carcinoma. *J Thorac Oncol*. 2023;19:829-838.

doi: 10.1016/j.jtho.2023.12.022

72. Storck S, Kennedy AL, Marcus KJ, *et al*. Pediatric NUT-midline carcinoma: Therapeutic success employing a sarcoma based multimodal approach. *Pediatr Hematol Oncol*. 2017;34(4):231-237.

doi: 10.1080/08880018.2017.1363839

73. Vorstenbosch LJMJ, Mavinkurve-Groothuis AMC, van den Broek G, Flucke U, Janssens GO. Long-term survival after relapsed NUT carcinoma of the larynx. *Pediatr Blood Cancer*. 2018;65(5):e26946.

doi: 10.1002/pbc.26946

74. Leeman R, Pinkney K, Bradley JA, *et al*. NUT carcinoma without upfront surgical resection: A case report. *J Pediatr Hematol Oncol*. 2021;43(5):e707-e710.

doi: 10.1097/MPH.0000000000001865

75. Lee JK, Louzada S, An Y, *et al*. Complex chromosomal rearrangements by single catastrophic pathogenesis in NUT midline carcinoma. *Ann Oncol*. 2017;28(4):890-897.

doi: 10.1093/annonc/mdw686

76. Davis A, Mahar A, Wong K, Barnet M, Kao S. Prolonged disease control on nivolumab for primary pulmonary NUT carcinoma. *Clin Lung Cancer*. 2021;22(5):e665-e667.

doi: 10.1016/j.cllc.2020.10.016

77. Li X, Shi H, Zhang W, *et al*. Immunotherapy and targeting the tumor microenvironment: Current place and new insights in primary pulmonary NUT carcinoma. *Front Oncol*. 2021;11:690115.

doi: 10.3389/fonc.2021.690115

78. Kloker LD, Calukovic B, Benzler K, *et al*. Case report: Immunovirotherapy as a novel add-on treatment in a patient with thoracic NUT carcinoma. *Front Oncol*. 2022;12:995744.

doi: 10.3389/fonc.2022.995744

79. Wang H, Weiss VL, Hoffman RD, *et al*. Salivary gland NUT carcinoma with prolonged survival in children: Case illustration and systematic review of literature. *Head Neck Pathol*. 2021;15(1):236-243.

doi: 10.1007/s12105-020-01141-3

80. Esteves G, Ferreira J, Afonso R, Martins C, Zagalo C, Félix A. HDAC overexpression in a NUT midline carcinoma of the parotid gland with exceptional survival: A case report. *Head Neck Pathol*. 2020;14(4):1117-1122.

doi: 10.1007/s12105-020-01130-6

81. Gov. C. *Open Label, Multi-center Study to Assess the Safety, Tolerability and Pharmacokinetics of CUDC-907 in Subjects With Advanced Relapsed Solid Tumors* [*EB/OL*]; 2019. Available from: https://clinicaltrials.gov/study/nct02307240?cond=cudc-907&rank=2 [Last accessed on 2023 Sep 22].

82. Shapiro GI, LoRusso P, Dowlati A, *et al*. A phase 1 study of RO6870810, a novel bromodomain and extra-terminal protein inhibitor, in patients with NUT carcinoma, other solid tumours, or diffuse large B-cell lymphoma. *Br J Cancer*. 2021;124(4):744-753.

doi: 10.1038/s41416-020-01180-1

83. Piha-Paul SA, Hann CL, French CA, *et al*. Phase 1 study of molibresib (GSK525762), a bromodomain and extra-terminal domain protein inhibitor, in NUT carcinoma and other solid tumors. *JNCI Cancer Spectr*. 2020;4(2):pkz93.

doi: 10.1093/jncics/pkz093

84. Lewin J, Soria JC, Stathis A, *et al*. Phase Ib trial with birabresib, a small-molecule inhibitor of bromodomain and extraterminal proteins, in patients with selected advanced solid tumors. *J Clin Oncol*. 2018;36(30):3007-3014.

doi: 10.1200/JCO.2018.78.2292

85. Baneckova M, Cox D. Top 10 basaloid neoplasms of the sinonasal tract. *Head Neck Pathol*. 2023;17(1):16-32.

doi: 10.1007/s12105-022-01508-8

86. French CA. Small-molecule targeting of BET proteins in cancer. *Adv Cancer Res*. 2016;131:21-58.

doi: 10.1016/bs.acr.2016.04.001

87. Reguerre Y, Lacour B, Andre N, *et al*. Epidemiology and management of rare paediatric tumours within the framework of the French Society for Children Cancer. *Bull Cancer*. 2010;97(9):1041-1045.

doi: 10.1684/bdc.2010.1169

88. Bisogno G, Ferrari A, Bien E, *et al*. Rare cancers in children - The EXPeRT initiative: A report from the European cooperative study group on pediatric rare tumors. *Klin Padiatr*. 2012;224(6):416-420.

doi: 10.1055/s-0032-1327608

89. Xin L, Zhuomiao Y. Expert consensus on the diagnosis and treatment of midline (NUT) cancer (2023 Edition). *Chin J Oncol Prev Treat*. 2023;15(5):463-476.

90. United Nations Statistics Division. *Population and Vital Statistics Report*. United Nations Statistics Division; 2024. Available from: https://unstats.un.org/unsd/demographic-social/products/vitstats/[EB/OL] [Last accessed on 2024 Apr 15].

ACCSCIENCE PUBLISHING

Tumor Discovery

REVIEW ARTICLE

Hypoxia-inducible factor-1α inhibition in renal cell carcinoma

Kinsey Morey[1], Santosh Nimkar[1], and Samir Dalia[2]*

[1]College of Osteopathic Medicine, Joplin Campus, Kansas City University, Joplin, Missouri, United States of America

[2]Department of Medical Oncology, Mercy Hospital, Joplin, Missouri, United States of America

Abstract

The tumorigenesis of clear cell renal cell carcinoma (ccRCC), an aggressive variant of renal cell carcinoma (RCC), is primarily attributable to the mutational inactivation of the Von Hippel–Lindau (VHL) gene. This mutation causes VHL syndrome, which is associated with tumor growth in various body parts, including the brain, spinal cord, eyes, adrenal glands, pancreas, kidney, and reproductive tract. RCC is the leading cause of death in patients with VHL syndrome. The VHL gene acts as a tumor suppressor that prevents the proliferation of various oncogenes by controlling the hypoxia-inducible factor (HIF). The HIF pathway is directly linked to the control of metabolic adaptation, cell proliferation, migration, angiogenesis, and apoptosis, which, in turn, is linked to ccRCC tumorigenesis. Consequently, many treatments have been developed to directly or indirectly inhibit HIF1α. Direct inhibition of HIF-1α was briefly explored but has not yet resulted in any treatment strategy approved by the Food and Drug Administration. Most prevalent are the indirect inhibitors targeting vascular endothelial growth factor receptors (VEGFR), the mammalian target of rapamycin (mTOR), and heat shock protein 90 (Hsp90). The VEGFR inhibitor category has the most FDA-approved drugs as they have been proven to be the most efficacious and safe early on. Thus, VEGFR inhibitors, along with mTOR inhibitors, have become the mainstay in RCC treatment. Most recently, therapies targeting HIF-2α inhibition have gained traction with FDA approval, whereas emerging therapies targeting direct inhibition of hsp90 have shown promise.

Keywords: Renal cell carcinoma; HIF-1α; HIF-2α; HIF-1α inhibitor; HIF-2α inhibitor; VEGF inhibitor; mTOR inhibitor

***Corresponding author:**
Samir Dalia
(samir.dalia@mercy.net)

Citation: Morey K, Nimkar S, Dalia S. Hypoxia-inducible factor-1α inhibition in renal cell carcinoma. *Tumor Discov*. 2024;3(4):4346. doi: 10.36922/td.4346

Received: July 27, 2024

Accepted: September 10, 2024

Published Online: October 8, 2024

1. Introduction

Renal cell carcinoma (RCC) originates from the kidney epithelium and constitutes approximately 2% of all cancers worldwide. Common risk factors include smoking, obesity, and hypertension (HTN), with approximately 2% being hereditary. The classic triad of RCC symptoms includes hematuria, abdominal pain, and a palpable mass, but most cases remain asymptomatic until advanced stages. Over 50% of RCCs are discovered incidentally, and 20 – 30% are metastatic at diagnosis. Metastases commonly occur in the lungs, bones, liver, and brain. Primary treatment is surgical resection, followed by medical therapy for locally advanced or metastatic disease as recurrence can

occur in 2 – 5% of patients without adjuvant treatment. Treatment can be challenging due to the poor response to chemotherapy and frequent recurrence.[1-3]

There are five types of RCCs: clear cell, chromophilic (papillary), chromophobic, oncocytic, and collecting duct. Clear cell RCC (ccRCC) is the most common, accounting for 75 – 85% of all RCCs.[3,4] Defects in the Von Hippel–Lindau (VHL) gene account for 60% of sporadic ccRCC cases. VHL is a tumor suppressor gene that regulates hypoxia-inducible genes (vascular endothelial growth factor [VEGF], transforming growth factor-alpha, and GLUT1) by controlling hypoxia-inducible factor (HIF).[2] HIF is a heterodimer that comprises alpha and beta subunits. HIF- is constitutively expressed, and unlike the alpha subunit, its expression is not influenced by oxygen levels in the cellular environment. In normoxic conditions, HIF-α is hydroxylated and acetylated for recognition by VHL. Once bound to VHL, HIF-α is ubiquitinated and targeted for proteasomal degradation, thus preventing the transcription of hypoxia-inducible genes. Under hypoxic conditions, the oxygen-dependent degradation domain senses the oxygen levels and interacts with the NH2-terminal transactivation domain to stabilize HIF-α; this prevents its recognition by VHL and subsequent degradation. Stabilized HIF-α translocates to the nucleus, dimerizes with HIF-β, and initiates gene transcription. The COOH-terminal transactivation domain binds co-activators to modulate HIF-α gene transcription. The HIF pathway regulates metabolic adaptation, cell proliferation, migration, angiogenesis, and apoptosis.[5,6] Loss of VHL results in the constitutive expression of HIF-α, which then leads to the overexpression of hypoxia-inducible genes and proliferation of epithelial cells.[2] HIF-α is encoded by three genes: HIF1-α, HIF2-α, and HIF3-α. HIF1-α and HIF2-α both respond to hypoxia and contribute to tumorigenesis when the HIF pathway is uncontrolled. The role of HIF3-α is less understood.[7]

VHL syndrome is an autosomal dominant familial cancer syndrome that is caused by mutations in the VHL gene on chromosome 3p.[3] This disorder occurs in 1/36,000 – 45,000 live births. Common manifestations of the disease include retinal and central nervous system (CNS) hemangiomas, ccRCC, pheochromocytomas, pancreatic neuroendocrine tumors, and endolymphatic sac tumors. Further, this syndrome can be diagnosed using one of the following three criteria: (1) the presence of at least two CNS/retinal hemangioblastomas; (2) the presence of at least one CNS/retinal hemangioblastoma and one other manifestation; or (3) at least one manifestation and a pathogenic mutation in the VHL gene or a first-degree relative with VHL syndrome. DNA sequencing and Southern blotting techniques can be used on peripheral leukocytes to detect VHL gene mutations. The disease usually manifests in patients in their 20s, with 95% of patients presenting with symptoms by the age of 34. The most common initial symptom is cerebellar hemangioblastomas, occurring in 35% of cases. RCC is rarely the first symptom, with only 7% of cases presenting RCC initially.[8] Genotype-phenotype correlations in VHL syndrome create subtypes based on the type of mutation in the VHL gene and disease features. Types 1A and 2B are associated with a higher incidence of RCC than the other types. In these cases, somatic inactivation of the VHL gene is the second requirement before progressing to malignancy.[9] RCC and renal cysts develop bilaterally and typically appear in patients in their 30s and 40s. By the age of 60, 70% of patients with VHL syndrome develop RCC. Hemangiomas and RCC are the leading causes of death in patients with VHL syndrome.[8]

RCC is highly vascularized tumors, tumors, primarily due to VHL mutations that activate the HIF pathway, leading to hyperactive angiogenesis.[10] These tumors exhibit elevated levels of HIF1-α. ccRCC shows the highest nuclear accumulation of HIF1-α among RCC types.[11] VHL gene mutations on chromosome 3p are present in over 80% of ccRCC cases, and more than 90% of all RCCs have a mutated or inactivated VHL gene. ccRCC is the most aggressive RCC subtype, and elevated HIF1-αα levels are linked to a poorer prognosis.[4,12] A study examining the correlation between HIF1-α levels and disease severity found that higher HIF1-α levels are linked to renal pelvis invasion, renal capsule rupture, and renal hilar invasion, along with increased nodal involvement. Patients with these characteristics had a worse prognosis and were more challenging to treat.[10] Another study investigated the survival of patients with RCC based on their HIF1-α expression levels. It was found that the median survival of those with high HIF1-α expression (>35%) was 13.5 months compared to 24.4 months for those with low HIF1-α expression (<35%).[11] In a study by Xu *et al*., downregulation of HIF1-α *in vitro* inhibited RCC cell growth, migration, and invasion, and induced caspase-dependent apoptosis. *In vivo* animal studies with downregulated HIF1-α RCC cell lines showed significant suppression of RCC cell proliferation, migration, and invasion under both normoxic and hypoxic conditions.[13] Overexpression of HIF1-α is associated with more aggressive biological behavior and reduced overall survival (OS).[14]

There are various treatments for RCC due to its poor response to traditional chemotherapy and its tendency to develop resistance. Inhibiting the HIF pathway has

garnered significant attention for its promising results in treating RCC and other cancers. The primary focus of these studies is on inhibiting the accumulation of HIF1-α or its downstream products. Direct HIF1-α inhibitors target the expression or function of HIF molecules by inhibiting mRNA expression, HIF protein synthesis, dimerization of the alpha and beta subunits, DNA binding with HIF, and HIF's transcriptional activities. Indirect HIF1-α inhibitors regulate molecules in the upstream or downstream pathways affecting HIF.[15] HIF2-α is another therapeutic target for RCC. Overexpression of HIF2-α promotes angiogenesis and tumor invasion, similar to HIF1-α, but complete loss of HIF2-α can also contribute to oncogenesis. Therefore, direct inhibitors of HIF2-α, which reduce its cellular concentration, are an appealing treatment for RCC. At present, HIF2-α inhibitors are used only in patients with VHL syndrome but show promise as an effective treatment for sporadic RCC.[7]

2. Methods

The initial search for articles was conducted through Google Scholar and PubMed using the keywords "Renal Cell Carcinoma," "RCC," "ccRCC," "HIF1-α," "HIF1-α inhibitor," "hypoxia-inducible factor," "VEGF inhibitor," and "VHL gene." Studies on drugs that inhibited HIF1-α and HIF2-α directly or indirectly and those on RCC were included in the study. The selected studies were further narrowed down to include studies on the treatment of locally advanced or metastatic RCC. Studies on HIF1-α inhibitors not targeting RCC, those conducted >2 years before FDA approval, and those not in English were excluded from the study.

3. Results

3.1. Direct HIF1-α inhibitors

Direct inhibition of HIF1-α impacts the expression or function of HIF molecules and is a less common therapeutic approach due to the numerous pathways controlled by HIF. At present, these therapies are not FDA-approved for RCC treatment, but several studies have investigated these drugs in combination with other approved treatments. These studies have shown promising results and could potentially be highly effective against RCC.[15,16]

3.2. VEGF inhibitors

The most commonly targeted molecules for treatment are the upstream and downstream components of the HIF pathway that can indirectly inhibit HIF1-α.[15] VEGF and VEGF receptor inhibitors are commonly used as targets for RCC treatment due to its the highly vascularized nature of these tumors. At present, there are eight FDA-approved RCC treatments in this category. The first drug in this category to receive FDA approval was sorafenib in 2005. Sorafenib is a tyrosine kinase inhibitor (TKI) of the VEGF receptor (VEGFR) that has been shown to delay progression and help preserve the patient's quality of life. In a trial study, sorafenib resulted in an OS that was 3.4 months longer than the placebo and an overall response that was 8% higher in patients with advanced RCC. Adverse events (AE) occurred in 13% of the patients, necessitating dose reduction. Some common AEs and toxicities of sorafenib include diarrhea (43%), rash (40%), hand-foot syndrome (30%), and HTN (17%).[17-19] The next drug to receive FDA approval was sunitinib in 2006, another VEGFR inhibitor similar to sorafenib, that replaced interferon-alpha (IFN-α) as the standard of care for RCC treatment. Compared with IFN-α, which has an average progression-free survival (PFS) of 5 months, sunitinib has an average PFS of 11 months. In patients with advanced RCC, sunitinib had an overall response rate that was 25% higher than IFN-α.[20-22] Patients receiving this therapy commonly presented with thrombocytopenia, leukopenia, neutropenia, fatigue, diarrhea, vomiting, and HTN. Considering the AEs and toxicities, 32% of the patients receiving sunitinib required dose reduction, and 38% needed a break in treatment.[23] Bevacizumab, an anti-VEGF antibody that targets and inhibits VEGFRs, was approved by the FDA in 2009. Compared with IFN-α alone, bevacizumab in combination with IFN-α had a longer PFS (10.2 vs. 5.4 months) and higher objective tumor response rates (31% vs. 13%).[17,24] Common Grade 3 or 4 AEs for bevacizumab include fatigue (35%), anorexia (17%), proteinuria (13%), and HTN (9%).[25] In 2009, pazopanib, a VEGFR inhibitor, was approved by the FDA for the treatment of metastatic RCC.[26] Compared with sunitinib, pazopanib had a longer PFS (9.8 vs. 4.3 months) and OS (14.4 vs. 8.9 months) but had a higher rate of treatment discontinuation due to toxicities (3% vs. 1%). Common side effects include aspartate transaminase (AST)/alanine transaminase (ALT) elevation, HTN, fatigue, anorexia, nausea, stomatitis, and diarrhea. The most common Grade 3 or 4 AEs are leukopenia, neutropenia, and ALT elevation.[27] Axitinib is a second-generation VEGFR inhibitor that was approved by the FDA in 2012 for the treatment of advanced RCC after one prior systemic therapy failure.[21,28] When used for the treatment of advanced ccRCC, axitinib in combination with avelumab, an anti-programmed death-ligand 1 antibody, showed antitumor activity and a longer PFS of 13.8 months compared with 8.4 months for sunitinib.[20] The most common Grade 3 or 4 AEs for patients receiving axitinib with avelumab were HTN (24.4%), diarrhea (5.1%), and fatigue (3%). Patients receiving axitinib combined with avelumab had similar

rates of Grade 3 and 4 AEs as those receiving sunitinib.[29] Cabozantinib was approved by the FDA in 2017 as the first-line treatment for advanced RCC.[30] In a trial that compared cabozantinib to sunitinib in patients with metastatic ccRCC, cabozantinib had a longer PFS (8.2 months vs. 5.6 months) and a significantly higher overall response rate (33% vs. 12%). The incidence of Grade 3 or 4 AEs was similar between the two groups. Among patients receiving cabozantinib, the most common Grade 3 or 4 AEs were HTN (28%), diarrhea (10%), palmar-plantar erythrodysesthesia (8%), and fatigue (6%).[31] Tivozanib was approved for advanced RCC after two or more prior systemic therapies.[32] Compared with sorafenib, tivozanib demonstrated improved PFS (11.9 vs. 9.1 months) and comparable OS (29.3 vs. 28.8 months) and ORR (33.1% vs. 23.3%) but lower rates of Grade 3 and 4 AEs (61% vs. 70%). Further, 4% of the patients on tivozanib had to discontinue treatment due to toxicities compared with 5% of those on sorafenib. The most common side effects of tivozanib are HTN, diarrhea, dysphonia, and palmar-plantar erythrodysesthesia. HTN (27%) and fatigue (5%) were the most common Grade 3 or 4 toxicities reported in patients on tivozanib.[33] Lenvatinib plus pembrolizumab, an immunotherapy, was approved by the FDA as the first-line therapy for advanced RCC in 2021.[34] Compared with sunitinib, the combination therapy of lenvatinib and pembrolizumab had greater PFS (23.9 vs. 9.2 months) and ORR (71% vs. 36%) but a higher rate of Grade 3 and 4 toxicities (82.4% vs. 71.8%). The most common AEs associated with lenvatinib and pembrolizumab were diarrhea, HTN, hypothyroidism, decreased appetite, and fatigue. The most common Grade 3 or 4 toxicities for the combination therapy were diarrhea, HTN, elevated lipase, and hypertriglyceridemia.[35] A comparison of FDA-approved treatments for RCC is outlined in Table 1. VEGF inhibitors provide many options for first-line treatment of RCC and initially have great results but patients commonly develop resistance and must switch to a different type of therapy.[21]

3.3. mTOR inhibitors

Indirect inhibitors of HIF1-α may also target upstream molecules to reduce its expression. Normally, VHL controls HIF1-α expression, but in cases of mutated VHL, as in RCC, this regulation fails.[36] mTOR activation increases HIF1-α expression and regulates cellular metabolism, growth, proliferation, and angiogenesis.[37,38] mTOR complex 1and mTOR complex 2 control HIF1-α expression; thus, inhibiting these complexes limit HIF1-α accumulation and block the G1-S cell cycle transition.[38,39] Besides promoting HIF1-α expression, mTOR stabilizes HIF1-α, allowing its nuclear translocation and accumulation. Rapamycin, an mTOR inhibitor, decreases HIF1-α stabilization and transcriptional activity in hypoxic cancer cells.[40] Temsirolimus, a single-agent mTOR inhibitor, has been FDA-approved since 2007 for first-line treatment of advanced RCC with poor prognosis. It has demonstrated improved PFS (3.8 vs. 1.9 months), OS (10.9 vs. 7.3 months), and ORR (8.6% vs. 4.8%) compared to IFN-α treatment. In addition, it resulted in fewer Grade 3 or 4 toxicities compared to IFN-α (67% vs. 78%).[1,36,41] Common AE with temsirolimus includes asthenia, rash, anemia, nausea, dyspnea, diarrhea, peripheral edema, hyperlipidemia, and hyperglycemia.[42] Everolimus, another mTOR inhibitor, was FDA-approved 2 years after temsirolimus for RCC treatment following VEGF-targeted therapy failure.[1,21,41] In a study of patients with metastatic RCC progression on VEGFR TKI, everolimus prolonged PFS (14.6 vs. 5.5 months) and OS (25.5 vs. 17.5 months) compared to placebo. The study also showed improved ORR (43% vs. 6%) in the everolimus arm. Despite prolonged survival, patients on everolimus had more AE/toxicities than the placebo arm (71% vs. 50%).[36] Motzer *et al.* found that anemia (12%), dyspnea (8%), hypertriglyceridemia (8%), and hyperglycemia (10%) are the most common Grade 3 or 4 AE in patients on everolimus.[43]

3.4. Hsp90 inhibitors

The accumulation of stabilized HIF1-α in the nucleus activates HIF signaling. Heat shock protein 90 (Hsp90), a chaperone molecule, ensures correct folding and protects HIF1-α from degradation.[40,44] Disruption of this association leads to ubiquitination and proteasomal degradation of HIF1-α.[45,46] Studies have shown that Hsp90 inhibitors lower HIF1-α protein levels regardless of the VHL status of the cells. Further, investigation of these drugs could lead to more effective treatments against RCC.[44,45]

3.5. HIF2-α inhibitors

HIF2-α is a major point of focus in research on RCC treatment and has emerged as a promising therapeutic target, including upstream proteins that regulate the concentration of HIF2-α. At present, there is one FDA-approved HIF2-α inhibitor. Belzutifan was approved for use in 2021 and has been used to treat tumors associated with VHL syndrome, including RCC, as an alternative to surgery for solid tumors.[47] This drug has demonstrated effectiveness in treating RCC in patients with VHL syndrome with an ORR of 49% and a 96% PFS at 24 months. The most common AEs for belzutifan include anemia, fatigue, headache, and dizziness. Although not yet approved for sporadic RCC, studies are underway to determine its efficacy for tumors other than those associated with VHL syndrome.[48]

Table 1. Comparison of HIF pathway inhibitors

Experimental arm	Therapy target	Approved use	PFS (months)	OS (months)	ORR	CRR	PRR	FDA Approval	AE	References
Sorafenib versus placebo	VEGF inhibitor	Advanced RCC	5.5 versus 2.8	19.3 versus 15.9	10% versus 2%	<1% versus 0%	10% versus 2%	2005	10% discontinued treatment; 13% required dose reduction	17-19
Sunitinib versus IFN-α	VEGFR inhibitor	Advanced RCC	11 versus 5	–	31% versus 6%	0% versus 0%	31% versus 6%	2006	38% required dose interruption; 32% required dose reduction	22,23
Bevacizumab +IFN-α versus single- agent IFN-α	anti-VEGF antibody	mRCC	10.2 versus 5.4	–	31% versus 13%	–	–	2009	Grade 3 or 4 – 79% versus 61%	21,24,25
Pazopanib versus sunitinib	VEGFR inhibitor	mRCC	9.8 versus 4.3	14.4 versus 8.9	36% versus 23%	0% versus 0%	36% versus 23%	2009	3% versus 1% discontinued treatment due to toxicities	26,27
Axitinib+ Avelumab (anti-PD-L1 antibody) versus sunitinib	VEGFR inhibitor	Advanced ccRCC after failure of one prior systemic therapy	13.8 versus 8.4	11.6 versus 10.7	55.2% versus 25.5%	4.4% versus 2.1%	50.7% versus 23.4%	2012	Grade 3 or 4 – 71.2% versus 71.5%	20,28,29
Cabozantinib versus sunitinib	VEGFR inhibitor	Advanced RCC	8.2 versus 5.6	30.3 versus 21.8	33% versus 12%	1.3% versus 0%	31.6% versus 12%	2017	Grade 3 or 4 – 67% versus 68%	30,31
Tivozanib versus sorafenib	VEGFR inhibitor	Advanced RCC following two or more prior systemic therapies	11.9 versus 9.1	29.3 versus 28.8	33.1% versus 23.3%	–	–	2021	Grade 3 or 4 – 61% versus 70%	32,33
Lenvatinib+ Pembrolizumab (immunotherapy) versus sunitinib	VEGFR inhibitor	Advanced RCC	23.9 versus 9.2	–	71% versus 36%	16.1% versus 4.2%	54.9% versus 331.9%	2021	Grade 3 or 4 – 82.4% versus 71.8%	34,35
Temsirolimus versus IFN-α	mTOR inhibitor	mRCC	3.8 versus 1.9	10.9 versus 7.3	8.6% versus 4.8%	–	–	2007	Grade 3 or 4 – 67% versus 78%	42
Everolimus+ Lenvatinib (VEGFR TKI) versus single-agent everolimus	mTOR inhibitor	RCC following prior TKI failure	14.6 versus 5.5	25.5 versus 17.5	43% versus 6%	2% versus 0%	41% versus 6%	2009	Grade 3 or 4 – 71% versus 50%	21,43
Belzutifan	HIF2-α inhibitor	VHL- syndrome associated solid tumors	96% at 24 months	–	49%	0%	49%	2021	Grade 3 or 4 – 15%	47,48

Abbreviations: CRR: complete response rate; ORR: objective response rate; OS: overall survival; PFS: progression-free survival; PRR: partial response rate; IFN-α: Interferon-alpha, VEGFR: Vascular endothelial growth factor receptor; TKI: Tyrosine kinase inhibitor; HIF: Hypoxia-inducible factor; RCC: Renal cell carcinoma; ccRCC: Clear cell renal cell carcinoma, mTOR: Mammalian target of rapamycin, VHL: Von Hippel–Lindau, AE: Adverse events.

4. Conclusion

The silent nature of RCC in its early stages makes early diagnosis difficult unless it is found accidentally. Consequently, many patients who are under treated for this disease have locally advanced or metastatic disease. In addition to late-stage diagnosis, the polymorphic nature of RCC and its propensity to develop drug resistance have made treatment challenging. Major advances have resulted from targeted therapies, beginning with sunitinib and, more recently, combination therapies of different types of targeted treatments. These developments have provided multiple options for first-line treatments for patients with metastatic disease. Although none of the current therapy lines are considered curative for mRCC, these drugs are promising in terms of improving patient outcomes. With the use of immunotherapies and targeted therapies such as HIF1-α inhibitors, VEGF inhibitors, and mTOR inhibitors, patients are living longer and enjoying a better quality of life than ever before.

Future research on RCC and its treatments could involve using machine learning to detect early signs of therapy failure and severe AE/toxicities, thereby personalizing treatment plans to enhance patients' quality of life during treatment. Studies of mitochondrial DNA across all RCC types may identify specific mutations linked to the diseases, leading to new potential drug targets. This review has limitations, including potential exclusions due to the keywords used in the initial search, which may have omitted studies with different terminologies. Publication bias may be present as only published studies were included in the study. In addition, restricting our search to English-language studies likely excluded an unknown percentage of published works. Focusing the review on therapies for advanced disease may have resulted in a lack of information on early-stage disease, which could have aided in understanding disease progression and early interventions.

Acknowledgments

None.

Funding

None.

Conflict of interest

The authors declare no conflicts of interest.

Author contributions

Conceptualization: Samir Dalia
Writing–original draft: Kinsey Morey
Writing–review & editing: All authors

Ethics approval and consent to participate

Not applicable.

Consent for publication

Not applicable.

Availability of data

Not applicable.

References

1. Bahadoram S, Davoodi M, Hassanzadeh S, Bahadoram M, Barahman M, Mafakher L. Renal cell carcinoma: An overview of the epidemiology, diagnosis, and treatment. *G Ital Nefrol*. 2022;39:2022-vol3.

2. Cohen HT, McGovern FJ. Renal-cell carcinoma. *N Engl J Med*. 2005;353(23):2477-2490.

   doi: 10.1056/NEJMra043172

3. Motzer RJ, Bander NH, Nanus DM. Renal-cell carcinoma. *N Engl J Med*. 1996;335(12):865-875.

   doi: 10.1056/NEJM199609193351207

4. Chen S, Wang Y, Xiong Y, *et al*. Wild-type IDH1 inhibits the tumor growth through degrading HIF-α in renal cell carcinoma. *Int J Biol Sci*. 2021;17(5):1250-1262.

   doi: 10.7150/ijbs.54401

5. Masoud GN, Li W. HIF-1α pathway: Role, regulation and intervention for cancer therapy. *Acta Pharma Sin B*. 2015;5(5):378-389.

   doi: 10.1016/j.apsb.2015.05.007

6. Weidemann A, Johnson RS. Biology of HIF-1alpha. *Cell Death Differ*. 2008;15(4):621-627.

   doi: 10.1038/cdd.2008.12

7. Toledo RA, Jimenez C, Armaiz-Pena G, Arenillas C, Capdevila J, Dahia PLM. Hypoxia-inducible factor 2 alpha (HIF2α) inhibitors: Targeting genetically driven tumor hypoxia. *Endocr Rev*. 2023;44(2):312-322.

   doi: 10.1210/endrev/bnac025

8. Chittiboina P, Lonser RR. Von Hippel-lindau disease. *Handb Clin Neurol*. 2015;132:139-156.

   doi: 10.1016/B978-0-444-62702-5.00010-X

9. Maher ER, Sandford RN. Von Hippel-lindau disease: An update. *Curr Genet Med Rep*. 2019;7(4):227-235.

   doi: 10.1007/s40142-019-00180-9

10. Medina Villaamil V, Aparicio Gallego G, Santamarina Caínzos I, Valladares-Ayerbes M, Antón Aparicio LM. Searching for Hif1-α interacting proteins in renal cell carcinoma. *Clin Transl Oncol*. 2012;14(9):698-708.

    doi: 10.1007/s12094-012-0857-4

11. Klatte T, Seligson DB, Riggs SB, *et al*. Hypoxia-inducible factor 1 alpha in clear cell renal cell carcinoma. *Clin Cancer Res*. 2007;13(24):7388-7393.

    doi: 10.1158/1078-0432.CCR-07-0411

12. Shen C, Beroukhim R, Schumacher SE, *et al*. Genetic and functional studies implicate HIF1α as a 14q kidney cancer suppressor gene. *Cancer Discov*. 2011;1(3):222-235.

    doi: 10.1158/2159-8290.CD-11-0098

13. Xu K, Ding Q, Fang Z, *et al*. Silencing of HIF-1α suppresses tumorigenicity of renal cell carcinoma through induction of apoptosis. *Cancer Gene Ther*. 2010;17(3):212-222.

    doi: 10.1038/cgt.2009.66

14. Tassoudi A, Stefanidis I, Eleftheriadis T, Tzortzis V, Tassoudis V, Ioannou M. Study of hypoxia induced factor-1alpha (HIF-1A) and carbonic anhydrase 9 (CAIX) in Clear Cell Renal Cell Carcinoma (ccRCC). *Arch Nephrol Urol*. 2021;4(2):50-62.

    doi: 10.26502/anu.2644-2833036

15. Fallah J, Rini BI. HIF inhibitors: Status of current clinical development. *Curr Oncol Rep*. 2019;21(1):6.

    doi: 10.1007/s11912-019-0752-z

16. Greenberger LM, Horak ID, Filpula D, *et al*. A RNA antagonist of hypoxia-inducible factor-1α, EZN-2968, inhibits tumor cell growth. *Mol Cancer Ther*. 2008;7(11):3598-3608.

    doi: 10.1158/1535-7163.MCT-08-0510

17. Costa LJ, Drabkin HA. Renal cell carcinoma: New developments in molecular biology and potential for targeted therapies. *Oncologist*. 2007;12(12):1404-1415.

    doi: 10.1634/theoncologist.12-12-1404

18. Drugs.com. *Nexavar FDA Approval History*. Available from: https://www.drugs.com/history/nexavar.html#:~:text=fda%20approved%3a%20yes%20%28first%20approved%20december%2020%2c%202005%29,for%3a%20renal%20cell%20carcinoma%2c%20hepatocellular%20carcinoma%2c%20thyroid%20cancer [Last accessed on 2024 Jul 14].

19. Escudier B, Eisen T, Stadler WM, *et al*. Sorafenib in advanced clear-cell renal-cell carcinoma. *N Engl J Med*. 2007;356(2):125-134.

    doi: 10.1056/NEJMoa060655

20. Kathuria-Prakash N, Drolen C, Hannigan CA, Drakaki A. Immunotherapy and metastatic renal cell carcinoma: A review of new treatment approaches. *Life* (*Basel*). 2021;12(1):24.

    doi: 10.3390/life12010024

21. Wiechno P, Kucharz J, Sadowska M, *et al*. Contemporary treatment of metastatic renal cell carcinoma. *Med Oncol*. 2018;35(12):156.

    doi: 10.1007/s12032-018-1217-1

22. Drugs.com. *Sutent* (*Sunitinib Malate*) *FDA Approval History*. Available from: https://www.drugs.com/history/sutent.html [Last accessed on 2024 Jul 14].

23. Motzer RJ, Hutson TE, Tomczak P, *et al*. Sunitinib versus interferon alfa in metastatic renal-cell carcinoma. *N Engl J Med*. 2007;356(2):115-124.

    doi: 10.1056/NEJMoa065044

24. Summers J, Cohen MH, Keegan P, Pazdur R. FDA drug approval summary: Bevacizumab plus interferon for advanced renal cell carcinoma. *Oncologist*. 2010;15(1):104-111.

    doi: 10.1634/theoncologist.2009-0250

25. Rini BI, Halabi S, Rosenberg JE, *et al*. Bevacizumab Plus interferon alfa compared with interferon alfa monotherapy in patients with metastatic renal cell carcinoma: CALGB 90206. *J Clin Oncol*. 2008;26(33):5422-5428.

    doi: 10.1200/JCO.2008.16.9847

26. Gupta S, Spiess PE. The prospects of pazopanib in advanced renal cell carcinoma. *Ther Adv Urol*. 2013;5(5):223-232.

    doi: 10.1177/1756287213495099

27. Kim JH, Park I, Lee JL. Pazopanib versus sunitinib for the treatment of metastatic renal cell carcinoma patients with poor-risk features. *Cancer Chemother Pharmacol*. 2016;78(2):325-332.

    doi: 10.1007/s00280-016-3093-8

28. Tyler T. Axitinib: Newly approved for renal cell carcinoma. *J Adv Pract Oncol*. 2012;3(5):333-335.

    doi: 10.6004/jadpro.2012.3.5.7

29. Motzer RJ, Penkov K, Haanen J, *et al*. Avelumab plus axitinib versus sunitinib for advanced renal-cell carcinoma. *N Engl J Med*. 2019;380(12):1103-1115.

    doi: 10.1056/NEJMoa1816047

30. Center for Drug Evaluation and Research. *FDA Grants Regular Approval to Cabometyx for First-Line Treatment of Advanced Renal Cell Carcinoma*. U.S. Food and Drug Administration, FDA. Available from: https://www.fda.gov/drugs/resources-information-approved-drugs/fda-grants-regular-approval-cabometyx-first-line-treatment-advanced-renal-cell-carcinoma#:~:text=on%20december%2019%2c%202017%2c%20the,renal%20cell%20carcinoma%20(rcc) [Last accessed on 2024 Jul 14].

31. Choueiri TK, Halabi S, Sanford BL, *et al*. Cabozantinib versus sunitinib as initial targeted therapy for patients with metastatic renal cell carcinoma of poor or intermediate risk: The alliance A031203 CABOSUN trial. *J Clin Oncol*. 2017;35(6):591-597.

    doi: 10.1200/JCO.2016.70.7398

32. Center for Drug Evaluation and Research. *FDA D.I.S.C.O.*

Burst Edition: FDA Approval of Fotivda (Tivozanib) for Adult Patients with Relapsed or Refractory Advanced Renal Cell Carcinoma Following Two or More Prior Systemic Therapies. U.S. Food and Drug Administration, FDA. Available from: https://www.fda.gov/drugs/resources-information-approved-drugs/fda-disco-burst-edition-fda-approval-fotivda-tivozanib-adult-patients-relapsed-or-refractory#:~:text=on%20march%2010%2c%202021%2c%20the,or%20more%20prior%20systemic%20therapies [Last accessed on 2024 Jul 14].

33. Motzer RJ, Nosov D, Eisen T, *et al*. Tivozanib versus sorafenib as initial targeted therapy for patients with metastatic renal cell carcinoma: Results from a Phase III trial. *J Clin Oncol*. 2013;31(30):3791-3799.

doi: 10.1200/JCO.2012.47.4940

34. Center for Drug Evaluation and Research. *FDA Approves Lenvatinib plus Pembrolizumab for Advanced Renal Cell Car*. U.S. Food and Drug Administration, FDA. Available from: https://www.fda.gov/drugs/resources-information-approved-drugs/fda-approves-lenvatinib-plus-pembrolizumab-advanced-renal-cell-carcinoma [Last accessed on 2024 Jul 14].

35. Motzer R, Alekseev B, Rha SY, *et al*. Lenvatinib plus pembrolizumab or everolimus for advanced renal cell carcinoma. *N Engl J Med*. 2021;384(14):1289-1300.

doi: 10.1056/NEJMoa2035716

36. Semenza GL. Evaluation of HIF-1 inhibitors as anticancer agents. *Drug Discov Today*. 2007;12(19-20):853-859.

doi: 10.1016/j.drudis.2007.08.006

37. Motzer RJ, Escudier B, Oudard S, *et al*. Efficacy of everolimus in advanced renal cell carcinoma: A double-blind, randomised, placebo-controlled phase III trial. *Lancet*. 2008;372(9637):449-456.

doi: 10.1016/S0140-6736(08)61039-9

38. Kuroshima K, Yoshino H, Okamura S, *et al*. Potential new therapy of Rapalink-1, a new generation mammalian target of rapamycin inhibitor, against sunitinib-resistant renal cell carcinoma. *Cancer Sci*. 2020;111(5):1607-1618.

doi: 10.1111/cas.14395

39. Faes S, Demartines N, Dormond O. Mechanistic target of rapamycin inhibitors in renal cell carcinoma: Potential, limitations, and perspectives. *Front Cell Dev Biol*. 2021;9:636037.

doi: 10.3389/fcell.2021.636037

40. Diaz-Gonzalez JA, Russell J, Rouzaut A, Gil-Bazo I, Montuenga L. Targeting hypoxia and angiogenesis through HIF-1alpha inhibition. *Cancer Biol Ther*. 2005;4(10):1055-1062.

doi: 10.4161/cbt.4.10.2195

41. Onnis B, Rapisarda A, Melillo G. Development of HIF-1 inhibitors for cancer therapy. *J Cell Mol Med*. 2009;13(9A):2780-2786.

doi: 10.1111/j.1582-4934.2009.00876.x

42. Hudes G, Carducci M, Tomczak P, *et al*. Temsirolimus, interferon alfa, or both for advanced renal-cell carcinoma. *N Engl J Med*. 2007;356(22):2271-2281.

doi: 10.1056/NEJMoa066838

43. Motzer RJ, Hutson TE, Glen H, *et al*. Lenvatinib, everolimus, and the combination in patients with metastatic renal cell carcinoma: A randomised, phase 2, open-label, multicentre trial. *Lancet Oncol*. 2015;16(15):1473-1482.

doi: 10.1016/S1470-2045(15)00290-9

44. Bohonowych JE, Peng S, Gopal U, *et al*. Comparative analysis of novel and conventional Hsp90 inhibitors on HIF activity and angiogenic potential in clear cell renal cell carcinoma: Implications for clinical evaluation. *BMC Cancer*. 2011;11(1):520.

doi: 10.1186/1471-2407-11-520

45. Isaacs JS, Jung YJ, Mimnaugh EG, Martinez A, Cuttitta F, Neckers LM. Hsp90 regulates a von Hippel lindau-independent hypoxia-inducible factor-1α-degradative pathway. *J Biol Chem*. 2002;277(33):29936-29944.

doi: 10.1074/jbc.M204733200

46. Albadari N, Deng S, Li W. The transcriptional factors HIF-1 and HIF-2 and their novel inhibitors in cancer therapy. *Expert Opin Drug Discov*. 2019;14(7):667-682.

doi: 10.1080/17460441.2019.1613370

47. Deeks ED. Belzutifan: First approval. *Drugs*. 2021;81(16):1921-1927.

doi: 10.1007/s40265-021-01606-x

48. Jonasch E, Donskov F, Iliopoulos O, *et al*. Belzutifan for renal cell carcinoma in von Hippel-lindau disease. *N Engl J Med*. 2021;385(22):2036-2046.

doi: 10.1056/NEJMoa2103425

ACCSCIENCE PUBLISHING

Tumor Discovery

REVIEW ARTICLE

Peroxisome proliferator-activated receptor agonists as an adjuvant for cancer therapy: A review

Binita Patel[1] and S. R. Kaid Johar[2]*

[1]Department of Life Sciences, School of Sciences, Gujarat University, Ahmedabad, Gujarat, India

[2]Department of Zoology, Biomedical Technology and Human Genetics, School of Sciences, Gujarat University, Ahmedabad, Gujarat, India

(This article belongs to the *Special Issue: Current Evidences in Cancer Chemoprevention*)

Abstract

Cancer is now one of the leading diseases responsible for the highest mortality rates worldwide. Cancer treatment is extremely intricate and is often associated with less targeted effects and more side effects. In the last few years, two significant revolutions in cancer treatment have altered treatment paradigms: immuno-oncology and the pursuit of actionable changes in oncogene-driven cancers. Significant obstacles continue to exist in both areas of cancer treatment. Next-generation sequencing technologies for molecular prescreening in clinical research are advancing, but their widespread clinical use is hindered by challenges related to the clinical interpretation of large genomic data. Moreover, cancer mono-chemotherapy is associated with issues such as inadequate efficacy, drug resistance, and systemic toxicity. It is not possible to administer cytotoxic drugs limitlessly. Combination therapy was developed in response to this circumstance, with the expectation of achieving high therapeutic efficacy at lower dosages of medication. Peroxisome proliferator-activated receptors (PPARs) are a group of essential lipid sensors and metabolic pathway regulators. In addition, they possess the ability to modulate immunity, inflammation, and endothelial nitric oxide synthase activation. Alongside their well-established functions, new insights into the roles of PPAR agonists in cancer research are emerging. After reviewing current research, it is evident that PPAR modulators have significant potential for managing cancer. This review aims to consolidate the functions of PPAR ligands alongside other cancer therapies. We provide a comprehensive perspective on the applicability of PPAR ligands in cancer treatment as an adjuvant.

Keywords: PPAR agonists; Adjuvant; Cancer; Synergism; Cancer therapy; Drug repurposing

***Corresponding author:**
S. R. Kaid Johar
(kaidjohar@gujaratuniversity.ac.in)

Citation: Patel B, Johar SRK. Peroxisome proliferator-activated receptor agonists as an adjuvant for cancer therapy: A review. *Tumor Discov*. 2024;3(4):4003. doi: 10.36922/td.4003

Received: June 21, 2024

Accepted: September 25, 2024

Published Online: November 5, 2024

1. Introduction

According to the World Health Organization, 97 million people died from cancer in 2022, with an estimated 20 million new cases. The estimated number of people who were alive 5 years after a cancer diagnosis was 53.5 million. In their lifetime, one in five

people will develop cancer; one in nine men and one in 12 women will die from the disease. The process of treating cancer has always been intricate. Conventional therapeutic modalities, including radiotherapy, chemotherapy, and surgery, have been employed to treat cancer.[1]

The main treatments for cancer are surgery and chemotherapy; however, patients frequently develop chemotherapeutic resistance within a few years after starting treatment.[2] Furthermore, side effects from chemotherapeutic drugs such as paclitaxel, carboplatin, and doxorubicin can significantly worsen quality of life. These side effects include weakness, itching, loss of appetite, hair loss, and facial flushing, among others. Consequently, novel therapeutic approaches and improved predictive markers for chemotherapy, targeted therapies, immunotherapy, and hormonal therapy are required.[3]

Advances in our understanding of the molecular mechanisms underlying cancer progression have made it possible to develop novel targeted therapies that are proving to be innovative and promising approaches for treating the disease.[4] As these therapies specifically target cancer cells while avoiding harm to non-target cells, they are becoming increasingly significant. The strategies used in targeted therapy include prodrugs, nanoparticulate antibody conjugates, small molecule inhibitors, and monoclonal antibodies. However, recent studies have revealed that the presence of molecularly diverse tumors can lead to treatment failures in several cases.[5-8] Furthermore, although it was anticipated that targeted therapy would cause fewer side effects than conventional chemotherapy, significant toxicities are still observed. Trastuzumab, for example, has been linked to congestive heart failure as a known adverse effect.[9] Common side effects of vascular endothelial growth factor (VEGF) inhibitors and VEGF receptor inhibitors include hypertension, thromboembolic events, slowed wound healing, and an elevated risk of bleeding, including tumor-related hemorrhage.[10]

By enhancing the immune response, immunotherapy enables the patient's immune system to destroy cancer cells. As a next-generation treatment for cancer, it has the potential to replace chemotherapy due to its effectiveness against multiple tumors and its innovative therapeutic properties.[11] There are two types of immunotherapy: active and passive. Active immunotherapy includes chimeric antigen receptor T cells, immunostimulatory vaccines, and genetically modified organisms that can recognize specific cancer antigens. Passive immunotherapy, on the other hand, involves using cytokines or checkpoint inhibitors to indirectly enhance the patient's immune response.[12] Although these treatments are novel, clinical trial results indicate that they are only effective against a limited number of cancers and can lead to unfavorable side effects, including cytokine release syndrome and a weakened immune response.[13] Although immunotherapy has been developed as an effective cancer treatment, immunotherapy-based drugs often have poor outcomes in solid tumors due to low infiltration of immune cells and decreased tumor immunogenicity, resulting in an immunosuppressive tumor environment.[14] Furthermore, the lack of appropriate preclinical models for validating distinct biomarkers, as well as inadequate methods for tumor tissue collection, makes it more difficult to assess predictive biomarkers.[15]

Usually, hormonal treatments prevent steroid ligands from attaching to the nuclear hormone receptor family, which includes estrogen receptor and androgen receptor (AR) in breast cancer and prostate cancer, respectively.[16] Various hormone receptors are expressed in cancer and mediate both growth stimulation and inhibition effects. Hormones such as gonadotropin-releasing hormones, gonadotropins, androgens, estrogens, and progestins have been evaluated in several clinical trials to understand the mechanisms of tumorigenesis.[17-20] However, resistance is a common cause of failure in single-agent hormonal therapy, and it is not the only factor at play. Therapies such as leuprorelin and enzalutamide can lead to resistance through various mechanisms, including mutations in the AR ligand-binding domain and the creation of variant AR proteins that can recognize antiandrogens (antagonists) as agonists.[21-23] In this comprehensive review, we have compiled the available research on the utilization of various peroxisome proliferator-activated receptor (PPAR) agonists as a combination therapy with known cancer modalities for different cancers.

2. Combination therapy for cancer

Considering the current situation, a synergistic approach that combines a chemotherapeutic agent with another agent can be employed to target similar or different genes for cancer treatment. Although the combination of cytotoxic drugs has garnered significant interest, concerns remain regarding the potential risks of drug toxicity, cross-resistance, and compromised quality of life.[24] Therefore, incorporating a biological agent alongside an established chemotherapeutic drug presents a promising alternative to optimize therapeutic outcomes while minimizing toxicity. By targeting various molecular pathways implicated in cancer development through diverse mechanisms of action, combination therapy aims to enhance treatment efficacy.[25,26] However, discovering novel therapeutic agents is a complex and resource-intensive process that entails multiple steps, substantial time, and costs, including clinical trials.[27] Thus, drug repurposing offers several advantages

in overcoming the challenges associated with finding new agents.[28] The process of using an already-approved medication or drug candidate for a new medical condition or treatment for which it was not previously recommended is known as "drug repurposing."[29,30] To expedite the drug discovery process and address the pressing needs in healthcare, drug repurposing has become essential. In drug repurposing, a drug is identified, preclinical models are used to assess its efficacy, and Phase II clinical trials are then conducted.[31] Among the various drugs that can be repurposed for synergistic cancer treatment, PPAR agonists show promising results.

3. PPARs

PPARs are a group of nuclear receptor superfamily members that play a major role in gene expression and metabolism regulation. PPARs bind to ligands and translocate to the cell nucleus. Together with their ligands, PPARs act as transcription factors that bind to specific DNA sequences known as peroxisome proliferator-responsive elements and heterodimerize with retinoid X receptors.[32] The PPAR superfamily comprises three subtypes: PPAR-α, PPAR-γ, and PPAR-β/δ. These PPAR subtypes share a relatively high similarity in molecular structure; however, there are significant differences in their biological functions, tissue distribution, and ligand affinities.[33] Figure 1 illustrates the differences between the PPAR subtypes and their interactions with DNA. PPAR-α expression is primarily found in the liver, brown adipose tissue, heart, kidney, and muscle tissue, where it regulates fatty acid β-oxidation and energy homeostasis.[34] PPAR-β/δ is ubiquitously expressed, often at high levels in skeletal muscle, adipose tissue, heart, and the gastrointestinal tract, and it regulates fatty acid metabolism and blood glucose levels.[35,36] PPAR-γ is highly expressed in the heart, muscle, gastrointestinal tract, kidney, adipose tissue, immune cells, and endothelial cells.[37] PPARs are also important lipid sensors and regulators of various metabolic pathways. They can promote endothelial nitric oxide synthase activation and modulate immune and inflammatory responses. In addition to their well-established roles, discoveries are being made regarding the functions of PPARs in cancer.[38,39] Previous studies have shown that the expression of PPAR-β/δ correlates with tumor proliferation, whereas the activation of PPAR-α and PPAR-γ is associated with tumor suppression. Such generalizations may be overly simplistic due to the complex regulatory signals of PPARs, and their intricate mechanisms require further investigation. Consequently, the role of PPARs in cancer has gradually become a focal point of research.[40] More specifically, initially recognized as key players in adipocyte differentiation and glucose regulation, PPAR-γ and PPAR-α have now been identified as therapeutic targets with a wide range of potential applications in cell differentiation, apoptosis, angiogenesis, epithelial–mesenchymal transition, and other biological processes that are deregulated in cancer.[41,42]

4. PPAR modulators

PPAR modulators are molecules that modulate the activity of PPAR receptors. PPAR agonists are compounds that activate the PPAR pathway. These ligands are developed to treat various diseases and disorders related to lipid metabolism, diabetes, and metabolic syndromes. PPAR-α agonists are primarily used to treat dyslipidemia, whereas PPAR-γ agonists are prescribed for the treatment of Type 2 diabetes. PPAR-α agonists include a class of chemicals called fibrates, which encompasses fenofibrate, gemfibrozil, bezafibrate, ciprofibrate, and clofibrate. Several other compounds, such as pemafibrate, Wy-14643 (pirinixic acid), and GW7674, are also known to act as PPAR-α agonists.[43] In addition to these, omega-3 fatty acids, curcumin, and sesquiterpenes are recognized for their PPAR-α agonist activity.[44] PPAR-γ agonists are the most widely used. Several other compounds, including natural compounds and synthetic derivatives, have been identified as PPAR-γ agonists. This group includes a class of drugs called thiazolidinediones (TZDs), whose antidiabetic properties were discovered in the early 1980s.[45] Various natural products derived from traditionally used medicinal plants and foods activate the PPAR-γ receptor.[46] Different fatty acids and fatty acid derivatives, such as eicosanoids (e.g., 8-S-hydroxyeicosatetraenoic acid [HETE] and leukotriene B4), can also activate PPAR-γ. In addition, several prostanoids, such as 15-deoxy-Δ12,14-prostaglandin J2 (15d-PGJ2) and 15-HETE, can activate PPAR-γ as well.[47] Many *in vivo* studies have shown that some natural activators of PPAR-γ (e.g., honokiol, amorphofurtin 1, amorphofurtin B, and amorphastilbol) improve metabolic parameters in diabetic animal models.[48-50] TZDs include pioglitazone, rosiglitazone, troglitazone (TGZ), rivoglitazone, and netoglitazone. Dual or pan-PPAR agonists have also been developed, including muraglitazar, tesaglitazar, and saroglitazar.[51-54] We have compiled a comprehensive review that summarizes the available literature supporting the beneficial effects of treatment with PPAR ligands in combination with existing therapies in cancer. Numerous examples exist where combination therapy has produced synergistic or additive effects on apoptosis, differentiation, and the ability to reduce cell proliferation and tumor burden.[55] Some studies indicate that pretreatment with PPAR ligands can overcome resistance and reduce toxicity.[56] Several mechanisms have been investigated to explain these protective effects.[57] This article focuses on studies that provide strong arguments

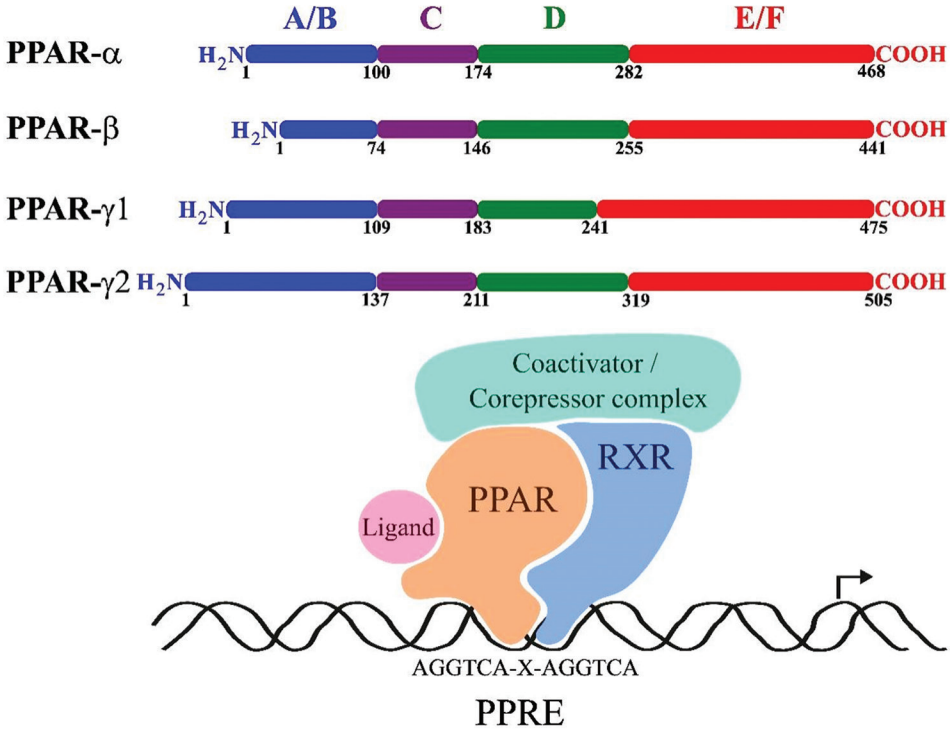

Figure 1. Peroxisome proliferator-activated receptor (PPARs) subtypes and their interaction with DNA. PPAR-α, PPAR-β, and PPAR-γ (γ1, and γ2) are the known PPAR subtypes. All subtypes of PPAR contain the A/B domain or AF-1 domain, C or DNA binding domain, D or hinge region, and E/F or ligand-binding domain (LBD). LBD has the ligand and retinoic acid receptor (RXR) interaction sites. It contains the AF-2 region, which is important for ligand-dependent trans-activation. The difference between the subtypes of PPAR at the A/B, D, and E/F domains determines its subtypes and the efficiency of its interaction with its ligands. The PPAR – RXR complex binds DNA at the peroxisome proliferator response elements.

for the use of PPAR ligands in conjunction with other treatment modalities as anticancer therapy for multiple types of cancer.

4.1. PPAR agonists for antiangiogenic effects

Angiogenesis, a crucial process in the tumor microenvironment involved in metastasis, is the natural progression through which new blood vessels form from existing ones. Growth factors that stimulate angiogenesis and inhibitors that regulate neovascularization act as controllers of this process.[58] The mutation of K-Ras and epidermal growth factor receptors is associated with resistance to conventional chemotherapeutic agents and other targeted therapies.[59] The treatment of PPAR-γ ligand (rosiglitazone) alongside carboplatin induces a dramatic depletion of mutant K-Ras and epidermal growth factor receptors in murine lung adenocarcinomas. In numerous genetically engineered mouse models of lung carcinoma, the combination treatment of rosiglitazone and carboplatin inhibits tumor aggressiveness, indicating its promise as a predominantly effective anticancer strategy.[60] Arachidonic acid (AA), a polyunsaturated fatty acid released from membrane phospholipids, is converted into different bioactive lipid mediators, such as epoxyeicosatrienoic acids (EETs), prostaglandins (PGs), and HETEs, through the action of cytochrome P450 (CYP) epoxygenases, cyclooxygenase (COX), or lipoxygenase pathways.[61] Among these, EETs are particularly potent proangiogenic eicosanoids and are positively linked with cancer progression.[62] PPAR-α ligand AVE8134, in conjunction with COX inhibitor therapy, synergistically halts lung cancer development and angiogenesis by downregulating CYP2c44 expression, reducing the synthesis of EETs (AA-derived EETs), increasing levels of 11-HETE, and altering the catalytic activity of COX enzymes.[63] N-(9-fluorenylmethyloxycarbonyl)-L-leucine (F-L-Leu), a novel PPAR-γ agonist, along with COX-2 inhibitors, induces an anti-tumorigenesis pathway in breast cancer cells. This integrated effect can be utilized at subclinical doses to reduce chemotherapy in women at high risk of developing breast cancer.[64] Malakouti *et al.* studied *CXCR4* and *CXCR7* gene expression to investigate the effects of co-administration of pioglitazone and doxorubicin on the breast cancer cell line MDA-MB-231. They observed that pioglitazone decreased the movement of MDA-MB-231 cells, possibly by upregulating the expression of *CXCR4* and *CXCR7* and

affecting other pathways related to cell migration, without increasing the expression of the surface proteins of these two receptors.[65]

4.2. PPAR agonists for antiproliferative and apoptotic effects

Apoptosis, the body's natural cell death process, is a key area of focus in anticancer treatment. In cancer, the suppression of the apoptotic pathway often occurs through the overexpression of antiapoptotic proteins and the underexpression of proapoptotic proteins. These changes can lead to resistance to chemotherapy, a commonly used cancer treatment method.[66] Several PPAR agonists have demonstrated antiproliferative and apoptosis-inducing effects when used in combination with chemotherapeutic agents, and the underlying pathways are illustrated in Figure 2. Treatment with PPAR-γ through the synthetic ligand TGZ and all-trans-retinoic acid significantly inhibited the growth of MCF7 tumors, which was correlated with the downregulation of Bcl-2 and resulted in significant apoptosis and fibrosis in these tumors.[67]

In certain cancer cell lines, ranpirnase and rosiglitazone work synergistically to reduce cell viability and accelerate cell death. For malignancies with elevated PI3K-dependent Fra-1 expression or survivin, the innovative combination of ranpirnase and rosiglitazone appears promising, as illustrated in Figure 2.[68] The combination of rosiglitazone and all-trans-retinoic acid lowers the expression of COX-2, matrix metallopeptidase 7 (MMP-7), and tissue inhibitor of metalloproteinase 1, induces cell cycle arrest at the G1 phase and consequently inhibits cell proliferation in the human colorectal cancer cell line HCT-15.[69] In hepatocellular carcinoma (HCC) cells treated with 5-fluorouracil, rosiglitazone activates the PPAR-γ signaling pathway, upregulating PTEN expression and downregulating COX-2 expression to promote cancer cell growth.[70] Fenofibrate, an agonist of PPAR-α, hinders cell proliferation and induces apoptosis in Ishikawa endometrial carcinoma cells. These effects are magnified by retinoic acid, an agonist of the retinoid X receptor. DNA content analysis indicates that progression through the G1/S phase of the cell cycle is inhibited. Independent component analysis of gene microarray experiments shows a reduction in the expression of cyclin D1 (*CCND1*) and related changes in cell cycle gene expression.[71]

A PPAR-γ agonist, TGZ, in combination with cisplatin, inhibited EHMES-10 cell growth through cell cycle arrest due to the overexpression of $p21^{waf1/cip1}$ and apoptosis. This synergism may provide therapeutic benefits for patients with malignant pleural mesothelioma.[72] The combination

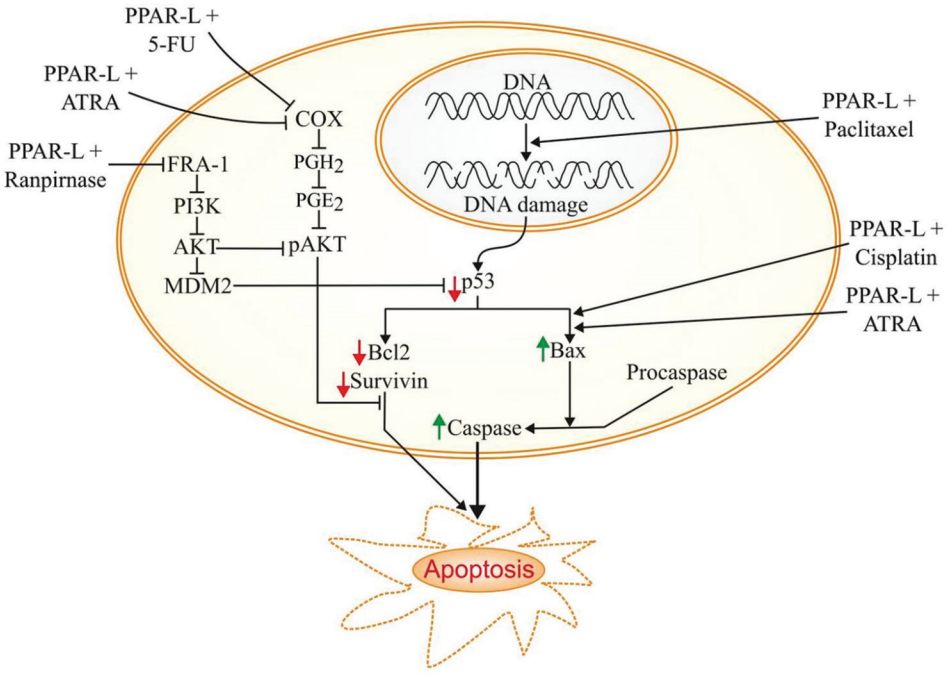

Figure 2. Effect of peroxisome proliferator-activated receptor (PPAR) agonists as an adjuvant on the proliferation and apoptosis of cancer cells. PPAR ligand along with paclitaxel, cisplatin, ranpirnase, all-trans-retinoic acid, and 5-fluorouracil exert more effects than cancer therapy alone. The effects of PPAR agonists were due to the decreased expression of Bcl2, survivin, PI3K, AKT, MDM2, and p53 and the increased expression of Bax. This finally leads to the activation of apoptotic pathways in cancer cells.

of the high-affinity PPAR-γ agonist RS5444 and paclitaxel exhibited a reduction in the proliferation rate of cells and minimized tumor growth of undifferentiated thyroid neoplasm carcinoma *in vivo*. Although RS5444 alone did not induce apoptosis, its combination with paclitaxel increased the apoptotic index twofold compared to paclitaxel alone.[73] Moreover, activation of PPAR-γ by its ligand pioglitazone intensifies the effects of cisplatin, inhibiting MDA-MB-231 cell survival compared to chemotherapy alone. This effect may be attributed to enhanced apoptosis resulting from the downregulation of the antiapoptotic protein Bcl-2 and increased levels of caspase-9 and cleaved PARP, as explained in Figure 2.[74] Pouya *et al.* illustrated that the co-delivery of capecitabine–pioglitazone-loaded triblock nanoparticles effectively destroyed colorectal cancer cells *in vitro*. This approach could achieve the co-delivery of capecitabine and pioglitazone, utilizing the potential of both drugs and increasing the longevity of patients with colorectal cancer.[75]

4.3. PPAR agonists for prevention of cell migration and invasion

The first stage of the metastatic cascade is invasion, which occurs when tumor cells migrate, infiltrate the surrounding tissue, and enter lymphatic and blood vessels to spread. A growing body of research suggests that mutations may drive and accelerate the invasion and migration of various cancer cell types.[76] The antimigration and anti-invasion effects of radiation were enhanced by rosiglitazone, a PPAR-γ agonist that decreased cell viability. Rosiglitazone increased the radiosensitivity of PANC1 xenografts and pancreatic cancer cells. According to microarray studies, the combination of rosiglitazone and radiation altered the expression of several genes and impacted various pathways.[77] In addition, a novel PPAR-γ ligand, CB13, inhibits cell growth by increasing lactate dehydrogenase release, decreasing cell viability, and enhancing caspase-3 and caspase-9 activities in non-small cell lung cancer (NSCLC) and radioresistant NSCLC cell lines (A549R and H460R). Furthermore, CB13 generates reactive oxygen species (ROS) and induces endoplasmic reticulum (ER) stress, leading to cell death. When CB13 is combined with radiation, ER stress, and cell death are significantly increased compared to using CB13 alone.[56]

Lyon *et al.* were the first to demonstrate that long-term *in vivo* treatment with a chemopreventive mixture, which includes selenium (an antioxidant), rosiglitazone, sodium phenylbutyrate or valproic acid (histone deacetylase inhibitors), and hydralazine (a cytosine-demethylating agent), could effectively block the development of premalignant lung cancer in the A/J mouse model treated with NNK (4-methylnitrosamino)-1-(3-pyridyl)-1-butanone.[78]

As shown in Figure 3, the PPAR agonist pioglitazone and the histone deacetylase inhibitor valproic acid synergistically regulate E-cadherin expression and inhibit the growth and invasion of prostate cancer compared to individual therapies.[79] The PPAR-γ agonist rosiglitazone, in combination with radiotherapy, enhances the effectiveness of radiotherapy to improve local tumor control, decrease the risk of distant metastasis, and delay tumor recurrence.[80] Survivin is the smallest member of the apoptosis inhibitor protein family, and its aberrant expression is correlated with tumor cell proliferation, progression, angiogenesis, resistance to therapy, and poor prognosis. Survivin is predominantly expressed in most human malignancies, including lung, pancreatic, and breast cancers, compared to normal tissues.[81] A natural PPAR-γ agonist, 15d-PGJ2 (15-Deoxy-Δ12,14-PGJ2), has been investigated for over a decade. Studies have shown that it possesses pro-apoptotic, anti-inflammatory, antiangiogenic, and anti-metastatic properties, along with significant anticancer effects.[82] Co-treatment with 15d-PGJ2 and survivin RNAi synergistically inhibits the stem cell phenotype and cell proliferation of bladder cancer *in vitro* by upregulating ROS production and generating oxidative stress mediated by NADPH oxidase 2. This study suggests that the combined treatment of survivin inhibitors and PPAR-γ agonists may have therapeutic significance in the clinical treatment of various cancers.[83]

4.4. PPAR agonists for induction of oxidative stress

ROS plays a major role in regulating normal cellular functions, but when they are uncontrolled, they can contribute to diseases such as cancer. Increased ROS generation has been observed in several studies, activating protumorigenic signaling, enhancing cell survival and proliferation, and promoting DNA damage and genetic instability.[84] However, it has also been discovered that higher concentrations of ROS can encourage antitumorigenic signaling by triggering oxidative stress-induced tumor cell death. Tumor cells adapt by producing higher levels of antioxidant proteins to detoxify excess ROS while maintaining protumorigenic signaling and resistance to apoptosis.[85] The effects of various PPAR agonists on elevating ROS levels in cancer cells are summarized in Figure 4.

The combination therapy of PPAR-γ ligands and COX-2 inhibitors has shown anti-inflammatory and antineoplastic effects *in vitro* and has been evaluated for its therapeutic potential in several preclinical and clinical studies.[86] As illustrated in Figure 4, PPAR-γ ligands can enhance γ-H2AX expression, thereby magnifying the DNA damage response induced by γ-radiation. Furthermore, the combined treatment significantly increased ROS generation, whereas

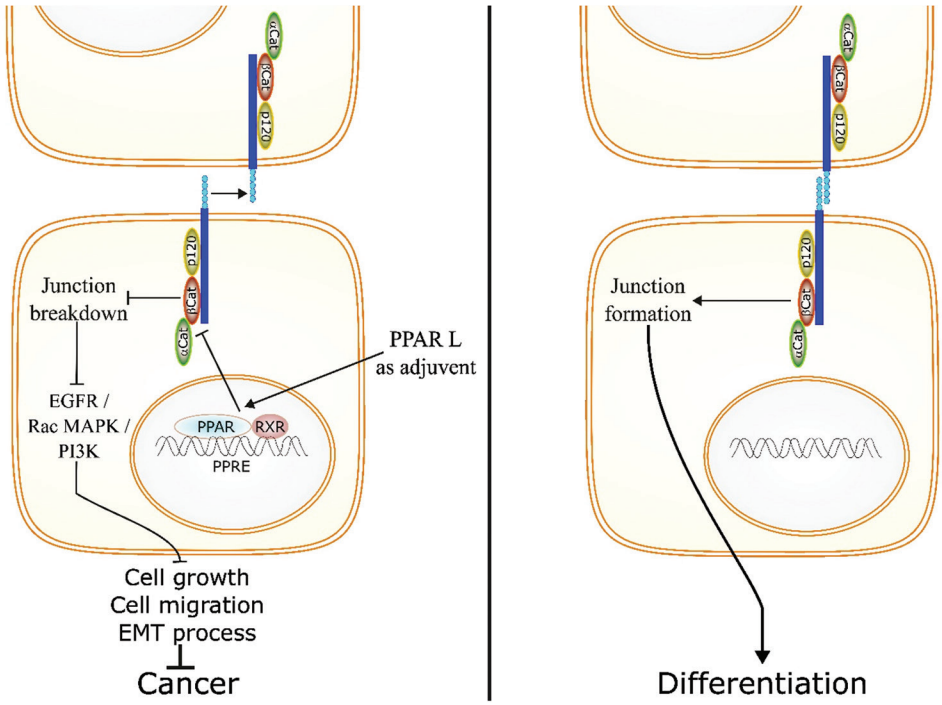

Figure 3. Effect of peroxisome proliferator-activated receptor (PPAR) agonists as an adjuvant on cell migration and invasion of cancer cells. PPAR ligand as an adjuvant regulates the expression of E-cadherin and effects the EGFR/MAPK/PI3K-AKT pathway. This leads to decreased cell growth, cell migration, and epithelial–mesenchymal transition in cancer cells

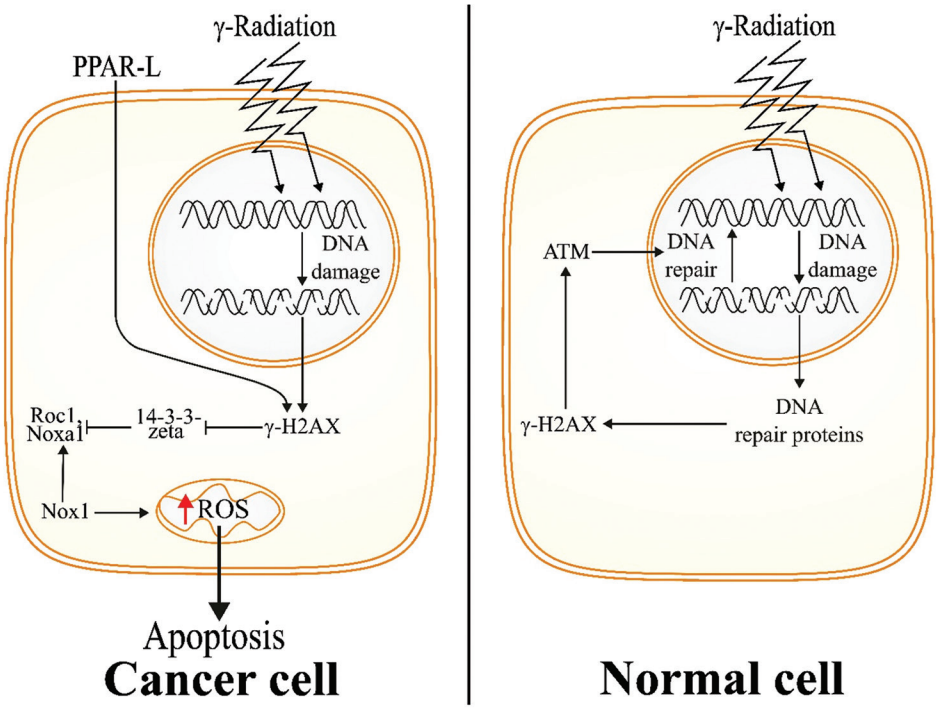

Figure 4. Effect of peroxisome proliferator-activated receptor (PPAR) agonists as adjuvants in inducing oxidative stress in cancer cells. PPAR ligand along with γ-radiation activates the γ-H2AX pathway to generate reactive oxygen species, which mediates the execution of apoptosis in cancer cells

the ROS scavenger N-acetylcysteine inhibited ROS production and the apoptotic cell death induced by this combination treatment.[87] The synergistic treatment of TGZ and heregulin increased the generation of superoxide in mitochondria, which disrupted mitochondrial potential and induced substantial cell death in breast cancer cells.[88]

4.5. PPAR agonists for suppression of multidrug resistance (MDR)

MDR is an acquired resistance that poses a major barrier to the successful treatment of cancer. One of the most common causes of MDR is the overexpression of P-glycoprotein (P-gp), which is encoded by the *MDR1* gene. This gene is a direct target of the Wnt/β-catenin signaling pathway, which plays a key role in cancer progression. The effects of various PPAR agonists on MDR are summarized in Figure 5. Pioglitazone, a PPAR-γ agonist, can modulate P-gp and overcome doxorubicin resistance in a patient-derived orthotopic xenograft model of osteosarcoma.[89] In addition, the PPAR-γ agonist rosiglitazone reverses ABCG2-mediated MDR expression by inhibiting ABCG2 transport activity and facilitating the translocation of ABCG2 from the cell surface to intracellular compartments through the PTEN/PI3K/AKT pathway.[90] It also downregulates the expression of FZD1 and MDR1/P-gp in a dose-dependent manner while significantly decreasing nuclear β-catenin levels and its transcriptional activity in ovarian cancer cells.[91]

Combination therapy using tumor necrosis factor-related apoptosis-inducing ligand (TRAIL) with PPAR ligands may offer a promising experimental approach, as PPAR ligands – particularly d15-PGJ2 – sensitize drug-resistant ovarian cancer cells to TRAIL-induced apoptosis.[92] In general, Wnt/β-catenin signaling is upregulated during inflammatory processes and oxidative stress in many cancers, whereas PPAR-γ is typically downregulated in these contexts. Therefore, PPAR-γ ligands have been shown to prevent cancer development by modulating the Wnt/β-catenin signaling pathway.[93]

4.6. PPAR agonists in clinical trials for cancer therapy

Clinical trials have been organized to evaluate the effects of PPAR agonists in combination with other therapies for the treatment of cancer. Efatutazone, also known as RS5444 and CS-7017, belongs to the TZD class of synthetic PPAR ligands and is an orally bioavailable, selective, and highly potent agonist of PPAR-γ, more so than second-generation TZDs such as pioglitazone and rosiglitazone.[94] When efatutazone is administered with other cytotoxic medications, its selective activation of the PPAR-γ subtype may be enhanced. Efatutazone

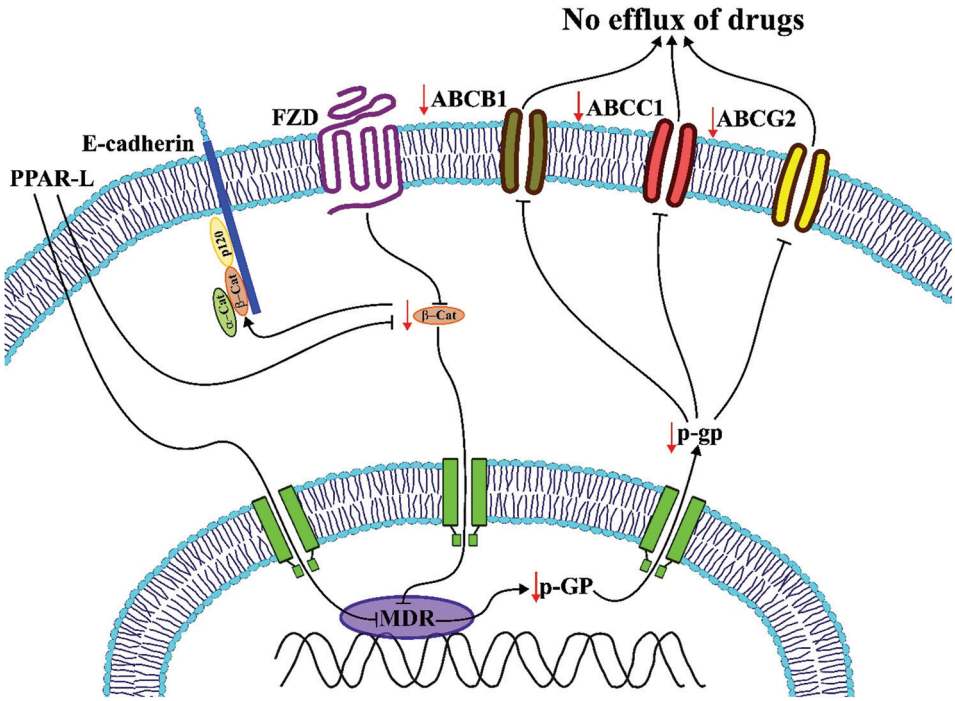

Figure 5. Effect of peroxisome proliferator-activated receptor (PPAR) agonists as an adjuvant in suppressing multidrug resistance in cancer cells. PPAR ligand sensitizes drug-resistant cancer cells by decreasing the expression of P-glycoprotein (P-gp). The reduced P-gp further reduces the expression of ABCB1, ABCC1, and ABCG2 and hence reduces the efflux of drugs from the cancer cells.

is being evaluated alongside paclitaxel in a Phase I trial for the treatment of anaplastic thyroid cancer, based on preclinical research showing that the drug inhibits cell proliferation by upregulating RhoB and p21 while promoting apoptosis.[73,95,96] In patients with advanced solid tumors, efatutazone has demonstrated acceptable safety, tolerability, and disease control when administered orally.[97] In Japanese patients with metastatic colorectal cancer, efatutazone combined with FOLFIRI (5-fluorouracil, levoleucovorin, and irinotecan) showed an acceptable safety profile and evidence of disease stabilization.[98] For patients with high-grade gliomas (glioblastoma or anaplastic glioma), a Phase II trial was initiated to examine the efficacy of continuously administered pioglitazone and rofecoxib in combination with low-dose chemotherapy (capecitabine or temozolomide). The study indicated that this novel regimen is well-tolerated and moderately effective.[99] Patients with advanced vascular malignancies participated in a pilot study assessing the effectiveness of metronomically scheduled, low-dose trofosfamide in combination with pioglitazone and rofecoxib, a selective COX-2 inhibitor, which may offer a new alternative for palliative care.[100] A Phase II trial was initiated to analyze the effectiveness of pioglitazone and rofecoxib combined with sequentially added angiostatic chemotherapy for patients with previously treated metastatic melanoma or soft-tissue sarcoma. This study demonstrated a novel and entirely orally administered chemotherapeutic regimen that is well tolerated in patients with chemotherapeutic malignancies.[101]

4.7. PPAR agonists as a supportive regimen for cancer immunotherapy

Immunotherapy has transformed cancer treatment in recent decades by modifying immune responses against tumor cells to enhance the effectiveness of conventional therapies such as chemotherapy and radiation. Programmed cell death protein 1 (PD-1) is a receptor present on immune cells that plays a crucial role in regulating the immune response. PD-1 restricts the entry and survival of T cells within the tumor microenvironment. However, targeting PD-1 with inhibitors allows T cells to infiltrate the tumor, thereby enhancing the effects of other cancer therapies.[102-104] PPAR agonists are a promising adjunct to immunotherapy, as they can boost the antitumor activity of T cells, even in an immunosuppressive tumor microenvironment. Research has shown that fenofibrate, an agonist of PPAR-α, can work synergistically with PD-1 blockers in cancer immunotherapy by altering the metabolism of effector T cells.[105] PD-1 blockade has also been found to work in conjunction with bezafibrate, an agonist of the PGC-1α/PPAR complex. In this context, fenofibrate increases fatty acid oxidation and mitochondrial respiratory capacity in CD8+ T lymphocytes, which enhances antitumor immunity when combined with PD-1 blockade.[106] TZDs have also been shown to inhibit TGF-β transcription, resulting in a significant reduction of the malignant phenotype in gliomas.[107,108] In addition, inhibiting TGF-β signaling improves survival and restores immune surveillance.[109]

4.8. PPAR agonists for altering tumor microenvironment

The PPAR subtypes may function differently depending on the type of cancer and the stage of the tumor. In addition, the effects of PPAR agonists can vary based on the tumor microenvironment. For instance, the expression of PPAR-γ in breast cancer cells inhibits the NF-κB signaling pathway, reducing the levels of proinflammatory, proangiogenic, and protransfer signaling molecules in the tumor microenvironment, including IL-6, IL-8, CXCR4, MMP-2, and MMP-9. This reduction inhibits tumor cell activity in breast cancer.[110,111] Tumor-associated macrophages (TAMs) are the most prevalent immune cells that promote neovascularization, immunosuppression, and chemoresistance within the tumor microenvironment.[112] The activation of PPAR-γ leads to lipid retention and PGE2 secretion, which causes macrophage polarization toward anti-inflammatory TAMs, converting the M1 phenotype into the M2 phenotype and diminishing the Stat3-mediated proinflammatory response.[113-116] In contrast, PPAR-α in the tumor microenvironment often negatively affects immune cells, leading to immunosuppression or cancer immune escape. Tumor-derived exosomes substantially activate PPAR-α in tumor-infiltrating dendritic cells, increasing intracellular lipid content and mitochondrial respiration, which triggers cytotoxic T-cell activation and immune dysfunction.[117] Cancer stem cells (CSCs) are frequently associated with the development of malignant tumors.[118] Stearoyl-CoA desaturase 1 is an ER enzyme that converts saturated fatty acids into monounsaturated fatty acids.[119] PPAR-α activates the stearoyl-CoA desaturase 1 pathway, which is significantly upregulated to maintain CSC stemness in human liver cancer.[120] Cells in the tumor microenvironment exhibit increased glucose uptake and glycolysis, enhanced glutamine depletion, and the dissolution of carbon and amino nitrogen. This becomes a direct source of energy for the cancer cells.[120-122] PPARs are known regulators of cellular metabolism, particularly carbohydrate and mitochondrial-linked metabolism. Thus, altering PPAR activity through their antagonists can modify the metabolism of cancer cells, which is related to the Warburg effect.[123-125]

4.9. PPAR and its associated genes as biomarkers for evaluating cancer therapy

The expression of PPAR and its associated genes is utilized as a biomarker to evaluate the effects of various cancer therapies. In HCC, molecular subtypes associated with the PPAR signaling pathway were identified through consensus clustering analyses. Based on this study, the authors developed a prognostic prediction model that relies on four gene signatures (*G6PD*, *SLC10A1*, *ABCC1*, and *PKIB*). These gene signatures are closely related to patient survival in HCC.[126] Zhang *et al*. validated a PPAR signaling pathway-based prognostic prediction model for uterine cervical cancer (UCC). They utilized the gene set enrichment analysis algorithm to calculate the PPAR scores of patients with cervical cancer. The study demonstrated that PPAR scores correlate with different sensitivities to immune checkpoint therapy. AC099568.2 was identified as a marker indicating the involvement of the PPAR pathway in patients with UCC.[127] The PPAR signaling pathway is also a potential biomarker for the detection of breast cancer. The study employed various bioinformatics and networking tools to identify 21 differentially expressed genes associated with the PPAR signaling pathway. The results indicated that four key genes – *RXRA*, *LPL*, *FABP4*, and *PPARG* – exhibited a high degree of interaction, suggesting that they may co-function in tumorigenesis by participating in the regulation of the PPAR signaling pathway.[128] Although the studies cited above have identified the use of PPAR-related proteins as biomarkers for cancer treatment, there are currently no studies that have identified biomarkers capable of detecting or explaining the effects of PPAR agonists on cancer progression and the efficacy of anticancer therapies utilizing PPAR agonists. In addition, further research is required to confirm the exact association between PPAR-related genes and cancer progression.

5. Conclusion

Due to its high morbidity and mortality rates, cancer has long been considered one of the most harmful illnesses. At present, combination therapy is widely recommended and practiced as a therapeutic intervention for cancer. One of the drugs suggested for use in combination therapy is PPAR agonists. PPAR agonists have shown significant promise in preventing tumor growth and metastasis in various cancers. Recent studies have elucidated the roles of PPAR ligands as adjuvants, helping to clarify their antitumor effects. PPAR ligands inhibit inflammation and immune responses, suppress cell proliferation, promote cell differentiation and apoptosis, and regulate fat and glucose metabolism. Therefore, it can be concluded that PPAR modulators do not play a primary role in the treatment of tumors but rather an auxiliary one. Despite their encouraging but paradoxical efficacy in reducing cancer metastasis and proliferation, PPAR ligands can increase tumor cell susceptibility to treatments such as radiation and chemotherapy. Among the several known PPAR agonists, only a few have been evaluated for their anticancer activity as adjuvants, whereas the anticancer activity of many other PPAR agonists remains unexplored. In addition, different types of cancer have distinct properties and may respond differently to PPAR agonists. However, such information is still lacking and represents a valuable area for further research.

Acknowledgments

None.

Funding

None.

Conflict of interest

The authors declare that they have no competing interest.

Author contributions

Conceptualization: S. R. Kaid Johar
Visualization: S. R. Kaid Johar
Writing–original draft: Binita Patel
Writing–review & editing: S. R. Kaid Johar

Ethics approval and consent to participate

Not applicable.

Consent for publication

Not applicable.

Availability of data

Not applicable.

References

1. Debela DT, Muzazu SG, Heraro KD, *et al*. New approaches and procedures for cancer treatment: Current perspectives. *SAGE Open Med*. 2021;9:20503121211034366.

   doi: 10.1177/20503121211034366

2. Yang C, Xia BR, Zhang ZC, Zhang YJ, Lou G, Jin WL. Immunotherapy for ovarian cancer: adjuvant, combination, and neoadjuvant. *Front Immunol*. 2020;11:577869.

   doi: 10.3389/fimmu.2020.577869

3. Lheureux S, Braunstein M, Oza AM. Epithelial ovarian cancer: Evolution of management in the era of precision medicine. *CA Cancer J Clin*. 2019;69(4):280-304.

doi: 10.3322/caac.21559

4. Wang ZB, Liu D, Lei G, Liu ZQ, Wu N, Wang J. Ovarian cancer-targeted medication: PARP inhibitors, anti-angiogenic drugs, immunotherapy, and more. *Front Pharmacol*. 2023;14:1222209.

   doi: 10.3389/fphar.2023.1222209

5. Padma VV. An overview of targeted cancer therapy. *Biomedicine* (*Taipei*). 2015;5(4):19.

   doi: 10.7603/s40681-015-0019-4

6. Lim ZF, Ma PC. Emerging insights of tumor heterogeneity and drug resistance mechanisms in lung cancer targeted therapy. *J Hematol Oncol*. 2019;12(1):134.

   doi: 10.1186/s13045-019-0818-2

7. Emran TB, Shahriar A, Mahmud AR, *et al*. Multidrug resistance in cancer: Understanding molecular mechanisms, immunoprevention and therapeutic approaches. *Front Oncol*. 2022;12:891652.

   doi: 10.3389/fonc.2022.891652

8. Safri F, Nguyen R, Zerehpooshnesfchi S, George J, Qiao L. Heterogeneity of hepatocellular carcinoma: From mechanisms to clinical implications. *Cancer Gene Ther*. 2024;31:1105-1112.

   doi: 10.1038/s41417-024-00764-w

9. Jackson C, Finikarides L, Freeman ALJ. The adverse effects of trastuzumab-containing regimes as a therapy in breast cancer: A piggy-back systematic review and meta-analysis. *PLoS One*. 2022;17(12):e0275321.

   doi: 10.1371/journal.pone.0275321

10. Shuel SL. Targeted cancer therapies: Clinical pearls for primary care. *Can Fam Physician*. 2022;68(7):515-518.

    doi: 10.46747/cfp.6807515

11. Levinson K, Dorigo O, Rubin K, Moore K. Immunotherapy in gynecologic cancers: What we know now and where we are headed. *Am Soc Clin Oncol Educ Book*. 2019;39:126-140.

    doi: 10.1200/EDBK_237967

12. Lobenwein D, Kocher F, Dobner S, Gollmann-Tepeköylü C, Holfeld J. Cardiotoxic mechanisms of cancer immunotherapy - A systematic review. *Int J Cardiol*. 2021;323:179-187.

    doi: 10.1016/j.ijcard.2020.08.033

13. Palaia I, Tomao F, Sassu CM, Musacchio L, Benedetti Panici P. immunotherapy for ovarian cancer: Recent advances and combination therapeutic approaches. *Onco Targets Ther*. 2020;13:6109-6129.

    doi: 10.2147/OTT.S205950

14. Muthukutty P, Woo HY, Ragothaman M, Yoo SY. Recent advances in cancer immunotherapy delivery modalities. *Pharmaceutics*. 2023;15(2):504.

    doi: 10.3390/pharmaceutics15020504

15. Li B, Jiang HY, Wang ZH, Ma YC, Bao YN, Jin Y. Effect of fenofibrate on proliferation of SMMC-7721 cells via regulating cell cycle. *Hum Exp Toxicol*. 2021;40(7):1208-1221.

    doi: 10.1177/0960327121991901

16. Jemal A, Siegel R, Ward E, Hao Y, Xu J, Thun MJ. Cancer statistics 2009. *CA Cancer J Clin*. 2009;59(4):225-249.

    doi: 10.3322/caac.20006

17. Gunthert AR, Grundker C, Hollmann K, Emons G. Luteinizing hormone-releasing hormone induces JunD-DNA binding and extends cell cycle in human ovarian cancer cells. *Biochem Biophys Res Commun*. 2002;294:11-15.

    doi: 10.1016/S0006-291X(02)00427-8

18. Gründker C, Emons G. The role of gonadotropin-releasing hormone in cancer cell proliferation and metastasis. *Front Endocrinol* (*Lausanne*). 2017;8:187.

    doi: 10.3389/fendo.2017.00187

19. Kara M, Ozcagli E, Fragkiadaki P, *et al*. Determination of DNA damage and telomerase activity in stanozolol-treated rats. *Exp Ther Med*. 2017;13(2):614-618.

    doi: 10.3892/etm.2016.3974

20. George A, McLachlan J, Tunariu N, *et al*. The role of hormonal therapy in patients with relapsed high-grade ovarian carcinoma: A retrospective series of tamoxifen and letrozole. *BMC Cancer*. 2017;17(1):456.

    doi: 10.1186/s12885-017-3440-0

21. Joseph JD, Lu N, Qian J, *et al*. A clinically relevant androgen receptor mutation confers resistance to second-generation antiandrogens enzalutamide and ARN-509. *Cancer Discov*. 2013;3(9):1020-1029.

    doi: 10.1158/2159-8290.CD-13-0226

22. Korpal M, Korn JM, Gao X, *et al*. An F876L mutation in androgen receptor confers genetic and phenotypic resistance to MDV3100 (enzalutamide). *Cancer Discov*. 2013;3(9):1030-1043.

    doi: 10.1158/2159-8290.CD-13-0142

23. Balbas MD, Evans MJ, Hosfield DJ, *et al*. Overcoming mutation-based resistance to antiandrogens with rational drug design. *Elife*. 2013;2:e00499.

    doi: 10.7554/eLife.00499

24. Feng LX, Li M, Liu YJ, Yang SM, Zhang N. Synergistic enhancement of cancer therapy using a combination of ceramide and docetaxel. *Int J Mol Sci*. 2014;15(3):4201-4220.

    doi: 10.3390/ijms15034201

25. Duarte D, Vale N. Evaluation of synergism in drug combinations and reference models for future orientations in oncology. *Curr Res Pharmacol Drug Discov*. 2022;3:100110.

doi: 10.1016/j.crphar.2022.100110

26. Rathaur P, Soni MN, Gelat B, Rawal R, Pandya HA, Johar K. Network pharmacology-based evaluation of natural compounds with paclitaxel for the treatment of metastatic breast cancer. *Toxicol Appl Pharmacol.* 2021;423:115576.

doi: 10.1016/j.taap.2021.115576

27. Rodrigues R, Duarte D, Vale N. Drug repurposing in cancer therapy: Influence of patient's genetic background in breast cancer treatment. *Int J Mol Sci*. 2022;23(8):4280.

doi: 10.3390/ijms23084280

28. Jourdan JP, Bureau R, Rochais C, Dallemagne P. Drug repositioning: A brief overview. *J Pharm Pharmacol.* 2020;72(9):1145-1151.

doi: 10.1111/jphp.13273

29. Oprea TI, Mestres J. Drug repurposing: Far beyond new targets for old drugs. *AAPS J*. 2012;14(4):759-763.

doi: 10.1208/s12248-012-9390-1

30. Patel B, Gelat B, Soni M, Rathaur P, Kaid Johar SR. Bioinformatics perspective of drug repurposing. *Curr Bioinform.* 2024;19(4):295-315.

doi: 10.2174/0115748936264692230921071504

31. Kulkarni VS, Alagarsamy V, Solomon VR, Jose PA, Murugesan S. Drug repurposing: An effective tool in modern drug discovery. *Russ J Bioorg Chem*. 2023;49(2):157-166.

doi: 10.1134/S1068162023020139

32. Botta M, Audano M, Sahebkar A, Sirtori CR, Mitro N, Ruscica M. PPAR agonists and metabolic syndrome: An established role? *Int J Mol Sci.* 2018;19(4):1197.

doi: 10.3390/ijms19041197

33. Mirza AZ, Althagafi II, Shamshad H. Role of PPAR receptor in different diseases and their ligands: Physiological importance and clinical implications. *Eur J Med* Chem. 2019;166:502-513.

doi: 10.1016/j.ejmech.2019.01.067

34. van Raalte DH, Li M, Pritchard PH, Wasan KM. Peroxisome proliferator-activated receptor (PPAR)-α: A pharmacological target with a promising future. *Pharm Res*. 2004;21:1531-1538.

doi: 10.1023/b: pham.0000041444.06122.8d

35. Corrales P, Vidal-Puig A, Medina-Gómez G. PPARs and metabolic disorders associated with challenged adipose tissue plasticity. *Int J Mol Sci.* 2018;19(7):2124.

doi: 10.3390/ijms19072124

36. Gross B, Pawlak M, Lefebvre P, Staels B. PPARs in obesity-induced T2DM, dyslipidaemia and NAFLD. *Nat Rev Endocrinol*. 2017;13(1):36-49.

doi: 10.1038/nrendo.2016.135.

37. Tyagi S, Gupta P, Saini AS, Kaushal C, Sharma S. The peroxisome proliferator-activated receptor: A family of nuclear receptors role in various diseases. *J Adv Pharm Technol Res.* 2011;2(4):236-240.

doi: 10.4103/2231-4040.90879

38. Tan Y, Wang M, Yang K, Chi T, Liao Z, Wei P. PPAR-α modulators as current and potential cancer treatments. *Front Oncol*. 2021;11:599995.

doi: 10.3389/fonc.2021.599995

39. Chi T, Wang M, Wang X, *et al*. PPAR-γ modulators as current and potential cancer treatments. *Front Oncol.* 2021;11:737776.

doi: 10.3389/fonc.2021.737776

40. Cheng HS, Tan WR, Low ZS, Marvalim C, Lee JYH, Tan NS. Exploration and development of PPAR modulators in health and disease: An update of clinical evidence. *Int J Mol Sci*. 2019;20(20):5055.

doi: 10.3390/ijms20205055

41. Kim SY, Kim MS, Lee MK, *et al*. PPAR-γ induces growth inhibition and apoptosis through upregulation of insulin-like growth factor-binding protein-3 in gastric cancer cells. *Braz J Med Biol Res.* 2015;48(3):226-233.

doi: 10.1590/1414-431X20144212

42. Skelhorne-Gross G, Nicol CJB. The key to unlocking the chemotherapeutic potential of PPAR-γ ligands: Having the right combination. *PPAR Res*. 2012;2012:946943.

doi: 10.1155/2012/946943

43. Panigrahy D, Kaipainen A, Huang S, *et al*. PPARα agonist fenofibrate suppresses tumor growth through direct and indirect angiogenesis inhibition. *Proc Natl Acad Sci*. 2008;105(3):985-990.

doi: 10.1073/pnas.0711281105

44. Rigano D, Sirignano C, Taglialatela-Scafati O. The potential of natural products for targeting PPARα. *Acta Pharm Sinica B*. 2017;7(4):427-438.

doi: 10.1016/j.apsb.2017.05.005

45. Chiarelli F, Marzio DD. Peroxisome proliferator-activated receptor-γ agonists and diabetes: Current evidence and future perspectives. *Vasc Health Risk Manag.* 2008;4(2):297-304.

doi: 10.2147/vhrm.s993

46. Ngoc LP, Man HY, Besselink H, Cam HD, Brouwer A, van der Burg B. Identification of PPAR-activating compounds in herbal and edible plants and fungi from Vietnam. *Ind Crops Prod*. 2019;129:195-200.

doi: 10.1016/j.indcrop.2018.12.003

47. Korbecki J, Bobiński R, Dutka M. Self-regulation of the inflammatory response by peroxisome proliferator-activated receptors. *Inflamm Res*. 2019;68:443-458.

doi: 10.1007/s00011-019-01231-1

48. Wu L, Guo C, Wu J. Therapeutic potential of PPARγ natural agonists in liver diseases. *J Cell Mol Med*. 2020;24(5):2736-2748.

doi: 10.1111/jcmm.15028

49. Park KS, Choi SH, Chung SS. Re-highlighting the action of PPARγ in treating metabolic diseases [version 1; referees: 2 approved]. *F1000Res*. 2018;7:1127.

doi: 10.12688/f1000research.14136.1

50. Wang L, Waltenberger B, Pferschy-Wenzig EM, *et al*. Natural product agonists of peroxisome proliferator-activated receptor gamma (PPARγ): A review. *Biochem Pharmacol*. 2014;92(1):73-89.

doi: 10.1016/j.bcp.2014.07.018

51. Lebovitz HE. Thiazolidinediones: The forgotten diabetes medications. *Curr Diab Rep*. 2019;19(12):151.

doi: 10.1007/s11892-019-1270-y

52. Krishnappa M, Patil K, Sharma S, *et al. Effectiveness of The PPAR Agonist Saroglitazar in Nonalcoholic Steatohepatitis: Positive Data from Preclinical and Clinical Studies*. Preprint (Version 1), Research Square; 2020.

doi: 10.21203/rs.3.rs-123364/v1

53. Harrity T, Farrelly D, Tieman A, *et al*. Muraglitazar, a novel dual (α/γ) peroxisome proliferator–activated receptor activator, improves diabetes and other metabolic abnormalities and preserves β-cell function in db/db mice. *Diabetes*. 2006;55(1):240-248.

doi: 10.1111/jcmm.15028

54. Fagerberg B, Edwards S, Halmos T, *et al*. Tesaglitazar, a novel dual peroxisome proliferator-activated receptor α/γ agonist, dose-dependently improves the metabolic abnormalities associated with insulin resistance in a non-diabetic population. *Diabetologia*. 2005;48:1716-1725.

doi: 10.1007/s00125-005-1846-8

55. Augimeri G, Giordano C, Gelsomino L, *et al*. The role of PPAR-γ ligands in breast cancer: From basic research to clinical studies. *Cancers* (*Basel*). 2020;12(9):2623.

doi: 10.3390/cancers12092623

56. Kim TW, Hong DW, Hong SH. CB13, a novel PPARγ ligand, overcomes radio-resistance via ROS generation and ER stress in human non-small cell lung cancer. *Cell Death Dis*. 2020;11(10):848.

doi: 10.1038/s41419-020-03065-w

57. Youssef J, Badr M. Peroxisome proliferator-activated receptors and cancer: Challenges and opportunities. *Br J Pharmacol*. 2011;164(1):68-82.

doi: 10.1111/j.1476-5381.2011.01383.x

58. Nguyen M, Shing Y, Folkman J. Quantitation of angiogenesis and antiangiogenesis in the chick embryo chorioallantoic membrane. *Microvasc Res*. 1994;47(1):31-40.

doi: 10.1006/mvre.1994.1003

59. Aviel-Ronen S, Blackhall FH, Shepherd FA, Tsao MS. K-ras mutations in non-small-cell lung carcinoma: A review. *Clin Lung Cancer*. 2006;8(1):30-38.

doi: 10.3816/CLC.2006.n.030

60. Girnun GD, Chen L, Silvaggi J, *et al*. Regression of drug-resistant lung cancer by the combination of rosiglitazone and carboplatin. *Clin Cancer Res*. 2008;14(20):6478-6486.

doi: 10.1158/1078-0432.CCR-08-1128

61. Xu YJ, Zheng Z, Cao C, Li J, Liu Y. Bioanalytical insights into the association between eicosanoids and pathogenesis of hepatocellular carcinoma. *Cancer Metastasis Rev*. 2018;37:269-277.

doi: 10.1007/s10555-018-9747-8

62. Panigrahy D, Kaipainen A, Greene ER, Huang S. Cytochrome P450-derived eicosanoids: the neglected pathway in cancer. *Cancer Metastasis Rev*. 2010;29:723-735.

doi: 10.1007/s10555-010-9264-x

63. Wu L, Wang W, Dai M, Li H, Chen C, Wang D. PPAR-α ligand, AVE8134, and cyclooxygenase inhibitor therapy synergistically suppress lung cancer growth and metastasis. *BMC Cancer*. 2019;19(1):1166.

doi: 10.1186/s12885-019-6379-5

64. Mustafa A, Kruger WD. Suppression of tumor formation by a cyclooxygenase-2 inhibitor and a peroxisome proliferator-activated receptor gamma agonist in an in vivo mouse model of spontaneous breast cancer. *Clin Cancer Res*. 2008;14(15):4935-4942.

doi: 10.1158/1078-0432.CCR-08-0958

65. Malakouti P, Mohammadi M, Boshagh MA, Amini A, Rezaee MA, Rahmani MR. Combined effects of pioglitazone and doxorubicin on migration and invasion of MDA-MB-231 breast cancer cells. *J Egypt Natl Canc Inst*. 2022;34(1):13.

doi: 10.1186/s43046-022-00110-x

66. Pfeffer CM, Singh ATK. Apoptosis: A target for anticancer therapy. *Int J Mol Sci*. 2018;19(2):448.

doi: 10.3390/ijms19020448

67. Elstner E, Müller C, Koshizuka K, *et al*. Ligands for peroxisome proliferator-activated receptorgamma and retinoic acid receptor inhibit growth and induce apoptosis of human breast cancer cells *in vitro* and in BNX mice. *Proc Natl Acad Sci U S A*. 1998;95(15):8806-8811.

doi: 10.1073/pnas.95.15.8806

68. Ramos-Nino ME, Littenberg B. A novel combination: ranpirnase and rosiglitazone induce a synergistic apoptotic effect by down-regulating Fra-1 and Survivin in cancer cells.

Mol Cancer Ther. 2008;7(7):1871-1879.

doi: 10.1158/1535-7163.MCT-08-0308

69. Miao R, Xu T, Liu L, *et al*. Rosiglitazone and retinoic acid inhibit proliferation and induce apoptosis in the HCT-15 human colorectal cancer cell line. *Exp Ther Med*. 2011;2(3):413-417.

doi: 10.3892/etm.2011.227

70. Cao LQ, Wang XL, Wang Q, *et al*. Rosiglitazone sensitizes hepatocellular carcinoma cell lines to 5-fluorouracil antitumor activity through activation of the PPARgamma signaling pathway. *Acta Pharmacol Sin*. 2009;30(9):1316-1322.

doi: 10.1038/aps.2009.119

71. Saidi SA, Holland CM, Charnock-Jones DS, Smith SK. *In vitro* and *in vivo* effects of the PPAR-alpha agonists fenofibrate and retinoic acid in endometrial cancer. *Mol Cancer*. 2006;5:13.

doi: 10.1186/1476-4598-5-13

72. Hamaguchi N, Hamada H, Miyoshi S, *et al*. *In vitro* and *in vivo* therapeutic efficacy of the PPAR-γ agonist troglitazone in combination with cisplatin against malignant pleural mesothelioma cell growth. *Cancer Sci*. 2010;101(9):1955-1964.

doi: 10.1111/j.1349-7006.2010.01632.x

73. Copland JA, Marlow LA, Kurakata S, *et al*. Novel high-affinity PPARgamma agonist alone and in combination with paclitaxel inhibits human anaplastic thyroid carcinoma tumor growth via p21WAF1/CIP1. *Oncogene*. 2006;25(16):2304-2317.

doi: 10.1038/sj.onc.1209267

74. Alqahtani QH, Alkharashi LA, Alajami H, Alkharashi I, Alkharashi L, Alhinti SN. Pioglitazone enhances cisplatin's impact on triple-negative breast cancer: Role of PPAR-γ in cell apoptosis. *Saudi Pharm J*. 2024;32(5):102059.

doi: 10.1016/j.jsps.2024.102059

75. Pouya FD, Salehi R, Rasmi Y, Kheradmand F, Fathi-Azarbayjani A. Combination chemotherapy against colorectal cancer cells: Co-delivery of capecitabine and pioglitazone hydrochloride by polycaprolactone-polyethylene glycol carriers. *Life Sci*. 2023;332:122083.

doi: 10.1016/j.lfs.2023.122083

76. Novikov NM, Zolotaryova SY, Gautreau AM, Denisov EV. Mutational drivers of cancer cell migration and invasion. *Br J Cancer*. 2021;124(1):102-114.

doi: 10.1038/s41416-020-01149-0

77. Wang Q, Peng H, Qi X, Wu M, Zhao X. Targeted therapies in gynecological cancers: A comprehensive review of clinical evidence. *Signal Transduct Target Ther*. 2020;5(1):137.

doi: 10.1038/s41392-020-0199-6

78. Lyon CM, Klinge DM, Do KC, *et al*. Rosiglitazone prevents the progression of preinvasive lung cancer in a murine model. *Carcinogenesis*. 2009;30(12):2095-2099.

doi: 10.1093/carcin/bgp260

79. Annicotte JS, Iankova I, Miard S, *et al*. Peroxisome proliferator-activated receptor gamma regulates E-cadherin expression and inhibits growth and invasion of prostate cancer. *Mol Cell Biol*. 2006;26(20):7561-7574.

doi: 10.1128/MCB.00605-06

80. Huang G, Yin L, Lan J, *et al*. Synergy between peroxisome proliferator-activated receptor γ agonist and radiotherapy in cancer. *Cancer Sci*. 2018;109(7):2243-2255.

doi: 10.1111/cas.13650

81. Chen X, Duan N, Zhang C, Zhang W. Survivin and tumorigenesis: Molecular mechanisms and therapeutic strategies. *J Cancer*. 2016;7(3):314.

doi: 10.7150/jca.13332

82. Bie Q, Dong H, Jin C, Zhang H, Zhang B. 15d-PGJ2 is a new hope for controlling tumor growth. *Am J Transl Res*. 2018;10(3):648-658.

83. Wang Y, Tan H, Xu D, *et al*. The combinatory effects of PPAR-γ agonist and survivin inhibition on the cancer stem-like phenotype and cell proliferation in bladder cancer cells. *Int J Mol Med*. 2014;34(1):262-268.

doi: 10.3892/ijmm.2014.1774

84. Nogueira V, Hay N. Molecular pathways: Reactive oxygen species homeostasis in cancer cells and implications for cancer therapy. *Clin Cancer Res*. 2013;19(16):4309-4314.

doi: 10.1158/1078-0432.CCR-12-1424

85. Arfin S, Jha NK, Jha SK, *et al*. Oxidative stress in cancer cell metabolism. *Antioxidants* (*Basel*). 2021;10(5):642.

doi: 10.3390/antiox10050642

86. Knopfová L, Smarda J. The use of Cox-2 and PPAR-γ signaling in anti-cancer therapies. *Exp Ther Med*. 2010;1(2):257-264.

doi: 10.3892/etm_00000040

87. Han EJ, Im CN, Park SH, Moon EY, Hong SH. Combined treatment with peroxisome proliferator-activated receptor (PPAR) gamma ligands and gamma radiation induces apoptosis by PPAR-γ-independent up-regulation of reactive oxygen species-induced deoxyribonucleic acid damage signals in non-small cell lung cancer cells. *Int J Radiat Oncol Biol Phys*. 2013;85(5):e239-e248.

doi: 10.1016/j.ijrobp.2012.11.040

88. Park BH, Lee SB, Stolz DB, Lee YJ, Lee BC. Synergistic interactions between heregulin and peroxisome proliferator-activated receptor-gamma (PPARgamma) agonist in breast cancer cells. *J Biol Chem*. 2011;286(22):20087-20099.

doi: 10.1074/jbc.M110.191718

89. Higuchi T, Sugisawa N, Miyake K, *et al*. Pioglitazone, an

agonist of PPAR-γ, reverses doxorubicin-resistance in an osteosarcoma patient-derived orthotopic xenograft model by downregulating P-glycoprotein expression. *Biomed Pharmacother*. 2019;118:109356.

doi: 10.1016/j.biopha.2019.109356

90. To KKW, Tomlinson B. Targeting the ABCG2-overexpressing multidrug resistant (MDR) cancer cells by PPAR-γ agonists. *Br J Pharmacol*. 2013;170(5):1137-1151.

doi: 10.1111/bph.12367

91. Zhang H, Jing X, Wu X, *et al*. Suppression of multidrug resistance by rosiglitazone treatment in human ovarian cancer cells through downregulation of FZD1 and MDR1 genes. *Anticancer Drugs*. 2015;26(7):706-715.

doi: 10.1097/CAD.0000000000000236

92. Bräutigam K, Biernath-Wüpping J, Bauerschlag DO, *et al*. Combined treatment with TRAIL and PPAR-γ ligands overcomes chemoresistance of ovarian cancer cell lines. *J Cancer Res Clin Oncol*. 2011;137(5):875-886.

doi: 10.1007/s00432-010-0952-2

93. Vallée A, Lecarpentier Y, Vallée JN. Targeting the canonical WNT/β-catenin pathway in cancer treatment using non-steroidal anti-inflammatory drugs. *Cells*. 2019;8(7):726.

doi: 10.3390/cells8070726

94. Chen L, Bush CR, Necela BM, *et al*. RS5444, a novel PPARγ agonist, regulates aspects of the differentiated phenotype in nontransformed intestinal epithelial cells. *Mol Cell Endocrinol*. 2006;251:17-32.

doi: 10.1016/j.mce.2006.02.006

95. Smallridge RC, Copland JA, Brose MS, *et al*. Efatutazone, an oral PPAR-γ agonist, in combination with paclitaxel in anaplastic thyroid cancer: Results of a multicenter phase 1 trial. *J Clin Endocrinol Metab*. 2013;98(6):2392-2400.

doi: 10.1210/jc.2013-1106

96. Marlow LA, Reynolds LA, Cleland AS, *et al*. Reactivation of suppressed RhoB is a critical step for the inhibition of anaplastic thyroid cancer growth. *Cancer Res*. 2009;69(4):1536-1544.

doi: 10.1158/0008-5472.CAN-08-3718

97. Pishvaian MJ, Marshall JL, Wagner AJ, *et al*. A phase 1 study of efatutazone, an oral peroxisome proliferator-activated receptor gamma agonist, administered to patients with advanced malignancies. *Cancer*. 2012;118(21):5403-5413.

doi: 10.1002/cncr.27526

98. Komatsu Y, Yoshino T, Yamazaki K, *et al*. Phase 1 study of efatutazone, a novel oral peroxisome proliferator-activated receptor gamma agonist, in combination with FOLFIRI as second-line therapy in patients with metastatic colorectal cancer. *Invest New Drugs*. 2014;32:473-480.

doi: 10.1007/s10637-013-0056-3

99. Hau P, Kunz-Schughart L, Bogdahn U, *et al*. Low-dose chemotherapy in combination with COX-2 inhibitors and PPAR-gamma agonists in recurrent high-grade gliomas-a phase II study. *Oncology*. 2008;73(1-2):21-25.

doi: 10.1159/000120028

100. Vogt T, Hafner C, Bross K, *et al*. Antiangiogenetic therapy with pioglitazone, rofecoxib, and metronomic trofosfamide in patients with advanced malignant vascular tumors. *Cancer*. 2003;98(10):2251-2256.

doi: 10.1002/cncr.11775

101. Reichle A, Bross K, Vogt T, *et al*. Pioglitazone and rofecoxib combined with angiostatically scheduled trofosfamide in the treatment of far-advanced melanoma and soft tissue sarcoma. *Cancer*. 2004;101(10):2247-2256.

doi: 10.1002/cncr.20574

102. Bahrambeigi S, Molaparast M, Sohrabi F, *et al*. Targeting PPAR ligands as possible approaches for metabolic reprogramming of T cells in cancer immunotherapy. *Immunol Lett*. 2020;220:32-37.

doi: 10.1016/j.imlet.2020.01.006

103. Odorizzi PM, Pauken KE, Paley MA, Sharpe A, Wherry EJ. Genetic absence of PD-1 promotes accumulation of terminally differentiated exhausted CD8+ T cells. *J Exp Med*. 2015;212(7):1125.

doi: 10.1084/jem.20142237

104. Tumeh PC, Harview CL, Yearley JH, *et al*. PD-1 blockade induces responses by inhibiting adaptive immune resistance. *Nature*. 2014;515(7528):568-571.

doi: 10.1016/j.ejca.2023.03.040

105. Zhang Y, Kurupati R, Liu L, *et al*. Enhancing CD8+ T cell fatty acid catabolism within a metabolically challenging tumor microenvironment increases the efficacy of melanoma immunotherapy. *Cancer Cell*. 2017;32(3):377-391.

doi: 10.1016/j.ccell.2017.08.004

106. Chowdhury PS, Chamoto K, Kumar A, Honjo T. PPAR-induced fatty acid oxidation in T cells increases the number of tumor-reactive CD8+ T cells and facilitates anti–PD-1 therapy. *Cancer Immunol Res*. 2018;6(11):1375-1387.

doi: 10.1158/2326-6066.CIR-18-0095

107. Han J, Alvarez-Breckenridge CA, Wang QE, Yu J. TGF-β signaling and its targeting for glioma treatment. *Am J Cancer Res*. 2015;5(3):945.

108. Coras R, Holsken A, Seufert S, *et al*. The peroxisome proliferator-activated receptor-γ agonist troglitazone inhibits transforming growth factor-β–mediated glioma cell migration and brain invasion. *Mol Cancer Ther*. 2007;6(6):1745-1754.

doi: 10.1158/1535-7163.MCT-06-0763

109. Tran TT, Uhl M, Ma JY, *et al*. Inhibiting TGF-β signaling restores immune surveillance in the SMA-560 glioma model. *Neuro Oncol*. 2007;9(3):259-270.

doi: 10.1215/15228517-2007-010

110. Papi A, De Carolis S, Bertoni S, *et al*. PPARγ and RXR ligands disrupt the inflammatory cross-talk in the hypoxic breast cancer stem cells niche. *J Cell Physiol*. 2014;229(11):1595-1606.

doi: 10.1002/jcp.24601

111. Rovito D, Gionfriddo G, Barone I, *et al*. Ligand-activated PPARγ downregulates CXCR4 gene expression through a novel identified PPAR response element and inhibits breast cancer progression. *Oncotarget*. 2016;7(40):65109.

doi: 10.18632/oncotarget.11371

112. Wang N, Wang S, Wang X, *et al*. Research trends in pharmacological modulation of tumor-associated macrophages. *Clin Transl Med*. 2021;11(1):e288.

doi: 10.1002/ctm2.288

113. Penas F, Mirkin GA, Vera M, *et al*. Treatment *in vitro* with PPARα and PPARγ ligands drives M1-to-M2 polarization of macrophages from T. cruzi-infected mice. *Biochim Biophys Acta*. 2015;1852(5):893-904.

doi: 10.1016/j.bbadis.2014.12.019

114. Souza-Moreira L, Soares VC, Dias SD, Bozza PT. Adipose-derived mesenchymal stromal cells modulate lipid metabolism and lipid droplet biogenesis via AKT/mTOR–PPARγ signalling in macrophages. *Sci Rep.* 2019;9(1):20304.

doi: 10.1038/s41598-019-56835-8

115. Gionfriddo G, Plastina P, Augimeri G, *et al*. Modulating tumor-associated macrophage polarization by synthetic and natural PPARγ ligands as a potential target in breast cancer. *Cells*. 2020;9(1):174.

doi: 10.3390/cells9010174

116. Christofides A, Konstantinidou E, Jani C, Boussiotis VA. The role of peroxisome proliferator-activated receptors (PPAR) in immune responses. *Metabolism*. 2021;114:154338.

doi: 10.1016/j.metabol.2020.154338

117. Sun J, Yu L, Qu X, Huang T. The role of peroxisome proliferator-activated receptors in the tumor microenvironment, tumor cell metabolism, and anticancer therapy. *Front Pharmacol*. 2023;14:1184794.

doi: 10.3389/fphar.2023.1184794

118. Nayak A, Warrier NM, Kumar P. Cancer stem cells and the tumor microenvironment: Targeting the critical crosstalk through nanocarrier systems. *Stem Cell Rev Rep.* 2022;18(7):2209-2233.

doi: 10.1007/s12015-022-10426-9

119. Min JY, Kim DH. Stearoyl-CoA desaturase 1 as a therapeutic biomarker: Focusing on cancer stem cells. *Int J Mol Sci*. 2023;24(10):8951.

doi: 10.3390/ijms24108951

120. Ma XL, Sun YF, Wang BL, *et al*. Sphere-forming culture enriches liver cancer stem cells and reveals Stearoyl-CoA desaturase 1 as a potential therapeutic target. *BMC Cancer*. 2019;19:1-2.

doi: 10.1186/s12885-019-5963-z

121. Altman BJ, Stine ZE, Dang CV. From Krebs to clinic: Glutamine metabolism to cancer therapy. *Nat Rev Cancer*. 2016;16(10):619-634.

doi: 10.1038/nrc.2016.114

122. Hay N. Reprogramming glucose metabolism in cancer: Can it be exploited for cancer therapy? *Nat Rev Cancer*. 2016;16(10):635-649.

doi: 10.1038/nrc.2016.77

123. Luo X, Cheng C, Tan Z, *et al*. Emerging roles of lipid metabolism in cancer metastasis. *Mol Cancer*. 2017;16(1):76.

doi: 10.1186/s12943-017-0646-3

124. Vamecq J, Colet JM, Vanden Eynde JJ, Briand G, Porchet N, Rocchi S. PPARs: interference with Warburg' effect and clinical anticancer trials. *PPAR Res*. 2012;2012(1):304760.

doi: 10.1155/2012/304760

125. Antonosante A, d'Angelo M, Castelli V, *et al*. The involvement of PPARs in the peculiar energetic metabolism of tumor cells. *Int J Mol Sci*. 2018;19(7):1907.

doi: 10.3390/ijms19071907

126. Shi Q, Zeng Y, Xue C, Chu Q, Yuan X, Li L. Development of a promising PPAR signaling pathway-related prognostic prediction model for hepatocellular carcinoma. *Sci Rep.* 2024 Feb 28;14(1):4926.

doi: 10.1038/s41598-024-55086-6

127. Zhang Y, Li X, Zhang J, *et al*. Development and validation of the promising PPAR signaling pathway-based prognostic prediction model in uterine cervical cancer. *PPAR Res*. 2023;2023(1):4962460.

doi: 10.1155/2023/4962460

128. Wang H, Yang Y, Luo Q, *et al*. The PPAR signaling pathway as a potential biomarker for the diagnosis of breast cancer. *Int J Clin Exp Med*. 2019;12(6):7327-7336.

ACCSCIENCE PUBLISHING

Tumor Discovery

REVIEW ARTICLE

Targeting the interplay between biomolecular condensates and regulatory RNAs in cancer

Palmiro Poltronieri[1]* and Sudipta Joardar[2]

[1]National Research Council of Italy, Department of Agrofood, Institute of Sciences of Food Productions, CNR-ISPA, Lecce, Apulia, Italy

[2]Autonomous University of Barcelona, Center for Research in Agricultural Genomics, Cerdanyola Del Valles, Barcelona, Spain

Abstract

Biomolecular condensates (BCs), RNA–protein complexes, have emerged as potential therapeutic targets for various cellular pathologies, including cancer. The mechanisms underlying liquid–liquid phase separation rely on the properties of proteins with intrinsically disordered regions and prion-like domains, which drive phase separation in conjunction with their RNA partners. These ribonucleoprotein complexes are distinct in their localization, compartmentalization, epigenetic regulation, and dynamics. BCs are categorized as either nuclear—such as promyelocytic leukemia nuclear bodies, speckles, paraspeckles, and Cajal bodies—or cytosolic, including stress granules (SGs), P bodies, and U bodies. Regulatory RNAs, assembled with protein partners through phase separation, exhibit oncogenic properties and perform key biological functions, including gene transcription, euchromatin/heterochromatin formation, mRNA splicing, mRNA translation, protein compartmentalization, and degradation. Epitranscriptome-modifying enzymes regulate the stability and oncogenic potential of noncoding RNAs (ncRNAs). These RNAs, along with their associated epitranscriptomic and protein modifications, play critical roles in the functioning and dissolution of condensates. Recent advancements in cancer therapy have focused on developing drugs targeting the epitranscriptomic machinery, including the writers, readers, and erasers of RNA modifications. Therapeutic strategies aim to target oncogenic RNAs, tumor-promoting proteins, and RNA–protein interaction domains. Several cancer therapeutic compounds have been developed using the PROTAC and RIBOTAC approaches. Moreover, small molecules targeting protein–RNA interactions and antisense oligonucleotides have been developed. Promising avenues in cancer therapeutics involve the inhibition of ncRNAs and their associated protein complexes, modulation of BCs, regulation of SGs and paraspeckles, and development of small molecule compounds with potential applications across various cancer types.

Keywords: Biomolecular condensates; Noncoding RNAs; RNA–protein interactions; Therapeutic targets; Cancer; Epitranscriptomics; Epigenetics

***Corresponding author:**
Palmiro Poltronieri
(palmiro.poltronieri@ispa.cnr.it)

Citation: Poltronieri P, Joardar S. Targeting the interplay between biomolecular condensates and regulatory RNAs in cancer. *Tumor Discov.* 2024;3(4):4657. doi: 10.36922/td.4657

Received: August 26, 2024

Accepted: October 25, 2024

Published Online: December 6, 2024

1. Introduction

Biomolecular condensates (BCs) are membraneless organelles (MLOs) that are crucial for intricate cellular biochemical reactions. Condensates within the nucleus include the

nucleolus and various ribonucleoprotein (RNP) granules, such as promyelocytic leukemia (PML) nuclear bodies, speckles, paraspeckles, Cajal bodies, DNA damage foci, and processing (P) bodies. In contrast, U bodies, stress granules (SGs), signalosomes, and the pyrenoid are found outside the nucleus. A single protein capable of simultaneously interacting with multiple copies of itself drives homotypic phase separation, whereas interaction with multiple other biomolecules leads to heterotypic phase separation, as observed in RNA–protein complexes.[1,2] Figure 1 illustrates a schematic of various MLOs and their cellular localization. In heterotypic phase separation, a molecule interacts with various biomolecules to aggregate and undergo liquid–liquid phase separation (LLPS). The structure of RNA and similar polymers, such as poly-ADP ribose (PAR), plays a pivotal role in determining the dense-phase identity within condensates.[3,4] RNA involvement in condensate formation near enhancers or promoters suggests regulatory roles of noncoding RNAs (ncRNAs). BCs are various, and this review discusses Bcs formed by ncRNAS and proteins.[3,5]

The role of RNA in condensates holds therapeutic potential, enabling innovative applications such as active ribozymes. The role of altered phase separation, oncogenic RNAs, and BC-forming proteins in cancer is well established.[6-13] Targeting condensates in cancer therapy aims to address condensatopathies, impair aberrant formation, inhibit target functions, and deliver drugs. This review focuses on the significance of BC formation, oncogenic RNAs, and RNAs, modified epigenetically or epigenetically and epitranscriptome regulation relevant to the field of cancer cell biology.

2. BC localization and compartmentalization

There are five mechanisms of messenger RNA (mRNA) localization: (1) diffusion and local entrapment, (2) stabilization and controlled degradation, (3) active transport by molecular motors, (4) vesicular trafficking through endosomes, and (5) integration into BCs.[13-17] A RNP particle undergoes various transitions throughout its lifetime; it leaves transcription sites, reaches nuclear speckles for splicing, moves into the cytoplasm through the nuclear pore, and appears in the cytoplasmic granules of specific cells. These granules include transport granules, P bodies for degradation, and SGs under stress conditions.[3,11] Collectively, these miniature LLPS structures are referred to as BCs.[12-14] Localized condensates consist of components that anchor the structure to specific functional cellular locations. For instance, in nuclei, proteins may bind to specific DNA or RNA sequences to form BCs, whereas in the cytoplasm, BCs are often located near the membrane.[15,16]

Compartmentalization is a critical determinant in achieving high local concentrations of biomolecules and their substrates while excluding functionally irrelevant molecules.[17-19] Another contributing factor is transcriptional bursting, during which a BC located in the promoter region of a gene can recruit RNA polymerase molecules.[20,21] Over short time frames, condensates can rapidly form

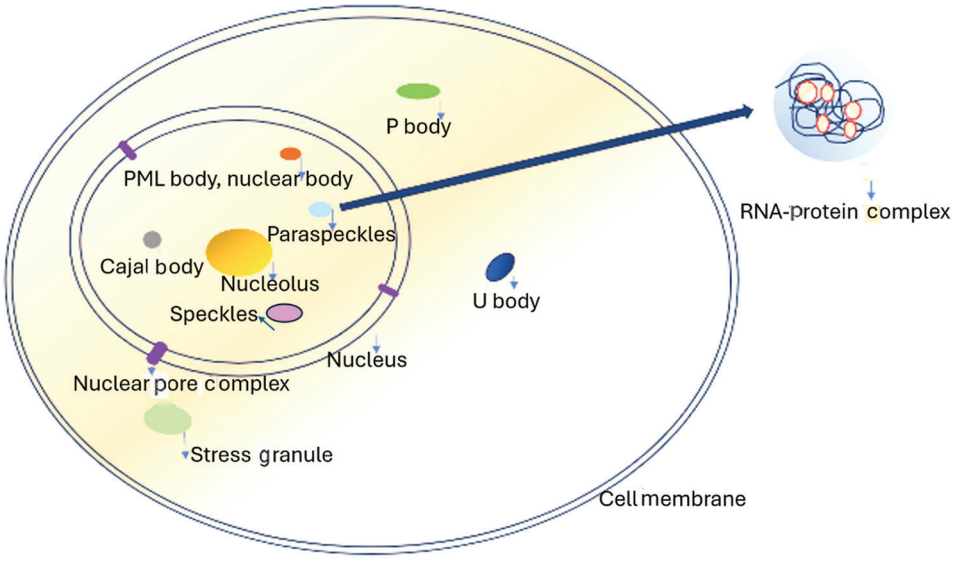

Figure 1. Occurrence of different biomolecular condensates inside the nucleus (promyelocytic leukemia nuclear bodies, paraspeckles, and Cajal bodies) and outside the nucleus (stress granules, P bodies, and U bodies). As an example, an RNA–protein complex representing a paraspeckle is marked outside the cell. Image created by the authors

and dissolve, providing cells with a mechanism to create temporary compartments. This allows biomolecules to be released and relocated when no longer needed at a specific site.[15] Furthermore, compartmentalization within condensates helps stabilize protein concentrations in cells, acting as a buffer against the inherent stochasticity of gene expression.[16-18]

2.1. Interactions between amino acids of protein partners and the role of post-translational modification (PTM)

In the nucleus, chromatin subdomains can undergo liquid–liquid phase separation driven by the IDRs of histone tails, leading to the formation of dense and dynamic droplets. Various proteins contribute to the aberrant formation of protein aggregates. These proteins often contain prion-like domains (PrLDs) enriched in uncharged polar amino acids, such as asparagine, glutamine, tyrosine, and glycine, which are essential for phase separation. One such protein is fused in sarcoma (FUS), which can self-assemble in paraspeckles. FUS, similar to TAR DNA-binding protein 43 (TDP-43), contains IDRs and PrLDs that drive protein aggregation within SGs, as observed in neurodegenerative diseases.[12,14,16] The tumor suppressor p53 protein is prone to amyloid-like aggregation, especially in its mutated forms, and the p53-MDM2 interaction is influenced by the presence of IDRs. Tau protein, which localizes in SGs and is relevant to Alzheimer's disease development, can also undergo LLPS.

Oppositely charged species regulate condensate formation based on RNA levels: low RNA levels promote formation, while excessive RNA levels trigger dissolution. Transcription and condensates create a feedback loop where short-lived RNA enhances condensate formation, and high RNA levels induce dissolution.[17,19] The phase separation of RNA-binding proteins depends on RNA length.[20] RNA structure determines dense-phase identity within BCs. For instance, Whi3, an ER-associated protein with a C-terminal RNA recognition motif (RRM), forms distinct RNA granules based on RNA structural differences, demonstrating RNA specificity.[21]

Lysines play a significant role in the condensation of BCs. This was studied in Alzheimer's-associated Tau protein, which exhibits a distinct phase separation mechanism compared with Tau/RNA coacervation.[22] Ukmar-Godec *et al.*[23] explored the role of lysine in disordered protein regions within P bodies, highlighting its ability to drive phase separation and form lysine/RNA coacervates. Glycine enhances fluidity, whereas glutamine and serine promote hardening. Amino acids such as arginine exhibit distinct properties in protein condensates, such as cation–π interactions between tyrosine and arginine as well as Coulomb interactions with the phosphate groups of nucleic acids. PTMs, including tyrosine and serine phosphorylation and arginine methylation, regulate LLPS. Arginine methyltransferases methylate the charged guanidine group of arginine, altering or inhibiting the electrostatic interactions required for phase separation. PTMs often accelerate LLPS by facilitating biorecognition, conformational changes, electrostatic interactions, and local accumulation of negative charges. Lysine ubiquitination increases Tau's propensity to form BCs but weakens Tau/RNA interactions. Conversely, lysine acetylation reverses LLPS, reducing Tau's localization in SGs. Tau acetylation blocks phase transition by neutralizing lysine-positive charges, thereby interrupting the electrostatic interactions between Tau residues and microtubules. Heterogeneous ubiquitination stabilizes droplets against dissolution.[24-26] Tau undergoes LLPS with DNA, mononucleosomes, and nucleosome arrays under low-salt conditions and localizes within droplets formed by nucleosomes and phosphorylated HP1α. Aberrant Tau hyperphosphorylation disrupts chromatin interactions and LLPS formation.[26] PTMs and RNA and protein modifications can influence condensate behavior.[24-26]

2.2. ncRNAs and small RNAs

Cellular RNA transcripts include mRNAs, rRNAs, tRNAs, and ncRNAs. Small RNAs include microRNAs (miRNAs), which are 22 nucleotides in length and play roles in the post-transcriptional control of target mRNAs, small interfering RNAs (SiRNAs), trans-acting small interfering RNAs (tasi-RNAs), and small nucleolar RNAs (sno-RNAs). Non-small RNAs include circular RNAs, noncapped RNAs (nap-RNAs), which are involved in gene expression regulation, and ncRNAs exceeding 500 nucleotides in length.

The majority of transcribed RNAs are functional.[27,28] Studies on RNA have employed siRNA libraries for high-throughput silencing of many ncRNAs as well as chromatin immunoprecipitation and RNA immunoprecipitation (RNA-IP) methods combined with next-generation sequencing to explore RNA functionality.[28] RNA modifications, such as 5′-end capping and polyadenylation (polyA tails), are essential for RNA localization and function. In addition, RNAs undergo epigenetic modifications, including those mediated by adenine deaminase and nucleotide-methylating enzymes.[27,29] These RNA modifications are transient and include methylation of adenine (m6A, m1A), cytosine (m6C), and guanine (m7G) as well as acetylation of adenine (ac4A).[27,30-32] These modifications can alter base pairing, reduce the affinity for complementary sequences, or mask target sites on proteins or mRNAs.

2.3. ncRNAs are required for LLPS, BC formation, and BC activity

ncRNAs, polyadenylated or nonpolyadenylated, perform diverse genome-regulatory functions, including encoding of micropeptides and miRNAs as well as acting as decoys for DNA–protein interactions. For example, p21-associated RNA DNA damage-activated (PANDA) acts as a decoy for nuclear transcription factor Y subunit-α (NF-YA), sequestering NF-YA from target gene promoters. ncRNAs can also function as miRNA sponges, sequestering miRNAs away from their mRNA targets. Both linear ncRNAs and circular RNAs (circRNAs) function as RNA sponges and compete endogenous RNAs (ceRNAs). CircRNAs are deregulated in various cancers (https://ngdc.cncb.ac.cn/circatlas/disease.php) and primarily function as RNA sponges, influencing target miRNAs based on cell type and miRNA expression profiles. The mechanism involves the interaction of three partners: circRNA/miRNA/protein target. miRNAs downregulate mRNA and target protein levels, whereas circRNAs block miRNAs through complementarity. Increased levels of miRNAs reduce target protein levels by blocking or degrading target mRNAs. Similar to ncRNAs, circRNAs may act as decoys, protecting amino acids in interacting partners from modifications or degradation or sequestering partners to prevent interactions with other proteins. These interactions are stoichiometric for ceRNAs and super-stoichiometric for RNA sponges. RNA sponges and RNA decoys are not discussed further here. CircRNAs, devoid of a 5′-cap structure and a 3′ poly(A) tail, are generated through a back-splicing process and can be translated through 5′ cap-independent internal translation initiation. In some cases, circRNAs are produced from protein-coding genes, such as circBRD7, derived from the bromodomain protein BRD7. Adenine methylation (m6A) modifications occur in ncRNAs, circRNAs, and protein-coding mRNAs. However, circRNA m6A methylation is more variable and occurs randomly, whereas ncRNA m6A methylation is more stable and tumor-type specific. Specific cases of circRNA functioning in the epigenetic regulation of transcription and its relationship with m6A modifications in cancer will be discussed in the following sections. RNAs have been found to act as oncogenes, contributing to cell proliferation and activation of oncogenic signals through overexpression or increased stability. Conversely, RNAs can function as tumor suppressors, blocking oncogenic signaling depending on the cellular context and specific functions (e.g., sponging oncogenic miRNAs, silencing promoters of genes involved in cell cycle regulation, proliferation, or antiapoptotic function). These tumor-suppressive RNAs are often downregulated in tumors.

In the formation of local condensates, ncRNAs can assemble proteins into chromatin-regulating complexes[33,34] and DNA damage repair complexes.[35]

In the following paragraphs, the roles of ncRNAs in cancer development will be described from the perspective of potential therapeutic approaches. RNA–protein complexes determine local LLPS and regulate cellular physiology and pathology. Local compartmentalization within BC loci is a critical determinant that facilitates the high local concentration of biomolecules and their substrates while excluding functionally irrelevant molecules.

Specific pathways and cellular responses that determine LLPS formation and function include mRNA transcription, mRNA splicing in speckles and paraspeckles, orchestration of chromatin domains, the DNA damage response in the nucleus, and stress responses through the formation of SGs in the cytoplasm. Unique ncRNAs are essential for the formation of certain BCs. For instance, NEAT1_2 is crucial for paraspeckle formation, whereas MALAT1 is recruited to speckles through interactions with multiple splicing-associated proteins, although it is not essential for speckle formation. These BCs, including speckles and paraspeckles, play vital roles in transcription and splicing. Specific pathways and cellular responses, such as the formation of euchromatin and heterochromatin and the activation or silencing of genes, rely on LLPS. These events occur through riboprotein complexes involved in assembling histone locus bodies and other BCs associated with chromatin regulation. In the nucleus, chromatin subdomains can undergo liquid–liquid phase separation driven by the IDRs of histone tails. This process results in the formation of dense, dynamic droplets, including histone locus bodies.

A significant number of ncRNAs function in concert with protein complexes to guide chromatin-modifying complexes to genomic sites. Polycomb (PcG) repressive complexes (PRC1 and PRC2) are involved in gene silencing, while mixed-lineage leukemia 1 (MLL) complexes promote gene activation. PRC2 represses genes by depositing repressive histone marks, such as H3K27me3 and H3K9me3, which lead to the formation of heterochromatin. Conversely, activating complexes deposit marks like H3K4me3 and H3K36me3, facilitating euchromatin formation. NcRNAs that serve as scaffolds for chromatin-modifying complexes guide these complexes to target genomic loci. In other cases, ncRNAs prevent chromatin-modifying complexes from recognizing specific gene promoters.

Histone marks are recognized by enzyme readers, including chromodomain, Tudor domain, PWWP domain, and PHD domain-containing enzymes. Bromodomain-containing protein 4 (BRD4) is an acetylated histone reader

at actively transcribed genes. It induces phase separation, leading to droplets with distinct physical properties. Acetylation of chromatin promotes a unique phase-separated state, with droplets that exhibit specific physical characteristics.[27] Acetylated chromatin is immiscible with heterochromatin containing non-acetylated chromatin. This property reflects the segregation of chromatin into subdomains within the cell. Chromatin forms phase-separated condensates, grouping regions with modified and unmodified chromatin states.

Repressed genes are located in heterochromatin regions marked by H3K27 methylation and non-acetylated nucleosomes, whereas active genes are associated with acetylated nucleosomes in euchromatin. Euchromatin and heterochromatin regions remain dynamically accessible to regulation by chromatin-modifying enzymes and protein readers of modified nucleosomes.[36,37]

Chrom-Seq methods utilize biotinylation tags combined with peptides that localize to specific chromatin regions and histone marks. One example is the mouse CBX7 peptide (containing a chromodomain between amino acids 2 and 76), and another is the Drosophila polycomb (dPC) protein. Fan *et al.*[38] used the Chrom-Seq method to identify RNAs proximal to H3K27me3 marks and validated their findings using RNA-IP quantitative PCR (RIP-qPCR). They identified 542 H3K27me3-associated ncRNAs. These histone marks define transcribed loci on euchromatin. Other ncRNAs that associate with H3K9me3 marks indicate repressed genes on heterochromatin. In some cases, ncRNAs are associated with both active and repressive PTMs; such ncRNAs are known as bivalent chromatin-associated RNAs. Double-site–interacting RNAs, which localize to both H4K20me3 and H3K4me3 marks, play roles in chromatin organization and RNA processing. H4K20me3-interacting RNAs are linked to cell differentiation, whereas H3K4me3-interacting RNAs are associated with metabolism and RNA processing.[36] H4K20me3 has been recognized as a key epigenetic regulator of chromatin structure and disease.[37]

A schematic summary of the various roles of ncRNAs in BC functioning is presented in a series of tables. Several of these ncRNAs have been the subject of cancer-related studies.[39] Tables 1-3 describe ncRNAs that act alongside protein complexes, guiding them to the target gene sites. Table 1 outlines ncRNAs involved in chromatin regulation, which guide Polycomb (PcG) repressive complexes (PRC) in PcG bodies to specific gene promoters for silencing. Table 2 describes ncRNAs that guide DNMT1 for CpG methylation at specific promoters. Table 3 details ncRNAs that guide chromatin-activating complexes and histone modification enzymes for gene activation.

3. NEAT1 and paraspeckles

Speckles and parapeckles regulate protein complexes competing with oncogene signaling. For instance, the interaction between sirtuin1 (SIRT1) and deleted in breast cancer 1 (DBC1), which then releases SIRT1 and enhances its deacetylation activity on p53. Consequently, the deacetylation of p53 reduces the transcription of its downstream target genes and promotes cell proliferation.[102] Paraspeckles are nuclear BCs that appear as chains of spheroids.[103-107] They involve over 60 proteins[106] and one RNA, namely, nuclear paraspeckle assembly transcript 1 (NEAT1). There are two variants of NEAT1: NEAT1_1, which is 3.7 kb in length, and NEAT1_2, which is 23 kb in length. Nascent 2,300-nucleotide–long NEAT1_2 transcripts recruit nuclear RNA-binding proteins to construct paraspeckles. NEAT1_2 is regulated by p53 and is a direct target of p53.[108] It is induced by stress related to DNA damage and replication stress.[109] NEAT1_1 is associated with cancer metabolism, enhanced glycolysis, and the Warburg effect.[110] NEAT1_2, which is essential for paraspeckle formation, recruits and retains proteins required for their assembly and is particularly noteworthy due to its presence in different variants.[105] NEAT1_2 is expressed in up to 50 copies per paraspeckle. The number of paraspeckles in a cell varies by cell type, with HeLa cells containing 13 – 17 foci/nucleus and NIH3T3 mouse fibroblasts containing 5 – 10 foci/nucleus.[106] Eight proteins are critical for paraspeckle nucleation: non-POU domain-containing octamer binding (NONO); splicing factor rich in proline and glutamine (SFPQ); paraspeckle protein component 1 (PSPC1); heterogeneous nuclear RNPs HNRNPA1, HNRNPA2, HNRNPK, and HNRNPH3; fused in sarcoma (FUS); DAZAP1; Brahma homolog component of SWI/SNF (BRG1); and the RNA-binding protein RBM14 (Figure 2). Notably, knockdown of these critical proteins leads to paraspeckle disintegration.[106]

In a search for paraspeckle modulators, An *et al.* identified several dual PI3K/mTOR inhibitors—Torin 1, PP242, LY3023414 (samotolisib), and INK128-as potent negative modulators of paraspeckles.[96] Rapamycin kinase T (ORK) inhibitors were also shown to inhibit PI3K. Additional dual PI3K/mTOR inhibitors, such as GSK1059615 and CAY10626, as well as the PI3K/mTOR/DNA-PK inhibitor PI-103, which has been used in clinical trials for chronic lymphocytic leukemia (CLL), similarly reduced either the NEAT1_2 area or the number of paraspeckles.

NEAT1_2-dependent clusters influence the interaction of proteins like FUS, which aggregate around RNA, with the RNA-binding protein RBP14 and paraspeckle proteins PSPC1, NONO, and SFPQ. During tumor progression, NEAT1_2, along with NONO, RBM14, and PSPC1, is

Table 1. RNAs that inhibit gene expression through PRC2 binding and deposition of H3K27me marks

Gene	Partner	Target	Modification	Tumor	References
LINC01133	EZH2, LSD1	KLF2, p21, E-cadherin	H3K27me	NSCLC	40
ANRIL-CDKN2B-AS1	PRC1–CBX7, PRC1	P14arf, p16ink4	H3K27me	-	41
LL22NC03-N64E9.1	PRC2	KLF2	H3K27me	CRC	42
HOTTIP	CTCF, DNMT1	MTUS1	-	NSCLC	43
ARHGAP27P1	PRC2	CDKIs p15, p16	H3K27me	-	44
SNHG7	PRC2	CDKIs	H3K27me	ovary	45
TUG1	PRC2	KLF2	H3K27me	HCC	46
SNHG6	PRC2	P21, KLF2	H3K27me	Osteosarcoma	47
DUXAP8	EZH2, LSD1	CDK1A, KLF2	H3K27me	Pancreas	48
SNHG20	PRC2	CDKis	H3K27me	NSCLC	49
PVT1	EZH2	miR-200b	H3K27me	Cervical cancer	50,51
UCA1	PRC2	P27	H3K27me	Breast cancer	52
MYLK-AS1	PRC2	LATS2	H3K27me	Gastric	53
HOXA-AS2	EZH2, LSD1	P21, KLF2	H3K27me	Colorectal	54
SNHG17	PRC2	CDKIs	H3K27me	Gastric	55
CHASERR, HASTER	unknown	Transcription factors CHD2 chromatin remodeler	-	Various	56
GIHCG	EZH2, DNMT1	miR-200b/a/429	H3K27me CpGme	Hepatocell HCC renal cell cancer	57
PVT1	PRC2	Apoptotic genes	H3K27me	MM	58
NEAT1	BRG1, SWI/SNF	GADD45A	Silencing	GC	59
LINC00675	LSD1	SPRY4	H3K4me2 demethylated	GC	57
HOXA11-AS	EZH2, LSD1, DNMT1	KLF2, PRSS8	H3K27 me3, H3K4 me demethylation	-	57
BST2/BISPR	-	Tetherin	Positive regulator of BST2/tetherin	Antiviral	57
SNHG12	HDAC9	miR-320a downregulated	Resistance to doxorubicin carboplatin sunitinib and temozolomide	OC, Osteosarcoma	60,61
SNHG13/DANCR	KAT6A (H3K23ac), EZH2	CDK inhibitors	-	CRC, endocrine cancers	62
SNHG14, SNHG15	EZH2, PRC2	-	-	Endocrine cancers	63
lincRNA-CMPK2, NRAV/NRIR	-	Block IFN response, downregulate IRENA	Stop protumor inflammatory cytokines	Macrophage antitumor response	64
FEZF2-AS1	LSD1	p21	H3K4me2	Gastric cancer	65
*LINC*0144660	LSD1	RASD1	Suppression by demethylating H3K4	Gastric cancer	66
SNHG22	EZH2	-	-	.	67
ATRX	EZH2	Xist targets	H3K27me	Chromatid silencing	68
XIST	PRC2, SMRT TRIM28, SHARP, HDAC3	RNA Pol II exclusion	Histone deacetylation	X chromosome silencing	69

(Cont'd...)

Table 1. ***(Continued)***

Gene	Partner	Target	Modification	Tumor	References
FIRRE	HnRNP U	X chromosome	H3K27me	Set up of specific chromosomal domains	70
CASC11	EZH2	PTEN	H3K27me	CRC, HCC	71
LNMAT1	EZH2	CADM	H3K27me	Melanoma	72,73
ZFAT-AS1	PRC2	CDX2	H3K27me	Glioma	74
LINC01271 (*MaTAR25*)	PUB	Tensin 1 promoter	Upregulates tensin 1 in focal adhesions, affecting migration	CRC, BC	64,75

Abbreviations: ANRIL: Antisense noncoding RNA in the INK4 locus; ARHGAP27: Rho GTPase activating protein 27, antisense. CASC11: Cancer susceptibility 11; CHASERR: CHD2 Adjacent suppressive regulatory RNA; FIRRE: Functional intergenic repeating RNA element; GIHCG: Gradually increased during hepatocarcinogenesis; IRENA: IFN-responsive nuclear factor-κB activator; LINC01271: Mammary tumor associated RNA 25 (MaTAR25) homolog; LNMAT1: Long noncoding RNA lymph node metastasis-associated transcript 1; NRAV/NRIR: Negative regulator of antiviral response; NRIR: PVT1: Plasmacytoma variant translocation 1; HOXA-AS: Homeobox gene A, antisense; HOTTIP: HOXA transcript at the distal tip; Xist: X-inactive specific transcript; ZFAT-AS1: Zinc finger and AT hook domain (ZFAT) antisense 1. Proteins. CADM: Cell adhesion molecule 1; CBX7: Chromobox protein homolog 7; CDKi: Cyclin-dependent kinase inhibitor; CDX2: Caudal-related homeobox transcription factor 2; CHD2: Chromodomain helicase DNA-binding protein 2; CTCF: CCCTC-binding factor; GADD45A: Growth arrest and DNA damage-inducible alpha; PTEN: Phosphatase and tensin homolog. Cancers. AML: Acute myeloid leukemia; BC: Breast cancer; CRC: Colorectal cancer; GC: Gastric cancer; HCC: Hepatocellular cancer; LC: Lung cancer; MM: Multiple myeloma; NSCLC: Non-small cell lung cancer; OC: Ovarian cancer.

Table 2. LncRNAs associated with DNMTs, silencing genes through CpG methylation

ncRNA	Recruitment	Target	Mechanism	References
DACOR	DNMT1	Fos, Jun, DNMT1	CpG methylation, Decoy	76
LINC0051	EZH2	PTEN	CpG methylation	77
HOTAIR	DNMT1	PTEN	CpG methylation	78
SAMD12-AS1	DNMT1	P53	CpG	79
KIF9-AS1	DNMT1	RAI2	CpG	80
ANRIL	Steric hindrance, block of Pol II binding	IGF2R	CpG methylated	81
HITT	EZH2, PRC2	Hif-1α	Triplex formation	82
CDKN2B-AS1/ANRIL	PRC2	CDKN2B	Triplex formation	83

Notes: A link to ncRNA databases can be found at https://lncipedia.org/db and http://www.noncode.org/; for RNAs related to biomolecular condensates, a link can be found at https://rps.renlab.org/#/Browse
Abbreviations: ANRIL: Antisense noncoding RNA in the INK4 locus; CDKN2B: Cyclin-dependent kinase inhibitor 2B; CpG: Cytosine-phosphate-guanine; DACOR: DNMT1-associated colon cancer repressed LncRNA; HIF-1α: Hypoxia inducible factor 1α; HITT: HIF-1α inhibitor at the translation level; HOTAIR: HOX transcript antisense RNA; IGF2R: Insulin growth factor 2 receptor; KIF9-AS: Kinesin family member 9-antisense; LINC0051: Long intergenic non-protein coding RNA 51; PTEN: Phosphatase and TENsin homolog deleted on chromosome 10; RAI2: Retinoic acid induced 2; SAMD12-AS: Sterile alpha motif domain-containing 12-Antisense.

upregulated in hepatocellular carcinoma (HCC) and is associated with poor survival outcomes.[111-117] NEAT1_2 is also overexpressed and dysregulated in multiple cancers, including breast, ovarian, prostate, and lung cancers, as well as multiple myeloma. Furthermore, elevated NEAT1 levels are linked to chemotherapy resistance and are associated with cancer stemness.[117] NEAT1 promotes resistance to cisplatin and taxol,[118] while downregulation or silencing of NEAT1 sensitizes tumors to these chemotherapeutic agents. NEAT1_2 also facilitates cancer progression and metastasis, particularly in thyroid cancer.[119,120] It has been suggested that NEAT1_2 could serve as a therapeutic target in HCC and papillary thyroid cancer using small molecule inhibitors.[121]

Paraspeckle components have been implicated in cancer development through expression analyses, knockout cell studies, and RNA silencing approaches. Proteins such as NONO, SFPQ, and PSPC1 have been extensively studied.[122-129] NONO, a core paraspeckle component, is involved in RNA- and DNA-tethered condensates and undergoes phase separation *in vitro*, which is sustained by nucleic acid binding. NONO plays a role in the transcription of super-enhancer-regulated genes, such as *HAND2* and *GATA2*. Inhibition of the RNA-binding ability

Table 3. Gene activation by lncRNAs through euchromatin regulation and histone marks

Gene	Interaction	Target	Histone mark	References
GClnc1	WDR5, KAT2A	SOD2 promoter	H3K4me3, H3K9ac	84
GCAWKR	WDR5, KAT2A	PTP4A1	H3K4me3, H3K9ac	85
LincRNA-P21	hnRNP K	P21	H3K4me3, H3K9ac	86
TM4SF19-AS1	WDR5	TM4SF19	H3K4me3	87
TARID	GADD45A	TCF21	CpG demethylation	88
CCAT1-L	CTCF, hnRNP K	MYC	Chromatin loop, NUP153 binding to cohesin	89
HOTTIP	WDR5, MLL/SET1	HOXA	H3K4me3	90
PVT1	CTCF, hnRNP K	MYC	Chromatin loop, NUP153 binding to cohesin	91
NRIP enhancer	Cohesin	ER-dependent genes	Chromatin loop nuclear receptor-interacting protein	92
HASTER	-	HNF1A	Promoter–enhancer interaction	93,94
lncPRESS1	SIRT6 deacetylase	Embryonic state	Preserves H3K56ac and H3K9ac	95
NEAT1_2	RBP14	Euchromatin binding	Paraspeckle condensates	96
THRIL	hnRNPs	TNF-α	Promoter/enhancer activation	97
HOTAIR	LSD1, HBXIP	MYC target genes	Lysine demethylation	98
NeST	WDR5	IFN-gamma	H3K4me	99
CircRNA0000285	Unknown	FUS involved in back-splicing to form circRNAs	Cervical cancer, proliferation, metastasis	100
circRap1b	KAT2A, KAT7	The HOXA5 gene H3K9ac mark, Fam3a antiapoptotic	Prevents stroke	101

Abbreviations: CCAT1-L: Colon cancer-associated transcript 1-long; circRap1b: Circular RNA from Ras-related protein 1b mRNA; CHD2: Chromodomain helicase DNA-binding protein 2; CpG: Cytosine-phosphate-guanine; Fam3A: Family with sequence similarity 3A, a cytokine-like protein; FUS: Fused-in sarcoma; HOXA5: Homeobox gene A5; IFN-gamma: Interferon-gamma; MYC: Viral myelocytomatosis homolog; NEAT1: Nuclear enriched abundant transcript 1; THRIL: TNFα and hnRNPL related immunoregulatory LincRNA; TARID: Tcf21 antisense RNA inducing demethylation; TNF-α: Tumor necrosis factor-α.

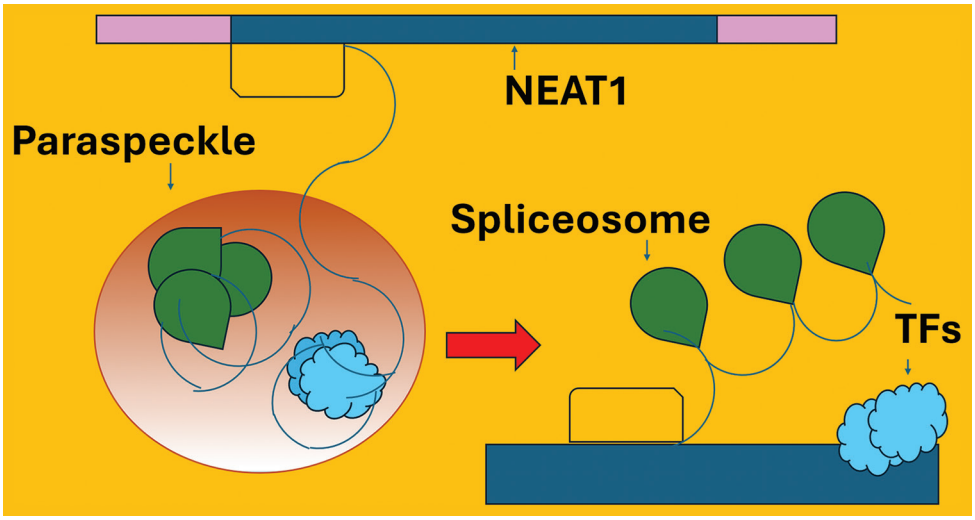

Figure 2. Function of paraspeckles in the transcription and splicing of mRNAs. The splicing factors NONO and SFPQ assemble with NEAT1_2 and then associate with PSPC1, HNRNPK, HNRNPA1, FUS, and RBM14, forming the NEAT1_2 ribonucleoprotein (RNP) complex. Image created by the authors

of NONO or its phase separation activity leads to decreased expression of *HAND2* and *GATA2*. This highlights the potential therapeutic application of compounds targeting the RNA-binding activity of NONO, particularly in neuroblastoma.[123]

The Drosophila behavior human splicing complex, comprising PSPC1, SFPQ, and NONO, plays a critical role in genome stability and gene regulation at both transcriptional and post-transcriptional levels. These functions depend on the heterodimerization of the proteins

and their subcellular compartmentalization, particularly within paraspeckles.[125]

PSPC1 potentiates IGF1R expression, enhancing cell adhesion and motility. It has been demonstrated that every component of paraspeckles is involved in this process. Knockdown experiments of PSPC1-interacting paraspeckle components, including NONO, FUS, and NEAT1, have shown that these are essential for PSPC1-regulated IGF1R expression.[126] Focal adhesion kinase and sarcoma kinase (Src) signaling pathways cooperate to increase cell adhesion and motility in HCC. Insulin-like growth factor 1 receptor (IGF1R), a membrane tyrosine kinase receptor, is a targetable molecule overexpressed in tumor metastasis, drug resistance, and poor prognosis across various cancers. In colorectal cancer (CRC), MALAT1 binds to SFPQ, releasing the oncogene PTBP2 from the SFPQ/PTBP2 complex.[130] In the same cancers, SFPQ depletion has been shown to be synthetically lethal in the presence of BRAF V600E mutations.[131] In addition, SFPQ promotes lung cancer malignancy[131] and contributes to the proliferation, migration, and invasion of HCC.[128] SFPQ condensates also sequester SMAD4, thereby preventing tumor-suppressive signaling through the TGF-β pathway.[129] PSPC1 interacts with lysine demethylase KDM5C, and both proteins are recognized as oncogenic factors in prostate cancer (PCa). Inhibition of KDM5C and PSPC1 using specific compounds shows potential as a therapeutic strategy for PCa.[132,133] In sporadic amyotrophic lateral sclerosis (ALS), NONO and PSPC1 remain localized within the nuclei of motor neurons,[134] whereas SFPQ and FUS exhibit nuclear loss, and TDP-43 displays cytoplasmic localization.[135]

RNA-binding proteins (RBPs) are critical components of BCs. Many RBPs colocalize with RNA polymerase II (Pol II) at promoter and enhancer loci. The paraspeckle protein PSPC1 utilizes RNAs as multivalent molecules to form transcription condensates, which are followed by the phosphorylation and release of Pol II.[136]

The PSPC1 protein contains a PrLD enriched in uncharged polar amino acids, such as asparagine, glutamine, and tyrosine. Glycine is also abundant and contributes to the liquid–gel phase separation properties of PSPC1. The PrLD domain contributes to the phase separation ability of PSPC1. Immunofluorescence assays have detected PSPC1 in mouse oocytes at the germinal vesicle (GV) stage. PSPC1 knockdown resulted in the blocking of oocyte maturation *in vitro*. Checkpoint kinase 1 (CHK1) is vital during the GV stage of mouse oocytes. PSPC1 interacts with the serine/threonine protein phosphatase PPP5C, which regulates CHK1 phosphorylation.[138]

PSPC1 also functions as an activator of transcription factors involved in epithelial-to-mesenchymal transition (EMT) and stemness. It sustains Myc activation and promotes tumor growth in breast and prostate cancer. PSPC1 enhances the secretion of transforming growth factor-β1 (TGF-β1) through interactions with phosphorylated nuclear Smad2/3. PSPC1 promotes a TGF-β1 prometastatic switch by altering the binding preference of Smad2/3 from tumor suppressor genes to prometastatic genes.[137,138]

In CRC, LOC105369504 expression is downregulated, leading to the inhibition of proliferation, invasion, migration, and EMT. LOC105369504 binds to PSPC1, regulating PSPC1 stability through the ubiquitin-proteasome pathway.[139]

The pro-oncogenic activities of PSPC1 are closely linked to those of the orphan nuclear receptor 4A1 (NR4A1, Nur77). NR4A1 knockdown decreases PSPC1 expression in various cell lines. Bisindole-derived NR4A1 antagonists (CDIMs) also induce PSPC1 downregulation in breast cancer.[140] Following NR4A1 silencing, genes associated with cancer stemness and EMT are also downregulated.

NEAT1_2-dependent clusters influence how proteins such as FUS, which aggregate around RNA, interact with the RNA-binding protein RBP14 and paraspeckle proteins PSPC1, NONO, and SFPQ. Activation of the mechanistic target of rapamycin (mTOR) reduces NEAT1_2 transcription, diminishes paraspeckles, and releases NONO, SFPQ, and RBP14, which are essential for RNA splicing.[141] Table 4 provides a detailed overview of ncRNAs necessary for the formation of different BC types.

3.1. Speckles and MALAT1

The ncRNA MALAT1 is a key RNA constituent of nuclear speckles and is overexpressed in cervical, colorectal, lung, breast, liver, and bladder tumors.[142] Elevated *MALAT1* expression is associated with poor prognosis and metastasis formation in lung cancer and other tumors.[143,144] Cells with aberrant *MALAT1* expression exhibit various dysregulated functions, with mechanisms of action often inconsistent and sometimes conflicting. It is plausible that the deregulation of oncogenic RNAs affects condensate function. MALAT1 is recruited to speckles through direct interactions with multiple splicing-associated proteins; however, it is not strictly required for speckle formation.[143] MALAT1, also known as *NEAT2*, is an ~8 kb highly abundant ncRNA conserved across vertebrates and considered an oncogene. Using capture hybridization analysis of RNA targets, researchers demonstrated MALAT1 binding to active genes, suggesting that both NEAT1 and MALAT1 contribute structurally to the organization of nuclear bodies at heavily transcribed sites.[144] Engreitz *et al.*[124] employed RNA–RNA interaction assays (RAP-RNA) and showed that MALAT1 localizes to actively transcribed

Table 4. ncRNAs required for the formation of biomolecular condensates (BCs) or interaction with protein components

Type	ncRNA	Interactome	Deregulated in cancer
Speckle	MALAT1	DBC1, PRPF6, SRSF, hnRNPs, ELAVL1/HuR	Breast cancer, CRC[102]
Paraspeckle	NEAT1_2	NONO, SFPQ, and PSPC1	Triple-negative BC, HCC[103]
PML body	DUXAP8	PTEN	Prostate, ovary, bladder, breast, pancreas, RCC, GC[48]
Stress granules (SGs)	RP11-435F13.2	ELAVL1 (HuR)	Pancreatic and esophageal cancer[57]
SG	NORAD	ALKBH5, AGO, DDX6	Various cancers[57]

Abbreviations: AGO: Argonaute; ALKBH5: ALKB homolog 5, erasing m6A; BC: Breast cancer; CRC: Colorectal cancer; DBC1: Depleted in breast cancer; DDX6: Death box family RNA-dependent helicase ATPase 6; DUXAP8: Double homeobox A pseudogene 8; GC: Gastric cancer; HuR: Human R antigen; MALAT1: Metastasis-associated lung adenocarcinoma transcript 1; NEAT1: Nuclear enhanced paraspeckle assembling transcript 1; NORAD: Noncoding RNA activated by DNA damage; PML: Promyelocytic leukemia; PRPF6: Pre-mRNA-processing factor; RCC: Renal cell carcinoma; SRSF: Serine/arginine-rich splicing factors.

genes through interactions with proteins that guide this RNA to nascent pre-mRNAs. MALAT1 functions as a scaffold for speckle proteins, facilitating the positioning of nuclear speckles at active gene loci.

3.2. PML bodies, p53 guardian of the genome, and cancer

PML bodies are dynamic nuclear MLO compartments[145] that compartmentalize diverse proteins, such as p53 and DNA repair protein complexes. PML bodies regulate various cellular processes, including apoptotic pathways and genome stability. Failures in DNA damage repair (DDR) result in chromosomal instability, a hallmark of cancer. Various ncRNAs contribute to DNA stability and repair, which are essential processes in cancer development.

PML bodies participate in activities such as transcription regulation, cell cycle control, antiviral defense, and apoptosis promotion. These functions are mediated by PTMs, such as phosphorylation by protein kinase 2 (PK2) and deubiquitination by USP7/HAUSP, which regulate protein ubiquitination for proteasomal degradation. PML bodies are also targeted by various oncolytic viruses.[146] The Momordica anti-HIV protein MAP30 has been shown to decrease HBV replication by inhibiting EBNA1, which directs PML proteins to degradation and promotes PML loss.[147]

Among the tripartite motif (TRIM) proteins, which include a series of RING-type E3 ligases, the TRIM 19 protein is encoded by *PML*. The N-terminal RBCC (RING, B-Box 1/2, coiled-coil) domain facilitates PML protein scaffold self-oligomerization. The C-terminus contains small ubiquitin-like modifier (SUMO) sites and a SUMO-interacting motif (SIM), which enhance granule assembly through SUMO and SIM arrays, promoting liquid-like condensate formation. In cancer, PML bodies exhibit diverse roles. In acute promyelocytic leukemia (APL), chromosomal translocation results in the fusion protein PML-RARα, which lacks C-terminal SIM and SUMOylation sites. This alteration impairs PML phase separation, causing dispersed microspeckles and concentrating transcriptional machinery at oncogenes, potentially impacting RNA splicing and contributing to oncogenesis. Novel therapeutic approaches targeting PML in cancer have been recently reviewed.[148]

Condensates are regulated at multiple levels, with alterations in their properties influencing their formation, viscoelasticity, dissolution, and other physicochemical aspects, ultimately modifying their functions. Several factors are critical for the regulation of BCs. Dysregulation in the concentration of components, chemical modifications, involvement of ncRNAs, and selective partitioning are observed in cancer cells. Among these, the concentration of biomolecules is a pivotal parameter in condensate dynamics. Condensation occurs when a critical threshold concentration is reached, which can be achieved through protein accumulation, inhibition of degradation, confinement within a membrane-bound compartment, or sequestration by binding to a substrate with multiple binding sites. Notably, the dissolution of condensates occurs during mitosis when the loss of the nuclear membrane reduces the concentration of nuclear components. Condensates reform in the nucleus once the nuclear envelope is re-established, facilitated by an increase in component concentrations through protein transport into the nucleus. Alterations in BCs are pervasive in cancer and are driven by diverse stresses within the tumor microenvironment. The phase separation of cancer-associated proteins influences numerous cellular processes, contributing to cancer development.

One notable role of ncRNAs interacting with condensates involves the activation of the tumor suppressor protein p53 and its downstream signaling pathways.[149] The p53 protein is prone to amyloid-like aggregation, particularly in its mutated forms. Interactions between p53 and MDM2, an E3 ubiquitin ligase that degrades p53, are influenced by IDRs. MDM2 inhibits p53 by inducing

its degradation and blocking its transcriptional activity, whereas p53 induces MDM2 expression, forming a regulatory feedback loop.[150] In the DNA repair pathway, phase-separated DNA repair foci containing the DNA damage-response factor p53-binding protein 1 (53BP1) also concentrate p53 protein.[151] Disruptions in these phase-separated foci impair the 53BP1-dependent induction of p53, reducing the expression of p53 target genes. Among the transcripts activated by p53,[152-154] several ncRNAs, such as LINC1, Guardin, and NEAT1_2, play significant roles, in addition to 53BP1.[155-157]

Since p53 acts as a tumor suppressor, its altered activity due to mutations, reduced concentration, or impaired signaling at DNA repair foci can promote cancer progression. In response to DNA damage, different repair mechanisms are activated depending on the type of damage. Double-strand breaks are repaired by mechanisms such as homologous recombination (HR), classical non-homologous end-joining (NHEJ), alternative end-joining, and single-strand annealing. Larger nucleotide adducts are repaired through nucleotide excision repair, whereas smaller base lesions are repaired through base excision repair. LINP1 ncRNA assembles proteins such as RPA, Ku70, Ku80, and ISWI, bringing in proximity breast cancer type 1 susceptibility protein (BRCA1), PAR polymerase 1 (PARP1), cadherin 4 (CDH4), and 53BP1.[158] NIHCOLE RNA acts as a scaffold for proteins, interacting with multiple Ku80 units and promoting phase separation, facilitating the formation of multimeric NHEJ complexes to optimize ligation efficiency.[159] It supports repair complexes like the XRCC4-DNA Ligase IV ligation complex. Another ncRNA, LRIK, binds to Ku70 – Ku80 heterodimers.

SNHG12 RNA stabilizes the interaction between DNA-PK and Ku70/Ku80, promoting NHEJ-based DNA repair. HITT RNA binds to ataxia-telangiectasia mutated (ATM) and prevents the formation of the MRE11-RAD50-NBS1 (MRN) complex, playing a role in both HR and NHEJ.[160]

Protein–protein interactions are crucial for assembling DNA repair complexes. BRCA1, through its leucine-zipper domain, interacts with PARP1, which performs poly-ADP-ribosylation, creating PAR chains that recruit PAR-binding proteins. MALAT1 forms a complex with PARP1 and ligase 3 (LIG3), facilitating HR. Inhibiting this complex has shown therapeutic benefits in prostate cancer and multiple myeloma.[161,162] H19, an ncRNA silenced in clonal sheep reproduction, increases BRCA1 stability by interfering with BRCA1 degradation mediated by ubiquitin ligases HUWE1 and UBE2T. Silencing H19 disrupts the DNA repair process and enhances sensitivity to PARP inhibitors (PARPi), offering potential therapeutic advantages.[163]

3.3. Microspeckles and superenhancers

Recent research has revealed that gain-of-function mutations in the miR-1400 seed sequence, caused by chondrocyte-activated superenhancers, lead to skeletal dysplasia, emphasizing the role of superenhancers in disease mechanisms. While the correlation between superenhancers and ncRNAs in controlling cell identity remains underexplored, it is proposed that super-enhancer-driven ncRNAs (SE-ncRNAs) are associated with tumor development and pathogenesis. RNA molecules facilitate condensate formation, initiate transcription, and contribute to the fusion or pairing of enhancer condensates with promoter sites, leading to transcriptional bursts. RNA-mediated feedback may terminate these transcriptional bursts, highlighting the roles of ncRNAs near enhancers or promoters.[91,93,94] Interactions between such RNAs and enhancers could regulate the rate and magnitude of transcriptional bursts. The accumulation of ncRNA near genes may influence condensate size or dissolution through feedback mechanisms. Furthermore, ncRNAs can modulate transcription by interacting with CTCF (CCCTC-binding factor), stabilizing genomic boundaries, and limiting the territory over which an enhancer or super-enhancer operates.[164,165] Functional crosstalk between superenhancers and ncRNAs—spanning gene regulation in cis and trans and the regulation of superenhancers by ncRNAs—has also been proposed. Noncoding mutations play a significant role in the dysregulation of superenhancers in cancer. For example, in approximately 5% of T-cell acute lymphoblastic leukemias (T-ALL), small insertions near the TAL1 gene induce ectopic super-enhancer creation. This presents a working hypothesis for studying how noncoding mutations trigger ectopic super-enhancer establishment.[165] Drugs targeting BCs, such as cyclopamine (a steroidal alkaloid[166]) and nucleolin,[167] could enable the pharmacological modulation of oncolytic virus replication and control transcription factors at cancer-driving superenhancers.

3.4. SGs

Key components of SGs include the Ras-GTPase-activating protein (GAP) SH3 domain-binding proteins G3BP1 and G3BP2, which are pivotal in cell behavior and cancer.[13,168,169] DDX3, a DEAD-box RNA helicase and RNA-binding protein,[170] localizes with DDX6 to SGs alongside Gle1A,[171] a DDX regulator, and CAPRIN1. DDX3 is essential for SG assembly, which occurs through nucleation mediated by the RNA decay factor G3BP1. G3BP1 prevents ribosome and initiation factor localization in silenced SG foci, assisted by other SG-associated proteins, such as DDX3, DDX6 (Rck/p54), Y-box-binding protein (YBX1/YB-1), translational suppressors TIA1 and TIAR, CAPRIN1,

USP10, poly-A-binding protein, and Lsm1. YB-1, with its low-complexity sequence domains, activates G3BP1 translation, thereby promoting SG assembly. Acetylation of YB-1, induced by entinostat, suppresses G3BP1 translation and SG formation. YB-1 interaction with G3BP1 also promotes metastasis in RCC by upregulating secreted phosphoprotein 1 (SPP1).

SGs play a critical role in enhancing tumor growth, invasiveness, migration, apoptosis inhibition, immune evasion, and metabolic reprogramming. SGs also contribute to the development of resistance against chemotherapy, immunotherapy, and radiotherapy across various cancer types.

A small molecule, C108, inhibits G3BP2, delays stress response, suppresses cancer cell metastasis, and promotes CD8 T-cell proliferation and infiltration, improving survival in animal models with breast tumor xenografts. LINC01554 protects G3BP2 against degradation through ubiquitination. RNA-seq analysis has revealed that hepatoma-derived growth factor (HDGF) is regulated by G3BP2. G3BP2 binds to HDGF mRNA, stabilizing its expression, while C108 inhibits G3BP2 function.[169]

Cancer cells exploit SGs as condensates to sequester drugs, protecting cellular components during stress. G3BP1, a key nucleation protein in SGs, is highly expressed in various cancers and promotes proliferation, migration, and invasion.[3] Although the mechanism underlying the upregulation of SG formation is not fully understood, G3BP1 expression is regulated by Y-box binding protein 1 (YB1), a nucleocytoplasmic shuttle protein. YB1 binds to the 5′ UTR of G3BP1 mRNA, promoting its translation. Notably, YB1 is highly expressed in sarcomas and nasopharyngeal cancers.[172] SG formation also favors cancer cells by inhibiting apoptosis.[173] Drug-based inhibition of SG components, such as DDX3, has been shown to reduce SG formation.[174] SG formation can also be triggered by lipid signaling molecules.[175] Independent of SG formation, G3BP1 contributes to cancer progression by participating in growth-related signaling pathways and promoting EMT in tumors.[176]

G3BPs (G3BP1 and G3BP2) regulate mRNA expression outside of SGs through interactions with RNA. They are implicated in cancer progression, invasion, metastasis, and viral infections by regulating SG dynamics, RNA stability, and tumorigenesis.[177] Consequently, compounds that target G3BPs, block SG formation, or promote SG dissolution hold potential as therapeutic agents. G3BPs may serve as therapeutic targets for both antiviral and anticancer strategies.[177-179]

G3BP1 is a central player in SG dynamics, with its RNA-binding ability essential for SG formation. The RNA-binding function of G3BP1 is impaired by acetylation at lysine 376 (K376) in its RRM domain.[178] A mutation mimicking this acetylation, K376Q, disrupts G3BP1 interaction with poly(A)-binding protein 1 (PABP1) but does not affect interactions with Caprin-1 or USP10. Substituting G3BP1 with its K376Q mutant or an RNA-binding-deficient mutant (F380L/F382L) blocks SG formation. During SG resolution, K376-acetylated G3BP1 is observed outside SGs.[178] MAGE-B2 (melanoma-associated antigen B2) suppresses SG initiation by reducing G3BP levels below the concentration critical for phase separation.[179] G3BP2 also induces changes in condensate and mRNA expression under endoplasmic reticulum (ER) stress.[168] Residues critical for G3BP condensation, such as V11, is essential for forming the G3BP-Caprin-1 complex and assembling SGs.[169]

During arsenite administration, oxidative stress or elongation factor eIF2 phosphorylation causes cell to enter a translation arrest phase. In this phase, RNAs are stalled within a ternary complex comprising eukaryotic initiation factor 2 (eIF2)/GTP/Met-tRNA. SGs play a critical role during this phase by sequestering mRNAs and inhibiting their translation until the stress subsides. Depending on the severity and type of stress, SGs may also lead to the processing or degradation of mRNAs. SGs contain enzymes of the RNA silencing pathway, including Argonaute2, trans-acting factors, Hsp90 complexes, and RBPs, which participate in the small RNA-mediated repression of RNA targets. Interestingly, viruses exploit SG formation to their advantage, either by facilitating the translation of their own RNAs or by binding to SG protein scaffolds to inhibit SG formation.[14,15]

SGs have been implicated in cancer development and neurodegenerative diseases. In human HCC tissues, four genes—*KPNA2*, *MEX3A*, *WDR62*, and *SFN*—are highly expressed. Knocking down any of these genes reduces HCC cell proliferation by disrupting SG formation.[180] A small molecule, C108, binds to G3BP2, decreasing PD-L1 mRNA and protein levels, increasing CD8 T-cell proliferation and infiltration, and improving survival and long-term cures in breast tumor-bearing mice.

Raloxifene, an estrogen receptor modulator, prevents SG dissolution in glioblastoma cells, induces protein synthesis failure, and promotes cell death during hypoxia. Thus, SG modulation can be a promising strategy to target the hypoxic niche of GBM tumors.

Knockdown of *G3bp1* and *G3bp2* prevents SG formation in response to eIF2α phosphorylation or eIF4A inhibition, although cells remain SG-competent under heat or osmotic stress. CAPRIN1 binding to G3BP promotes SG formation, whereas USP10 binding inhibits

it. G3BP, through its RGG motif, interacts with 40S ribosomal subunits, and this motif is essential for G3BP-mediated SG assembly. G3BP facilitates SG condensation through S149 phosphorylation and its interactions with CAPRIN1 or USP10.[169] CAPRIN1 is a phase-separating protein with significant roles in dendritic spines and SG formation, often in association with ncRNAs.[181] SG-associated CAPRIN1 is involved in the progression of nasopharyngeal carcinoma.[182] In ovarian cancer, the upregulation of SNHG8 RNA enhances its binding with CAPRIN1, positively regulating its expression and promoting the stability of catenin beta 1 (CTNNB1) and Axin.[183] These interactions activate Wnt/β-catenin signaling, thereby facilitating cell migration and EMT and maintaining the stemness of ovarian cancer cells. Given their pivotal role in cellular stress responses, SGs are promising therapeutic targets for cancer treatment.[184] For example, small peptides derived from the G3BP1 sequence have shown encouraging results in cancer therapy.[185]

CAPRIN1 is an RNA-binding protein that confers specificity to enzymes depositing the (m6A) mark on RNAs, particularly near stop codons. An *et al.* demonstrated that TRA2A and CAPRIN1 promote the methylation of m6A sites colocalized with their RNA-binding targets. CAPRIN1 interacts with METTL3 and METTL14, forming the m6A methyltransferase METTL3/METTL14 complex, which associates with Wilms' tumor 1-associated protein (WTAP).[186]

3.5. P bodies

P bodies are dynamic structures similar to SGs and are organized during stress-induced translational arrest. They serve as sites for mRNA silencing and decay. Specific RBPs are essential for P body formation, including DEAD-box RNA helicase 6 (DDX6), LSM14A, and eukaryotic translation initiation factor 4E transporter (EiF4E), which participate in the nucleation process. Other P body-associated proteins include SAMD4A, AJUBA, YB-1, and Wilms' tumor-1 interacting protein (WTIP). Enzymes such as DCP1A and DCP2 and enhancers of mRNA decapping proteins (EDC3 and EDC4) reinforce the protein interaction network and are required for stress-induced P body formation.

P bodies are closely linked to tumor progression. In CRC, DCP1A is highly expressed, and this upregulation correlates with advanced tumor-node-metastasis stage, worse prognosis, increased lymph node metastasis, tumor invasiveness, and lower survival rates. In mammary epithelial cells, treatment with TGF-β promotes P body formation and EMT. Activation of autophagy can clear P bodies, thereby blocking EMT.

P bodies are enriched in mRNAs with m6A modifications, attracting the m6A reader YTHDF2, which colocalizes with P body markers DCP1A, DDX6, and EDC4. DCP1A is post-translationally modified through ubiquitination by the E3 ubiquitin ligase TRAF6 and phosphorylation. These PTMs favor interactions with P body factors such as DCP2, EDC4, and XRN1, enhancing P body formation. Notably, phosphorylation promotes mRNA storage, whereas ubiquitination drives mRNA decay.

Knockdown of DDX6 in a mouse model of late-stage BC prevents P body formation, inhibits EMT, and reduces metastatic nodule size and number. Snail zinc finger transcription factors, which are key regulators of EMT, are recruited to P bodies by the RNA-binding protein muscleblind-like 1 (MBNL1), suppressing metastasis formation.

Y-box binding protein 1 (YB-1) activates SNAIL transcription, promoting EMT and cell invasiveness in BC. This mechanism is also significant in pancreatic cancer and in resistance to gemcitabine. YB-1 additionally protects against oxidative stress by regulating NRF2, a transcription factor with antioxidant functions. Several inhibitors of YB-1 have been identified, including PI3K/mTOR inhibitors, which suppress YB-1 activity.[184]

3.6. Regulation of ncRNAs at the epitranscriptome level

RNA modifications, particularly m6A and m5C, are critical regulators of RNA structure, stability, and function.[27] The deposition of m6A induces structural changes in ncRNAs, altering ncRNA-protein interactions, regulating transcription, influencing subcellular localization, and stabilizing ncRNAs. Other RNA modifications include m7G and acetylation marks, such as m1A in MALAT1 and Ac4C on cytosine.[27,187,188] NAT10 is the enzyme responsible for the deposition of N4-acetylcytidine (Ac4C), a modification implicated in cancer.[189] NAT10 serves as a metastasis suppressor in CRC, acetylating RNA CTC-490G23.2, which binds to polypyrimidine tract-binding protein 1 (PTBP1) and increases alternative splicing of CD44 in esophageal squamous cell carcinoma. However, NAT10 may also act as a metastasis promoter and EMT inducer by stabilizing COL5A1 mRNA through direct binding.[190]

The N6-adenosine–methyltransferase complex catalytic subunit (METTL3) is an S-adenosylmethionine (SAM)-dependent enzyme. The methyltransferase complex, formed by METTL3 and METTL14 and associated with WTAP, methylates adenines, producing m6A-modified RNAs. Interestingly, METTL14 acts as a chromatin

regulator independent of its RNA m6A methyltransferase activity,[191,192] as it colocalizes with repressive H3K27me3 marks on chromatin. METTL14 binds to H3K27me3 and KDM6Brecruits facilitating H3K27me3 demethylation, a process essential for the transition from embryonic stem cells to differentiated cells.[193] Another methyltransferase complex (MTC) is formed by the association of RNA-binding motif protein 15 (RBM15), vir-like m6A methyltransferase-associated protein (VIRMA), zinc finger CCHC-type containing 4 (ZCCHC4), and zinc finger CCCH-type containing 13 (ZC3H13).[27]

Regarding internal m7G (N7-methylguanosine) writers, METTL1 forms a protein complex with WD repeat domain 4 (WDR4). This complex is active on tRNAs, rRNAs, mRNAs (enhancing mRNA translation), and miRNAs. The insulin-like growth factor 2 mRNA-binding protein (IGF2BP) family serves as readers of m6A modifications, regulating the stability of m6A-modified mRNAs. m6A influences RNA-driven phase separation by altering RNA–RNA and RNA–protein interactions. For example, the loading of m6A readers facilitates phase separation.[194] Notably, IGFBP2/3 act as m6A readers, binding ncRNAs and promoting the stability of m6A-modified mRNAs.[27] Other m6A readers include eukaryotic initiation factor (eIF3), proteins of the heterogeneous nuclear RNP (HNRNP) family, and YTHDF1 and YTHDF2, which contain the YT521-B homologous (YTH) domain.

The cytoplasmic protein YTHDF2 binds to m6A marks, either leading to degradation of m6A-modified RNAs by erasers or facilitating the localization and translation of bound mRNAs through interactions with translation initiation factors. In the nucleus, YTHDC1 regulates pre-mRNA splicing by recruiting splicing factors.

Demethylases such as fat mass- and obesity-associated protein (FTO) and alkylation repair AlkB homolog protein 5 (ALKBH5) remove m6A modifications. PSPC1, a regulatory subunit of ALKBH5, binds to K235-acetylated ALKBH5, enhancing its recognition of m6A-modified RNAs and promoting its erasing activity. Elevated K235 acetylation of ALKBH5 is observed in cancers and is linked to tumorigenesis.[132] Table 5 highlights the ncRNAs and circRNAs regulated by m6A-associated enzymes.

An internal N7-methylguanosine (m7G) modification in ncRNAs has been identified as a significant factor in resistant acute myeloid leukemia (AML).[188] However, limited information exists on m7G readers and erasers.

Each ncRNA possesses unique properties, with m6A modifications sometimes enhancing stability through interactions with m6A readers, while in other cases, they make ncRNAs susceptible to degradation through recognition by m6A erasers. This variability, coupled with cell type-specific interactions with m6A writers, readers, and erasers, contributes to differences in cancer susceptibility and progression. Different cancers exhibit distinct expression levels of m6A-modifying enzymes, further influencing cancer development and therapeutic outcomes.

Similar to ncRNAs, there is a dynamic crosstalk between circRNAs and m6A modifications. CircRNAs impact cancer response to chemotherapeutics through mechanisms such as modulating drug transport, DNA repair, apoptosis, the TME, autophagy, EMT, cancer stem cells, and glycolysis.[209]

4. Epitranscriptome regulation of ncRNAs and cancer therapeutics

Recent databases have compiled information on ncRNAs involved in epigenetic regulation.[207,208] A significant resource, curated by Yulia Medvedeva's laboratory at the Institute of Bioengineering, Russian Academy of Science, lists over 4,100 such ncRNAs and is accessible at https://github.com/lab-medvedeva/himorna-frontend. Similar to how amino acid charges and PTMs[209] confer new properties, epitranscriptomic modifications in ncRNAs influence interaction strength, base pairing, and RNA stability.

The METTL3 inhibitor STM2457 entered phase I clinical trials in 2022, demonstrating inhibition of proliferation in AML.[211] S-adenosylmethionine (SAM), an essential cofactor, is required for both DNMT1 (a DNA methylating enzyme) and METTL3.[212,213] METTL3A, a component of the m6A writer complex, is a key target in cancers with elevated m6A levels. METTL3 inhibitors, including STC-15, have been tested in clinical trials.[214]

Various epitranscriptomic modifications of ncRNAs affect RNA stability and function in cancer. Researchers have developed drugs targeting the writers, readers, and erasers of m6A modifications.[211-214,216] Promising anticancer effects have been reported for inhibitors targeting the METTL3–METTL14 methylation complex. These inhibitors exhibit diverse chemical structures, such as adenine derivatives, sinefungin, UZH derivatives, CDIBA derivatives, STM2457, and eltrombopag.[217] In addition, compounds such as mitoxantrone, suramin, KH3, and eltrombopag inhibit the RNA-binding domain of ELAVL/HuR, demonstrating antiangiogenic properties.[217] Notably, various METTL3 inhibitors entered phase 1 clinical trials for AML in 2022.[211,214,217] Researchers have explored two main approaches: developing m6A writer inhibitors[217] and allosterically activating m6A writing complexes. Drug compounds targeting METTL14, a transcriptional

Table 5. m6A modification: Role of ncRNA interactions with m6A writers, readers, and erasers

lncRNA	Interaction	Modified	Effect	References
FEZF1-AS1	IGF2BP1 sequestration	m6A	Apoptosis	195
DARS1-AS1	METTL3-METTL14	m6A	Proliferation	196
THOR	Readers YTHDF1 and YTHDF2	m6A	Oncogenesis	197
LNCAROD	METTL3-METTL14	m6A	Prevents YBX1 degradation	198
GAS5	Reader YTHDF3	m6A	GAS5 degradation	199
LINC021	IGF2BP2	m6A	MSX1 stability	200
LINC0047	METTL3	m6A	PTEN-m6A degradation	125
CASC11	ALKBH5	m6A	Decrease in m6A UBE2T	200
NEAT1_2	ALKBH5, YTHDF2	m6A	Destabilize mRNA	201,202
PVT1	Silencing ALKBH5	m6A	Decrease levels	58
LEAWBIH	YTHDC1	m6A	Recruits H3K9me2 demethylase KDM3B	203
MALAT1	The serine/arginine-rich splicing factor TRA2A forms a complex with writers METTL14, RBMX, KIAA1429	m6A	lncRNA m6A methylation	204
LINC00022	FTO	m6A	Block degradation by YTHDF2	205
DANCR	IGF2BP2	m6A	Stabilized DANCR	206
circARHGAP35/ circDLC1	METTL3, HNRNPL	m6A	Promotes its translation, producing an oncogenic protein	102
circDDIT4	METTL3-WTAP	m6A	Suppresses anoctamin (ANO7) binding to ELAVL1/HuR, reduces PC progression	189
circRBM33	METTL3/YTHDC1	m6A	RNA stability, abdominal aortic aneurysm	207
circ0049271	WTAP	m6A	IGF2BP3 binding, regulation of the TGF-b/ SMAD signal, and promotion of EMT in gastric cancer	208
circPTPRA, circNSUN, circ1662, circMEG3	WTAP writer complex, IGF2BP1 binding, recruitment of YTHDF3 and YTHDC1	m6A	Cytoplasmic export and formation of protein ternary complexes	209
circMARK2	METTL3	m6A	Cytoplasmic export, Lin28B stabilization, Wilms tumor progression	210

Note: An extensive database (http://www.xjtlu.edu.cn/biologicalsciences/m7ghub) is available as a tool to check RNA modifications.
Abbreviations: FTO: Fat mass and obesity; ALHB1: AlkB homolog protein 5; IGF2BP1: Insulin-like growth factor mRNA-binding protein 1; METTL3: Methyltransferase 3, N6-adenosine-methyltransferase complex catalytic subunit; CircARHGAP35/CircDLC1: Rho GTPase activating protein 35 circular RNA; CircDDIT4: Damage inducible transcript 4 circular RNA; CircPPTRA; Protein tyrosine phosphatase receptor type A circular RNA; DARS1-AS1: Aspartyl-tRNA synthetase, antisense; FEZF1-AS: FEZ family zinc finger1, antisense; GAS5: Growth arrest specific 5; LNCAROD: LncRNA activating regulator of DKK1; DANCR: Differentiation antagonizing non-protein coding RNA; LEAWBIH: Long noncoding RNA epigenetically activating Wnt/β-catenin signaling in HCC.

activator, have also been identified.[191,215] New studies are investigating the role of m7G modification in cancer through METTL1 activity, with efficient inhibitors undergoing testing.[218]

Studies have also focused on inhibitors and activators of m6A readers. IGF2BP1 and IGF2BP2 inhibitors have shown antiproliferative effects.[219-222] For instance, SU056, an azopodophyllotoxin-derived small molecule, effectively inhibits IGF2BP2, promoting apoptosis and RNA degradation while reducing splicing pathways, with inhibitory effects in ovarian, lung, and breast cancers and AML.[219] Silencing the YTHDF1 m6A reader using vesicle-like nanoparticles encapsulating YTHDF1-siRNA enhanced immune responses and improved anti-PD-1 therapy outcomes *in vivo*.[223]

ONC213 suppressed mitochondrial respiration, elevated α-ketoglutarate by inhibiting α-ketoglutarate dehydrogenase (αKGDH), and exhibited potent antileukemia activity with minimal toxicity. ALK-04 is a selective ALKBH5 inhibitor.[220]

Several classes of FTO inhibitors have been developed to target m6A erasers,[224] including metal-chelating inhibitors, substrate-competitive inhibitors, and various

structural scaffolds.[225,226] Blocking FTO activity with inhibitors such as FB23 and FB23-2, developed by Huang *et al.*,[225] increased m6A levels and inhibited AML cell growth. These inhibitors, which bind to FTO and block its demethylase activity, hold promise as therapeutic agents for AML.

Inhibitors of the RNA-binding protein IGF2BP have shown significant potential as anticancer agents.[225] Recent advancements in small molecules targeting m6A regulators were reviewed by Feng *et al.* in 2024.[226] Novel compounds with high binding specificity and selectivity for m6A readers, including YTHFD1-YTHFD3 and YTHFC2, have been proposed for therapeutic applications in AML, owing to their antiproliferative effects.[227]

In tumors with low m6A levels, such as certain breast cancers, m6A erasers exhibit increased activity. In these cases, small molecule activators of m6A writers, such as METTL3, may be effective. Depending on the tumor type and ncRNAs involved, m6A writers may require either inhibition or activation using suitable drugs.

4.1. Epigenetic modifications, cancer, and clinical therapeutics

Phase separation properties in cellular processes depend on amino acids favoring this transition, with charges and influencing their behavior.[209] Lysine and arginine residues, found in both histones and other associated proteins, are primary targets of epigenetic modifications.

Several inhibitors targeting histone mark writers, readers, and erasers have been identified and tested in clinics trials. SET domain proteins, including lysine-specific demethylase 1 (LSD1) and the histone-lysine N-methyltransferase 2 family (MLL1-4SETD1A, SETD1B), are prominent targets.

Lysine methyltransferase (KMT) enzymes, such as EZH1 and EZH2, are integral to the PRC complex, relying on the catalytic SET domain. KMT activity, including that of NSD1, depends on S-adenosylmethionine (SAM) availability, which inversely correlates with nicotinamide-N-methyltransferase (NNMT) activity. NNMT produces 1-methyl nicotinamide, a methyl sink for SAM-derived methyl groups. FIDAS-5, a methionine-adenosyltransferase (MAT2A) inhibitor, has been shown to reduce tumor size in 5TGM1 murine cells. MAT2A inhibition by FIDAS-5 enhances the effects of bortezomib, a proteasome inhibitor, in MM.

EZH2 overexpression has been observed in lymphoma and other cancers. Tazemetostat, an EZH2 inhibitor, has been approved for treating epithelioid sarcoma.[227] Novel inhibitors have been designed to block EZH2 and histone-modifying enzymes.[229] Targeting EZH2 activity prevents histone methylation at chromatin sites, enhancing heterochromatin accessibility through inhibition of H3K27 methylation. Small sequences such as AC1NOD4Q and AC1Q3QWB have been developed to block EZH2's interaction with ncRNAs.[229] These peptides prevent the PRC2 complex from engaging ncRNAs and exerting histone methylation. Administration of AC1Q3QWB increases the antitumor activity of 3-deazaneplanocin (DZNep), an S-adenosyl homocysteine hydrolase inhibitor targeting histone methyltransferases (HMTs), including EZH2.[230] CC-90011, a reversible LSD1 inhibitor, has entered phase I human trials.[227] This dual approach targets histone methylation by inhibiting either histone methyltransferases like EZH2 in cases of hypomethylation or histone demethylases like LSD1 in cases of hypodemethylation. In addition, the interaction between lncRNAs and EZH2 has been identified as a promising therapeutic target in cutaneous melanoma.[73] METEOR-1, a phase I study of GSK3326595 (EPZ015938), a first-in-class protein arginine methyltransferase 5 (PRMT5) inhibitor, is underway in advanced solid tumors.[228]

Epigenetic and epitranscriptomic mechanisms significantly influence the levels of ncRNAs and circRNAs, which play critical roles in cancer progression. Consequently, these enzymes must be targeted using specific drugs.[231]

Numerous companies are actively developing novel small molecules targeting epigenetic enzymes. Well-known examples include HDAC inhibitors such as heliostat,[232] vorinostat,[233] amidepsine,[234] and panobinostat, which is approved for T-cell lymphoma treatment, as well as thioamide,[235] approved for treating leukemia and multiple myeloma.[236]

In blood malignancies such as AML,[237] effective treatments have been achieved using 5-azacitidine,[238] decitabine,[239] and guadecitabine, which target DNMTs. Similarly, inhibitors of m5C methylase, such as azacitidine, decitabine, and cytidine analogs, are approved therapies for blood tumors.

A recent study on long noncoding RNAs (lncRNAs) has provided insight into their roles in therapeutic resistance.[29] For example, APAF1-binding lncRNA (ABL) promotes proliferation and drug resistance in gastric cancer by inhibiting apoptosis and caspase activation. It achieves this by binding to APAF1 and preventing its interaction with cytochrome c. Encapsulated liposomal siRNAs targeting ABL have been shown to restore chemotherapy sensitivity. Another example is ARHGAP5-AS1, which facilitates m6A modification of ARHGAP5 mRNA, stabilizing it by recruiting the m6A writer METTL3 in the cytoplasm, thereby inducing chemoresistance in gastric cancer.

Drugs that inhibit enzymes involved in PTMs can disrupt condensate behavior and influence epitranscriptome modifications of RNA. These modifications include m6A, m6Am (dimethyladenosine), m1A, m5C, m7G, and ac4C, which are regulated by PTMs. The dependencies of transcriptomic modifications on PTM regulation are illustrated in Figure 3.[241] PTMs such as phosphorylation (targeted by kinase inhibitors), acetylation (targeted by HAT and HDAC inhibitors), ADP-ribosylation (targeted by PARP inhibitors), methylation (targeted by histone methyltransferase inhibitors), lactation, acylation (targeted by sirtuin inhibitors), 2-hydroxyisobutyrylation, citrullination, and ubiquitination can be targeted by drugs already approved for human therapeutics. The significance of these PTMs, particularly epitranslational modifications, has been comprehensively reviewed along with an updated list of inhibitors targeting m6A writers, readers, and erasers.[241] Understanding the mechanisms underlying drug resistance provides critical insights into optimizing drug efficacy in clinical settings.

4.2. Targeting ncRNAs to overcome resistance against drug inhibitors

The first phase of research focused on understanding the cooperative mechanisms between ncRNAs and antiapoptotic factors in tumor cells. In the laboratory, significant progress has been made through the application of oligonucleotide libraries, RNA silencing, antisense oligonucleotides (ASOs), short hairpin RNAs (shRNAs), and single guide RNAs (sgRNAs) for CRISPR/Cas technology.[242-245] CRISPR/Cas9-based gene editing has been particularly effective, enabling high-throughput

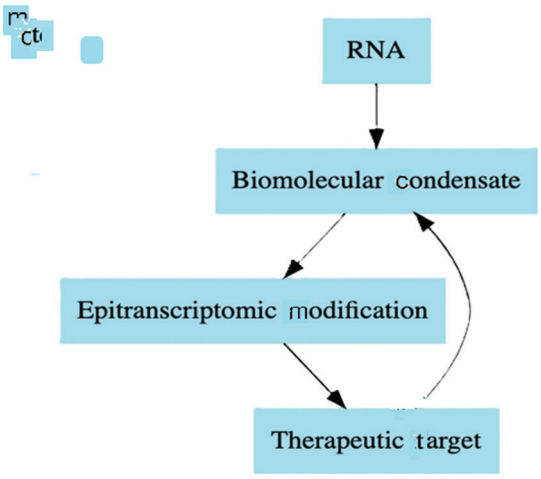

Figure 3. A schematic illustrating the involvement of PTM regulation of proteins and intrinsically disordered domain-containing proteins in the formation of LLPS, with a role for epitranscriptome modifications of RNAs in their stability and recognition by RNA-binding proteins. Image created by the authors

delivery of synthetic sgRNAs in conjunction with the Cas9 nuclease to target RNAs. Liu *et al.* compared chemical inhibitors of methylation enzymes with CRISPRoff/on methylation editing systems.[244] CRISPRoff is a relatively recent gene editing technology based on ZNF10 KRAB, Dnmt3A, and Dnmt3L domains, combined with catalytically inactive Cas9 (dCas9). This method allows researchers to manipulate the methylation landscape and alter gene expression without modifying the genome sequence. CRISPRon, on the other hand, facilitates the reversal of epigenetic changes induced by CRISPRoff by employing sgRNA-dCas9 complexes fused with DNA demethylases. Research using CRISPR technology, such as UCA1 knockout, has shown efficacy when combined with apoptosis regulation.[245]

Defective or dysregulated proteins can also be targeted using proteolysis targeting chimeras (PROTACs).[245-247] PROTACs enable protein knockdown with high efficiency at nanomolar concentrations. A few ncRNAs have been identified that contribute to chemoresistance and unresponsiveness to kinase inhibitors. For instance, some ncRNAs promote the oncogenicity of BRAF mutations and confer resistance to BRAF inhibitors (BRAFi) in melanoma cells. These ncRNAs, overexpressed in BRAFi-resistant cell lines, induce gain-of-function phenotypes.[248] Remarkably, BRAF-resistant cell lines respond well to PROTAC-based BRAF inhibition, offering advantages over conventional inhibitors.[249] In addition, small molecules have been identified that efficiently bind RNAs,[206] enabling the targeting of epigenetic alterations.

Several therapeutic approaches have been developed to inhibit ncRNAs in BCs. These include novel ribonuclease-targeting chimeras (RIBOTAC)[249,250] RNA therapeutics[251,252] that selectively regulate RNA-modifying enzymes, and targeting major SG proteins.

4.3. Targeting the mechanisms of therapy resistance by ncRNA knockdown

Gene silencing and knockdown methods are commonly used to inhibit ncRNAs. Antisense oligonucleotides (ASOs) and small interfering RNAs (siRNAs) suppress the expression of target genes in a sequence-specific manner. Catalytic nucleic acids, such as ribozymes, also suppress transcripts by cleaving mRNAs and template RNAs.[251]

Oncogenic RNAs can be targeted through RNA silencing with ASOs as well as small molecules that interact with RNA-binding protein domains.[252-255]

Cancers are frequently associated with chromosomal instability (CIN). Various approaches are being employed to restore sensitivity to radiotherapy and chemotherapy by targeting the CIN pathway. One strategy is to accelerate CIN

pathways, generating less-fit karyotypes. In gastrointestinal cancers, the ncRNA colon cancer-associated transcript 2 (CCAT2) plays a role in an RNA–protein complex formed by WD40-containing protein block-of-proliferation 1 (BOP1) and aurora kinase B (AURKB). This complex disrupts chromosome segregation, causing chaotic cell division. The CCAT2–BOP1–AURKB network is linked to 5-fluorouracil and oxaliplatin resistance.[256] The presence of active AURK, functional BOP1, and highly expressed CCAT2 RNA is crucial for driving chaotic cell division in this context.

Targeting ncRNAs often aims to overcome chemotherapy resistance. Researchers have tested nanoparticle-mediated RNA interference to knock down ncRNAs using delivery systems such as nanoparticles, liposomes, and PEG-conjugated particles. In triple-negative breast cancer (TNBC), the role of DANCR ncRNA has been identified. Silencing DANCR with siRNA technology resulted in decreased proliferation and blocked tumor growth. Following DANCR downregulation, EZH2 activity was restored, silencing the promoters of CD44 and ABCG2.[257] Another strategy is to inhibit CIN and therapeutically address genetically frozen cancer cell populations. To provide oncologists with safe and cost-effective medications, establishing production lines capable of synthesizing large quantities of modified oligonucleotides is crucial.

The European Medicines Agency has issued guidelines on RNA-based medicines,[258] highlighting advances in chemical modifications of ASOs, sequence engineering, and tumor-specific delivery methods.[259] In 2022, Benhamou designed an oncogenic noncoding RNA inhibitor by selecting optimal sequences from an RNA library and comparing them with a DNA library.[259] This pioneering work has laid the groundwork for developing efficient ncRNA-targeting drugs.

Patents have already been filed for targeting miR-22 in cancer and metabolism. ASO-based drugs are being developed for therapeutic applications. Examples include oligonucleotides antisense to protein-coding genes (e.g., BCL-2, VEGF, AP1) and antagomiRs targeting small RNAs, such as anti-miR-155 for cutaneous T-cell lymphomas and anti-miR-122. Miravirsen has demonstrated efficacy in primates for liver diseases, and other oligonucleotides function as miRNA mimics.

Efforts to standardize RNA-based therapeutics and address technical challenges have been optimized to preserve bioactivity from production to delivery. Nucleic acid-based drugs and delivery systems are now mature enough for industrial production, ensuring safe and efficient delivery to patients.

4.4. Targeting the interaction between BC components and the role of PTM

This section highlights how mutations in cancer gene fusions affect phase separation properties, potentially driving cancer initiation and progression. Insights into this mechanism can inform therapy design for cancers associated with aberrant phase separation. A central player in this process is the speckle-type POZ (Poxvirus and Zinc finger) protein (SPOP), which serves as a substrate adaptor for cullin 3 RING E3 ubiquitin ligase. SPOP facilitates the ubiquitination and proteasomal degradation of oncogenic proteins, exerting anti-proliferative effects. Localized in nuclear speckles, SPOP oligomerization and substrate interaction induce the formation of nuclear phase-separated droplets, known as SPOP droplets. These droplets facilitate the ubiquitination of substrates like DAXX (death domain-associated protein), marking them for proteasomal turnover. Studies have shown that the co-expression of DAXX with SPOP forms condensates enriched in SPOP/DAXX, facilitating DAXX ubiquitination and subsequent degradation.[260] Cancer-associated SPOP mutations disrupt the recruitment of DAXX and prevent the nucleation of SPOP/DAXX condensates, stabilizing DAXX instead. DAXX, in turn, promotes tumor development by repressing p53 activity. Its cytoplasmic and nuclear accumulation contributes to malignancy.[260]

Genetic systems can be leveraged to deliver proteins capable of dissolving p53 aggregates, potentially through mechanisms involving DAXX degradation, or to develop crosslinked mimic condensates for selective drug delivery. Synthetic peptides and nucleic acid-based oligonucleotides (e.g., RNA mimics, RNA sponges, siRNAs, and ASOs) hold promise for targeting mutant phenotypes. Investigating the dynamics of mutant p53 can enhance our understanding of protein misfolding and aggregation mechanisms. Novel drugs targeting abnormal phase transitions and p53 aggregation may have significant potential for clinical oncology applications.[11] Inhibition of mutant p53 aggregation by small molecules could effectively block tumor proliferation and migration.

Certain chemotherapeutics preferentially accumulate in specific BCs due to interactions linked to the drug's affinity for its target. For instance, cisplatin tends to accumulate in transcriptional condensates, whereas tamoxifen localizes in ER-alpha condensates. Estrogen-induced mediator (MED) activity dilutes transcriptional condensates, along with tamoxifen concentrations in these BCs. Interestingly, some therapeutics selectively interfere with condensates, presenting opportunities to regulate compartments critical for disease development.

Emerging evidence highlights the interplay between ncRNAs and epigenetic enzymes, particularly through

established and validated epigenetic drugs. Concurrently, small molecules targeting RNAs and their interacting partners are being explored for applications in RNA therapeutics.

Drugs that inhibit enzymes involved in PTMs can influence condensate behavior and modify oncogenic activities localized in these condensates. Alterations in the charges of residues within protein–protein interaction domains can impact proteins with IDR or prion-like domains ability to form BCs and undergo LLPS.

While chemotherapies aim to induce cancer cell death, certain drugs (e.g., bortezomib, sorafenib, 5-fluorouracil (5-FU), lapatinib, morusin, 5-azacytidine, 6-thioguanine, cisplatin, oxaliplatin, doxorubicin, and sodium selenite) paradoxically enhance cancer cell survival by promoting SG formation. For instance, K-RAS-dependent tumors upregulate SG formation.[261] Targeting or reducing SGs and their functions may yield therapeutic benefits. A notable PTM affecting condensate formation is myristoylation. In lung cancer cells, EZH2 myristoylation induces phase-separated liquid droplets containing EZH2, leading to compartmentalization, activation of STAT3, and enhanced cell proliferation.[262,263] Inhibiting myristoylation may potentially suppress cell growth. The subsequent section will discuss approaches for SG inhibition and specific cases of oncogenic protein chimeras impacting BCs in cancer.

4.5. Targeting the interaction between intrinsically disordered proteins and their partners

Proteins essential for BC formation, such as G3BP1, which assembles SGs, are promising targets for interfering with stress responses in cancer.[168,176] Key residues like V11 in G3BP are necessary for the formation of the G3BP–Caprin-1 complex; mutations at these sites block SG assembly. This opens the possibility for small compounds targeting protein interactions and specific G3BP domains to disrupt SG and BC formation or stability.[176,264] Small molecule interactors of SG proteins have shown potential in addressing cancer resistance to environmental stresses.[264,265]

SG inhibitory peptides (SIPs), derived from Caprin1 and USP10, have been fused with cell-penetrating peptides to create cancer inhibitors such as TAT-SIP-C1/2 and SIP-U1-Antp. These SIPs disrupt SGs[265] and enhance the sensitivity of cancer cells to sorafenib.

Inhibitors based on small compounds targeting the disordered regions of proteins have shown promise, with some progressing to clinical trials or therapeutic approval. For example, AC1Q3QWB selectively disrupts HOTAIR-mediated PRC2 recruitment, preventing silencing of gene promoters.[206]

In pancreatic cancer, the inhibitor ZW-115 targets the stress-inducible nuclear protein 1 (NUPR1), an intrinsically disordered protein, triggering apoptosis in PDAC cells that depend on K-RAS expression.[259,260]

The androgen receptor (AR), involved in nuclear condensates, has transiently stable secondary structures that are targeted by small molecules. Antiandrogens and abiraterone used in androgen-deprivation therapy induce the expression of constitutively active AR splice variants (AR-Vs), which promote resistance to radiotherapy by aiding DDR. Small molecules such as EPI-001 (ralaniten) selectively bind to the transactivation domain of AR, forming a binding pocket that blocks AR-DNA interaction. Other molecules like ETI-516 and EPI-7170 (a derivative of EPI-001) also block AR transcriptional activity and condensate formation in prostate cancer. EPI-7170 is currently in clinical trials (NCT04421222).[266] The ReACp53 peptide (patent WO2014182961A1) inhibits p53 amyloid-like aggregation, effectively targeting high-grade serous ovarian carcinomas (HGSOC).[267] BAY 249716 stabilizes both wild-type p53 and its mutants (R175H and Y220C),[11,268] while ADH-6 rescues mutant p53 activity. The aminothiazole compound BAY 1892005 covalently binds to mutant p53 variants (e.g., R175H, R282W, and Y220C) and dissolves nuclear condensates. In addition, PRIMA-1 reactivates mutated p53, inducing apoptosis under normoxic and hypoxic conditions, whereas nutlin-3 inhibits the MDM2-p53 interaction, increasing p53 stability and longevity.

Small molecule ligands have been screened from libraries of backbone-modified compounds for their RNA-binding capabilities. For example, diphenylfuran (DPF) compounds targeting MALAT1 bind to its triple helix, inducing RNA degradation.[269]

Small molecules targeting RNAs are under development with promising therapeutic applications. In alignment with the experimental work by Kovachka,[253] Meyer *et al.*[270] described receptor tyrosine kinase inhibitors (RTKis). RTKis can serve as RNA binders and can be reprogrammed and repurposed, given that they are FDA-approved drugs. For instance, the RTKi dovitinib inhibited the biogenesis of oncogenic miR-21 through direct interaction,[270] paving the way for designing small molecule RNA inhibitors to minimize off-target effects. Recently, the FDA approved a small molecule capable of interacting with the U1 snRNP complex of the splicing machinery. Risdiplam, tested in clinical trials for both infantile and later-onset spinal muscular atrophy (SMA), is now an orally administered drug for SMA treatment.[271] Furthermore, small molecules targeting RNA G-quadruplexes have been explored for the downregulation of K-RAS and N-RAS mRNAs and

are under development for addressing the GGGGCC repeat expansion in C9orf72, a mutation linked to ALS and frontotemporal dementia. For instance, DB1273 promotes G-quadruplex formation, reducing RNA foci and dipeptide translation in a Drosophila model of the neurological disease derived from all three independent C9orf72 repeat expansion iPSC lines and Drosophila with adult-onset ubiquitous expression of 36 G4C2 repeats which causes neurodegeneration due to arginine-rich proteins.[271] Recent work by Xiao *et al.* reviewed machine learning approaches for studying small molecules targeting RNAs and provided a list of FDA-approved drugs based on oligonucleotide technology. Their work highlighted the potential of machine learning in identifying RNA structures and prospective structural targets for small molecules.[272] Moreover, Kim and Kim reviewed the current understanding of RNAs, including circRNAs, and the therapeutic frontiers in targeting regulatory RNAs.[273]

In cell-specific pathways and responses, such as chromatin foci formation, transcription activation, and DNA damage response, BC formation is essential and depends on liquid–gel phase separation. These MLOs can be targeted by small molecules that block protein domains. One such BC target is the nuclear speckle, demonstrated by the use of diphenylfuran to target MALAT1.

Regarding the relationship between BCs and cancer, notable work has been conducted on the splicing factor ZMAT2. This protein contains two disordered regions critical for the formation of spliceosome complex condensates and regulates the expression of the tripartite motif protein 28 (TRIM28),[274,275] also known as Krüppel-Associated Box (KRAB)-Associated Protein 1 (KAP1). TRIM28 is a SUMOylation and RING-type ubiquitin-E3 ligase involved in the degradation of programmed cell death ligand 1 (PD-L1), thereby modulating immunosuppression in cancers. Targeting immune checkpoints has become a focus in cancer therapy. Verteporfin, for example, inhibits PD-L1 expression through Golgi-related autophagy mechanisms, interfering with the interaction of TRIM28 with interferon regulatory factor 1 and blocking PD-L1 induction. ZMAT2 also has RNA-binding activity and promotes phase transition, playing a role in the maturation of TRIM28 mRNA during the formation of protein-nucleic acid condensates. By upregulating TRIM28, this process reduces ROS accumulation in HCC and supports cell proliferation. Finally, SGs, as previously discussed, contribute to cancer cells' resistance to chemotherapy.

Pharmacological inhibition of DDX3 has been shown to attenuate SG assembly.[173] Consequently, small compounds targeting protein interactions and specific G3BP domains could be used in combination with novel drugs and small molecule interactors of SG proteins[264,265] to modulate SG stability.[176,265] This strategy could help overcome cancer resistance to environmental stress and chemotherapy. The eIF2α phosphorylation-induced SG assembly occurs during chemotherapy and involves various serine/threonine protein kinases, including GCN2, HRI, PKR, and PERK. Natural compounds such as psammaplysin F[276] reduce phosphorylated eIF2α levels, while cannabidiol attenuates the formation of SGs and BCs in glioblastoma. Similarly, medium-chain fatty acids, such as lauric acid, lipoic acid, and their amides,[277] show inhibitory effects. Notably, lipoamide has been demonstrated to inhibit SGs.[277]

Lipoamide reduces the formation of cytoplasmic FUS-linked SGs induced by arsenate and mitigates SG formation triggered by mitochondrial electron transport chain inhibition and hyperosmotic stress. However, it does not affect SGs formed in response to heat shock or glycolysis inhibition. This suggests that lipoamide functions as either an antioxidant or an inhibitor of specific BC forms. Importantly, lipoamide selectively inhibits SGs without affecting other BCs, such as Cajal bodies, nucleoli, and DNA damage foci.[277]

BCs can be targeted through three primary mechanisms. The first involves targeting the driver components, i.e., proteins and nucleic acids, to downregulate or inactivate them. The second focuses on disrupting physicochemical interactions essential for BC formation involving proteins and nucleic acids. The third strategy involves stabilizing or destabilizing condensates using drugs that partition into a BC, thereby modulating its activity.[13] Table 6 provides a summary of the inhibitors discussed in this section (Table 6).

Arsenic compounds, such as sodium arsenite, play a role in oxidative stress-induced SG formation, in which DDX3 acetylation is involved.[278] Arsenic trioxide (ATO), a highly toxic compound, has been used to induce PML-RARα degradation and inhibit PML nuclear bodies, particularly in PML-RARα translocation. Arsenite and ATO exhibit a dual role in paraspeckle formation, depending on the dose and duration of application. ATO promotes the formation of speckles and processing bodies by inducing spliceosome activity, induces SGs, and inhibits PML bodies by degrading PML-RARα. Trisenox was approved in 2002 as a drug for the treatment of multiple myeloma (MM). In 2004, the FDA approved its use for hepatocellular carcinoma therapy, and in 2018, the combination of Trisenox/Tretinoin was also approved. In addition, a phase II clinical trial in patients with refractory peripheral T-cell lymphoma (rPTCL) demonstrated the antitumor activity of darinaparsin, an organic arsenical compound comprising dimethylated arsenic conjugated to glutathione.[278]

Table 6. Molecules acting on intrinsically disordered proteins and biomolecular condensates (BCs)

Compound	Target	Application	References
AC1Q3QWB	HOTAIR-EZH2 binding	Various cancers, BC favors euchromatin	206
RK33 inhibits ATPase 16D inhibits helicase	DDX3, resulting in the block of SGs assembly	CRC, head/neck cancer, PC, brain cancer, drug resistance	173
G3BP inhibitor G3Ia nSP3 peptide	Block the interaction of G3BP with caprin 1 and USP10 and dissolves the preformed SG	VCP multisystem proteinopathy	168,176
ZW-115	Stress-inducible NUPR1	Induces apoptosis, K-RAS tumors, PDAC	259,260
TAT-SIP-C1/2, TAT-SIP-U1-Antp	Inhibitory peptides (SIPs) derived from Caprin 1 and USP10	Induce sensitivity to sorafenib	265
Ralaniten, EPI-7170	Blocks AR binding to DNA	Prostate cancer, androgen resistant	266
ReACp53 peptides	Bind p53 intrinsically disordered region	High-grade serous ovarian carcinoma	267
Aminothiazole BAY 249716, BAY 1892005	Stabilize p53 variants R175H, R282W and Y220C	Dissolution of the nuclear condensates	11,268
PRIMA-1, ADH-6	Reactivates mutated p53	Induce apoptosis in normoxia and hypoxia	268
Nutlin-3 p	Prevents the MDM2-p53 interaction	Increases the p53 shelf-life	268
Dyphenylfurans (DPF)	Triple helix containing MALAT1	Degradation of MALAT1 in overexpressing cancers	269
Dovitinib	Multiple RTK inhibitors	Blocks miR-21 biogenesis	270
Small molecule DB1273	RNA G-quadruplexes targets	K-RAS and N-RAS-bearing cancer	271
Verteporfin	Blocks TRIM28 interaction with IRF1	Inhibits IRF-induced PD-L1 expression and Golgi-related autophagy mechanisms	274,275
Psammaplysin F	Decreases the levels of phosphorylated eIF2α, inhibits SG formation after eIF2 phosphorylation	Improves chemotherapy, increases the efficacy of bortezomib sorafenib	276
Cannabidiol, lipoamide	Attenuates the formation of SGs and BCs	GBM; reduce FUS-linked stress granules induced by arsenate	277,278
Trisenox/Tretinoin	Inhibit PML bodies	Induce PML-RARa degradation HCC, MM	278,281
VTP50469	Disrupts the interactions between the NUP98 fusion proteins and chromatin	Therapy for NUP98-rearranged leukemia	282
Emodin, MLN4924, and TSA	Increase the levels of PML protein	Restore PML body activity	282
MLN4924	NEDDylation inhibitor	Suppresses APL	282
SU056, fisetin, CX-5461	Y-box-binding protein 1 (YB1)	CRC, melanoma, block invasiveness in BC	184
PI3K/mTOR dual inhibitors: GSK1059615, CAY10626, samotolisib, 4Torin 1, PP242, PI-103, LY3023414, INK128	Inhibit NEAT1_2 and paraspeckle	CLL therapy	96
Dual PI3K/TOR inhibitor BEZ235	Inhibit YB-1 expression	Favors radiotherapy cytotoxicity in CRC, blocks EMT, and invasiveness in melanoma	184
YK-4-279	Targets the IDR of EWS-FLI1	Ewing sarcoma tumors	280,281
SHP2 inhibitors AB-3068, TNO155, RMC-4630, and RLY-1971	Therapy of SHP2 mutations inducing BC formation and promoting MAPK signaling, leading to ERK1/2 activation	Trials in solid cancers	282
Elvitegravir	Disrupts SRC-1 condensates, P bodies, YAP/TEAD/SRC-1 BCs	Suppresses the growth of YAP-dependent tumors, favors anti-PD-1 immunotherapy	282

(Cont'd...)

Table 6. ***(Continued)***

Compound	Target	Application	References
Reserpine	Induce cell death through BAX and MST-1 upregulation and downregulation of Bcl2, LATS-1, and YAP	Antiproliferative effects on MDA-MB-231	283
pH-responsive hexapeptide (VEALYL)	Swelling of lysosomes	Chemotherapy of MDR-overexpressing tumors	284
Actinomycin D (ActD), etoposide, flavopiridol	Inhibit paraspeckles	Reduction in size	285
AKT inhibitor TAS0612, everolimus	Inhibits YB-1 phosphorylation	Reverse resistance to tamoxifen in BC	287
2,4-dihydroxy-5-pyrimidinyl imidothiocarbomate, 6-O-angeloylplenolin sesquiterpene lactone	Block YB-1 translocation to the nuclei	YB-1 cannot induce target genes, blocking BC growth	287
MG132 proteasome inhibitor	Activates GCN2 for the hyperphosphorylation of eIF2-alpha	Cells defective in UPR, B-cell lymphoma, leukemias; hyper phosphorylated eIF2a increases bortezomib anticancer activity through eradication of quiescent cancer cells	288
ISRIB peptide		Pulmonary veno-occlusive disease, Fragile X syndrome, neurodegenerative diseases, diseases involving SG formation	289,290
FYVE finger-containing phosphoinositide kinase) modulator plus an integrated stress response antagonist	Induce a MiT/TFE transcription factor promoting lysosomal gene translation	Improve glucocerebrosidase function in Gaucher patient-derived fibroblasts	291

Abbreviations: CLL: Chronic lymphocytic leukemia; PDAC: Pancreatic ductal adenocarcinoma; PML: Promyelocytic leukemia protein; GBM: Glioblastoma multiforme.

Pancreatic cancer cells have been shown to be sensitive to 1,6-hexanediol, an LLPS inhibitor that also modulates kinase and phosphatase activities. Experimentally applied to cell cultures, 1,6-hexanediol reduced pancreatic cancer growth in an orthotopic BxPC-3 xenograft model using the BXPC-3 human pancreatic adenocarcinoma cell line. This compound inhibits the stability of SGs and disrupts weak intermolecular hydrophobic interactions, likely through alterations in hydrogen bonding. Transcriptional studies revealed that 1,6-hexanediol downregulates *myc* expression as well as other genes involved in key signaling pathways, including cytokine-cytokine receptor interactions, Wnt signaling pathway, extracellular matrix-integrin/cadherin receptor interactions, mitogen-activated protein kinase (MAPK) signaling, and focal adhesion pathways.[277]

Therapeutic approaches aimed at modifying cancer phenotypes (proliferation, invasiveness, and chemotherapy unresponsiveness) are collectively referred to as condensate-modifying therapeutics (c-mods). The targets of c-mods include the regulation of physical properties, macromolecular networks, composition, dynamics, and functions of specific BCs.[280]

Several oncogenes are influenced by ncRNA regulation, making these ncRNAs potential targets for small molecules that inhibit their activity. For instance, the ncRNA MTAR1 recruits IGF2BPs into condensates, promoting their interaction with PABP1 and enhancing the stability and translation of *myc* Mrna.[241] Similarly, MNX1-AS1, which is upregulated in NSCLC, facilitates MYC-mediated transcriptional activation. MNX1-AS1 induces IGF2BP1 phase separation, thereby increasing its interaction with the mRNAs *E2F1* and *myc*, both of which encode oncogenic transcription factors and promote NSCLC cell proliferation.[241] Since the MYC signaling pathway is oncogenic, it can serve as a key target for therapeutic strategies.

The PML nuclear body, a BC formed through LLPS, is relevant in leukemias where mutations in *PML* render patients resistant to arsenic-targeted therapy.[281]

The induction of LLPS by NUP98 fusion oncoproteins (FOs) is implicated in leukemia. Nearly 30 NUP98-FOs have been identified, associated with 5% of pediatric acute myeloid leukemia (pAML) cases and 50% of chemotherapy-resistant pAML cases.[281] Strategies to counteract the oncogenic activity of NUP98-FOs depend on the specific fusion protein involved. These strategies may include targeting transcriptional and epigenetic machinery (e.g., HDAC inhibitors), addressing alterations in cooperating partners, or disrupting signaling and cell cycle pathways. For instance, VTP50469 disrupts interactions between NUP98 fusion proteins and chromatin in

NUP98-rearranged leukemia models.[282] To restore PML body activity, molecules such as emodin, MLN4924, and TSA increase PML protein levels. MLN4924, an inhibitor of neddylation, has been shown to suppress APL development. Synthetic protein disaggregates, such as modified Hsp104 variants, can disaggregate condensates formed by the EWS-FLI and FUS-CHOP fusion proteins.[282]

YB-1 represents another promising therapeutic target, as it is involved in both P bodies and SGs. Various approaches have demonstrated positive impacts on YB-1 inhibition. TOR kinase inhibitors, such as rapamycin, also inhibit PI3K: PI3K/TOR inhibitors and suppress NEAT1_2 and paraspeckles. The dual PI3K/TOR inhibitor BEZ235 reduces YB-1 expression, inhibits cancer growth, and enhances the cytotoxicity of radiotherapy in CRC.[184] In addition, the AKT inhibitor TAS0612, which acts on p70S6K and p90RSK, inhibits YB-1 phosphorylation and reverses antiestrogen resistance in BC. SU056 (azopodophyllotoxin) directly binds to YB-1. Fisetin, a small molecule, inhibits the AKT–YB-1 interaction, thereby preventing cancer migration in prostate tumors. It also reduces melanoma tumor growth *in vivo* through a dual mechanism: inhibition of RSK kinase activity and reduction of YB-1 protein levels. Fisetin forms a complex with RSK2, which then binds to YB-1. Furthermore, CX-5461 inhibits RNA polymerase I and blocks YB-1 activity. The compound 2,4-dihydroxy-5-pyrimidinyl imidothiocarbomate (DPI) prevents YB-1 nuclear translocation, downregulates target gene expression, and inhibits BC growth. Similarly, the sesquiterpene lactone 6-O-angeloylplenolin blocks YB-1 nuclear translocation and downregulates the expression of the multidrug efflux pump MDR1 in colon cancer.

LLPS plays a crucial role in the transcriptional programs regulated by Yes-associated protein (YAP) and the transcriptional coactivator with PDZ-binding motif (TAZ), both key components and regulators of Hippo signaling. The complex formed by YAP/TAZ promotes P body formation in various cancer cell lines. P bodies act as downstream effectors of YAP/TAZ. The interaction between YAP/TEAD and steroid receptor coactivator 1 (SRC-1) is critical for the formation of SRC-1/YAP/TEAD condensates, which promote YAP transcription. Interestingly, the anti-HIV drug elvitegravir disrupts SRC-1 condensates and suppresses the growth of YAP-dependent tumors.[282]

YAP condensates are associated with resistance to anti-PD-1 immunotherapy. These BCs concentrate epigenetic enzymes such as histone acetylase, making drugs targeting these enzymes potentially beneficial when combined with existing therapies.

The methanolic extract (RTE) from *Rauvolfia tetraphylla* and its isolated compound, reserpine, exhibit antiproliferative effects on the TNBC cell line MDA-MB-231. Reserpine-treated cells cease proliferation and undergo apoptosis through the upregulation of BAX and MST-1 and the downregulation of Bcl2, LATS-1, and YAP. Consequently, YAP levels decline, the TEAD-YAP complex fails to form, and cell growth is inhibited.[283]

The transcriptional coactivators YAP and TAZ, which interact with PDZ-binding domains, serve as downstream effectors of the Hippo kinase cascade. YAP/TAZ plays significant roles in cell growth, differentiation, tissue development, and carcinogenesis. Recent studies reveal that in addition to the Hippo kinase cascade, several non-Hippo kinases regulate YAP/TAZ signaling, influencing tumorigenesis and progression. YAP/TAZ oncogenes also promote P body formation across various cancer cell lines. Mechanistically, this involves the transcriptional activation of P body-related genes (e.g., SAMD4A, AJUBA, and WTIP) and the suppression of the tumor suppressor gene PNRC1. Re-expression of PNRC1 or knockdown of P body core genes (e.g., DDX6, DCP1A, and LSM14A) demonstrates that P bodies attenuate cell proliferation, migration, and tumor growth induced by YAP overexpression in CRC. Since P bodies act as downstream effectors of YAP/TAZ, re-expressing PNRC1 or disrupting P bodies may serve as potential therapeutic strategies for YAP-driven tumors.

An additional treatment avenue involves targeting cancers with deregulated phase transitions caused by IDRs. For example, YK-4-279 targets the IDR of phase-separating EWS-FLI1 and blocks its interaction with RNA helicase A in Ewing sarcoma tumors.[280-282] Wild-type SHP2 (protein tyrosine phosphatase non-receptor type 11) forms BCs in response to factors such as EGF and FGF. Mutations in SHP2 that promote BC formation drive MAPK signaling, leading to ERK1/2 activation. Several SHP2 allosteric inhibitors, including AB-3068, TNO155, RMC-4630, and RLY-1971, are under clinical evaluation for solid cancers.[282]

Advancements in permeable peptide and material design have also shown promise in LLPS regulation.[284] An aromatic motif-based pH-responsive hexapeptide (VEALYL), referred to as the lysosome-targeting peptide, was derived from the insulin sequence. Cancer cells internalize this peptide through endocytosis, triggering proton-induced phase separation within lysosomes, transitioning from solution to hydrogel. This hydrogelation increases lysosomal volume and permeability, causing lysosomal rupture and subsequent cancer cell death. Lysosomal assemblies have been shown to enhance the efficacy of chemotherapy against multidrug-resistant cells in xenografted tumors.[284]

Paraspeckle disintegration has been achieved using DNA intercalators. Actinomycin D (ActD) binds to the DNA minor groove, promoting paraspeckle disassembly and resulting in smaller condensates. While ActD administration reduces the size of NEAT1_2 speckles, it does not alter their number. Meanwhile, core paraspeckle proteins SFPQ and NONO remain localized to the perinucleolar caps.

Because DNA-binding molecules can induce double-strand breaks, it has been demonstrated that paraspeckle disintegration is not linked to DNA damage or RNA polymerase inhibition. An increase in smaller NEAT1_2 paraspeckles was observed following treatment with etoposide, a topoisomerase II inhibitor, and flavopiridol, an inhibitor of cyclin-dependent kinases. In contrast, the microtubule inhibitor vincristine had no effect, as it does not bind to dsDNA.[285]

The structural basis of double-stranded DNA helix binding underpins the assembly and maintenance of paraspeckles, speckles, and other nuclear ncRNA-based condensates. This insight opens new avenues for studying the mechanisms of drugs such as etoposide, actinomycin D, and mithramycin A, which are widely used in osteosarcoma treatment. Targeting P bodies also holds potential for cancer therapy. A recent review discussed the therapeutic implications of modulating P body formation.[184,286,287]

Hyperphosphorylation of eIF2a enhances the anticancer activity of bortezomib by eradicating quiescent cancer cells and inhibiting their survival. Under ER stress, the transmembrane protein kinase/endoribonuclease inositol-requiring enzyme 1 (IRE1) is activated, clustering into ER membrane-bound condensates associated with SGs. IRE1α clusters tether SGs to the ER in response to various stressors. This clustering facilitates the splicing of XBP1 mRNA to produce the XBP1 isoform 2, which is involved in the unfolded protein response.[288] Diseases linked to XBP1 dysfunction include bipolar disorders, B-cell lymphomas, and leukemias. XBP1 is frequently overexpressed in BCs and metastatic malignancies. MG132, a proteasome inhibitor, has been shown to activate GCN2.

The integrated stress response (ISR) inhibitor, ISRIB (M7425, AbMole, Huston, USA), is a selective small molecule inhibitor of eukaryotic translation initiation factor 2-alpha kinase 3, also known as protein kinase R (PKR)-like ER kinase (PERK) signaling. ISRIB effectively reverses eIF2α phosphorylation and disassembles SGs. When administered to be stressed cells with preformed SGs, ISRIB induces their rapid disassembly, releasing mRNAs into the RNA pool for active translation. ISRIB reverses the translational inhibition caused by stress and eIF2α phosphorylation. ISRIB prevents SG formation induced by eIF2α phosphorylation, ER stress from unfolded protein retention, thapsigargin, and arsenite (an SG inducer).

Notably, P bodies remain functional and unaffected by ISRIB treatment or stressors. ISRIB increases the activity of eIF2B, eIF5, and other initiation factors by directly or indirectly reversing the effects of phosphorylated eIF2α. It acts as a molecular glue, linking eIF2B tetramers to decameric active enzymes.

A hollow nanoparticle-based delivery system was developed for ISRIB. PEGylated copper sulfide nanoparticles (HCuS NPs) encapsulating ISRIB, combined with phase-change material lauric acid (LA), were used in photothermal therapy (PTT). This light-controlled ISRIB release inhibited SG formation during PTT, enhancing the antitumor effect and inducing immunogenic cell death (ICD).[289] In addition, a pH-driven and NIR photo-responsive smart drug delivery system (IL@H-PP) promoted the production of ROS by tumor-associated macrophages (TAMs). TAMs were repolarized toward an M1 phenotype, remodeling the tumor microenvironment from immunosuppressive to immunity-competent. ISRIB has demonstrated therapeutic potential beyond cancer treatment. It has shown promise in addressing pulmonary veno-occlusive disease, Fragile X syndrome, neurodegenerative disorders associated with SG formation, eIF2α phosphorylation, and cognitive impairment.[289,290]

Inhibition of the ISR has also been explored for the treatment of diseases beyond cancer. In lysosomal storage disorders, two compounds (patent U.S. Ser. No. 63/675,391) have been found to enhance glucocerebrosidase function in Gaucher patient-derived fibroblasts through an MiT/TFE transcription factor that promotes lysosomal gene translation. An ISR antagonist was combined with a PIKfyve (FYVE finger-containing phosphoinositide kinase) modulator to improve cellular glucocerebrosidase activity. This combination likely succeeded because ISR signaling appears to be slightly activated by treatment with either of these small molecules individually.[291]

5. Application of emerging technologies in BC studies

The potential of RNA to adopt diverse structures within or outside condensates can be utilized for innovative therapeutic purposes. This includes enzymatic RNA molecules, known as ribozymes, exhibiting activity exclusively within condensates. These structures influence RNA–RNA interactions, affecting the material properties of RNA-seeded condensates and impacting RNA sorting during the development of phase-separated assemblies. Analyzing RNA structures in dense phases and the supramolecular formations within them poses significant

challenges, resulting in limited data on RNA structure within BCs. A key obstacle is isolating this specific RNA quantitatively. A recently reported needle-shearing method has proven effective for RNA extraction in this context. RNA structural biology is crucial for advancing knowledge, with cryo-EM SPA revealing protein-free RNA structures. RNA structure determination using cryo-EM methods provides useful information, including resolving maps of RNA-based systems. These data can offer subnanometer resolution and coordinate estimation, especially when combined with multidimensional chemical mapping and computational modeling, such as with Rosetta DRRAFTER. The "Ribosolve" pipeline aids in validating macromolecular complexes.[292] Applying this workflow to ncRNA modules may uncover new structural elements.

Super-resolution microscopy, based on various techniques, produces images with a resolution surpassing the diffraction limit, achieving the 30-nm range. A series of fluorophores, acting in complementary absorbance zones and emitting light at separate times and wavelengths, enables resolving images over time. Among these methods are super-resolution optical fluctuation imaging and single-molecule localization methods (SMLM). Examples of applications include imaging cell nuclei and mitotic stages. Stimulated emission depletion microscopy (STED), a frontline method in recent years, uses two laser pulses: an excitation pulse to excite fluorophores and a STED pulse for de-excitation through stimulated emission. Spectral precision distance microscopy resolves multiple light sources by isolating a few at a time. Cryogenic optical localization in 3D (COLD) localizes fluorescent sites within small- to medium-sized biomolecules at near-Angstrom resolution. Binding-activated localization microscopy is a potential approach for SMLM. Stochastic optical reconstruction microscopy, another frontline method, is similar to photo-activated localization microscopy (PALM) and fluorescence photo-activation localization microscopy, which exploit sequential activation and time-resolved localization of photoswitchable fluorophores to produce high-resolution images. PALM of mEos3.2 fluorescent protein tags combined with DNA-PAINT revealed BC organization and patterns in a cell cycle–dependent manner. Spectrally resolved SMLM (SR-SMLM) combined with an environment-sensitive dye for displacement/diffusivity mapping (SMdM) analyzed distinct hydrophobic nanodomains at the condensate surface.[293-296] Xia, Doudna, and colleagues[290] developed single-molecule live-cell fluorescence *in situ* hybridization (smLiveFISH), employing a programmable RNA-guided CRISPR–Csm complex with catalytically inactivated Csm for specific and durable RNA binding.[297] Using smLiveFISH, they visualized single NOTCH2 and MAP1B mRNA transcripts in living cells, identifying mechanisms such as cotranslational translocation of NOTCH2 mRNA at the ER and MAP1B mRNA transfer to the cell periphery. These technologies provide insights into mRNA mislocalization and BC dysregulation in diseases and cancer.[15] New frontiers on treatment of cancers by targeting RNA modifications and BC dysregulation with new drugs are surging interest and could be applied in a clinical setting.[298]

6. Conclusion

In conclusion, this review highlights the frontier of condensate- and oncogenic RNA-targeted drug discovery, pointing to potential breakthroughs in therapeutic interventions. The role of BCs, including SGs, cancer-associated proteins, and tumor suppressors and repressors, in cancer cell biology and their dysregulation within the cancer milieu has gained attention. Several avenues exist for developing cancer therapeutics. The first involves targeting oncogenic ncRNAs, potentially delivering drugs to specific cell types to prevent their role in forming phase-separated condensates with oncogenic potential. This can be achieved through RNA silencing through shRNA or ASO or by targeting triple helix structures. The second approach focuses on targeting domains responsible for RNA–protein interactions. A third strategy is the use of drugs aimed at epigenetic enzymes. The final approach involves validating compounds that chemically disrupt BC formation or target the protein organizers of BCs. Future research directions in BCs hold significant promise, offering not only a deeper understanding of degenerative diseases and cancer but also paving the way for advancements in clinical applications.

Acknowledgments

None.

Funding

None.

Conflict of interest

The authors declare that they have no competing interests.

Author contributions

Conceptualization: Palmiro Poltronieri
Visualization: Sudipta Joardar
Writing – original draft: Sudipta Joardar
Writing – review & editing: Palmiro Poltronieri

Ethics approval and consent to participate

Not applicable.

Consent for publication

Not applicable.

Availability of data

Not applicable.

Further disclosure

Part of the work has been presented in the virtual conference "International Forum on Traditional and Alternative Medicine" on November 16, 2023.

References

1. Boeynaems S, Alberti S, Fawzi NL, *et al.* Protein phase separation: A new phase in cell biology. *Trends Cell Biol*. 2018;28(6) 420-435.

   doi: 10.1016/j.tcb.2018.02.004

2. Banani SF, Lee HO, Hyman AA, Rosen MK. Biomolecular condensates: Organizers of cellular biochemistry. *Nat Rev Mol Cell Biol*. 2017;18(5):285-298.

   doi: 10.1038/nrm.2017.7

3. Guillén-Boixet J, Kopach A, Holehouse AS, *et al.* RNA-induced conformational switching and clustering of G3BP drive stress granule assembly by condensation. *Cell*. 2020;181:346-361.e17.

   doi: 10.1016/j.cell.2020.03.049

4. Rhine K, Odeh HM, Shorter J, Myong S. Regulation of biomolecular condensates by Poly(ADP-ribose). *Chem Rev*. 2023;123(14):9065-9093.

   doi: 10.1021/acs.chemrev.2c00851

5. Fay MM, Anderson PJ. The role of RNA in biological phase separations. *J Mol Biol*. 2018;430(23):4685-4701.

   doi: 10.1016/j.jmb.2018.05.003

6. Lavalée M, Curdy N, Laurent C, Fournié JJ, Franchini DM. Cancer cell adaptability: Turning ribonucleoprotein granules into targets. *Trends Cancer*. 2021;7(10):902-915.

   doi: 10.1016/j.trecan.2021.05.006

7. Taniue K, Akimitsu N. Aberrant phase separation and cancer. *FEBS J*. 2022;289(1):17-39.

   doi: 10.1111/febs.15765

8. Mullard A. Biomolecular condensates pique drug discovery curiosity. *Nat Rev Drug Discov*. 2019;18:324-326.

   doi: 10.1038/d41573-019-00069-w

9. Conti BA, Oppikofer M. Biomolecular condensates: New opportunities for drug discovery and RNA therapeutics. *Trends Pharmacol Sci*. 2022;43(10):820-837.

   doi: 10.1016/j.tips.2022.07.001

10. Chakravarty AK, Mcgrail DJ, Lozanoski TM, *et al.* Biomolecular condensation: A new phase in cancer research. *Cancer Discov*. 2022;12:2031-2043.

    doi: 10.1158/2159-8290.CD-21-1605

11. Silva JL, Foguel D, Ferreira VF, *et al.* Targeting biomolecular condensation and protein aggregation against cancer. *Chem Rev*. 2023;123(14):9094-9138.

    doi: 10.1021/acs.chemrev.3c00131

12. Kilgore HR, Young RA. Learning the chemical grammar of biomolecular condensates. *Nat Chem Biol*. 2022;18(12):1298-1306.

    doi: 10.1038/s41589-022-01046-y

13. Maqsood Q, Sumrin A, Saleem MZ, *et al.* An insight into cancer from biomolecular condensates. *Cancer Screen Prevent*. 2023;2(3):177-190.

    doi: 10.14218/CSP.2023.00018

14. Ginell GM, Holehouse AS. An introduction to the stickers-and-spacers framework applied to biomolecular condensates. *Methods Mol Biol*. 2023;2563:95-116.

    doi: 10.1007/978-1-0716-2663-4_4

15. Otis JP, Mowry KL. Hitting the mark: Localization of mRNA and biomolecular condensates in health and disease. *Wiley Interdiscipl Rev RNA*. 2023;14(6):e1807.

    doi: 10.1002/wrna.1807

16. Villegas JA, Heidenreich M, Levy ED. Molecular and environmental determinants of biomolecular condensate formation. *Nat Chem Biol*. 2022;18(12):1319-1329.

    doi: 10.1038/s41589-022-01175-4

17. Schmidt HB, Görlich D. Transport selectivity of the nuclear pores, phase separation, and membraneless organelles. *Trends Biochem Sci*. 2016;41(1):46-61.

    doi: 10.1016/j.tibs.2015.11.001

18. Forman-Kay JD, Ditlev JA, Nosella ML, Lee HO. What are the distinguishing features and size requirements of biomolecular condensates and their implications for RNA-containing condensates? *RNA*. 2022;28:36-47.

    doi: 10.1261/rna.079026.121

19. Kwon I, Kato M, Xiang S, *et al.* Phosphorylation-regulated binding of RNA polymerase II to fibrous polymers of low-complexity domains. *Cell*. 2013;155(5):1049.

    doi: 10.1016/j.cell.2013.10.033

20. Peran I, Mittag T. Molecular structure of the biomolecular condensates. *Curr Opin Struct Biol*. 2020;60:17-26.

    doi: 10.1016/j.sbi.2019.09.007

21. Holmes KJ, Klass DM, Guiney EL, Cyert MS. Whi3, an S. cerevisiae RNA-binding protein, is a component of stress granules that regulates levels of its target mRNAs. *PLoS One*.

2013;8(12):e84060.

doi: 10.1371/journal.pone.0084060

22. Ukmar-Godec T, Wegmann S, Zweckstetter M. Biomolecular condensation of the microtubule-associated protein tau. *Semin Cell Dev Biol*. 2020;99:202-214.

doi: 10.1016/j.semcdb.2019.06.007

23. Ukmar-Godec T, Hutten S, Grieshop MP, *et al.* Lysine/RNA-interactions drive and regulate biomolecular condensation. *Nat Commun*. 2019;10(1):2909.

doi: 10.1038/s41467-019-10792-y

24. Boyko S, Surewicz WK. Tau liquid-liquid phase separation in neurodegenerative diseases. *Trends Cell Biol*. 2022;32(7):611-623.

doi: 10.1016/j.tcb.2022.01.011

25. Abasi LS, Elathram N, Movva M, Deep A, Corbett KD, Debelouchina GT. Phosphorylation regulates tau's phase separation behavior and interactions with chromatin. *Commun Biol*. 2024;7(1):251.

doi: 10.1038/s42003-024-05920-4

26. Parolini F, Tira R, Barracchia CG, *et al.* Ubiquitination of Alzheimer's-related tau protein affects the liquid-liquid phase separation in a site- and cofactor-dependent manner. *Int J Biol Macromol*. 2022;201:173-181.

doi: 10.1016/j.ijbiomac.2021.12.191

27. Farooqi AA, Fayyaz S, Poltronieri P, Calin G, Mallardo M. Epigenetic deregulation in cancer: Enzyme players and noncoding RNAs. *Semin Cancer Biol*. 2022;83:197-207.

doi: 10.1016/j.semcancer.2020.07.013

28. Mattick JS, Amaral PP, Carninci P, *et al.* Long noncoding RNAs: Definitions, functions, challenges and recommendations. *Nat Rev Mol Cell Biol*. 2023;24:430-447.

doi: 10.1038/s41580-022-00566-8

29. Poltronieri P. Regulatory RNAs: Role as scaffolds assembling protein complexes and their epigenetic deregulation. *Explor Target Antitumor Ther*. 2024;5(4):841-876.

doi: 10.37349/etat.2024.00252

30. Cusenza VY, Tameni A, Neri A, Frazzi R. lncRNA epigenetics: The significance of m6A and m5C lncRNA modifications in cancer. *Front Oncol*. 2023;13:1063636.

doi: 10.3389/fonc.2023.1063636

31. Bure IV, Nemtsova MV, Kuznetsova EB. Histone modifications and non-coding RNAs: Mutual epigenetic regulation and role in pathogenesis. *Int J Mol Sci*. 2022;23:5801.

doi: 10.3390/ijms23105801

32. Yang X, Liu M, Li M, *et al.* Epigenetic modulations of noncoding RNA: A novel dimension of Cancer biology. *Mol Cancer*. 2020;19:64.

doi: 10.1186/s12943-020-01159-9

33. Gibson BA, Doolittle LK, Schneider WG, Gerlich DW, Redding S, Rosen MK. Organization of chromatin by intrinsic and regulated phase separation. *Cell*. 2019;179:470-484.

doi: 10.1016/j.cell.2019.08.037

34. Nylund P, Garrido-Zabala B, Kalushkova A, Wiklund HJ. The complex nature of lncRNA-mediated chromatin dynamics in multiple myeloma. *Front Oncol*. 2023;13:1303677.

doi: 10.3389/fonc.2023.1303677

35. Hu WL, Jin L, Xu A, *et al.* GUARDIN is a p53-responsive long noncoding RNA that is essential for genomic stability. *Nat Cell Biol*. 2018;20:492-502.

doi: 10.1038/s41556-018-0066-7

36. Kurup JT, Kidder BL. Identification of H4K20 me3-and H3K4 me3-associated RNAs using CARIP-Seq expands the transcriptional and epigenetic networks of embryonic stem cells. *J Biol Chem*. 2018;293(39):15120-15135.

doi: 10.1074/jbc.RA118.004974

37. Agredo A, Kasinski AL. Histone 4 lysine 20 tri-methylation: A key epigenetic regulator of chromatin structure and disease. *Front Genet*. 2023;14:1243395.

doi: 10.3389/fgene.2023.1243395

38. Fan L, Sun W, Lyu Y, *et al.* Chrom-seq identifies RNAs at chromatin marks. *Sci Adv*. 2024;10(31):eadn1397.

doi: 10.1126/sciadv.adn1397

39. Ahmad A, Poltronieri P, Uddin S. Editorial: LncRNAs in cancer metastasis and therapy resistance. *Front Oncol*. 2021;11:813274.

doi: 10.3389/fonc.2021.813274

40. Zang C, Nie FQ, Wang Q, *et al.* Long noncoding RNA LINC01133 represses KLF2, P21 and E-cadherin transcription through binding with EZH2 and LSD1 in non-small cell lung cancer. *Oncotarget*. 2016;7:11696-11707.

doi: 10.18632/oncotarget.7077

41. Kong Y, Hsieh CH, Alonso LC. ANRIL: A lncRNA at the CDKN2A/B locus with roles in cancer and metabolic disease. *Front Endocrinol* (*Lausanne*). 2018;9:405.

doi: 10.3389/fendo.2018.00405

42. Lian Y, Yan C, Ding J, *et al.* A novel lncRNA, LL22NC03-N64E9.1, represses KLF2 transcription by binding with EZH2 in colorectal cancer. *Oncotarget*. 2017;8:59435-59445.

doi: 10.18632/oncotarget.19738

43. Quagliata L, Matter MS, Piscuoglio S, *et al.* Long noncoding RNA HOTTIP/HOXA13 expression is associated with disease progression and predicts the outcome in hepatocellular carcinoma patients. *Hepatology.*

2014;59:911-923.

doi: 10.1002/hep.26740

44. Zhang G, Xu Y, Zou C, *et al.* The long noncoding RNA ARHGAP27P1 inhibits gastric cancer cell proliferation and cell cycle progression by epigenetically regulating p15 and p16. *Aging* (*Albany NY*). 2019;11:9090-9110.

doi: 10.18632/aging.102377

45. Bai Z, Wu Y, Bai S, *et al.* Long noncoding RNA SNHG7 Is activated by SP1 and exerts oncogenic properties by interacting with EZH2 in ovarian cancer. *J Cell Mol Med*. 2020;24:7479-7489.

doi: 10.1111/jcmm.15373

46. Huang MD, Chen WM, Qi FZ, *et al.* Long noncoding RNA TUG1 is upregulated in hepatocellular carcinoma and promotes cell growth and apoptosis by epigenetically silencing KLF2. *Mol Cancer*. 2015;14:165.

doi: 10.1186/s12943-015-0431-0

47. Ruan J, Zheng L, Hu N, *et al.* Long noncoding RNA SNHG6 promotes osteosarcoma cell proliferation by regulating p21 and KLF2. *Arch Biochem Biophys*. 2018;646:128-136.

doi: 10.1016/j.abb.2018.03.036

48. Lian Y, Yang J, Lian Y, Xiao C, Hu X, Xu H. DUXAP8, a pseudogene-derived lncRNA, promotes the growth of pancreatic carcinoma cells by epigenetically silencing CDKN1A and KLF2. *Cancer Commun* (*Lond*). 2018;38:64.

doi: 10.1186/s40880-018-0333-9

49. Chen Z, Chen X, Chen P, *et al.* Long noncoding RNA SNHG20 promotes non-small cell lung cancer cell proliferation and migration by epigenetically silencing of P21 expression. *Cell Death Dis*. 2017;8:e3092.

doi: 10.1038/cddis.2017.484

50. Statello L, Guo CJ, Chen LL, Huarte M. Gene regulation by long noncoding RNAs and its biological functions. *Nat Rev Mol Cell Biol*. 2021;22:96-118.

doi: 10.1038/s41580-020-00315-9

51. Cai Z, Cao C, Ji L, *et al.* RIC-seq for global in situ profiling of RNA-RNA spatial interactions. *Nature*. 2020;582(7812):432-437.

doi: 10.1038/s41586-020-2249-1

52. Huang J, Zhou N, Watabe K, *et al.* Long noncoding RNA UCA1 promotes breast tumor growth by suppressing p27 (Kip1). *Cell Death Dis*. 2014;5:e1008.

doi: 10.1038/cddis.2013.541

53. Luo J, Xiang H. LncRNA MYLK-AS1 acts as an oncogene by epigenetically silencing large tumor suppressor 2 (LATS2) in gastric cancer. *Bioengineered*. 2021;12:3101-3112.

doi: 10.1080/21655979.2021.1944019

54. Ding J, Xie M, Lian Y, *et al.* Long noncoding RNA HOXA-AS2 represses P21 and KLF2 expression transcription by binding with EZH2 and LSD1 in colorectal cancer. *Oncogenesis*. 2017;6:e288.

doi: 10.1038/oncsis.2016.84

55. Zhang G, Xu Y, Wang S, *et al.* LncRNA SNHG17 promotes gastric cancer progression by epigenetically silencing of p15 and p57. *J Cell Physiol*. 2019;234(4):5163-5174.

doi: 10.1002/jcp.27320

56. Rom A, Melamed L, Gil N, *et al.* Regulation of CHD2 expression by the Chaserr long noncoding RNA gene is essential for cell viability. *Nat Commun*. 2019;10:5092.

doi: 10.1038/s41467-019-13075-8

57. Jiang X, Li Q, Zhang S, Song C, Zheng P. Long noncoding RNA GIHCG induces cancer progression and chemoresistance and indicates poor prognosis in colorectal cancer. *Onco Targets Ther*. 2019;12:1059-1070.

doi: 10.2147/OTT.S192290

58. Li L, Chen J, Wang A, Yi K. ALKBH5 regulates ovarian cancer growth via demethylating long noncoding RNA PVT1 in ovarian cancer. *J Cell Mol Med*. 2023;28(2):e18066.

doi: 10.1111/jcmm.18066

59. Ma P, Pan Y, Yang F, *et al.* KLF5-Modulated lncRNA NEAT1 contributes to tumorigenesis by acting as a scaffold for BRG1 to silence GADD45A in gastric cancer. *Mol Ther Nucleic Acids*. 2020;22:382-395.

doi: 10.1016/j.omtn.2020.09.003

60. Abildgaard C, do Canto LM, Rainho CA, *et al.* The long non-coding RNA SNHG12 as a mediator of carboplatin resistance in ovarian cancer via epigenetic mechanisms. *Cancers* (*Basel*). 2022;14(7):1664.

doi: 10.3390/cancers14071664

61. Huang X, Chen J, Li H, *et al.* LncRNA SNHG12 suppresses adipocyte inflammation and insulin resistance by regulating the HDAC9/Nrf2 axis. *FASEB J*. 2024;38(13):e23794.

doi: 10.1096/fj.202400236RR

62. Zhang KJ, Tan XL, Guo L. The long noncoding RNA DANCR regulates the inflammatory phenotype of breast cancer cells and promotes breast cancer progression via the EZH2-dependent suppression of SOCS3 transcription. *Mol Oncol*. 2020;14(2):309-328.

doi: 10.1002/1878-0261.12622

63. Xie F, Huang Q, Wang C, *et al.* Downregulation of the long noncoding RNA SNHG14 suppresses cell proliferation and invasion by regulating EZH2 in pancreatic ductal adenocarcinoma (PDAC). *Cancer Biomark*. 2020;27(3):357-364.

doi: 10.3233/CBM-190908

64. Cable J, Heard E, Hirose T, *et al.* Noncoding RNAs: Biology and applications: A Keystone symposia report. *Ann N Y Acad Sci*. 2021;1506:118-141.

doi: 10.1111/nyas.14713

65. Liu YW, Xia R, Lu K, *et al.* LincRNA FEZF1-AS1 represses p21 expression to promote gastric cancer proliferation through LSD1-Mediated H3K4me2 demethylation. *Mol Cancer*. 2017;16(1):39.

doi: 10.1186/s12943-017-0588-9

66. Lian Y, Yan C, Lian Y, *et al.* Long intergenic non-protein-coding RNA 01446 facilitates the proliferation and metastasis of gastric cancer cells by interacting with the histone lysine-specific demethylase LSD1. *Cell Death Dis*. 2020;11(7):522.

doi: 10.1038/s41419-020-2729-0

67. Mao X, Ji T, Liu A, Weng Y. ELK4-mediated lncRNA SNHG22 promotes gastric cancer progression through interacting with EZH2 and regulating miR-200c-3p/Notch1 axis. *Cell Death Dis*. 2021;12(11):957.

doi: 10.1038/s41419-021-04228-z

68. Sarma K, Cifuentes-Rojas C, Ergun A, *et al.* ATRX directs binding of PRC2 to Xist RNA and polycomb targets. *Cell*. 2014;159:869-883. Erratum in *Cell*. 2014;159:1228. Erratum in Cell. 2015;160:568-569.

doi: 10.1016/j.cell.2014.10.019

69. McHugh CA, Chen CK, Chow A, *et al.* The Xist lncRNA interacts directly with SHARP to silence transcription through HDAC3. *Nature*. 2015;521:232-236.

doi: 10.1038/nature14443

70. Lu Y, Liu X, Xie M, *et al.* The NF-κB-responsive long noncoding RNA FIRRE regulates the posttranscriptional regulation of inflammatory gene expression by interacting with hnRNPU. *J Immunol*. 2017;199(10):3571-3582.

doi: 10.4049/jimmunol.1700091

71. Wang B, Xu W, Hu C, *et al.* Critical roles of the lncRNA CASC11 in tumor progression and cancer metastasis: The biomarker and therapeutic target potential. *Genes Dis*. 2020;9(2):325-333.

doi: 10.1016/j.gendis.2020.11.016

72. Mou K, Zhang X, Mu X, *et al.* LNMAT1 promotes invasion-metastasis cascade in malignant melanoma by epigenetically suppressing CADM1 expression. *Front Oncol*. 2019;9:569.

doi: 10.3389/fonc.2019.00569

73. Wozniak M, Czyz M. lncRNAs-EZH2 interaction as promising therapeutic target in cutaneous melanoma. *Front Mol Biosci*. 2023;10:1170026.

doi: 10.3389/fmolb.2023.1170026

74. Zhang F, Ruan X, Ma J, *et al.* DGCR8/ZFAT-AS1 promotes CDX2 transcription in a PRC2 complex-dependent manner to facilitate the malignant biological behavior of glioma cells. *Mol Ther*. 2020;28(2):613-630.

doi: 10.1016/j.ymthe.2019.11.015

75. Chang KC, Diermeier SD, Yu AT, *et al.* MaTAR25 lncRNA regulates the Tensin1 gene to impact breast cancer progression. *Nat Commun*. 2020;11(1):6438.

doi: 10.1038/s41467-020-20207-y

76. Somasundaram S, Forrest ME, Moinova H, *et al.* DNMT1-associated lincRNA DACOR1 reprograms genome-wide DNA methylation in colon cancer. *Clin Epigenet*. 2018;10:127.

doi: 10.1186/s13148-018-0555-3

77. Wang Q, Mao X, Luo F, Wang J. LINC00511 promotes gastric cancer progression by regulating SOX4 and epigenetically repressing PTEN to activate PI3K/AKT pathway. *J Cell Mol Med*. 2021;25:9112-9127.

doi: 10.1111/jcmm.16656

78. Dai Z, Liu X, Zeng H, Chen Y. Long noncoding RNA HOTAIR facilitates pulmonary vascular endothelial cell apoptosis via DNMT1-mediated hypermethylation of the Bcl-2 promoter in COPD. *Respir Res*. 2022;23(1):356.

doi: 10.1186/s12931-022-02234-z

79. Lu GH, Zhao HM, Liu ZY, Cao Q, Shao RD, Sun G. LncRNA SAMD12-AS1 promotes the progression of gastric cancer via DNMT1/p53 axis. *Arch Med Res*. 2021;52(7):683-691.

doi: 10.1016/j.arcmed.2021.04.004

80. Yu Y, Lu X, Yan Y, *et al.* lncRNA KIF9-AS1 accelerates hepatocellular carcinoma growth by recruiting DNMT1 to promote RAI2 DNA methylation. *J Oncol*. 2022;2022:3888798.

doi: 10.1155/2022/3888798

81. Hao A, Wang Y, Stovall DB, Wang Y, Sui G. Emerging roles of LncRNAs in the EZH2-regulated oncogenic network. *Int J Biol Sci*. 2021;17(13):3268-3280.

doi: 10.7150/ijbs.63488

82. Wang X, Wang Y, Li L, *et al.* lncRNA coordinates with Ezh2 to inhibit HIF-1α transcription and suppress cancer cell adaptation to hypoxia. *Oncogene*. 2020;39(9):1860-1874.

doi: 10.1038/s41388-019-1123-9

83. Aguilo F, Di Cecilia S, Walsh MJ. Long non-coding RNA ANRIL and polycomb in human cancers and cardiovascular disease. *Curr Top Microbiol Immunol*. 2016;394:29-39.

doi: 10.1007/82_2015_455

84. Sun TT, He J, Liang Q, *et al.* LncRNA GClnc1 promotes gastric carcinoma and may act as a modular scaffold of WDR5 and KAT2A complexes to specify the histone modification pattern. *Cancer Discov*. 2016;6(7):784-801.

doi: 10.1158/2159-8290.CD-15-0921

85. Ma M, Zhang Y, Weng M, *et al.* lncRNA GCAWKR promotes gastric cancer development by scaffolding the chromatin modification factors WDR5 and KAT2A. *Mol Ther*. 2018;26(11):2658-2668.

doi: 10.1016/j.ymthe.2018.09.002

86. Dimitrova N, Zamudio JR, Jong RM, *et al.* LincRNA-p21 activates p21 in cis to promote Polycomb target gene expression and to enforce the G1/S checkpoint. *Mol Cell*. 2014;54(5):777-790.

doi: 10.1016/j.molcel.2014.04.025

87. Luo M, Xie L, Su Y, *et al.* TM4SF19-AS1 facilitates the proliferation of lung squamous cell carcinoma by recruiting WDR5 to mediate TM4SF19. *Mol Cell Probes*. 2022;65:101849.

doi: 10.1016/j.mcp.2022.101849

88. Arab K, Park YJ, Lindroth AM, *et al.* Long noncoding RNA TARID directs the demethylation and activation of the tumor suppressor TCF21 via GADD45A. *Mol Cell*. 2014;55:604-614.

doi: 10.1016/j.molcel.2014.06.031

89. Ghafouri-Fard S, Dashti S, Taheri M. The HOTTIP (HOXA transcript at the distal tip) lncRNA: Review of oncogenic roles in humans. *Biomed Pharmacother*. 2020;127:110158.

doi: 10.1016/j.biopha.2020.110158

90. Xiang JF, Yin QF, Chen T, *et al.* Human CRC-specific CCAT1-L lncRNA regulates long-range chromatin interactions at the MYC locus. *Cell Res*. 2014;24(5):513-531.

doi: 10.1038/cr.2014.35

91. Hakami MA, Hazazi A, Khan FR, *et al.* PVT1 lncRNA in lung cancer: A key player in tumorigenesis and therapeutic opportunities. *Pathol Res Pract*. 2024;253:155019.

doi: 10.1016/j.prp.2023.155019

92. Li W, Notani D, Ma Q, *et al.* Functional roles of enhancer RNAs for estrogen-dependent transcriptional activation. *Nature*. 2013;498(7455):516-520.

doi: 10.3390/ijms21103711

93. Ferrer J, Dimitrova N. Transcription regulation by long noncoding RNAs: Mechanisms and disease relevance. *Nat Rev Mol Cell Biol*. 2024;25(5):396-415.

doi: 10.1038/s41580-023-00694-9

94. Beucher A, Miguel-Escalada I, Balboa D, *et al.* The HASTER lncRNA promoter is a cis-acting transcriptional stabilizer of HNF1A. *Nat Cell Biol*. 2022;24(10):1528-1540.

doi: 10.1038/s41556-022-00996-8

95. Jain AK, Xi Y, McCarthy R, *et al.* LncPRESS1 is a p53-regulated LncRNA that safeguards pluripotency by disrupting SIRT6-mediated de-acetylation of histone H3K56. *Mol Cell*. 2016; 64:967-981.

doi: 10.1016/j.molcel.2016.10.039

96. An H, Elvers KT, Gillespie JA, *et al.* A toolkit for the identification of the NEAT1_2/paraspeckle modulators. *Nucleic Acids Res*. 2022;50(20):e119.

doi: 10.1093/nar/gkac771

97. Li Z, Chao TC, Chang KY, *et al.* The long noncoding RNA THRIL regulates TNFα expression through its interaction with hnRNPL. *Proc Natl Acad Sci U S A*. 2014;111(3):1002-1007.

doi: 10.1073/pnas.1313768111

98. Li Y, Wang Z, Shi H, *et al.* HBXIP and LSD1 Scaffolded by lncRNA hotair mediate transcriptional activation by c-Myc. *Cancer Res*. 2016;7:293-304.

doi: 10.1158/0008-5472.CAN-14-3607

99. Gomez JA, Wapinski OL, Yang YW, *et al.* The NeST long ncRNA controls microbial susceptibility and epigenetic activation of the interferon-γ locus. *Cell*. 2013;152(4):743-754.

doi: 10.1016/j.cell.2013.01.015

100. Swaminathan G, Rogel-Ayala DG, Armich A, Barreto G. Implications in cancer of nuclear micro RNAs, long non-coding RNAs, and circular RNAs bound by PRC2 and FUS. *Cancers* (*Basel*). 2024;16(5):868.

doi: 10.3390/cancers16050868

101. Lei P, Guo Q, Hao J, *et al.* Exploring the evolving roles and clinical significance of circRNAs in head and neck squamous cell carcinomas. *J Cancer*. 2024;15:3984-3994.

doi: 10.7150/jca.96614

102. Chen R, Liu Y, Zhuang H, *et al.* Quantitative proteomics revealed that the long noncoding RNA MALAT1 interacts with DBC1 to regulate p53 acetylation. *Nucleic Acids Res*. 2017;45(17):9947-9959.

doi: 10.1093/nar/gkx600

103. Yamazaki T, Souquere S, Chujo T, *et al.* Functional domains of NEAT1 architectural lncRNA induce paraspeckle assembly through phase separation. *Mol Cell*. 2018;70(6):1038-1053.e7.

doi: 10.1016/j.molcel.2018.05.019

104. Nakagawa S, Yamazaki T, Hirose T. Molecular dissection of nuclear paraspeckles: Toward understanding the emerging world of the RNP milieu. *Open Biol*. 2018;8:180150.

doi: 10.1098/rsob.180150

105. Hirose T, Yamazaki T, Nakagawa S. Molecular anatomy of the architectural NEAT1 noncoding RNA: The domains, interactors, and biogenesis pathway required to build phase-separated nuclear paraspeckles. *Wiley Interdiscipl Rev RNA*. 2019;10(6):e1545.

doi: 10.1002/wrna.1545

106. Fox AH, Nakagawa S, Hirose T, Bond CS. Paraspeckles: Where long noncoding RNA meets phase separation. *Trends Biochem Sci*. 2018;43(2):124-135.

doi: 10.1016/j.tibs.2017.12.001

107. Todorovski V, McCluggage F, Li Y, *et al.* Confined environments induce polarized paraspeckle condensates. *Commun Biol*. 2023;6(1):145.

doi: 10.1038/s42003-023-04528-4

108. Mello SS, Sinow C, Raj N, *et al.* Neat1 is a p53-inducible lincRNA essential for transformation suppression. *Genes Dev*. 2017;31(11):1095-1108.

doi: 10.1101/gad.284661.116

109. Taiana E, Favasuli V, Ronchetti D, *et al.* Long noncoding RNA NEAT1 targeting impairs the DNA repair machinery and triggers antitumor activity in multiple myeloma. *Leukemia*. 2020;34:234-244.

doi: 10.1038/s41375-019-0542-5

110. Smith NE, Spencer-Merris P, Fox AH, Petersen J, Michael MZ. The long and the short of it: NEAT1 and cancer cell metabolism. *Cancers* (*Basel*). 2022;14(18):4388.

doi: 10.3390/cancers14184388

111. Kessler SM, Hosseini K, Hussein UK, *et al.* Hepatocellular carcinoma and nuclear paraspeckles: Induction of chemoresistance and prediction for poor survival. *Cell Physiol Biochem*. 2019;52(4):787-801.

doi: 10.33594/000000055

112. Takakuwa H, Yamazaki T, Souquere S, *et al.* The shell protein composition specified by the lncRNA NEAT1 domains dictates the formation of paraspeckles as distinct membraneless organelles. *Nat Cell Biol*. 2023;25(11):1664-1675.

doi: 10.1038/s41556-023-01254-1

113. Long F, Li X, Pan J, *et al.* The role of lncRNA NEAT1 in human cancer chemoresistance. *Cancer Cell Int*. 2024;24(1):236.

doi: 10.1186/s12935-024-03426-x

114. Jia X, Wei L, Zhang Z. NEAT1 overexpression indicates a poor prognosis and induces chemotherapy resistance via the miR-491-5p/SOX3 signaling pathway in ovarian cancer. *Front Genet*. 2021;12:616220.

doi: 10.3389/fgene.2021.616220

115. Ma F, Lei YY, Ding MG, Luo LH, Xie YC, Liu XL. LncRNA NEAT1 interacted with DNMT1 to regulate malignant phenotype of cancer cell and cytotoxic T cell infiltration via epigenetic inhibition of p53, cGAS, and STING in lung cancer. *Front Genet*. 2020;11:250.

doi: 10.3389/fgene.2020.00250

116. Mamontova V, Trifault B, Gribling-Burrer AS, *et al.* NEAT1 promotes genome stability via m^6A methylation-dependent regulation of CHD4. *Genes Dev.* 2024; 38(17-20):915-930.

doi: 10.1101/gad.351913.124

117. Shin VY, Chen J, Cheuk IWY, *et al.* Long noncoding RNA NEAT1 confers an oncogenic role in triple-negative breast cancer by modulating chemoresistance and cancer stemness. *Cell Death Dis*. 2019;10(4):270.

doi: 10.1038/s41419-019-1513-5

118. Dong P, Xiong Y, Yue J, *et al.* Long non-coding RNA NEAT1: A novel target for diagnosis and therapy in human tumors. *Front Genet*. 2018;9:471.

doi: 10.3389/fgene.2018.00471

119. Peng X, Zhang K, Ma L, Xu J, Chang W. The role of long non-coding RNAs in thyroid cancer. *Front Oncol*. 2020;10:941.

doi: 10.3389/fonc.2020.00941

120. Sun W, Qin Y, Wang Z, *et al.* The NEAT1_2/miR-491 axis modulates papillary thyroid cancer invasion and metastasis through TGM2/NFκb/FN1 signaling. *Front Oncol*. 2021;11:610547.

doi: 10.3389/fonc.2021.610547

121. Sun W, Lan X, Zhang H, *et al.* NEAT1_2 functions as a competing endogenous RNA to regulate ATAD2 expression by sponging microRNA-106b-5p in papillary thyroid cancer. *Cell Death Dis*. 2018;9(3):1-15.

doi: 10.1038/s41419-018-0418-z

122. Schell B, Legrand P, Fribourg S. Crystal structure of SFPQ-NONO heterodimer. *Biochimie*. 2022;198:1-7.

doi: 10.1016/j.biochi.2022.02.011

123. Zhang S, Cooper JA, Chong YS, *et al.* NONO enhances mRNA processing of super-enhancer-associated GATA2 and HAND2 genes in neuroblastoma. *EMBO Rep.* 2023;24(2):e54977.

doi: 10.15252/embr.202254977

124. Engreitz JM, Sirokman K, McDonel P, *et al.* RNA-RNA interactions enable specific targeting of noncoding RNAs to nascent Pre-mRNAs and chromatin sites. *Cell*. 2014;159(1):188-199.

doi: 10.1016/j.cell.2014.08.018

125. Lee PW, Marshall AC, Knott GJ, *et al.* Paraspeckle subnuclear bodies depend on the dynamic heterodimerisation of DBHS RNA-binding proteins via their structured domains. *J Biol Chem*. 2022;298(11):102563.

doi: 10.1016/j.jbc.2022.102563

126. Jen HW, Gu DL, Lang YD, Jou YS. PSPC1 potentiates IGF1R expression to augment cell adhesion and motility. *Cells*. 2020;9(6):1490.

doi: 10.3390/cells9061490

127. Yang L, Yang J, Jacobson B, *et al.* SFPQ promotes lung cancer

malignancy *via* regulation of CD44 v6 expression. *Front Oncol*. 2022;12:862250.

doi: 10.3389/fonc.2022.862250

128. Lin Y, Zhong W, Lin Q, *et al.* SFPQ promotes the proliferation, migration and invasion of hepatocellular carcinoma cells and is associated with poor prognosis. *Am J Cancer Res*. 2023;13(6):2269-2284.

129. Xiao M, Wang F, Chen N, *et al.* Smad4 sequestered in SFPQ condensates prevents TGF-β tumor-suppressive signaling. *Dev Cell*. 2024;59(1):48-63.e8.

doi: 10.1016/j.devcel.2023.11.020

130. Ji Q, Zhang L, Liu X, *et al.* Long noncoding RNA MALAT1 promotes tumor growth and metastasis in colorectal cancer by binding to SFPQ and releasing the oncogene PTBP2 from the SFPQ/PTBP2 complex. *Br J Cancer*. 2014;111:736-748.

doi: 10.1038/bjc.2014.383

131. Klotz-Noack K, Klinger B, Rivera M, *et al.* SFPQ depletion is synthetically lethal with BRAFV600E in colorectal cancer cells. *Cell Rep.* 2020;32(12):108184.

doi: 10.1016/j.celrep.2020.108184

132. Zhang XL, Chen XH, Xu B, *et al.* K235 acetylation couples with PSPC1 to regulate the m6A demethylation activity of ALKBH5 and tumorigenesis. *Nat Commun*. 2023;14(1):3815.

doi: 10.1038/s41467-023-39414-4

133. Lemster AL, Weingart A, Bottner J, *et al.* Elevated PSPC1 and KDM5C expression indicates poor prognosis in prostate cancer. *Hum Pathol*. 2023;138:1-11.

doi: 10.1016/j.humpath.2023.05.007

134. Tyzack GE, Manferrari G, Newcombe J, Luscombe NM, Luisier R, Patani R. Paraspeckle components NONO and PSPC1 are not mislocalized from motor neuron nuclei in sporadic ALS. *Brain*. 2020;143(8):e66.

doi: 10.1093/brain/awaa205

135. Harley J, Hagemann C, ASerio A, Patani R. TDP-43 and FUS mislocalization in VCP mutant motor neurons is reversed by pharmacological inhibition of the VCP D2 ATPase domain. *Brain Commun*. 2021;3:fcab166.

doi: 10.1093/braincomms/fcab166

136. Shao W, Bi X, Pan Y, *et al.* Phase separation of RNA-binding protein promotes polymerase binding and transcription. *Nat Chem Biol*. 2022;18(1):70-80.

doi: 10.1038/s41589-021-00904-5

137. Yeh HW, Hsu EC, Lee SS, *et al.* PSPC1 mediates TGF-β1 autocrine signaling and Smad2/3 target switching to promote EMT, stemness and metastasis. *Nat Cell Biol*. 2018;20(4):479-491.

doi: 10.1038/s41556-018-0062-y.

138. Li J, Cui P, Sun Q, *et al.* PSPC1 regulates CHK1 phosphorylation through phase separation and participates in mouse oocyte maturation. *Acta Biochim Biophys Sin* (*Shanghai*). 2021;53(11):1527-1537.

doi: 10.1093/abbs/gmab123

139. Zhan T, Cheng X, Zhu Q, *et al.* LncRNA LOC105369504 inhibits tumor proliferation and metastasis in colorectal cancer by regulating PSPC1. *Cell Death Discov*. 2023;9(1):89.

doi: 10.1038/s41420-023-01384-3

140. Mohankumar K, Shrestha R, Safe S. Nuclear receptor 4A1 (NR4A1) antagonists target paraspeckle component 1 (PSPC1) in cancer cells. *Mol Carcinog*. 2022;61(1):73-84.

doi: 10.1002/mc.23362

141. Zhang H, Su X, Burley SK, Zheng XFS. mTOR regulates aerobic glycolysis through NEAT1 and nuclear paraspeckle-mediated mechanisms in hepatocellular carcinoma. *Theranostics*. 2022;12:3518-3533.

doi: 10.7150/thno.72581

142. Hussein MA, Valinezhad K, Adel E, Munirathinam G. MALAT-1 is a key regulator of epithelial-mesenchymal transition in cancer: A potential therapeutic target for metastasis. *Cancers* (*Basel*). 2024;16(1):234.

doi: 10.3390/cancers16010234

143. Nakagawa S, Ip JY, Shioi G, *et al.* Malat1 is not an essential component of nuclear speckles in mice. *RNA*. 2012;18:1487-1499.

doi: 10.1261/rna.033217.112

144. Arratia F, Fierro C, Blanco A, *et al.* Selective concurrence of the long non-coding RNA MALAT1 and the polycomb repressive complex 2 to the promoter regions of active genes in MCF7 breast cancer cells. *Curr Issues Mol Biol*. 2023;45(6):4735-4748.

doi: 10.3390/cimb45060301

145. Frappier L. Viral disruption of promyelocytic leukemia (PML) nuclear bodies by hijacking host PML regulators. *Virulence*. 2011;2(1):58-62.

doi: 10.4161/viru.2.1.14610

146. Huang WH, Su WM, Wang CW, *et al.* The Momordica anti-HIV protein MAP30 abrogates the Epstein-Barr virus nuclear antigen 1-dependent functions in host cells. *Heliyon*. 2023;9(11):e21486.

doi: 10.1016/j.heliyon.2023.e21486

147. D'Amico F, Mukhopadhyay R, Ovaa H, Mulder MPC. Targeting TRIM proteins: A quest toward drugging an emerging protein class. *Chembiochem*. 2021;22(12):2011-2031.

doi: 10.1002/cbic.202000787

148. Dodel M, Guiducci G, Dermit M, *et al.* TREX reveals proteins that bind to specific RNA regions in living cells. *Nat*

Methods. 2024;21(3):423-434.

doi: 10.1038/s41592-024-02181-1

149. Sullivan KD, Galbraith MD, Andrysik Z, Espinosa JM. Mechanisms of transcriptional regulation by p53. *Cell Death Differ*. 2018;25(1):133-143.

doi: 10.1038/cdd.2017.174

150. Wang S, Zhao Y, Aguilar A, Bernard D, Yang CY. Targeting the MDM2-p53 protein-protein interaction for new cancer therapy: Progress and challenges. *Cold Spring Harb Perspect Med*. 2017;7(5):a026245.

doi: 10.1101/cshperspect.a026245

151. Stubbs FE, Flynn BP, Rivers CA, *et al.* Identification of a novel GR-ARID1a-P53BP1 protein complex involved in DNA damage repair and cell cycle regulation. *Oncogene*. 2022;41(50):5347-5360.

doi: 10.1038/s41388-022-02516-2

152. Kozłowska J, Kolenda T, Poter P, *et al.* Long intergenic non-coding RNAs in HNSCC: From "Junk DNA" to important prognostic factor. *Cancers* (*Basel*). 2021;13(12):2949.

doi: 10.3390/cancers13122949

153. Lin T, Hou PF, Meng S, *et al.* Emerging roles of p53-related lncRNAs in cancer progression: A systematic review. *Int J Biol Sci*. 2019;15(6):1287-1298.

doi: 10.7150/ijbs.33218

154. Adriaens C, Standaert L, Barra J, *et al.* p53 induces formation of NEAT1 lncRNA-containing paraspeckles that modulate replication stress response and chemosensitivity. *Nat Med*. 2016;22(8):861-868.

doi: 10.1038/nm.4135

155. Cheng Y, Huang N, Yin Q, *et al.* LncRNA TP53TG1 plays an anti-oncogenic role in cervical cancer by synthetically regulating transcriptome profile in HeLa cells. *Front Genet*. 2022;13:981030.

doi: 10.3389/fgene.2022.981030

156. Shao M, Ma H, Wan X, Liu Y. Survival analysis for long noncoding RNAs identified TP53TG1 as an antioncogenic target for breast cancer. *J Cell Physiol*. 2020;235:6574-6581.

doi: 10.1002/jcp.29517

157. Liao D, Liu X, Yuan X, *et al.* Long non-coding RNA tumor protein 53 target gene 1 promotes cervical cancer development via regulating microRNA-33a-5p to target forkhead box K2. *Cell Cycle*. 2022;21(6):572-584.

doi: 10.1080/15384101.2022.2026705

158. Zhao K, Wang X, Xue X, Li L, Hu Y. A long noncoding RNA sensitizes genotoxic treatment by attenuating ATM activation and homologous recombination repair in cancers. *PLoS Biol*. 2020;18:e3000666.

doi: 10.1371/journal.pbio.3000666

159. Unfried JP, Marín-Baquero M, Rivera-Calzada Á, *et al.* Long noncoding RNA NIHCOLE promotes the ligation efficiency of DNA double-strand breaks in hepatocellular carcinoma. *Cancer Res*. 2021;81(19):4910-4925.

doi: 10.1158/0008-5472.CAN-21-0463

160. Sharma V, Khurana S, Kubben N, *et al.* A BRCA1-interacting lncRNA regulates homologous recombination. *EMBO Rep*. 2015;16:1520-1534.

doi: 10.15252/embr.201540437

161. Yadav A, Biswas T, Praveen A, *et al.* Targeting MALAT1 augments sensitivity to PARP inhibition by impairing homologous recombination in prostate cancer. *Cancer Res Commun*. 2023;3:2044-2061.

doi: 10.1158/2767-9764.CRC-23-0089

162. Hu Y, Lin J, Fang H, *et al.* Targeting the MALAT1/PARP1/LIG3 complex induces DNA damage and apoptosis in multiple myeloma. *Leukemia*. 2018;32:2250-2262.

doi: 10.1038/s41375-018-0104-2

163. Zhao J, Xu J, Wu M, *et al.* LncRNA H19 regulates breast cancer DNA damage response and sensitivity to PARP inhibitors via binding to ILF2. *Int J Mol Sci*. 2023;24:9157.

doi: 10.3390/ijms24119157

164. Wang Y, Nie H, He X, *et al.* The emerging role of super enhancer--derived noncoding RNAs in human cancer. *Theranostics*. 2020;10(24):11049.

doi: 10.7150/thno.49168

165. Saldaña-Meyer R, Rodriguez-Hernaez J, Escobar T, *et al.* RNA interactions are essential for CTCF-mediated genome organization. *Mol Cell*. 2019;76(3):412-422.e5.

doi: 10.1016/j.molcel.2019.08.015

166. Diot C, Richard CA, Risso-Ballester J, *et al.* Hardening of respiratory syncytial virus inclusion bodies by cyclopamine proceeds through perturbation of the interactions of the M2-1 protein with RNA and the P protein. *Int J Mol Sci*. 2023;24(18):13862.

doi: 10.3390/ijms241813862

167. Etibor TA, Vale-Costa S, Sridharan S, *et al.* Defining basic rules for hardening influenza A virus liquid condensates. *Elife*. 2023;12:e85182.

doi: 10.7554/eLife.85182

168. Liboy-Lugo JM, Espinoza CA, Sheu-Gruttadauria J, *et al.* Protein-protein interactions with G3BPs drive stress granule condensation and gene expression changes under cellular stress. bioRxiv [Preprint]. 2024.

doi: 10.1101/2024.02.06.579149

169. Alam U, Kennedy D. Rasputin a decade on and more promiscuous than ever? A review of G3BPs. *Biochim Biophys Acta Mol Cell Res*. 2019;1866(3):360-370.

doi: 10.1016/j.bbamcr.2018.09.001

170. Shih JW, Wang WT, Tsai TY, Kuo CY, Li HK, Wu Lee YH. Critical roles of the RNA helicase DDX3 and its interactions with eIF4E/PABP1 in stress granule assembly and stress response. *Biochem J*. 2012;441(1):119-129.

doi: 10.1042/BJ20110739

171. Aditi, Folkmann AW, Wente SR. Cytoplasmic hGle1A regulates stress granules by modulation of translation. *Mol Biol Cell*. 2015;26(8):1476-1490.

doi: 10.1091/mbc.E14-11-1523

172. Zhan Y, Chen X, Zheng H, *et al.* YB1 associates with oncogenetic roles and poor prognosis in nasopharyngeal carcinoma. *Sci Rep*. 2022;12(1):3699.

doi: 10.1038/s41598-022-07636-z

173. Cui BC, Sikirzhytski V, Aksenova M, *et al.* Pharmacological inhibition of DEAD-Box RNA Helicase 3 attenuates stress granule assembly. *Biochem Pharmacol*. 2020;182:114280.

doi: 10.1016/j.bcp.2020.114280

174. Kitajima H, Maruyama R, Niinuma T, *et al.* TM4SF1-AS1 inhibits apoptosis by promoting stress granule formation in cancer cells. *Cell Death Dis*. 2023;14(7):424.

doi: 10.1038/s41419-023-05953-3

175. Kang W, Wang Y, Yang W, Zhang J, Zheng H, Li D. Research progress on the structure and function of G3BP. *Front Immunol*. 2021;12:718548.

doi: 10.3389/fimmu.2021.718548

176. Freibaum BD, Messing J, Nakamura H, *et al.* Identification of small molecule inhibitors of G3BP-driven stress granule formation. *J Cell Biol*. 2024;223(3):e202308083.

doi: 10.1083/jcb.202308083

177. Mukhopadhyay C, Zhou P. Role(s) of G3BPs in human pathogenesis. *J Pharmacol Exp Ther*. 2023;387(1):100-110.

doi: 10.1124/jpet.122.001538

178. Gal J, Chen J, Na DY, Tichacek L, Barnett KR, Zhu H. Acetylation of lysine-376 of G3BP1 regulates RNA binding and stress granule dynamics. *Mol Cell Biol*. 2019;39(22):e00052-19.

doi: 10.1128/MCB.00052-19

179. Lee AK, Klein J, Fon Tacer K, *et al.* Translational repression of G3BP in cancer and germ cells suppresses stress granules and enhances stress tolerance. *Mol Cell*. 2020;79(4):645-659.e9.

doi: 10.1016/j.molcel.2020.06.037

180. Li M, Fan X, Zhao J, Wang D. Establishment and validation of a four-stress granule-related gene signature in hepatocellular carcinoma. *J Clin Transl Hepatol*. 2024;12(1):1-14.

doi: 10.14218/JCTH.2023.00019

181. Chen S, Cao X, Zhang J, Wu W, Zhang B, Zhao F. circVAMP3 drives CAPRIN1 phase separation and inhibits hepatocellular carcinoma by suppressing c-Myc translation. *Adv Sci* (*Weinh*). 2022;9:e2103817.

doi: 10.1002/advs.202103817

182. Zhang M, Peng S. The association and clinical relevance of the phase-separating protein CAPRIN1 with noncoding RNA. *Cell Stress Chaperones*. 2023;28(2):125-132.

doi: 10.1007/s12192-023-01320-5

183. Schneider C, Schneider G. Stress granules-membraneless organelles as therapeutic targets in pancreatic cancer. *EMBO Mol Med*. 2024;16(3):429-431.

doi: 10.1038/s44321-024-00040-2

184. Kim A, Shim S, Kim YH, Kim MJ, Park S, Myung JK. Inhibition of Y-Box binding protein 1 suppresses cell growth and motility in colorectal cancer. *Mol Cancer Ther*. 2020;19(2):479-489.

doi: 10.1158/1535-7163.MCT-19-0265

185. Wang F, Li J, Fan S, *et al*. Targeting stress granules: A novel therapeutic strategy for human diseases. *Pharmacol Res*. 2020;161:105143.

doi: 10.1016/j.phrs.2020.105143

186. An S, Huang W, Huang X, *et al.* Integrative network analysis identifies cell-specific trans regulators of m6A. *Nucleic Acids Res*. 2020;48:1715-1729.

doi: 10.1093/nar/gkz1206

187. Zhang Y, Jing Y, Wang Y, *et al.* NAT10 promotes gastric cancer metastasis via N4-acetylated COL5A1. *Signal Transduct Target Ther*. 2021;6:173.

doi: 10.1038/s41392-021-00489-4

188. Han J, Liu Q, Zhou Y, Li D, Wang R. Landscape of internal N7-methylguanosine of long noncoding RNA modifications in resistant acute myeloid leukemia. *BMC Genomics*. 2023;24:425.

doi: 10.1186/s12864-023-09526-8

189. Kong Z, Lu Y, Yang Y, *et al.* m6A-Mediated biogenesis of circDDIT4 inhibits prostate cancer progression by sequestrating ELAVL1/HuR. *Mol Cancer Res*. 2023;21:1342-1355.

doi: 10.1158/1541-7786.MCR-22-0271

190. Yu XM, Li SJ, Yao ZT, *et al.* N4-acetylcytidine modification of lncRNA CTC-490G23.2 promotes cancer metastasis through interacting with PTBP1 to increase CD44 alternative splicing. *Oncogene*. 2023;42:1101-1116.

doi: 10.1038/s41388-023-02628-3

191. Dou X, Huang L, Xiao Y, *et al.* METTL14 is a chromatin regulator independent of its RNA N6-methyladenosine methyltransferase activity. *Protein Cell*. 2023;14(9):683-697.

doi: 10.1093/procel/pwad009

192. Hu J, Lin H, Wang C, Su Q, Cao B. METTL14-mediated RNA methylation in digestive system tumors. *Int J Mol Med*. 2023;52(3):86.

doi: 10.3892/ijmm.2023.5289

193. Wang J, Wang S, Yang H, *et al.* Methyltransferase like-14 suppresses growth and metastasis of non-small-cell lung cancer by decreasing LINC02747. *Cancer Sci*. 2024;115(9):2931-2946.

doi: 10.1111/cas.16254

194. Lee JH, Wang R, Xiong F, *et al.* Enhancer RNA m6A methylation facilitates transcriptional condensate formation and gene activation. *Mol Cell*. 2021;81(16):3368-3385.e9.

doi: 10.1016/j.molcel.2021.07.024

195. Long X, Wen F, Li J, Huang X. LncRNA FEZF1-AS1 accelerates multiple myeloma progression by regulating IGF2BP1/BZW2 signaling. *Hematol Oncol*. 2023;41(4):694-703.

doi: 10.1002/hon.3157

196. Shen W, Zhu M, Wang Q, *et al.* DARS-AS1 recruits METTL3/METTL14 to bind and enhance DARS mRNA m(6)A modification and translation for cytoprotective autophagy in cervical cancer. *RNA Biol*. 2022;19:751-763.

doi: 10.1080/15476286.2022.2079889

197. Liu H, Xu Y, Yao B, Sui T, Lai L, Li Z. A novel N6-methyladenosine (m6A)-dependent fate decision for the lncRNA THOR. *Cell Death Dis*. 2020;11:613.

doi: 10.1038/s41419-020-02833-y

198. Ban Y, Tan P, Cai J, *et al.* LNCAROD is stabilized by m6A methylation and promotes cancer progression via forming a ternary complex with HSPA1A and YBX1 in head and neck squamous cell carcinoma. *Mol Oncol*. 2020;14:1282-1296.

doi: 10.1002/1878-0261.12676

199. Ni W, Yao S, Zhou Y, *et al.* Long noncoding RNA GAS5 inhibits the progression of colorectal cancer by interacting with and triggering YAP phosphorylation and degradation and is negatively regulated by the m6A reader YTHDF3. *Mol Cancer*. 2019;18:143.

doi: 10.1186/s12943-019-1079-y

200. Chen F, Li M, Wang L. LncRNA CASC11 promotes hepatocellular carcinoma progression via upregulation of UBE2T in a m6A-dependent manner. *Front Oncol*. 2021;11:772671.

doi: 10.3389/fonc.2021.772671

201. Zhang J, Guo S, Piao HY, *et al.* ALKBH5 promotes invasion and metastasis of gastric cancer by decreasing methylation of the lncRNA NEAT1. *J Physiol Biochem*. 2019;75:379-389.

doi: 10.1007/s13105-019-00690-8

202. Liu T, Wang H, Fu Z, *et al.* Methyltransferase-like 14 suppresses growth and metastasis of renal cell carcinoma by decreasing long noncoding RNA NEAT1. *Cancer Sci*. 2022;113:446-458.

doi: 10.1111/cas.15212

203. Wei H, Huang L, Lu Q, *et al.* N6-methyladenosine-modified LEAWBIH drives hepatocellular carcinoma progression through epigenetically activating Wnt/β-catenin signaling. *J Hepatocellular Carcinoma*. 2023;10:1991-2007.

doi: 10.2147/JHC.S433070

204. Bei M, Hao S, Lin K, *et al.* Splicing factor TRA2A contributes to esophageal cancer progression via a noncanonical role in lncRNA m6 A methylation. *Cancer Sci*. 2023;114:3216-3229.

doi: 10.1111/cas.15870

205. Su T, Liu J, Zhang N, *et al.* New insights into the interplay between m6A modifications and microRNA or lncRNA in gastrointestinal cancers. *Front Cell Dev Biol*. 2023;11:1157797.

doi: 10.3389/fcell.2023.1157797

206. Hu X, Peng WX, Zhou H, *et al.* IGF2BP2 regulates DANCR by serving as an N6-methyladenosine reader. *Cell Death Differ*. 2020;27(6):1782-1794.

doi: 10.1038/s41418-019-0461-z

207. Xu Y, Weng X, Qiu J, Wang S. Biogenesis of circRBM33 mediated by N6-methyladenosine and its function in abdominal aortic aneurysm. *Epigenetics*. 2024;19(1):2392401.

doi: 10.1080/15592294.2024.2392401

208. Zhang Y, Chen Z, Song J, Qian H, Wang Y, Liang Z. The role of m6A modified circ0049271 induced by MNNG in precancerous lesions of gastric cancer. *Heliyon*. 2024;10(16):e35654.

doi: 10.1016/j.heliyon.2024.e35654

209. Liu F, Gu W, Shao Y. Cross-talk between circRNAs and m6A modifications in solid tumors. *J Transl Med*. 2024;22(1):694.

doi: 10.1186/s12967-024-05500-4

210. Shu G, Zhao Z, Zhao T, *et al.* N6-methyladenosine modification of circMARK2 enhances cytoplasmic export and stabilizes LIN28B, contributing to the progression of Wilms tumor. *J Exp Clin Cancer Res*. 2024;43(1):191.

doi: 10.1186/s13046-024-03113-9

211. Yankova E, Blackaby W, Albertella M, *et al.* Small-molecule inhibition of METTL3 as a strategy against myeloid leukemia. *Nature*. 2021;593:597-601.

doi: 10.1038/s41586-021-03536-w

212. Fiorentino F, Menna M, Rotili D, Valente S, Mai A. METTL3 from target validation to the first small-molecule inhibitors: A medicinal chemistry journey. *J Med Chem*. 2023;66(3):1654-1677.

doi: 10.1021/acs.jmedchem.2c01601

213. Qing Y, Dong L, Gao L, *et al.* R-2-hydroxyglutarate attenuates aerobic glycolysis in leukemia by targeting the FTO/m^{6}A/PFKP/LDHB axis. *Mol Cell*. 2021;81:922-939.e9.

doi: 10.1016/j.molcel.2020.12.026

214. Ofir-Rosenfeld Y, Rausch O, McMahon J, *et al.* STC-15, an oral small molecule inhibitor of the RNA methyltransferase METTL3, inhibits tumor growth through activation of anti-cancer immune responses and synergises with immune checkpoint blockade. *J Immunother Cancer*. 2022;10:A1-A1603.

215. Guan Q, Lin H, Miao L, *et al.* Functions, mechanisms, and therapeutic implications of METTL14 in human cancer. *J Hematol Oncol*. 2022;15:13.

doi: 10.1186/s13045-022-01231-5

216. Albert L, Xu J, Wan R, Srinivasan V, Dou Y, Vázquez O. Controlled inhibition of methyltransferases using photoswitchable peptidomimetics: Toward an epigenetic regulation of leukemia. *Chem Sci*. 2017;8:4612-4618.

doi: 10.1039/c7sc00137a

217. Lee JH, Choi N, Kim S, Jin MS, Shen H, Kim YC. Eltrombopag as an allosteric inhibitor of the METTL3-14 complex affecting the m6A methylation of RNA in acute myeloid leukemia cells. *Pharmaceuticals* (*Basel*). 2022;15(4):440.

doi: 10.3390/ph15040440

218. Nai F, Flores Espinoza MP, Invernizzi A, *et al.* Small-molecule inhibitors of the m7G-RNA writer METTL1. *ACS Bio Med Chem Au*. 2023;4(2):100-110.

doi: 10.1021/acsbiomedchemau.3c00030

219. Li F, Li W. Readers of RNA modification in cancer and their anticancer inhibitors. *Biomolecules*. 2024;14(7):881.

doi: 10.3390/biom14070881

220. Dahlem C, Abuhaliema A, Kessler SM, *et al.* First small-molecule inhibitors targeting the RNA-binding protein IGF2BP2/IMP2 for cancer therapy. *ACS Chem Biol*. 2022;17(2):361-375.

doi: 10.1021/acschembio.1c00833

221. Wallis N, Oberman F, Shurrush K, *et al.* A small molecule inhibitor of Igf2bp1 represses Kras and a prooncogenic phenotype in cancer cells. *RNA Biol*. 2022;19(1):26-43.

doi: 10.1080/15476286.2021.2010983

222. Feng P, Chen D, Wang X, *et al.* Inhibition of the m6A reader IGF2BP2 as a strategy against T-cell acute lymphoblastic leukemia. *Leukemia*. 2022;36(9):2180-2188.

doi: 10.1038/s41375-022-01651-9

223. Bao Y, Zhai J, Chen H, *et al.* Targeting m6A reader YTHDF1 augments antitumour immunity and boosts anti-PD-1 efficacy in colorectal cancer. *Gut*. 2023;72:1497-1509.

doi: 10.1136/gutjnl-2022-328845

224. Chanda S, Lepikhov K, Dahlem C, *et al.* Gene editing and small molecule inhibitors of the RNA binding protein IGF2BP2/IMP2 show its potential as an anti-cancer drug target. *Front Biosci (Landmark Ed)*. 2024;29(1):41.

doi: 10.31083/j.fbl2901041

225. Huang Y, Su R, Sheng Y, *et al.*, Small-Molecule Targeting of Oncogenic FTO Demethylase in Acute Myeloid Leukemia. *Cancer Cell*. 2019, 35(4):677-691.e10.

doi: 10.1016/j.ccell.2019.03.006

226. Feng G, Wu Y, Hu Y, *et al.* Small molecule inhibitors targeting m6A regulators. *J Hematol Oncol*. 2024;17(1):30.

doi: 10.1186/s13045-024-01546-5

227. Zálešák F, Nai F, Herok M, *et al.* Structure-based design of a potent and selective YTHDC1 ligand. *J Med Chem*. 2023;67:9516-9535.

doi: 10.1021/acs.jmedchem.4c00599

228. Hollebecque A, Salvagni S, Plummer R, *et al.* Clinical activity of CC-90011, an oral, potent, and reversible LSD1 inhibitor, in advanced malignancies. *Cancer* (*Basel*). 2022;128(17):3185-3195.

doi: 10.1002/cncr.34366

229. Sahafnejad Z, Ramazi S, Allahverdi A. An update of epigenetic drugs for the treatment of cancers and brain diseases: A comprehensive review. *Genes* (*Basel*). 2023;14(4):873.

doi: 10.3390/genes14040873

230. Li Y, Ren Y, Wang Y, *et al.* A compound AC1Q3QWB selectively disrupts HOTAIR-mediated recruitment of PRC2 and enhances the cancer therapy of DZNep. *Theranostics*. 2019;9:4608-4623.

doi: 10.7150/thno.35188

231. Yang L, Tang L, Min Q, *et al.* Emerging role of RNA modification and long noncoding RNA interaction in cancer. *Cancer Gene Ther*. 2024;31(6):816-830.

doi: 10.1038/s41417-024-00734-2

232. Poole RM. Belinostat: First global approval. *Drugs*. 2014;74:1543-1554.

doi: 10.1007/s40265-014-0275-8

233. Mann BS, Johnson JR, Cohen MH, Justice R, Pazdur R. FDA approval summary: Vorinostat for treatment of advanced primary cutaneous T-cell lymphoma. *Oncologist*. 2007;12:1247-1252.

doi: 10.1634/theoncologist.12-10-1247

234. VanderMolen KM, McCulloch W, Pearce CJ, Oberlies NH. Romidepsin (Istodax, NSC 630176, FR901228, FK228, depsipeptide): A natural product recently approved for cutaneous T-cell lymphoma. *J Antibiotics* (*Tokyo*). 2011;64:525-531.

doi: 10.1038/ja.2011.35

235. Lu X, Ning Z, Li Z, Cao H, Wang X. Development of chidamide for peripheral T-cell lymphoma, the first orphan drug approved in China. *Intractable Rare Dis Res*. 2016;5:185-191.

doi: 10.5582/irdr.2016.01024

236. Garnock-Jones KP. Panobinostat: First global approval. *Drugs*. 2015;75:695-704. Erratum in *Drugs*. 2015;75:929.

doi: 10.1007/s40265-015-0388-8

237. Ghasemi S. Cancer's epigenetic drugs: Where they are in the cancer medicines? *Pharmacogen J*. 2020;20:367-379.

doi: 10.1038/s41397-019-0138-5

238. Zhou Z, Li HQ, Liu F. DNA methyltransferase inhibitors and their therapeutic potential. *Curr Top Med Chem*. 2018;18:2448-2457.

doi: 10.2174/1568026619666181120150122

239. Kantarjian HM, Roboz GJ, Kropf PL, *et al.* Guadecitabine (SGI-110) in treatment-naive patients with acute myeloid leukemia: Phase 2 results from a multicenter, randomized, phase 1/2 trial. *Lancet Oncol*. 2017;18:1317-1326.

doi: 10.1016/S1470-2045(17)30576-4

240. Poltronieri P, Joardar S. Unravelling the interplay between biomolecular condensates and RNA in cancer and diseases. *J Biol Regul Homeost Agents*, 2024;38(8):5627-5652.

doi: 10.23812/j.biol.regul.homeost.agents.20243808.453

241. Chen XH, Guo KX, Li J, Xu SH, Zhu H, Yan GR. Regulations of m6A and other RNA modifications and their roles in cancer. *Front Med*. 2024;18(4):622-648.

doi: 10.1007/s11684-024-1064-8

242. Gilbert LA, Horlbeck MA, Adamson B, *et al.* Genome-scale CRISPR-mediated control of gene repression and activation. *Cell*. 2014;159:647-661.

doi: 10.1016/j.cell.2014.09.029

243. Shamloo S, Kloetgen A, Petroulia S, *et al.* Integrative CRISPR activation and small molecule inhibitor screening for lncRNA mediating BRAF inhibitor resistance in melanoma. *Biomedicines*. 2023;11:2054.

doi: 10.3390/biomedicines11072054

244. Liu C, Tang H, Hu N, *et al.* Methylomics and cancer: The current state of methylation profiling and marker development for clinical care. *Cancer Cell Int*. 2023;23:242.

doi: 10.1186/s12935-023-03074-7

245. Zhen S, Lu J, Chen W, Zhao L, Li X. Synergistic antitumor effect on bladder cancer by rational combination of programed cell death 1 blockade and CRISPR-Cas9-mediated long non-coding RNA urothelial carcinoma associated 1 knockout. *Hum Gene Ther*. 2018;29:1352-1363.

doi: 10.1089/hum.2018.048

246. Gao J, Hou B, Zhu Q, *et al.* Engineered bioorthogonal POLY-PROTAC nanoparticles for tumor-specific protein degradation and precise cancer therapy. *Nat Commun*. 2022;13(1):4318.

doi: 10.1038/s41467-022-32050-4

247. Wang C, Zhang Y, Chen W, Wu Y, Xing D. New-generation advanced PROTACs as potential therapeutic agents in cancer therapy. *Mol Cancer*. 2024;23(1):110.

doi: 10.1186/s12943-024-02024-9

248. Zhao LP, Rao XN, Zheng RR, *et al.* Carrier-free nano-PROTACs to amplify photodynamic therapy induced DNA damage through BRD4 degradation. *Nano Lett*. 2023;23(13):6193-6201.

doi: 10.1021/acs.nanolett.3c01812

249. Alabi S, Jaime-Figueroa S, Yao Z, *et al.* Mutant-selective degradation by BRAF-targeting PROTACs. *Nat Commun*. 2021;12:920.

doi: 10.1038/s41467-021-21159-7

250. Haj-Yahia S, Nandi A, Benhamou RI. Targeted degradation of structured RNAs via ribonuclease-targeting chimeras (RiboTacs). *Expert Opin Drug Discov*. 2023;18(8):929-942.

doi: 10.1080/17460441.2023.2224960

251. Tong Y, Lee Y, Liu X, *et al.* Programing inactive RNA-binding small molecules into bioactive degraders. *Nature*. 2023;618(7963):169-179.

doi: 10.1038/s41586-023-06091-8

252. Ly HH, Daniel S, Soriano SKV, Kis Z, Blakney AK. Optimization of lipid nanoparticles for saRNA expression and cellular activation using a design-of-experiment approach. *Mol Pharmacol*. 2022;19(6):1892-1905.

doi: 10.1021/acs.molpharmaceut.2c00032

253. Kovachka S, Panosetti M, Grimaldi B, Azoulay S, Di Giorgio A, Duca M. Small-molecule approaches to targeting RNA. *Nat Rev Chem*. 2024;8:120-135.

doi: 10.1038/s41570-023-00569-9

254. Hargrove AE. Small molecule-RNA targeting: Starting with the fundamentals. *Chem Commun* (*Camb*). 2020;56:14744-14756.

doi: 10.1039/d0cc06796b

255. Berdnikova DV. Photoswitches for controllable RNA binding: A future approach in RNA-targeting therapy. *Chem Commun* (*Camb*). 2021;57:10819-10826.

doi: 10.1039/d1cc04241f

256. Chen B, Dragomir MP, Fabris L, *et al.* The long noncoding RNA CCAT2 induces chromosomal instability through BOP1-AURKB signaling. *Gastroenterology*. 2020;159:2146-2162.

doi: 10.1053/j.gastro.2020.08.018

257. Sha S, Yuan D, Liu Y, Han B, Zhong N. Targeting long noncoding RNA DANCR inhibits triple-negative breast cancer progression. *Biol Open*. 2017;6(9):1310-1316.

doi: 10.1242/bio.023135

258. Ehmann F, Kuhn A, Pasmooij AMG, *et al.* Report of the European medicines agency conference on RNA-based medicines. *Nucleic Acid Ther*. 2024;34:4-11.

doi: 10.1089/nat.2023.0021

259. Benhamou RI, Suresh BM, Tong Y, *et al.* DNA-encoded library versus RNA-encoded library selection enables design of an oncogenic noncoding RNA inhibitor. *Proc Natl Acad Sci U S A*. 2022;119:e2114971119.

doi: 10.1073/pnas.2114971119

260. Bouchard JJ, Otero JH, Scott DC, *et al.* Cancer mutations in the tumor suppressor SPOP disrupt the formation of active, phase-separated compartments. *Mol Cell*. 2018;72(1):19-36.e8.

doi: 10.1016/j.molcel.2018.08.027

261. Grabocka E, Bar-Sagi D. Mutant KRAS enhances tumor cell fitness by upregulating stress granules. *Cell*. 2016;167(7):1803-1813.e12.

doi: 10.1016/j.cell.2016.11.035

262. Zhang J, Zeng Y, Xing Y, *et al.* Myristoylation-mediated phase separation of EZH2 compartmentalizes STAT3 to promote lung cancer growth. *Cancer Lett*. 2021;516:84-98.

doi: 10.1016/j.canlet.2021.05.035

263. Xu WX, Qu Q, Zhuang HH, *et al.* The burgeoning significance of liquid-liquid phase separation in the pathogenesis and therapeutics of cancers. *Int J Biol Sci*. 2024;20(5):1652-1668.

doi: 10.7150/ijbs.92988

264. Li J, Zhang Y, Gu J, *et al.* Stress granule core protein-derived peptides inhibit assembly of stress granules and improve sorafenib sensitivity in cancer cells. *Molecules* (*Basel*). 2024;29(9):2134.

doi: 10.3390/molecules29092134

265. Bechara C, Sagan S. Cell-penetrating peptides: 20 years later, where do we stand? *FEBS Lett.* 2013;587:1693-1702.

doi: 10.1016/j.febslet.2013.04.031

266. Chen Y, Lan T. N-terminal domain of androgen receptor is a major therapeutic barrier and potential pharmacological target for treating castration resistant prostate cancer: A comprehensive review. *Front Pharmacol*. 2024;15:1451957.

doi: 10.3389/fphar.2024.1451957

267. Kamagata K, Ariefai M, Takahashi H, *et al.* Rational peptide design for regulating the liquid-liquid phase separation on the basis of the residue-residue contact energy. *Sci Rep.* 2022;12(1):13718.

doi: 10.1038/s41598-022-17829-1

268. Lemos C, Schulze L, Weiske J, *et al.* Identification of small molecules that modulate mutant p53 condensation. *iScience*. 2020;23(9):101517.

doi: 10.1016/j.isci.2020.101517

269. Donlic A, Zafferani M, Padroni G, *et al.* Regulation of the MALAT1 triple helix stability and *in vitro* degradation by diphenylfuran. *Nucleic Acids Res*. 2020;48:7653-7664.

doi: 10.1093/nar/gkaa585

270. Meyer SM, Tanaka T, Taghavi A, Baisden JT, Grefe M, Disney MD. Optimization of a protein-targeted medicine into an RNA-specific small molecule. *ACS Chem Biol*. 2023;18(11):2336-2342.

doi: 10.1021/acschembio.3c00476

271. False JP, Donlic A, Hargrove AE. Targeting RNA with small molecules: From fundamental principles toward the clinic. *Chem Soc Rev*. 2021;50(4):2224-2243.

doi: 10.1039/d0cs01261k

272. Xiao H, Yang X, Zhang Y, Zhang Z, Zhang G, Zhang BT. RNA-targeted small-molecule drug discoveries: a machine-learning perspective. *RNA Biol*. 2023;20(1):384-397.

doi: 10.1080/15476286.2023.2223498

273. Kim T, Kim TK. Regulatory RNA: From molecular insights to therapeutic frontiers. *Exp Mol Med*. 2024;56(6):1233-1234.

doi: 10.1038/s12276-024-01267-2

274. Li K, Wang H, Jiang B, Jin X. TRIM28 in cancer and cancer therapy. *Front Genet*. 2024;15:1431564.

doi: 10.3389/fgene.2024.1431564

275. Zhu Y, Li J, Li S, *et al.* ZMAT2 condensates regulate the alternative splicing of TRIM28 to reduce cellular ROS accumulation, thereby promoting the proliferation of HCC cells. *Cell Commun Signal*. 2024;22(1):407.

doi: 10.1186/s12964-024-01790-9

276. Christen KE, Davis RA, Kennedy D. Psammaplysin F increases the efficacy of bortezomib and sorafenib through the regulation of stress granule formation. *Int J Biochem Cell Biol*. 2019;112:24-38.

doi: 10.1016/j.biocel.2019.04.008

277. Mitrea DM, Mittasch M, Ferreira Gomes B, Klein IA, Murcko MA. Modulation of biomolecular condensates: A novel approach to drug discovery. *Nat Rev Drug Discov*. 2022;21(11):841-862.

doi: 10.1038/s41573-022-00505-4

278. Wheeler RJ, Lee OH, Poser I, *et al. Small Molecules for Modulating Protein Driven Liquid-Liquid Phase Separation in Treating Neurodegenerative Disease*. BioRixv preprint.

doi: 10.1101/721001

279. Qu M, He Q, Bao H, *et al.* The multiple roles of arsenic compounds in phase separation and membraneless organelle formation determine their therapeutic efficacy in tumors. *J Pharm Anal*. 2024;14(8):100957.

doi: 10.1016/j.jpha.2024.02.011

280. Li X, Yu Z. Role of liquid-liquid phase separation in cancer: Mechanisms and therapeutic implications. *Cancer Innov*. 2024;3(5):e144.

doi: 10.1002/cai2.144

281. Zhang W, Li Z, Wang X, Sun T. Phase separation is regulated by posttranslational modifications and participates in the development of human diseases. *Heliyon*. 2024;10(13):e34035.

doi: 10.1016/j.heliyon.2024.e34035

282. Liu Z, Qin Z, Liu Y, *et al.* Liquid-liquid phase separation: roles and implications in future cancer treatment. *Int J Biol Sci*. 2023;19(13):4139-4156.

doi: 10.7150/ijbs.81521

283. Balavaishnavi B, Kamaraj M, Nithya TG, Santhosh P, GokilaLakshmi S, Shaik MR. Regulation of hippo signaling-mediated apoptosis by *Rauvolfia tetraphylla* in triple-negative breast cancer. *Med Oncol*. 2024;41(5):103.

doi: 10.1007/s12032-024-02341-5

284. Wang J, Hu L, Zhang H, Fang Y, Wang T, Wang H. Intracellular condensates of oligopeptides for targeting lysosomes and addressing multiple drug resistance of cancer. *Adv Mater*. 2022;34(1):e2104704.

doi: 10.1002/adma.202104704

285. Grosch M, Ittermann S, Rusha E, *et al.* Nucleus size and DNA accessibility are linked to the regulation of paraspeckle formation in cellular differentiation. *BMC Biol*. 2020;18:42.

doi: 10.1186/s12915-020-00770-y

286. Jia Y, Jia R, Dai Z, *et al.* Stress granules in cancer: Adaptive dynamics and therapeutic implications. *iScience*. 2024;27(8):110359.

doi: 10.1016/j.isci.2024.110359

287. Dinh NTM, Nguyen TM, Park MK, Lee CH. Y-box binding protein 1: Unraveling the multifaceted role in cancer development and therapeutic potential. *Int J Mol Sci*. 2024;25(2):717.

doi: 10.3390/ijms25020717

288. Shen X, Peng X, Guo Y, *et al.* YAP/TAZ enhances P-body formation to promote tumorigenesis. *Elife*. 2024;12:RP88573.

doi: 10.7554/eLife.88573

289. Tong F, Hu H, Xu Y, *et al.* Hollow copper sulfide nanoparticles carrying ISRIB for the sensitized photothermal therapy of breast cancer and brain metastases by inhibiting stress granule formation and reprograming tumor-associated macrophages. *Acta Pharmacol Sin B*. 2023;13:3471-3488.

doi: 10.1016/j.apsb.2022.11.003

290. Zyryanova AF, Kashiwagi K, Rato C, *et al.* ISRIB blunts the integrated stress response by allosterically antagonizing the inhibitory effect of phosphorylated eIF2 on eIF2b. *Mol Cell*. 2021;81:88-103.e6.

doi: 10.1016/j.molcel.2020.10.03

291. Hou WC, Massey LA, Rhoades D, *et al.* A PIKfyve modulator combined with an integrated stress response inhibitor to treat lysosomal storage diseases. *Proc Natl Acad Sci U S A*. 2024;121(34):e2320257121.

doi: 10.1073/pnas.2320257121

292. Cao X, Zhang Y, Ding Y, Wan Y. Identification of RNA structures and their roles in RNA functions. *Nat Rev Mol Cell Biol*. 2024;25(10):784-801.

doi: 10.1038/s41580-024-00748-6

293. He C, Wu CY, Li W, Xu K. Multidimensional super-resolution microscopy unveils nanoscale surface aggregates in the aging of FUS condensates. *J Am Chem Soc*. 2023;145(44):24240-24248.

doi: 10.1021/jacs.3c08674

294. Choi AA, Xu K. Single-molecule diffusivity quantification unveils ubiquitous net charge-driven protein-protein interaction. *J Am Chem Soc*. 2024;146(15):10973-10978.

doi: 10.1021/jacs.4c02475

295. Yao RW, Rosen MK. Advanced surface passivation for high-sensitivity studies of biomolecular condensates. *Proc Natl Acad Sci U S A*. 2024;121(22):e2403013121.

doi: 10.1101/2024.02.12.580000

296. Paul S, Mondal S, Shenogina I, Cui Q. The molecular basis for the increased stability of the FUS-LC fibril at the anionic membrane- and air-water interfaces. *Chem Sci*. 2024;15(34):13788-13799.

doi: 10.1039/d4sc02295e

297. Xia C, Colognori D, Jiang X, Xu K, Doudna JA. Single-molecule live-cell RNA imaging with CRISPR-Csm. bioRxiv [Preprint]. 2024:2024.07.14.603457.

doi: 10.1101/2024.07.14.603457

298. Guan A, Wong JJ. Targeting RNA modifications with pharmacological agents: New frontiers in cancer therapy. *Cancer Med*. 2024;13(7):e6989.

ACCSCIENCE PUBLISHING

Tumor Discovery

ORIGINAL RESEARCH ARTICLE

Bioinformatics approach to identifying potential cancer-associated mutations in *CCL2*

Shah Kamal[1†], Najeeb Ullah[1†], Amanullah Amanullah[1], Mariam Ahmed Mujtaba[2], Kashif Ali Khan[3], Cheng Deng[1*], Shanshan Lai[1*], and Mohammad Amjad Kamal[4,5,6,7,8*]

[1]Jiangsu Key Laboratory for Biodiversity and Biotechnology, College of Life Sciences, Nanjing Normal University, Nanjing, China

[2]Department of Biotechnology, Women University Mardan, East Canal Road Mardan, 23200, Pakistan

[3]Department of Pharmacy, Shaheed Benazir Bhutto University Sheringal, Dir Upper, Pakistan

[4]Institutes for Systems Genetics, Frontiers Science Center for Disease-related Molecular Network, West China School of Nursing, West China Hospital, Sichuan University, Chengdu, China

[5]King Fahd Medical Research Center, King Abdulaziz University, Jeddah, Saudi Arabia

[6]Department of Pharmacy, Faculty of Allied Health Sciences, Daffodil International University, Dhaka, Bangladesh

Abstract

Chemokine C-C motif ligand 2 (CCL2), also known as monocyte chemoattractant protein 1 or small inducible cytokine A2, is a cytokine from the CC chemokine family. It plays a crucial role in recruiting monocytes, memory T-cells, and dendritic cells to inflammatory sites resulting from tissue injury or infection. C-C motif chemokine receptor 2 (CCR2) is a chemokine receptor that may influence lymphocyte function. The interaction between CCL2 and CCR2 is essential for inflammatory responses and cancer regulation, as it attracts monocytes and macrophages to tumor sites, facilitating tumor growth and metastasis. Given the importance of CCL2 in regulating cell trafficking and cancer progression, we employed a bioinformatics approach to examine the effects of oncogenic missense mutations in *CCL2* on CCR2 activation. We used precise computational methods to identify the molecular characteristics responsible for the altered activity and interactions, thereby enhancing our understanding of the molecular mechanisms underlying disease progression. We generated a three-dimensional model of the CCL2 protein with the identified mutations using the I-TASSER algorithm. The effects of these mutations on the protein's stability and functional properties were evaluated using various prediction tools, and molecular dynamics simulations were conducted using WebGro software. Our analysis of 83 *CCL2* missense mutations identified 10 disease-causing mutations, including C59G, which was directly linked to cancer. The C59G mutation increases the binding interaction between CCL2 and CCR2. The C59G position was determined to be highly conserved, and substitutions of cysteine (C) 59 with glycine (G) altered CCL2 activity. Our results suggest that this mutation alters the CCL2–CCR2 binding activity, lowering the risk of developing cancer and defending against pathogen invasion during the neutrophil-mediated innate immune response.

Keywords: CCL2; Molecular dynamic simulation; Colorectal cancer; Point mutation

†These authors contributed equally to this work.

***Corresponding authors:**
Cheng Deng
(dengcheng2014@126.com)
Mohammad Amjad Kamal
(ma.kamal@wchscu.cn)
Shanshan Lai
(lss7259@163.com)

Citation: Kamal S, Ullah N, Amanullah A, *et al*. Bioinformatics approach to identifying potential cancer-associated mutations in *CCL2*. *Tumor Discov*. 2024;3(4):3891.
doi: 10.36922/td.3891

Received: June 7, 2024

Accepted: September 5, 2024

Published Online: October 21, 2024

[7]Centre for Global Health Research, Saveetha Medical College and Hospital, Saveetha Institute of Medical and Technical Sciences, Chennai, Tamil Nadu, India
[8]Enzymoics, 7 Peterlee Place, Hebersham, Novel Global Community Educational Foundation, NSW, Australia
(This article belongs to the *Special Issue: Colorectal Cancer: Best Tools for Diagnosis to Management Strategies*)

1. Introduction

Chemokine C-C motif ligand 2 (CCL2), also known as monocyte chemoattractant protein 1 (MCP-1) or small inducible cytokine A2, is an important cytokine in the CC chemokine family.[1] CCL2 adopts a β-trefoil fold, which is a common protein fold that provides plasticity for recognizing various targets.[2] Monomeric CCL2 binds to its receptor, C-C motif chemokine receptor 2 (CCR2), through a single, topologically novel binding site.[3] CCL2 penetrates the extracellular portion of the CCR2 transmembrane domain and interacts with the receptor through its N-terminal glutamine. There are numerous hydrophobic and polar interactions between CCL2 and the Gα-protein of the CCR2 receptor complex, which contribute to the receptor's constitutive activity.[4]

CCL2 plays a crucial role in regulating cellular mechanics by attracting monocytes, memory T-cells, and dendritic cells to inflammation sites resulting from tissue injury or infection.[5] This small cytokine is primarily secreted by monocytes, macrophages, and dendritic cells and is involved in various physiological processes, including immune cell recruitment, antitumor activity, and granuloma formation.[6] CCL2 interacts with cell surface receptors, such as CCR2 and CCR4, and exhibits chemotactic activity for monocytes and basophils.[7] Its effects extend to diseases characterized by monocytic infiltrates, such as psoriasis, rheumatoid arthritis, atherosclerosis, and certain cancers. In cancer, CCL2 has been demonstrated to promote cell proliferation, migration, and metastasis, underscoring its potential as a therapeutic target for cancer treatment.[8,9]

Chemokines can induce the release of stored promalignant chemokines from breast tumor cells, highlighting the substantial tumor-promoting role of chemokine coexpression in breast cancer progression.[10-12] Epithelial ovarian cancer cells produce MCP-1, which is likely the major source of this chemokine. This production may contribute to the accumulation of tumor-associated macrophages, which can subsequently influence tumor behavior.[13,14] Cancer cells and macrophages interact to promote tumor angiogenesis, a crucial process in cancer progression. Specifically, MCP-1 has been linked to the progression of human esophageal carcinoma by facilitating angiogenesis, enhancing macrophage recruitment, and promoting the development of new blood vessels.[15,16] Moreover, MCP-1 produced by human gastric carcinoma cells plays a crucial role in angiogenesis. It attracts and activates macrophages, which then aid in forming new blood vessels and promote tumor growth.[17] MCP-1 has a limited role in eliciting an immune response in renal cell carcinomas, as assessed by the parameters analyzed in this study.[18] The simultaneous induction of tumor necrosis factor-alpha (TNF-α), urokinase-type plasminogen activator, interleukin (IL)-8, and MCP-1 can enhance the interaction of tumor and inflammatory cells, thereby increasing cytotoxicity and promoting tumor suppression.[19] MCP-1 can potentiate the effects of bacterial endotoxins by activating macrophages to become tumoricidal, potentially suppressing metastasis.[20] The chemokine MCP-1 plays an important role in promoting tumor progression and angiogenesis across various cancer types, including breast, ovarian, esophageal, and gastric carcinomas. MCP-1 production by tumor cells contributes to the recruitment and activation of tumor-associated macrophages, supporting cancer growth and metastasis.

Computational analysis has become increasingly vital for identifying harmful mutations and predicting the effects of missense mutations on protein structures and functions. This type of analysis is now a key tool in designing new drugs and therapies for genetic diseases.[21] In this study, we evaluated the potential significance of mutations in *CCL2* that can impact its protein functions and ligand interactions. Initially, we used various computational algorithms, including meta-single nucleotide polymorphism (SNP),[22] PolyPhen-2,[23] and Pmut,[24] to categorize harmful mutations. We further employed the Functional Analysis through Hidden Markov Models (FATHMM) server to identify specific genetic variants associated with cancer development or initiation among disease-causing mutations. This approach allowed us to distinguish between cancer-promoting mutations and those related to other disease phenotypes, providing valuable insights into the specific role of certain variants in cancer pathogenesis.[25] In addition to the sequence-based analysis, we employed structure-based computational tools, such as mCSM,[26] SDM,[27] and DUET,[28] to predict the impact of the identified mutations on the structure and stability of the corresponding proteins.

One missense mutation in *CCL2* was selected based on its cancer association for further investigation. The

I-TASSER server was used to generate a structural model incorporating the specified missense mutation in *CCL2*.[29] The model underwent molecular dynamics (MD) simulations and three-dimensional (3D) modeling through WebGro to evaluate how the mutation affected the stability and functionality of the CCL2 protein.[30] WebGro software was then used to perform MD simulations on the mutant CCL2 model, enabling the assessment of its stability and potential functional consequences compared to the native protein. A thorough analysis of the impact of the missense mutation on the protein structure and function was facilitated by this integrated computational approach that combines structure prediction with MD[31] (Figure 1).

Molecular docking studies offer valuable insights into the binding dynamics and interactions between CCL2 and CCR2, highlighting the potential for therapeutic interventions in diseases mediated by this signaling pathway. Molecular docking analyses have identified the critical residues in CCL2, such as T16, N17, and R18, which are essential for forming stable complexes with CCR2. These interactions involve both hydrophobic interactions and hydrogen bonds, which collectively contribute to the binding affinity of CCL2 (ligand) with CCR2 (receptor).[3] For instance, the binding of the compound baicalin (BA) to CCL2 is facilitated by substantial hydrophobic interactions with residues such as I20 and V51 and hydrogen bonds with residues such as T16 and S17. The binding energy calculated for CCL2 interactions with CCR2, that is, approximately −6.3 kcal/mol for the interaction between BA and human CCL2, indicates the formation of a favorable and stable ligand–receptor complex.[3] Understanding these molecular interactions through docking studies provides valuable insights into drug design. By targeting the CCL2–CCR2 interaction, researchers can develop antagonists that disrupt this pathway. These antagonists hold promise as therapeutic agents for the treatment of inflammatory and autoimmune diseases as well as certain cancers where CCL2/CCR2 signaling plays an important role.

CCL2 mutations can substantially alter the protein's structure and function and potentially affect its binding affinity to the CCR2 receptor. This may impact the recruitment and activation of tumor-associated macrophages, thereby influencing angiogenesis and tumor progression. This mutation could also modulate the immune response to CCL2, potentially influencing antitumor immunity and macrophage tumoricidal activity. Overall, *CCL2* mutations could have profound implications for the tumorigenic potential of this chemokine in cancer development. However, further research is required to elucidate the specific genetic and epigenetic factors that influence the expression and activity of *CCL2* mutations.

2. Material and methods

2.1. Collection of datasets

In this study, we collected data on *CCL2* missense mutations from the Ensembl database (release 109) (https://www.

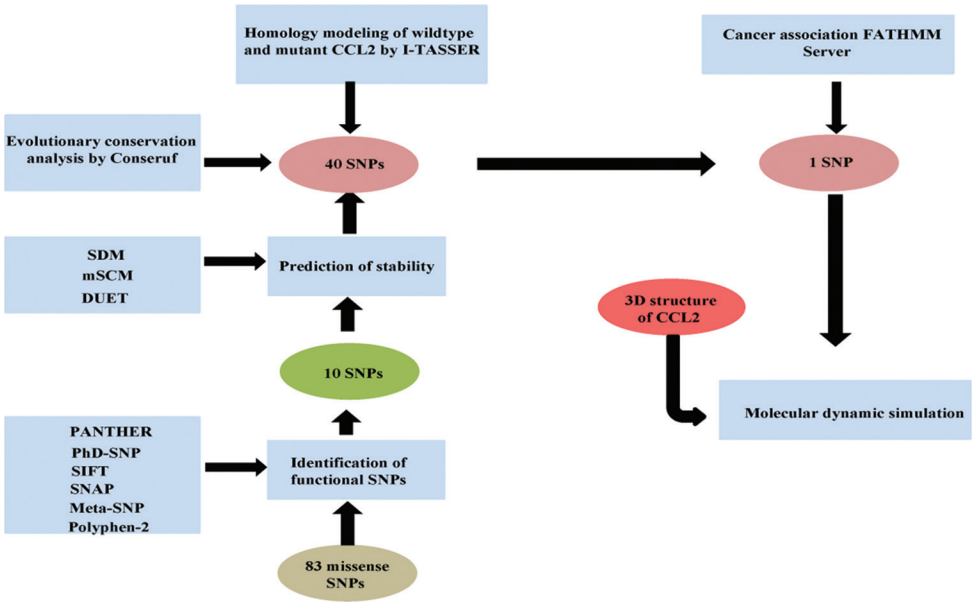

Figure 1. Flowchart illustrating the stepwise analysis of missense SNPs in human CCL2, employing computational tools to investigate 83 missense SNPs. Initially, six tools identified 10 SNPs with functional effects, including 40 highly destabilizing SNPs. One mutation, C59G, was predicted as the most high-risk missense SNP and subjected to molecular dynamics simulations.
Abbreviations: SNP: Single-nucleotide polymorphism; CCL2: Chemokine C-C motif ligand 2.

ensembl.org), which provides comprehensive genomic information (Ensembl ID: ENSG00000108691).[32] This dataset was chosen due to its extensive collection of genomic variations. In addition, data were obtained from the UniProtKB database (https://www.uniprot.org), which includes sequence details in FASTA format (UniProt ID: P13500), and the National Center for Biotechnology Information (NCBI) (https://www.ncbi.nlm.nih.gov).[33,34] Structural information regarding CCL2 was retrieved from the Protein Data Bank (PDB) (CCL2 PDB ID: 2LIE, and CCR2 PDB ID: 2LWL) through the website http://www.rcsb.org/.[35]

2.2. Computational prediction of mutation pathogenicity

To assess the effects of mutations on CCL2 proteins, we used computational methods essential for distinguishing between single-nucleotide variations that are detrimental, benign, or cancerous. Accurate evaluation of the functional impacts of these genetic alterations is essential for identifying disease-causing mutations. Meta-SNP (http://snps.biofold.org/meta-snp/) is a web-based tool that uses multiple predictive algorithms to assess the potential pathogenicity of protein mutations.[22] We employed meta-SNP to assess mutation pathogenicity by integrating the predictions from algorithms such as SNAP,[36] PhD-SNP, Panther,[37] and SIFT.[38]

Meta-SNP is a reliable tool for predicting how mutations affect protein functions. It combines results from various algorithms using a random forest technique, which involves 100 decision trees within the WEKA library. This method ensures the precise assessment of a mutation's impact on its protein function.[39] The meta-SNP algorithm was trained on the SV-2009 dataset through a 20-fold cross-validation procedure and provides dependable predictions of disease-causing variants.[22] It outputs a probability score between 0 and 1, with scores above 0.5 indicating a higher likelihood of the mutation being pathogenic.[40]

Next, we used the Polyphen-2 web server (http://genetics.bwh.harvard.edu/pph2/), which is an automated tool designed to predict the potential effects of amino acid substitutions on the structure and function of human proteins.[41] This site features an input form that enables users to query either a single amino acid substitution or a coding, non-synonymous SNP that is annotated in the dbSNP database.[23]

2.3. Computational assessment of protein stability

Mutations can affect a protein's structure and stability, resulting in changes in free energy (ΔΔG in Kcal/mol). The difference between the mutated (ΔGm) and original (ΔGw) proteins' free energy indicates a change in stability, where negative ΔΔG indicates destabilization, whereas positive ΔΔG indicates stabilization.[27,42] Various computational tools, including mCSM, SDM, and DUET, were employed to assess the impact of mutations on CCL2 protein stability and function, providing valuable insights into how specific mutations alter protein behavior.[27]

The SDM online tool, available at http://marid.bioc.cam.ac.uk/sdm2, accurately predicts the impact of mutations on protein stability through *in silico* analysis. It examines variations in amino acid substitutions tolerated by homologous proteins with known 3D structures in specific environments, providing valuable insights into how mutations can affect protein behavior and stability.[27,43,44]

The mCSM computational technique uses machine learning to predict the effects of missense mutations on CCL2 protein stability and function. It employs graph-based signatures to depict how mutations impact the interaction network among residues. By integrating evolutionary information, complex network metrics, and energetic factors, mCSM creates an accurate predictive model. It is available at http://structure.bioc.cam.ac.uk/mcsm.[21,26] The mCSM method evaluates how mutations affect protein structure and interactions with other proteins and nucleic acids. It provides insights into how mutations contribute to disease development, improving our understanding of the molecular mechanisms of various diseases. This computational approach clarifies the effects of mutations on protein stability, function, and interactions, enhancing our understanding of disease pathogenesis.[45,46]

DUET (http://structure.bioc.cam.ac.uk/duet) is a computational tool that predicts changes in protein stability due to individual mutations. It combines two methods to calculate the change in folding free energy (ΔΔG in Kcal/mol), with negative ΔΔG values indicating destabilizing mutations and positive values indicating stabilizing mutations.[28,47] DUET uses support vector machines trained with sequential minimal optimization to integrate the predictions from mCSM and SDM. This machine learning technique leverages the strengths of both methods to provide a comprehensive assessment of how missense mutations affect protein stability. By combining these predictive capabilities, DUET enhances the accuracy and reliability of mutation impact predictions on protein stability.[48]

2.4. Evaluating cancer-related mutations using the FATHMM server

The FATHMM server, available at http://fathmm.biocompute.org.uk, was used to assess the cancer relevance of deleterious mutations in *CCL2*. This web server predicts the functional consequences of both coding and noncoding

variants, including their potential association with cancer, where scores below the default threshold of −0.75 indicate a potential cancer link. FATHMM helps distinguish between cancer-related mutations and non-pathogenic germline polymorphisms.[25,49] Using FATHMM, we aimed to deepen our understanding of the genetic basis of cancer by evaluating the impact of harmful mutations on disease progression, identifying clinically significant mutations, and advancing our knowledge of cancer development.[25]

2.5. Sequence conservation analysis of CCL2

The ConSurf web server (http://consurf.tau.ac.il) analyzes the evolutionary patterns of amino acids in proteins to identify regions critical for structure and function. Using a query sequence or structure, the server automatically gathers homologous sequences, performs multiple sequence alignment, and constructs a phylogenetic tree that illustrates their evolutionary relationships. This information is then utilized within a probabilistic framework to estimate the evolutionary rates for each position in the sequence.[50]

2.6. Structural modeling of CCL2 point mutation sites

To create a mutant model of CCL2 featuring the targeted mutation C59C (native) and C59G (mutant), the crystal structure of the native peptides was initially downloaded from the PDB. Subsequently, the I-TASSER server (https://zhanglab.ccmb.med.umich.edu/I-TASSER/), which uses a multiple threading approach, was employed to construct the intended mutant model.[29]

2.7. Quality evaluation of the protein model

The CCL2 protein is a complex molecule composed of amino acids, with its function intricately linked to its specific 3D structure. Understanding CCL2's structure can provide valuable insights into its function, interactions with other molecules, and potential roles in biological processes, such as the immune system and inflammation.[51] The I-TASSER server was used to generate protein models of mutant and native CCL2.[29] The quality assessment process included an analysis of the stereochemical characteristics of the models, such as the bond lengths, bond angles, and torsion angles. This evaluation aimed to confirm that the protein models exhibit a conformation that is both geometrically and chemically reasonable. Deviations from expected values in the stereochemical features of the model could suggest potential errors in the model.[52] The protein models were validated by comparing them with experimental data to ensure that they aligned with the known structural properties of CCL2 protein, which verified the accuracy of the predicted models by examining how accurately they matched with the actual protein structure, thereby ensuring the reliability of the models.[53]

The reliability of the mutant and native CCL2 protein models was ensured by validating their stereochemical quality using the Rampage server (https://servicesn.mbi.ucla.edu/PROCHECK). This involved analyzing the residue-by-residue geometry and overall structure geometry to assess the accuracy of models.[54]

2.8. MD simulation

MD simulation is a computational technique used to simulate the dynamic movement of atoms and molecules throughout a period. By simulating movements and interactions of biological molecules, such as proteins, MD provides detailed insights into their molecular structures, dynamics, and interactions, which are often difficult to obtain through experimental methods alone.[55,56] The accuracy of MD simulation results relies heavily on the quality of the protein model.[57] Key factors for a high-quality protein model include an accurate representation of the native structure, selection of a suitable force field, inclusion of surrounding solvent and relevant environmental factors, and facilitation of post-simulation analysis.[58,59] Addressing these aspects improves the credibility and biological significance of the findings derived from MD simulations.

The native and mutant models of CCL2 proteins with the highest I-TASSER score, indicating their optimal conformation, were selected for further analysis.[29] To examine the effects of the identified mutations on the CCL2 protein structure at the molecular level, we performed an MD simulation using WebGro software.[60] This revealed how native C59C and mutant C59G influenced the structure of CCL2 during a 100-ns simulation, and the MD simulation system was neutralized by introducing sodium or chlorine ions to balance the total charges. Before MD simulation, the steepest descent algorithm was used for system minimization through 5000 iterations[61] (The simulations were performed at a constant temperature of 300 K and a pressure of 1.0 bar, with a 0.15 M NaCl concentration. Approximately 1000 frames were generated per 100-ns simulation.[62]

As a crucial initial step, we performed protein docking to predict the binding location of the molecule within the protein's active site. This process provided essential insights into the subsequent MD simulations, allowing for the detailed examination of the protein's structure and function.[63,64] MD simulations produced multiple trajectories, including root mean square deviation (RMSD), root mean square fluctuation (RMSF), radius of gyration (Rg), solvent-accessible surface area (SASA), and hydrogen bonds.[65,66]

The RMSD profiles of protein–ligand complexes were analyzed using the WebGRO server. The best-docked

complexes were prepared for MD simulations using the GROMOS 43a1 force field.[65] RMSD measures the average distance between the atoms of two superimposed molecular structures. It is commonly used in bioinformatics to assess the similarity of 3D structures, particularly in the study of protein conformations.[61] RMSD is calculated using the formula:

$$\text{RMSD} = \sqrt{1/N \sum_{i=1}^{n} (\delta i)^2} \quad \text{(I)}$$

where δi represents the distance between the corresponding atoms in the two structures, and *N* is the number of atoms considered. Typically, RMSD is calculated for the backbone heavy atoms or alpha carbon (Cα) atoms.

RMSF is a measure of the average deviation of atomic positions from their mean positions over time in MD simulations. It quantifies the fluctuations of individual atoms or residues, providing insights into the flexibility and mobility of different regions within a protein structure. RMSF is calculated as the square root of the variance of the fluctuations around the average position[62] using the formula:

$$\text{RMSF} = \sqrt{(\gamma i - \gamma i)^2} \quad \text{(II)}$$

where γi represents the coordinates of atom *i,* and ⟨γi⟩ is its ensemble average position. High RMSF values indicate regions with considerable mobility, whereas low values suggest rigidity.

To gain insights into the hydrogen bonding characteristics of the proteins, we analyzed the hydrogen bond geometries. As the positions of hydrogen atoms are uncertain in these structures, they were excluded from the analysis. In total, 4195 hydrogen bonds were identified and categorized into four types based on the donor and acceptor atom origins: main-chain to main-chain (MC-MC), main-chain to side-chain, side-chain to main-chain, and side-chain to side-chain. The MC-MC hydrogen bonds were further classified according to the secondary structures, including alpha helices, beta strands, and non-secondary structures.

Furthermore, we investigated the correlations between hydrogen bond geometry and environmental factors, such as atomic depth, secondary structure, and partial charge. Atomic depth was defined as the distance to the nearest bulk water molecule. This analysis provides a comprehensive understanding of the characteristics and determinants of hydrogen bonding in high-resolution protein structures.

2.9. Examination of alterations in CCL2 protein secondary structure

The Database of Secondary Structure in Proteins tool analyzes hydrogen bonding and other secondary structures of CCL2 proteins – indicators to classify protein residues – as well as changes in secondary structures between native and mutant CCL2 proteins.[66]

2.10. Docking of CCL2-native and -mutant proteins with receptor CCR2

The objective of molecular docking for the ligand–receptor (CCL2–CCR2) binding process is to construct an accurate binding free energy landscape and estimate the binding affinity and binding kinetics. We introduced a novel hybrid docking (HDOCK) protocol that integrates template-based and template-free approaches to enhance protein–protein docking accuracy. Unlike traditional methods that focus on docking monomer proteins, HDOCK utilizes homologous complex structures of the proteins involved. Initially, homologous complexes were identified using BLAST searches of the PDB, with a sequence identity cutoff set at 25%. Among multiple hits, the optimal template was selected based on the highest sequence coverage, sequence similarity, and resolution. This selected homologous complex structure was then used as a docking template, incorporating potential binding interface information. By leveraging the structural information from the homologous complexes, HDOCK substantially improves the prediction accuracy of protein–protein interactions.[67] The individual protein structures are modeled using the homologous complexes as templates, either by superimposing them onto available homologous complexes or through homology modeling.[68] In our study, the individual component structures of the modeled complex were separated and subjected to a global sampling of potential binding modes using our hierarchical protein–protein docking algorithm. This approach allows for a comprehensive exploration of possible interaction interfaces between the proteins.[69,70] Symmetric docking was achieved by constraining the translational degrees of freedom to ensure symmetry along a specific axis. In cases where no complex structure templates were available, the individual protein structures for docking were modeled using their homologous monomer structures with Modeller.[71] The binding modes obtained from the docking simulations were evaluated and ranked according to their binding energy scores. To group similar conformations, an RMSD cutoff of 5.0 Å was applied for clustering. From the resulting clusters, the top 100 binding modes were examined and the best 10 models were selected for submission to the Critical Assessment of Predicted Interactions initiative.

3. Results

The results of this study demonstrated the considerable impact of mutations in the *CCL2* gene on the molecular stability, functionality, and structure of the resulting

protein. The altered protein might not perform its normal functions effectively, potentially contributing to disease development or progression. Advanced computational methods were employed to assess protein stability, identify cancer-causing mutations, and predict pathogenicity.[72,73]

3.1. Collection of missense mutations

To explore the potential effects of *CCL2* mutation on protein function, we collected a comprehensive dataset comprising 83 mutations from a publicly accessible database. These mutations were located across various coding regions of the gene, enabling a thorough assessment of their potential effects on protein functionality.

3.2. Missense mutation analysis

The deleterious effects of mutations can be anticipated by evaluating the importance of the affected peptides. To analyze the 83 missense mutations in *CCL2*, computational tools such as Polyphen-2 and Meta-SNP (comprising Panther, PhD-SNP, SIFT, and SNAP) were employed (Table 1). The results revealed that 10 mutations were likely disease-causing and distributed across various protein domains.

3.3. CCL2 mutations affect protein stability

Three algorithms, mCSM, SDM, and DUET, were used to predict the effects of 83 mutations on CCL2 protein stability. The results are shown in Table 2. mCSM predicted that 40 mutations in CCL2 were likely highly destabilizing.

3.4. Identification of cancer-causing mutations in CCL2

Using the FATHMM server, 83 CCL2 mutations were analyzed to assess their potential involvement in cancer development or progression. The analysis results suggest that the C59G mutation alters the binding dynamics between CCL2 and CCR2, potentially reducing the risk of cancer and enhancing the immune response to pathogen invasion.

3.5. Conservation analysis of CCL2 mutations

The C59G mutation, identified as a cancer-causing mutation, was selected for further analysis. We utilized the ConSurf server to investigate the conservation and spatial distribution of the C59G mutation, which offered valuable insights into its potential functional implications.[50] ConSurf analysis revealed that the C59G mutation occurred at a highly conserved position, obtaining the maximum conservation score of 9 on the ConSurf scale (Figure 2A and B). These findings prompted further computational investigations into the potential effects of this mutation on the stability and function of the CCL2 protein.

3.6. Structure validation of native and mutant CCL2 proteins

The reference model for the native protein was the 3D structure of CCL2 (PDB ID 2LIE). The I-TASSER server was used to identify the template proteins with similar folds in the PDB database and generate 10,000 conformations (decoys) based on a mutant sequence.[74] I-TASSER used the SPICKER tool to group the generated conformations through pairwise structural alignments, identifying models with structural similarities. This process typically results in five clusters, each containing multiple models with identical structures. I-TASSER then selects a representative model from each cluster to generate five final models that best represent the diverse conformations predicted.[74] The model displaying the highest confidence score (C-score) was selected for subsequent analysis.[75] Ramachandran plots were used to assess the model's quality by examining the distribution of the protein backbone torsion angles (ϕ and ψ) and identifying any structural issues.[76] The Ramachandran plot analysis revealed that 90% of native residues and 89% of mutant residues were positioned in the favored region of the native CCL2 structure, indicating a high degree of structural similarity (Figure 3).

3.7. MD simulation of CCL2

To investigate the effects of the C59G mutation on the CCL2 protein, a 100-ns MD simulation was performed. The simulation tracked various structural parameters, including secondary structure elements, to monitor the protein's behavior and identify any changes in its conformational dynamics.

The RMSD was computed for the backbone residues of both the native and mutant CCL2 proteins to assess their deviation from their initial structures throughout the simulation and quantify the extent of structural variation. The RMSD values for the mutant CCL2 protein (C59G) were substantially higher than those of the native protein (Figure 3A), indicating a higher degree of structural instability in the mutant structure. This suggests that the C59G mutation introduced substantial conformational changes, potentially affecting the protein's stability and function. MD simulations revealed that the native CCL2 protein remained structurally stable throughout the simulation and that the mutant proteins, particularly C59G, exhibited a longer stabilization period. The RMSD values for the mutant proteins steadily increased between 15 and 30 ns, indicating a higher degree of structural deviation from the initial conformation. In contrast, the RMSD values for the native C59C–CCL2 protein remained relatively stable, which suggests that the C59G mutation

Table 1. Harmful mutation predictions using in silico online tools

Serial number	Mutants	Prediction of deleterious mutation													
		Panther		PhD-SNP		SIFT		SNAP		Meta-SNP		PolyPhen-2			
		Analysis	Score	Analysis	Score	Analysis	Score	Analysis	Score	Analysis	Score	Analysis	Score	Sensitivity	Specificity
1	M1L	Disease	0.982	Normal	0.153	Normal	0.15	Normal	0.25	Normal	0.248	Benign	0.4	0.84	0.79
2	K2E	Normal	0.466	Normal	0.12	Normal	0.41	Normal	0.34	Normal	0.128	Possibly damaging	0.637	0.8	0.84
3	K2T	Disease	0.567	Normal	0.075	Normal	0.42	Normal	0.275	Normal	0.085	Possibly damaging	0.86	0.72	0.89
4	K2R	Normal	0.255	Normal	0.05	Normal	0.44	Normal	0.095	Normal	0.082	Benign	0.209	0.88	0.74
5	V3I	Normal	0.196	Normal	0.033	Normal	0.27	Normal	0.13	Normal	0.071	Benign	0.181	0.89	0.73
6	V3G	Disease	0.696	Normal	0.242	Disease	0.01	Normal	0.46	Normal	0.422	Possibly damaging	0.959	0.63	0.92
7	S4F	Disease	0.871	Normal	0.208	Normal	0.11	Normal	0.485	Normal	0.383	Possibly damaging	0.99	0.51	0.95
8	A5V	Normal	0.266	Normal	0.037	Normal	0.42	Normal	0.175	Normal	0.075	Benign	0.139	0.9	0.71
9	A5T	Normal	0.269	Normal	0.047	Normal	0.48	Normal	0.145	Normal	0.074	Benign	0.098	0.91	0.68
10	I13T	Normal	0.169	Normal	0.05	Normal	0.44	Normal	0.16	Normal	0.076	Benign	0.002	0.99	0.18
11	I13V	Normal	0.127	Normal	0.082	Normal	0.38	Normal	0.145	Normal	0.089	Benign	0.004	0.98	0.35
12	A14E	Normal	0.482	Disease	0.571	Normal	0.08	Disease	0.585	Normal	0.498	Possibly damaging	0.839	0.73	0.88
13	A15P	Disease	0.727	Disease	0.749	Normal	0.08	Disease	0.62	Disease	0.653	Possibly damaging	0.921	0.68	0.91
14	T16S	Normal	0.122	Normal	0.103	Normal	0.55	Normal	0.13	Normal	0.096	Benign	0.086	0.91	0.67
15	I18N	Normal	0.119	Normal	0.346	Normal	0.31	Normal	0.37	Normal	0.293	Benign	0.001	0.99	0.09
16	I18T	Normal	0.285	Normal	0.088	Normal	0.41	Normal	0.19	Normal	0.056	Benign	0.001	0.99	0.09
17	P19L	Normal	0.148	Normal	0.134	Normal	0.76	Normal	0.245	Normal	0.167	Benign	0.003	0.98	0.26
18	P19Q	Normal	0.262	Normal	0.123	Normal	0.35	Normal	0.32	Normal	0.136	Possibly damaging	0.449	0.83	0.8
19	Q20R	Normal	0.351	Normal	0.498	Normal	0.47	Disease	0.55	Disease	0.609	Possibly damaging	0.691	0.78	0.85
20	A23T	Normal	0.374	Normal	0.369	Normal	0.55	Normal	0.37	Normal	0.302	Benign	0.348	0.85	0.78
21	A23S	Normal	0.384	Normal	0.213	Normal	0.88	Normal	0.155	Normal	0.249	Possibly damaging	0.603	0.81	0.83
22	A27G	Normal	0.183	Normal	0.081	Normal	1	Normal	0.37	Normal	0.092	Benign	0.028	0.94	0.59
23	A27V	Disease	0.619	Normal	0.324	Normal	0.17	Disease	0.585	Normal	0.484	Possibly damaging	0.876	0.71	0.89
24	N29K	Normal	0.286	Normal	0.425	Normal	0.69	Disease	0.58	Normal	0.304	Benign	0.098	0.91	0.68
25	P31A	Normal	0.274	Normal	0.355	Normal	0.11	Disease	0.66	Normal	0.314	Benign	0.119	0.9	0.7
26	Y36C	Disease	0.903	Disease	0.717	Disease	0.01	Disease	0.745	Disease	0.795	Possibly damaging	0.976	0.59	0.93
27	N37D	Normal	0.19	Normal	0.2	Normal	0.26	Disease	0.56	Normal	0.25	Benign	0.21	0.88	0.74
28	T39I	Normal	0.222	Normal	0.18	Normal	0.6	Disease	0.515	Normal	0.145	Benign	0.021	0.95	0.56
29	T39A	Normal	0.178	Normal	0.229	Normal	0.59	Disease	0.62	Normal	0.244	Benign	0.006	0.97	0.45
30	N40D	Normal	0.226	Normal	0.384	Normal	0.45	Normal	0.415	Normal	0.33	Benign	0.022	0.95	0.57

(Cont'd...)

Table 1. *(Continued)*

Serial number	Mutants	Prediction of deleterious mutation													
		Panther		PhD-SNP		SIFT		SNAP		Meta-SNP		PolyPhen-2			
		Analysis	Score	Analysis	Score	Analysis	Score	Analysis	Score	Analysis	Score	Analysis	Score	Sensitivity	Specificity
31	N40K	Normal	0.128	Normal	0.245	Normal	0.65	Normal	0.415	Normal	0.248	Benign	0.023	0.95	0.57
32	R41K	Normal	0.182	Normal	0.072	Normal	0.77	Normal	0.405	Normal	0.084	Benign	0.002	0.99	0.18
33	K42I	Disease	0.703	Disease	0.634	Normal	0.12	Disease	0.665	Disease	0.669	Possibly damaging	0.936	0.66	0.91
34	S44L	Normal	0.468	Normal	0.482	Disease	0.02	Disease	0.53	Normal	0.49	Benign	0.02	0.95	0.56
35	V45M	Normal	0.11	Normal	0.054	Normal	0.25	Normal	0.41	Normal	0.069	Benign	0.026	0.94	0.58
36	V45A	Normal	0.161	Normal	0.116	Normal	0.53	Normal	0.475	Normal	0.116	Benign	0.103	0.91	0.69
37	R47K	Normal	0.173	Normal	0.223	Normal	0.36	Normal	0.43	Normal	0.241	Benign	0.1	0.91	0.68
38	L48F	Disease	0.653	Normal	0.416	Disease	0.02	Disease	0.68	Disease	0.582	Possibly damaging	0.997	0.27	0.98
39	A49E	Normal	0.207	Normal	0.08	Normal	0.96	Normal	0.41	Normal	0.076	Benign	0.007	0.97	0.46
40	A49V	Normal	0.241	Normal	0.084	Normal	0.4	Normal	0.41	Normal	0.08	Benign	0.015	0.95	0.54
41	A49T	Normal	0.152	Normal	0.074	Normal	0.53	Normal	0.345	Normal	0.085	Benign	0.015	0.95	0.54
42	A49P	Normal	0.291	Normal	0.404	Normal	0.23	Disease	0.635	Normal	0.328	Possibly damaging	0.587	0.81	0.83
43	S50N	Normal	0.434	Normal	0.311	Normal	0.16	Disease	0.58	Normal	0.325	Possibly damaging	0.651	0.79	0.84
44	Y51H	Disease	0.845	Disease	0.647	Disease	0.01	Disease	0.86	Disease	0.733	Possibly damaging	0.998	0.18	0.98
45	R53G	Disease	0.743	Disease	0.539	Normal	0.21	Disease	0.685	Disease	0.661	Possibly damaging	0.906	0.69	0.9
46	I54V	Normal	0.253	Normal	0.085	Normal	0.28	Disease	0.51	Normal	0.089	Benign	0.075	0.92	0.66
47	T55S	Disease	0.662	Normal	0.455	Normal	0.53	Disease	0.585	Disease	0.6	Possibly damaging	0.718	0.78	0.85
48	S56N	Normal	0.234	Normal	0.216	Normal	0.26	Disease	0.62	Normal	0.236	Benign	0.107	0.91	0.69
49	S56R	Disease	0.627	Normal	0.485	Normal	0.31	Disease	0.685	Disease	0.612	Possibly damaging	0.965	0.62	0.93
50	S57C	Disease	0.812	Disease	0.518	Disease	0.01	Disease	0.64	Disease	0.637	Possibly damaging	0.976	0.59	0.93
51	C59G	Disease	0.992	Disease	0.857	Disease	0	Disease	0.83	Disease	0.916	Possibly damaging	1	0	1
52	K61I	Disease	0.525	Normal	0.223	Normal	0.53	Normal	0.445	Normal	0.296	Possibly damaging	0.487	0.83	0.81
53	K67R	Normal	0.244	Normal	0.043	Normal	0.41	Normal	0.42	Normal	0.086	Benign	0.029	0.94	0.59
54	K67D	Normal	0.498	Normal	0.211	Normal	0.2	Disease	0.605	Normal	0.26	Possibly damaging	0.712	0.78	0.85
55	K67T	Normal	0.464	Normal	0.105	Normal	0.61	Normal	0.435	Normal	0.111	Benign	0.178	0.89	0.73
56	T68I	Disease	0.98	Disease	0.626	Disease	0.02	Disease	0.685	Disease	0.56	Possibly damaging	0.967	0.61	0.93
57	I69V	Normal	0.196	Normal	0.124	Normal	0.14	Normal	0.34	Normal	0.12	Benign	0.006	0.97	0.45
58	A71T	Normal	0.25	Normal	0.128	Disease	0.04	Disease	0.63	Normal	0.175	Benign	0.41	0.84	0.79
59	A71V	Normal	0.369	Normal	0.159	Disease	0.01	Disease	0.645	Normal	0.21	Possibly damaging	0.653	0.79	0.84
60	E73G	Disease	0.581	Normal	0.454	Normal	0.1	Disease	0.64	Disease	0.509	Benign	0.208	0.88	0.74

(Cont'd...)

Table 1. ***(Continued)***

Serial number	Mutants	Prediction of deleterious mutation													
		Panther		PhD-SNP		SIFT		SNAP		Meta-SNP		PolyPhen-2			
		Analysis	Score	Analysis	Score	Analysis	Score	Analysis	Score	Analysis	Score	Analysis	Score	Sensitivity	Specificity
61	I74N	Disease	0.885	Disease	0.771	Disease	0.01	Disease	0.725	Disease	0.772	Possibly damaging	0.964	0.62	0.92
62	D77E	Normal	0.269	Normal	0.409	Disease	0.04	Disease	0.685	Normal	0.325	Benign	0.311	0.86	0.77
63	D77G	Disease	0.661	Disease	0.67	Disease	0.01	Disease	0.71	Disease	0.691	Possibly damaging	0.933	0.67	0.91
64	P78S	Disease	0.548	Disease	0.517	Disease	0.01	Disease	0.76	Disease	0.728	Possibly damaging	0.941	0.66	0.91
65	P78H	Disease	0.886	Disease	0.557	Disease	0	Disease	0.805	Disease	0.732	Possibly damaging	0.998	0.18	0.98
66	K79E	Normal	0.289	Normal	0.219	Normal	0.4	Normal	0.47	Normal	0.245	Benign	0.049	0.93	0.63
67	K79R	Normal	0.347	Normal	0.154	Normal	0.19	Normal	0.43	Normal	0.162	Benign	0.285	0.86	0.76
68	K81N	Disease	0.554	Normal	0.234	Normal	0.21	Normal	0.465	Normal	0.342	Benign	0.364	0.85	0.78
69	W82L	Disease	0.986	Disease	0.622	Disease	0	Disease	0.795	Disease	0.75	Possibly damaging	1	0	1
70	V83A	Disease	0.977	Normal	0.406	Disease	0.01	Disease	0.695	Disease	0.62	Possibly damaging	0.992	0.49	0.95
71	V83L	Disease	0.965	Normal	0.466	Disease	0.01	Disease	0.675	Disease	0.63	Possibly damaging	0.941	0.66	0.91
72	Q84R	Normal	0.304	Normal	0.289	Normal	0.13	Normal	0.48	Normal	0.309	Benign	0.097	0.91	0.68
73	D85Y	Disease	0.714	Normal	0.334	Disease	0.01	Disease	0.56	Disease	0.519	Possibly damaging	0.98	0.57	0.94
74	M87V	Normal	0.139	Normal	0.061	Normal	0.4	Disease	0.525	Normal	0.1	Benign	0.02	0.95	0.56
75	M87K	Disease	0.596	Normal	0.252	Disease	0.02	Disease	0.745	Normal	0.372	Benign	0.128	0.9	0.7
76	D88N	Normal	0.132	Normal	0.024	Normal	0.32	Normal	0.23	Normal	0.063	Benign	0.004	0.98	0.35
77	D88V	Normal	0.191	Normal	0.061	Disease	0.03	Normal	0.465	Normal	0.112	Benign	0.103	0.91	0.69
78	H89P	Normal	0.443	Normal	0.322	Normal	0.21	Disease	0.65	Normal	0.343	Possibly damaging	0.722	0.78	0.85
79	K92R	Normal	0.16	Normal	0.042	Normal	0.38	Normal	0.16	Normal	0.066	Benign	0.008	0.96	0.48
80	T96A	Normal	0.232	Normal	0.027	Normal	0.42	Disease	0.56	Normal	0.084	Benign	0.071	0.92	0.66
81	P97L	Normal	0.168	Normal	0.035	Normal	0.41	Normal	0.48	Normal	0.055	Benign	0.012	0.96	0.52
82	P97T	Normal	0.245	Normal	0.034	Normal	0.68	Normal	0.45	Normal	0.05	Benign	0.033	0.94	0.6
83	T99S	Normal	0.091	Normal	0.006	Normal	0.42	Disease	0.51	Normal	0.081	Benign	0	1	0

Table 2. Prediction of protein stability using in silico tools

Serial number	Mutants	Protein stability prediction					
		SDM		mCSM		DUET	
		ΔΔGkcal/mol	Prediction	ΔΔGkcal/mol	Prediction	ΔΔGkcal/mol	Prediction
1	M1L	0	Destabilizing	−0.528	Destabilizing	−0.079	Destabilizing
2	K2E	−0.08	Destabilizing	0.15	Stabilizing	0.411	Stabilizing
3	K2T	−0.39	Destabilizing	−0.419	Destabilizing	−0.251	Destabilizing
4	K2R	−0.24	Destabilizing	−0.297	Destabilizing	−0.066	Destabilizing
5	V3I	0.11	Stabilizing	−0.864	Destabilizing	−0.547	Destabilizing
6	V3G	−0.38	Destabilizing	−1.907	Destabilizing	−1.798	Destabilizing
7	S4F	0.58	Stabilizing	−1.339	Destabilizing	−1.047	Destabilizing
8	A5V	−0.18	Destabilizing	−0.527	Destabilizing	−0.257	Destabilizing
9	A5T	−0.37	Destabilizing	−1.443	Destabilizing	−1.2	Destabilizing
10	I13T	−0.96	Destabilizing	−1.451	Destabilizing	−1.33	Destabilizing
11	I13V	−0.1	Destabilizing	−1.056	Destabilizing	−0.804	Destabilizing
12	A14E	−0.13	Destabilizing	−2.421	Destabilizing	−2.148	Destabilizing
13	A15P	−1.96	Destabilizing	−0.606	Destabilizing	−0.767	Destabilizing
14	T16S	−0.78	Destabilizing	−1.357	Destabilizing	−1.302	Destabilizing
15	I18N	−1.39	Destabilizing	−2.458	Destabilizing	−2.435	Destabilizing
16	I18T	−2.02	Destabilizing	−2.715	Destabilizing	−2.85	Destabilizing
17	P19L	1.29	Stabilizing	−0.789	Destabilizing	−0.197	Destabilizing
18	P19Q	−0.23	Destabilizing	−0.973	Destabilizing	−0.68	Destabilizing
19	Q20R	0.56	Stabilizing	0.009	Stabilizing	0.357	Stabilizing
20	A23T	−0.81	Destabilizing	−1.028	Destabilizing	−0.853	Destabilizing
21	A23S	−1.39	Destabilizing	−0.951	Destabilizing	−0.886	Destabilizing
22	A27G	−2.55	Destabilizing	−1.264	Destabilizing	−1.617	Destabilizing
23	A27V	−1.46	Destabilizing	−0.774	Destabilizing	−0.831	Destabilizing
24	N29K	0.44	Stabilizing	0.144	Stabilizing	0.606	Stabilizing
25	P31A	−0.2	Destabilizing	−0.91	Destabilizing	−0.671	Destabilizing
26	Y36C	0.09	Stabilizing	0.42	Stabilizing	0.633	Stabilizing
27	N37D	0.15	Stabilizing	0.276	Stabilizing	0.634	Stabilizing
28	T39I	1.33	Stabilizing	−0.053	Destabilizing	0.493	Stabilizing
29	T39A	1.34	Stabilizing	−0.876	Destabilizing	−0.322	Destabilizing
30	N40D	−0.38	Destabilizing	0.119	Stabilizing	0.347	Stabilizing
31	N40K	−0.2	Destabilizing	0.131	Stabilizing	0.451	Stabilizing
32	R41K	−0.19	Destabilizing	−0.038	Destabilizing	0.192	Stabilizing
33	K42I	0.47	Stabilizing	0.158	Stabilizing	0.452	Stabilizing
34	S44L	1.24	Stabilizing	0.062	Stabilizing	0.585	Stabilizing
35	V45M	−0.26	Destabilizing	−0.396	Destabilizing	−0.295	Destabilizing
36	V45A	0.19	Destabilizing	−0.971	Stabilizing	−0.641	Destabilizing
37	R47K	−0.1	Destabilizing	−0.316	Destabilizing	−0.058	Destabilizing
38	L48F	−0.66	Destabilizing	−1.439	Destabilizing	−1.493	Destabilizing
39	A49E	0.72	Stabilizing	−0.528	Destabilizing	0.007	Stabilizing
40	A49V	1.41	Stabilizing	−0.416	Destabilizing	0.201	Stabilizing
41	A49T	0.29	Stabilizing	−0.942	Destabilizing	−0.546	Destabilizing

(Cont'd...)

Table 2. ***(Continued)***

Serial number	Mutants	Protein stability prediction					
		SDM		mCSM		DUET	
		ΔΔGkcal/mol	Prediction	ΔΔGkcal/mol	Prediction	ΔΔGkcal/mol	Prediction
42	A49P	−1.14	Destabilizing	−0.416	Destabilizing	−0.366	Destabilizing
43	S50N	0.07	Stabilizing	−1.123	Destabilizing	−0.858	Destabilizing
44	Y51H	−1.23	Destabilizing	−2.402	Destabilizing	−2.457	Destabilizing
45	R53G	0.37	Stabilizing	−1.393	Destabilizing	−1.084	Destabilizing
46	I54V	−2.38	Destabilizing	−1.695	Destabilizing	−2.05	Destabilizing
47	T55S	−0.71	Destabilizing	−0.468	Destabilizing	−0.319	Destabilizing
48	S56N	0.28	Stabilizing	−0.564	Destabilizing	−0.226	Destabilizing
49	S56R	0.9	Stabilizing	−0.645	Destabilizing	−0.226	Destabilizing
50	S57C	0.62	Stabilizing	−0.491	Destabilizing	−0.162	Destabilizing
51	C59G	−0.6	Destabilizing	−1.767	Destabilizing	−1.667	Destabilizing
52	K61I	1.4	Stabilizing	0.437	Stabilizing	0.915	Stabilizing
53	K67R	0	Destabilizing	−0.699	Destabilizing	−0.435	Destabilizing
54	K67D	−0.83	Destabilizing	−1.817	Destabilizing	−1.832	Destabilizing
55	K67T	−0.14	Destabilizing	−1.275	Destabilizing	−1.086	Destabilizing
56	T68I	0.13	Stabilizing	−0.148	Destabilizing	0.111	Stabilizing
57	I69V	−0.03	Destabilizing	−0.347	Destabilizing	−0.033	Destabilizing
58	A71T	−1.12	Destabilizing	−0.861	Destabilizing	−0.738	Destabilizing
59	A71V	0.38	Stabilizing	−0.472	Destabilizing	−0.071	Destabilizing
60	E73G	0.56	Stabilizing	−1.152	Destabilizing	−0.846	Destabilizing
61	I74N	−1.35	Destabilizing	−1.567	Destabilizing	−1.522	Destabilizing
62	D77E	−0.5	Destabilizing	−0.784	Destabilizing	−0.609	Destabilizing
63	D77G	0.22	Stabilizing	−1.093	Destabilizing	−0.874	Destabilizing
64	P78S	−0.77	Destabilizing	−1.976	Destabilizing	−1.844	Destabilizing
65	P78H	1.14	Stabilizing	−1.898	Destabilizing	−1.331	Destabilizing
66	K79E	0.25	Stabilizing	−0.115	Destabilizing	0.229	Stabilizing
67	K79R	−0.11	Destabilizing	−0.144	Destabilizing	0.11	Stabilizing
68	K81N	−0.88	Destabilizing	−0.001	Destabilizing	0.044	Stabilizing
69	W82L	0.63	Stabilizing	−2.029	Destabilizing	−1.49	Destabilizing
70	V83A	−0.69	Destabilizing	−1.948	Destabilizing	−1.924	Destabilizing
71	V83L	0.14	Stabilizing	−0.428	Destabilizing	−0.079	Destabilizing
72	Q84R	0.13	Stabilizing	−0.043	Destabilizing	0.245	Stabilizing
73	D85Y	−0.37	Destabilizing	−0.479	Destabilizing	−0.514	Destabilizing
74	M87V	0.14	Stabilizing	−1.727	Destabilizing	−1.309	Destabilizing
75	M87K	−0.19	Destabilizing	−1.477	Destabilizing	−1.02	Destabilizing
76	D88N	−0.34	Destabilizing	−0.639	Destabilizing	−0.469	Destabilizing
77	D88V	−0.11	Destabilizing	0.312	Stabilizing	0.518	Stabilizing
78	H89P	−2.03	Destabilizing	0.226	Stabilizing	−0.113	Destabilizing
79	K92R	−0.37	Destabilizing	−0.162	Destabilizing	0.048	Stabilizing
80	T96A	1.15	Stabilizing	−0.191	Destabilizing	0.318	Stabilizing
81	P97L	0.84	Stabilizing	−0.258	Destabilizing	0.246	Stabilizing
82	P97T	0.28	Stabilizing	−0.404	Destabilizing	−0.002	Destabilizing
83	T99S	0	Destabilizing	−0.626	Destabilizing	−0.32	Destabilizing

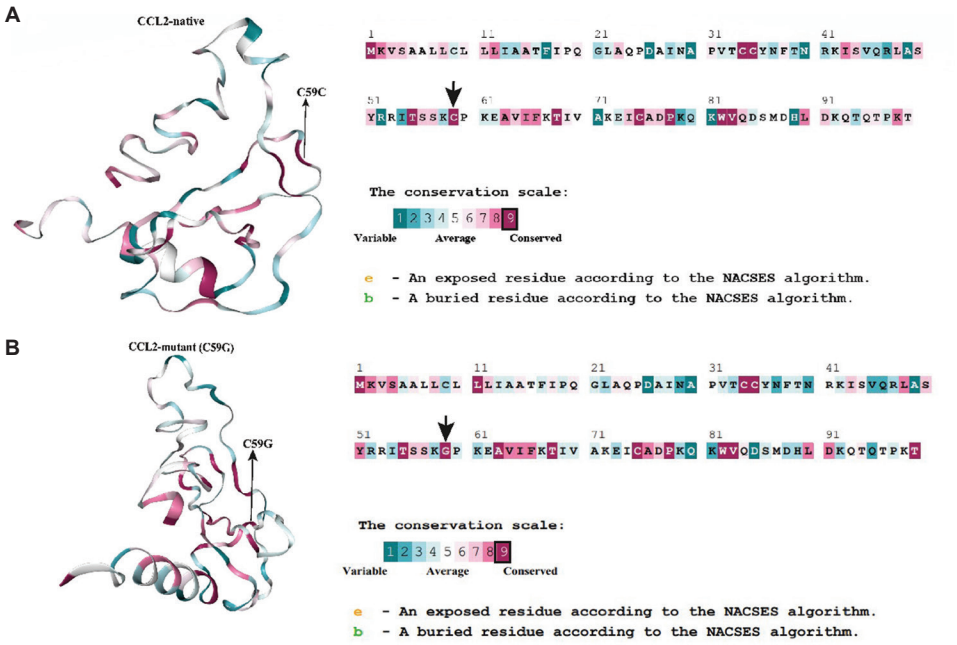

Figure 2. The ConSurf server was used to analyze the residue conservation of the C59G mutation in CCL2. The results are displayed in a colored format to visualize the evolutionary conservation of these residues within the protein structure. (A) represents the C59 residue, while (B) indicates the position of the C59G mutation. This mutation lies within the most conserved region of the CCL2 protein structure. The conservation of this region suggests its critical role in the protein's function and stability.
Abbreviation: CCL2: Chemokine C-C motif ligand 2.

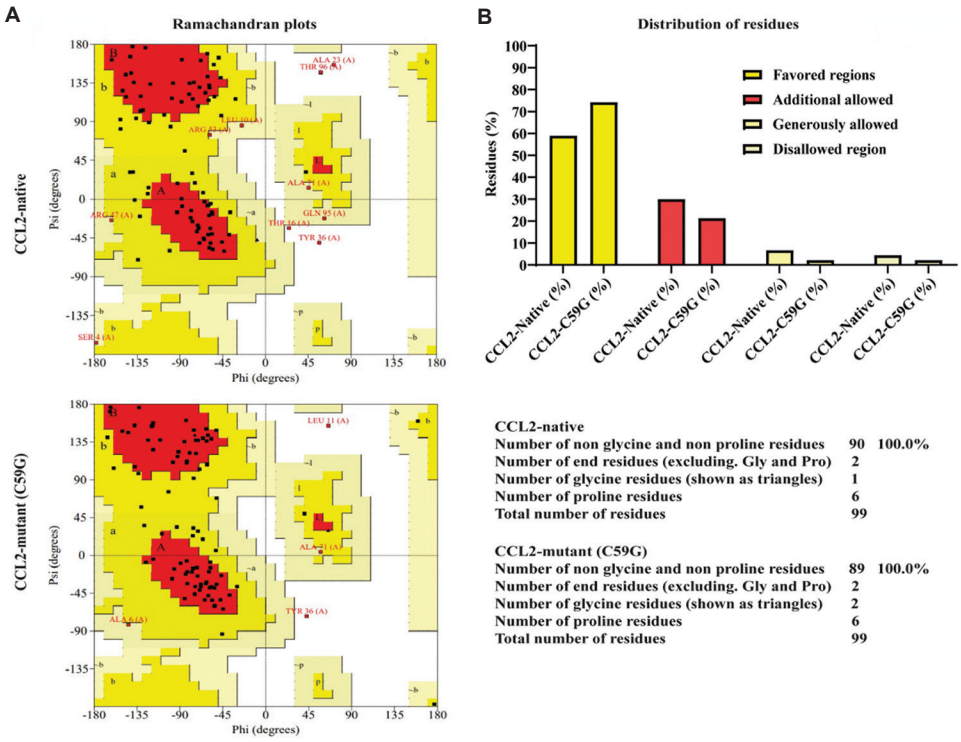

Figure 3. (A and B) Ramachandran plot analysis was used to evaluate the structural quality of the native and mutant CCL2 proteins by examining the distribution of residues within the plot. The results are presented in a colored format to facilitate easier visualization and interpretation of the evolutionary conservation of these residues within the protein structure.
Abbreviation: CCL2: Chemokine C-C motif ligand 2.

introduced considerable conformational changes that required more time to reach equilibrium (Figure 4A).

To assess the impact of mutations on the stability and dynamics of the CCL2 protein, the RMSF of the Cα atoms was calculated. This analysis aimed to understand how mutations affect the dynamics of the residues and compare these effects with those of the native protein. In general, the RMSF values of the mutant structures demonstrated higher flexibility than those of the native structures, particularly in regions spanning residues 5 – 80. Specifically, these regions exhibited significant fluctuations in RMSF values, ranging from 0.1 to 0.7 Å, which indicated increased dynamic behavior in these areas (Figure 4B).

After analyzing the intramolecular hydrogen bonds, a noticeable decrease in the number of hydrogen bonds formed during the simulation in the mutant protein was observed compared to the native structure. Assessment of the intramolecular hydrogen bonds indicated that the native protein maintained a relatively stable number of hydrogen bonds, ranging from 40 to 80, whereas the mutant protein exhibited more variability, with the number of hydrogen bonds fluctuating between 40 and 69. This implies that the mutant protein underwent increased flexibility and structural alterations compared to the native CCL2 protein (Figure 5A and B).

Essential dynamics (ED) analysis was conducted to identify correlated movements within both the native and mutant peptides of CCL2. The cumulative sum of the eigenvalues revealed that significant fluctuations were mainly observed in the first two eigenvectors for both types of proteins. This concentration of fluctuations in the first two eigenvectors indicates that these principal components (PCs) capture the primary motions of the system. Subsequently, the trajectories of both native and mutant simulations were plotted onto phase space along PC1 and PC2 at 300 K to visualize these motions (Figure 5C and D).

The Rg analysis revealed that the mutant protein was less compact compared to the native protein. The Rg value for the mutant protein ranged from 1.3 nm to 1.45 nm, which reflected increased flexibility and structural changes. Conversely, the native protein demonstrated a higher compactness with Rg values between 1.4 nm and 1.3 nm. This suggests that the mutations notably affected the protein's structural compactness and flexibility (Figure 6A and B).

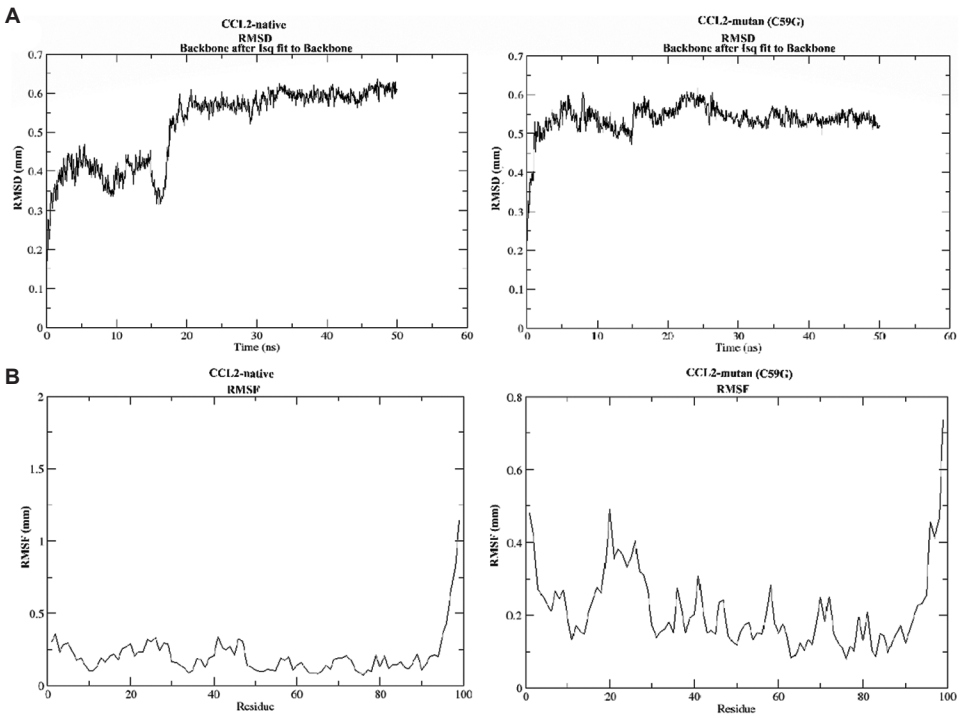

Figure 4. The RMSD and RMSF were used as measures to assess the structural alterations and dynamic fluctuations in the proteins. (A) Molecular dynamics simulations were conducted on both native and C59G mutant CCL2 proteins for 100 ns to explore the impacts of mutations on protein stability. The RMSD of the backbone was calculated over time to quantify the structural changes. (B) The RMSF of backbone alpha carbon (Cα) atoms in the native CCL2 protein structure was examined throughout the simulation duration. The results are depicted on a plot, where the Y-axis represents RMSF values and the X-axis corresponds to each atom in the protein structure.
Abbreviations: RMSD: root mean square deviation; RMSF: root mean square fluctuation; CCL2: Chemokine C-C motif ligand 2.

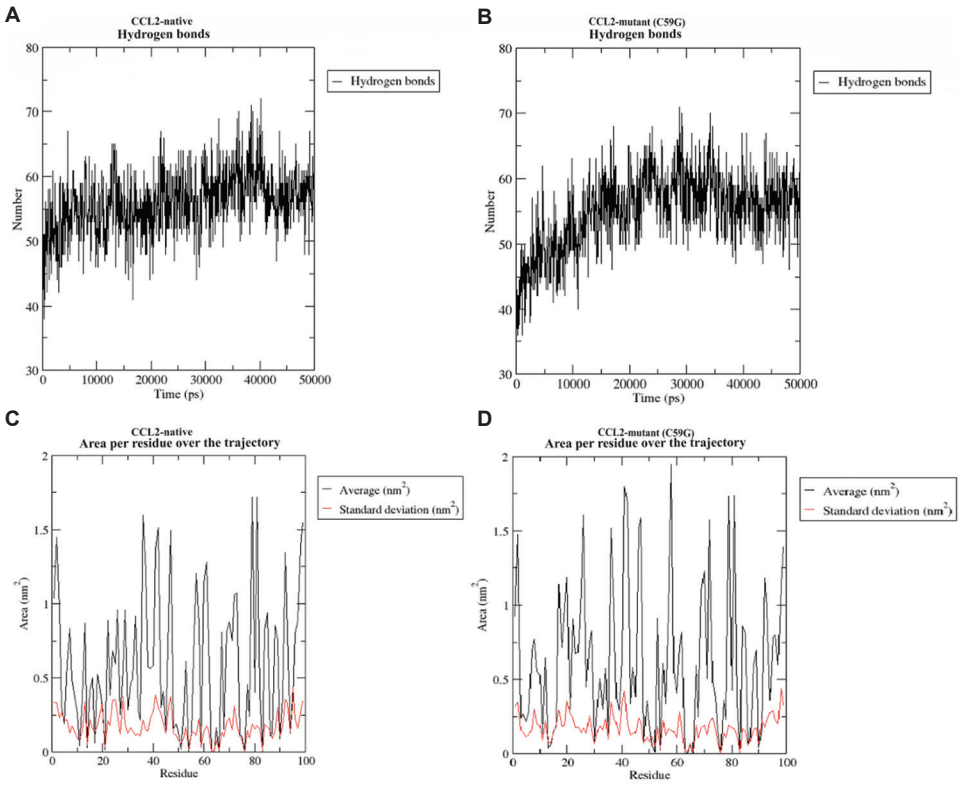

Figure 5. Hydrogen bonding and two-dimensional projection of native and mutant CCL2 proteins. (A) represents the average number of intermolecular hydrogen bonds in native CCL2, while (B) shows the average number of intermolecular hydrogen bonds in the CCL2-C59G mutant structures as a function of time. (C and D) depict the projection of the motion of the protein in phase space for CCL2-native and CCL2-C59G, respectively.
Abbreviation: CCL2: Chemokine C-C motif ligand 2.

Throughout the simulation, the SASA of both the native and mutant CCL2 proteins was monitored. The native protein exhibited a consistent SASA value, ranging from 55 to 65 nm² throughout the simulation period. In contrast, the mutant protein displayed a higher and more variable SASA, ranging from 60 to 75 nm², with significant fluctuations observed over time. This variation in SASA suggests that the mutant protein underwent substantial changes in its solvent accessibility, potentially affecting its stability and interactions with other molecules (Figure 6C and D).

During the simulation, the native protein maintained a stable SASA value, indicating its stability. Conversely, the mutant structures exhibited higher SASA values with notable fluctuations, suggesting increased solvent accessibility and alterations in its interactions with other molecules.

3.8. Hydrogen bonding analysis of native and mutant CCL2 proteins

MD simulations were used to monitor the interactions between CCR2 and CCL2. The majority of the important protein–peptide interactions were hydrogen bonds (Figure 7). A timeline of these interactions was generated to highlight the key hydrogen bonds formed during the simulations. The number of hydrogen bonds formed between CCR2 and CCL2 is an essential parameter to assess the stability of the complex. Our results revealed that the native CCL2–C59C complex exhibits a lower average number of hydrogen bonds (total hydrogen bonds: 3350) (Figure 7A). In contrast, the C59G mutation in CCL2 leads to an increase in hydrogen bond formation (total hydrogen bonds: 4195) (Figure 7B). This directly correlates with the binding affinity and stability of the receptor–ligand interaction, which suggests that the C59G mutation enhances receptor–ligand interactions by promoting stronger and more stable hydrogen bonding.

3.9. Effects of CCL2 mutants on the protein secondary and tertiary structures

The I-TASSER-modeled structure of CCL2 (native and mutant) was evaluated using UCSF Chimera calculations for homology modeling. This evaluation involved comparative modeling by satisfaction of spatial restraints, which requires a known related structure (i.e., a template) and a target-template sequence alignment. The

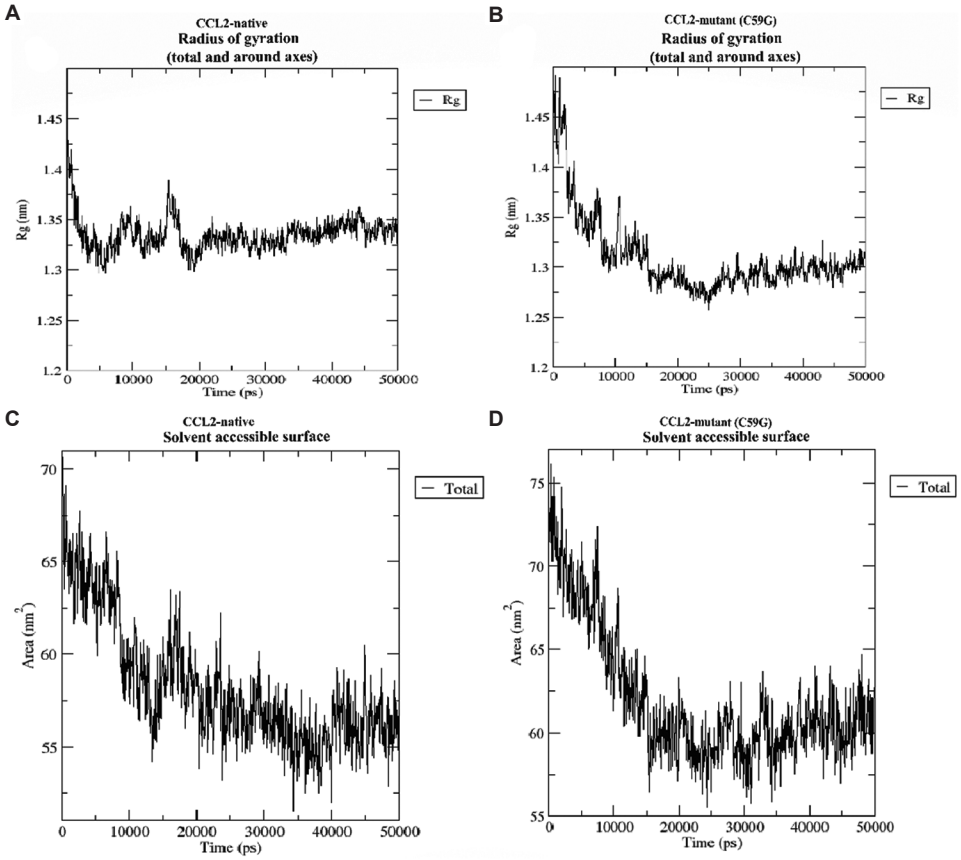

Figure 6. Rg and SASA analysis. (A and B) The Rg of Cα atoms in the native and mutant structures was monitored throughout the simulation. The native protein consistently maintained a stable Rg value, whereas the mutant structures displayed notable fluctuations, suggesting alterations in compactness. (C and D) SASA of both the native and mutant structures over time
Abbreviations: Rg: radius of gyration; SASA: solvent-accessible surface area; Cα: alpha carbon.

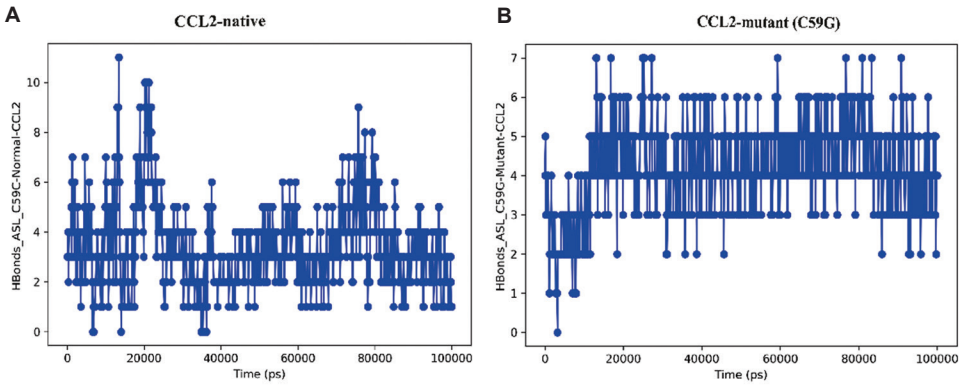

Figure 7. Protein contact hydrogen bond. (A) Representation of the hydrogen bonds of the native CCL2–C59C. (B) Representation of the hydrogen bonds of the mutant CCL2–C59G. Simulation time is presented in picoseconds.
Abbreviation: CCL2: Chemokine C-C motif ligand 2.

Chimera interface to Modeller allows for the generation of theoretical models of a protein using at least one known related structure and a target-template sequence alignment.[77] Homology modeling was performed on the native and mutant CCL2 proteins to investigate the spatial arrangement of the conserved amino acids, particularly cysteine (C59) and glycine (G59). This approach allowed for the assessment of how the C59G mutation affects

the local structural environment and the overall protein conformation. I-TASSER was used to generate a 3D model of the CCL2 protein based on the cysteine (C59) and glycine (G59) structures. The model was selected due to its high C-score, indicating a high confidence level in the predicted structure. This computational method enabled the prediction of the protein tertiary structure. According to I-TASSER modeling results, the predicted structure of the native CCL2 protein has a C-score of −1.20, a TM-score of 0.56 ± 0.15, and an RMSD of 6.4 ± 3.9 Å. Similarly, the mutant CCL2 protein was predicted to have a comparable structure, with a C-score of −1.10, a TM-score of 0.54 ± 0.14, and an RMSD of 6.2 ± 3.7 Å. These values suggest that both models have a moderate confidence level and a correct global topology, despite some local structural variations.

The mutation of a cysteine (C) to glycine (G) in the CCL2 protein substantially affected both its secondary and tertiary structures. This is mainly due to the differing side-chain properties of these amino acids, which can alter local interactions and disrupt hydrogen bonding networks. In addition, the mutation's impact on electrostatic interactions and hydrophobic forces can alter the protein's overall folding and stability. These structural alterations can significantly influence the protein's function, solubility, and susceptibility to aggregation.[78,79]

In the present study, we observed changes in the bond distances between the amino acids in the CCL2 protein. The native CCL2 structure with K58 and C59 had bond distances of 9.6 and 6.5 Å, respectively. In contrast, the mutant G59 structure with K58 and P60 had bond distances of 11.7 and 7.1 Å, respectively. The observed changes in bond distances suggest notable structural differences in the mutant protein compared to the native structure. The mutant protein displays structural variations compared to the native protein, as indicated by distance measurements and C-scores (Figure 8A and B). Cysteine at position 59 is a positively charged amino acid that participates in electrostatic interactions. Substituting cysteine with glycine eliminates this positive charge, disrupting electrostatic interactions. Furthermore, cysteine can form disulfide bonds, which can alter the protein's overall structure. These changes can significantly affect the protein's function, stability, and interactions with other molecules.[80,81] These findings highlight the structural variations in CCL2 among proteins and critical mutations, providing crucial insights into their functional implications.

3.10. Molecular docking of native and mutant CCL2 with CCR2

The molecular docking results of native and mutant CCL2 with the CCR2 receptor were obtained using the HDOCK online tool, which revealed significant insights into their binding interactions. Native CCL2 displayed binding affinity to CCR2, with the top 10 minimum docking scores being −176.10, −160.30, −159.82, −156.20, −155.16, −153.10, −152.99, −151.07, −150.53, and −150.21 kcal/mol (Figure 9A). The lowest score of −176.10 kcal/mol indicates the most favorable binding interaction. Similarly, mutant CCL2 also exhibited robust binding affinity to CCR2, with top docking scores of −175.86, −172.30, −168.52, −161.03, −160.64, −159.83, −159.64, −158.47, −155.39, and −153.79 kcal/mol (Figure 9B). Although the mutant CCL2 had slightly higher minimum docking scores than the native CCL2, the scores indicate strong binding interactions. The comparison of the native and mutant CCL2 forms revealed that the mutant CCL2 had a marginally better minimum docking score (−175.86 kcal/mol) than the native form (−176.10 kcal/mol) (Figure 9), suggesting a slightly higher binding affinity for CCR2. However, the overall similarity in the docking scores indicates that the mutation alters the binding affinity of CCL2 to CCR2. These findings suggest that mutant CCL2 has a strong binding affinity for the CCR2 receptor and that the mutation impacts CCL2's ability to interact with its receptor. Further experimental validation and structural analysis are required to fully elucidate the functional implications of this mutation on CCL2–CCR2 signaling.

4. Discussion

CCL2 interacts with CCR2 through its N-terminal β strand, which is a critical component of the chemokine receptor binding process.[82] The CCL2–CCR2 signaling pathway plays a crucial role in the pathophysiology of various disorders, including chronic obstructive pulmonary disease, asthma, cystic fibrosis, and cancer. In the context of cancer, the interaction between CCL2, which is released by cancer cells, and CCR2 in the tumor microenvironment is essential for the progression and metastasis of cancer.[9,83] Previous research has shown that CCL2 promotes tumor growth and metastasis by recruiting macrophages and immune cells to the tumor microenvironment.[84] The CCL2–CCR2 axis is a critical factor in the progression of various cancers, including prostate, pancreatic, breast, lung, kidney, bladder, and colorectal cancers. In prostate cancer, CCL2 promotes tumor growth and migration through the PI3K/Akt signaling pathway and contributes to resistance against castration and chemotherapy, making it a potential therapeutic target.[85] In pancreatic ductal adenocarcinoma, high levels of CCL2 correlate with a poor prognosis and facilitate angiogenesis, and CCR2 inhibitors have shown promise in enhancing treatment outcomes.[86] In breast cancer, CCL2 enhances cell migration and is implicated in triple-negative breast cancer, suggesting that targeting

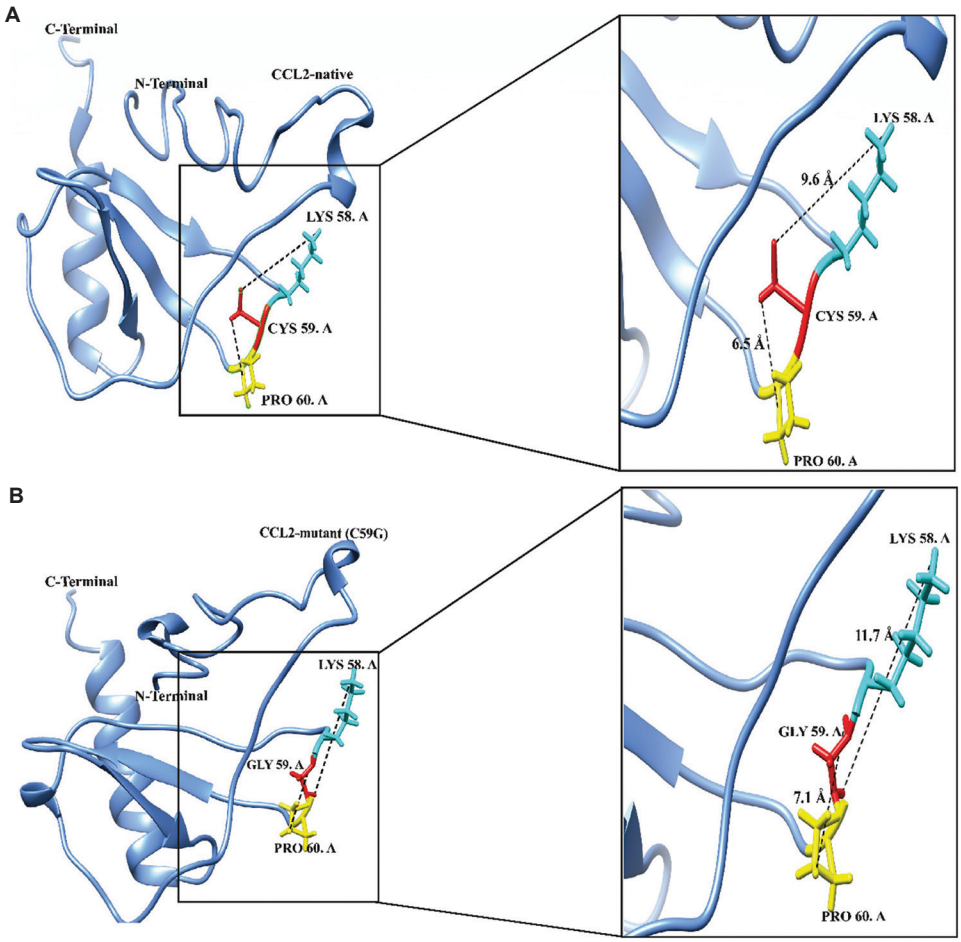

Figure 8. Mutation of cysteine (C59) to glycine (G59) in the CCL2 protein led to substantial structural changes. (A) Native CCL2 structure, where the bond distances between C59 and the neighboring amino acids K58 and P60 were 9.6 and 6.5 Å, respectively. (B) CCL2 mutant G59 structure, where these bond distances increased to 11.7 Å between G59 and K58 and 7.1 Å between G59 and P60. These changes in bond distances indicate that the mutation disrupted the local interactions and altered the overall folding of the protein.
Abbreviation: CCL2: Chemokine C-C motif ligand 2.

this axis helps overcome therapy resistance.[84] In lung cancer, CCL2 recruits myeloid-derived suppressor cells (MDSCs) and tumor-associated macrophages, reducing the effectiveness of immune checkpoint inhibitors, whereas its inhibition increases chemotherapy sensitivity.[87] In renal cell carcinoma, the elevated expression of CCL2 is linked to poor survival, promoting angiogenesis, and the accumulation of MDSCs.[88] CCL2 also enhances bladder cancer cell migration and infiltration, indicating that its blockade may improve responses to both chemotherapy and immunotherapy.[89] In colorectal cancer, CCL2 is involved in metastasis and angiogenesis, highlighting its potential as a prognostic marker and therapeutic target.[9] Overall, targeting the CCL2–CCR2 axis presents a promising strategy for cancer treatment across multiple tumor types. Our findings on the C59G mutation offer insights into its potential role in modulating CCL2 activity and influencing tumor progression. Further investigation in cohorts of patients with cancer is needed to validate this mutation's clinical relevance and potential as a therapeutic target.

CCL2 plays a critical role in macrophage recruitment and activation. Mutations that affect CCL2's ability to bind to its receptor CCR2 could alter macrophage behavior, impacting inflammatory responses and tumor-associated macrophage dynamics.[90] For example, mutations that impair CCL2 function might reduce macrophage infiltration into tumors, potentially affecting tumor growth and metastasis.[5] Monocytes migrate into tissues by activating integrins on their surface through the CCL2–CCR2 axis. This activation facilitates the processes of rolling and adhesion, which allow monocytes to pass through the vascular endothelium and enter the tissues.[91] The CCL2–CCR2 axis activates monocytes, macrophages,

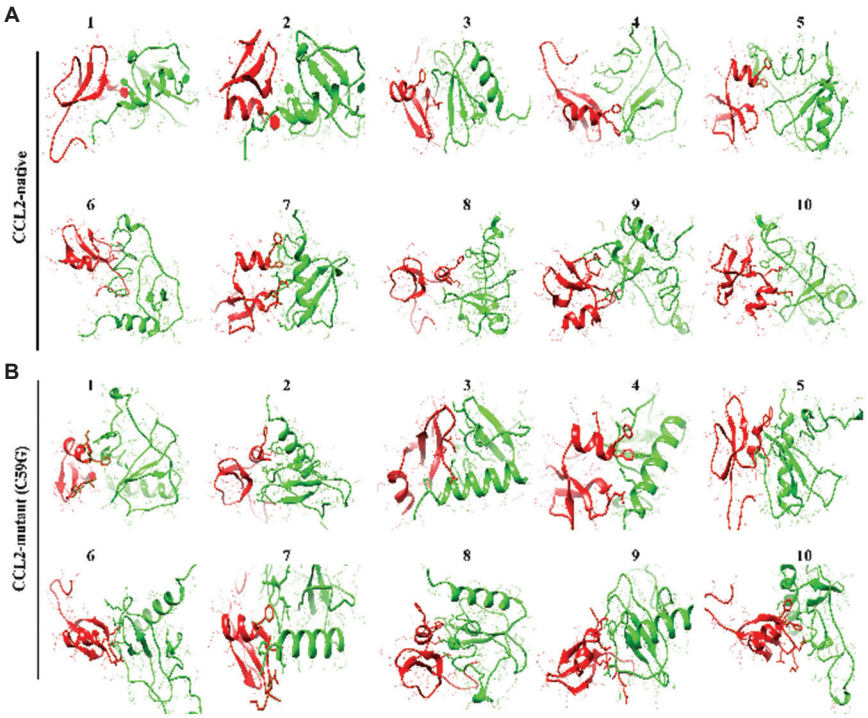

Rank	Docking Score	Confidence Score	Ligand rmsd (Å)
1	-176.10	0.6276	94.85
2	-160.30	0.5513	96.67
3	-159.82	0.5489	85.09
4	-156.70	0.5310	93.02
5	-155.16	0.5238	103.75
6	-153.10	0.5155	74.74
7	-152.99	0.5149	87.08
8	-151.07	0.5053	101.22
9	-150.53	0.5026	117.04
10	-150.21	0.5010	83.08

Rank	Docking Score	Confidence Score	Ligand rmsd (Å)
1	-175.86	0.6265	97.01
2	-172.30	0.6097	83.29
3	-168.52	0.5916	83.48
4	-161.03	0.5549	89.16
5	-160.64	0.5530	86.36
6	-159.83	0.5490	115.62
7	-159.64	0.5481	88.42
8	-158.47	0.5422	106.61
9	-155.39	0.5269	115.72
10	-153.79	0.5189	115.28

Figure 9. Molecular docking results of native and mutant CCL2 with the CCR2 receptor using the HDOCK online tool. (A) The native form of CCL2 displayed a strong binding affinity to CCR2, with the top 10 minimum docking scores ranging from −176.10 to −150.21 kcal/mol. The lowest score of −176.10 kcal/mol indicates the most favorable binding interaction. (B) The mutant form of CCL2 also demonstrated robust binding affinity to CCR2, with top docking scores between −175.86 and −153.79 kcal/mol.
Abbreviations: CCL2: Chemokine C-C motif ligand 2; CCR2: C-C motif chemokine receptor 2.

memory T lymphocytes, and natural killer cells, resulting in the release of pro-inflammatory cytokines such as IL-1, IL-6, and TNF. In addition, macrophages activated by CCL2 secrete tissue repair factors, including vascular endothelial growth factor, platelet-derived growth factor, and transforming growth factor.[92] Functional assays are required to evaluate how these mutations influence activities such as macrophage migration and cytokine production. Understanding these effects could reveal new therapeutic opportunities for modulating macrophage responses in inflammatory diseases and cancer.

Using computational tools, our analysis of 83 mutations extracted from a public database predicted that ten of these mutations were likely to be deleterious and potentially impact the function of the CCL2 protein (Table 1). FATHMM analysis only identified one (C59G) mutation as a cancer-causing or cancer-promoting mutation, indicating its potential role in tumorigenesis (Table 3). The C59G mutation was selected for further analysis, and a conservation study revealed that the C and G positions were highly conserved, with a conservation score of 9 (Figure 2A and B). A previous study discovered that the double mutants R199H/D265H and R203H/D265H as well as the triple mutant R199H/R203H/D265H in CXCR1 were unable to trigger an IL-8-dependent calcium response.[93] Identifying the specific locus of a mutated amino acid can provide valuable insights into how the mutation alters the protein's overall structure and function.[94] Many studies have extensively explored how the location of mutations within a protein structure impacts its function. By examining the relationship between the mutation location and its effects on protein structure, stability, and function, these studies aim to elucidate disease development and progression.[95,96] Using I-TASSER, we modeled the structures of native and mutant CCL2 proteins (Figures 3-5) to perform a MD simulation analysis. This approach allowed us to investigate the structural changes caused by the mutation and its potential impact on the protein's function and overall structure. The RMSD data from the simulations revealed that the mutant CCL2 protein exhibited a distinct and significant pattern of deviation throughout the simulation period, differing from the behavior observed in the native protein (Figure 4A). The simulation results indicated that the mutation substantially destabilizes the CCL2 protein, resulting in structural changes distinct from those observed in the native protein, thereby impacting its stability and overall structure. The RMSF data supported the hypothesis that the mutation destabilizes the protein structure. RMSF

Table 3. Cancer association prediction of CCL2 mutations using the FATHMM server

S. No.	Cancer association			S. No.	Cancer association		
	Mutation	Prediction	Score		Mutation	Prediction	Score
1	M1L	Passenger/Other	3.83	43	S50N	Passenger/Other	3.33
2	K2E	Passenger/Other	3.71	44	Y51H	Passenger/Other	3.02
3	K2T	Passenger/Other	3.68	45	R53G	Passenger/Other	3.51
4	K2R	Passenger/Other	3.8	46	I54V	Passenger/Other	3.44
5	V3I	Passenger/Other	4.03	47	T55S	Passenger/Other	3.48
6	V3G	Passenger/Other	3.85	48	S56N	Passenger/Other	3.41
7	S4F	Passenger/Other	3.99	49	S56R	Passenger/Other	3.4
8	A5V	Passenger/Other	4.17	50	S57C	Passenger/Other	3.36
9	A5T	Passenger/Other	4.08	51	C59G	Cancer	−2.04
10	I13T	Passenger/Other	4.13	52	K61I	Passenger/Other	3.54
11	I13V	Passenger/Other	4.22	53	K67R	Passenger/Other	3.53
12	A14E	Passenger/Other	3.9	54	K67D	Passenger/Other	3.49
13	A15P	Passenger/Other	3.85	55	K67T	Passenger/Other	3.8
14	T16S	Passenger/Other	4.08	56	T68I	Passenger/Other	3.14
15	I18N	Passenger/Other	4.03	57	I69V	Passenger/Other	3.61
16	I18T	Passenger/Other	4.1	58	A71T	Passenger/Other	3.78
17	P19L	Passenger/Other	4.13	59	A71V	Passenger/Other	3.74
18	P19Q	Passenger/Other	4.13	60	E73G	Passenger/Other	3.54
19	Q20R	Passenger/Other	4.07	61	I74N	Passenger/Other	3.35
20	A23T	Passenger/Other	3.97	62	D77E	Passenger/Other	3.43
21	A23S	Passenger/Other	4.06	63	D77G	Passenger/Other	3.43
22	A27G	Passenger/Other	3.72	64	P78S	Passenger/Other	2.23
23	A27V	Passenger/Other	3.71	65	P78H	Passenger/Other	2.19
24	N29K	Passenger/Other	3.74	66	K79E	Passenger/Other	3.58
25	P31A	Passenger/Other	3.63	67	K79R	Passenger/Other	3.42
26	Y36C	Passenger/Other	3.53	68	K81N	Passenger/Other	3.44
27	N37D	Passenger/Other	3.52	69	W82L	Passenger/Other	2.93
28	T39I	Passenger/Other	3.73	70	V83A	Passenger/Other	2.91
29	T39A	Passenger/Other	3.71	71	V83L	Passenger/Other	2.96
30	N40D	Passenger/Other	3.79	72	Q84R	Passenger/Other	3.6
31	N40K	Passenger/Other	3.83	73	D85Y	Passenger/Other	3.45
32	R41K	Passenger/Other	3.6	74	M87V	Passenger/Other	3.49
33	K42I	Passenger/Other	3.34	75	M87K	Passenger/Other	3.3
34	S44L	Passenger/Other	3.53	76	D88N	Passenger/Other	3.64
35	V45M	Passenger/Other	3.49	77	D88V	Passenger/Other	3.56
36	V45A	Passenger/Other	3.54	78	H89P	Passenger/Other	3.53
37	R47K	Passenger/Other	3.57	79	K92R	Passenger/Other	3.66
38	L48F	Passenger/Other	3.37	80	T96A	Passenger/Other	3.72
39	A49E	Passenger/Other	3.72	81	P97L	Passenger/Other	3.87
40	A49V	Passenger/Other	3.63	82	P97T	Passenger/Other	3.83
41	A49T	Passenger/Other	3.57	83	T99S	Passenger/Other	4.1
42	A49P	Passenger/Other	3.52				

analysis revealed distinct fluctuation patterns in the mutant protein compared to the native structure, indicating that the mutation significantly impacted protein stability and dynamics (Figure 4B). The analysis showed a substantial increase in residue-level variation in the mutant protein, suggesting that the mutation caused notable changes in the protein's conformation and increased its flexibility.

Analysis of the intramolecular hydrogen bonds in the CCL2 protein revealed a notable decrease in the number of hydrogen bonds formed in the mutant protein compared to the native structure during the simulation. This reduction suggests an increase in the flexibility of the mutant protein and significant structural differences between the two forms (Figure 5A and B). To elucidate the structural dynamics of the native and mutant CCL2 proteins, an ED analysis was performed. This approach enabled the identification of correlated movements within both protein structures, providing insights into the molecular mechanisms underlying their functional differences. Examination of the sum of the eigenvalues revealed that the primary fluctuations were confined to the first two eigenvectors for both the native and mutant proteins. This finding suggests that these PCs capture the main motions within the system (Figure 5C and D).

Analysis of the Rg plot indicated that the amino acid substitution at position G59 had a destabilizing effect on the protein's structure, which led to reduced protein compactness (Figure 6A and B). This finding was supported by SASA analysis, which revealed higher SASA values for the mutant protein, indicating a substantial structural transition (Figure 6C and D). The observed conformational changes strongly suggest that the amino acid substitution in the mutant protein significantly altered its overall structure. Furthermore, the mutation resulted in a less stable, more flexible, and less compact structure compared to the native protein. Our results collectively indicate that the mutation had a profound impact on protein structure and stability.

Previous studies have shown the synergistic value of combining *in silico* approaches and wet laboratory experiments to gain a comprehensive understanding of biological processes.[97,98] The combination of computational methods and experimental techniques has emerged as a potent strategy for predicting and confirming hypotheses across various biological systems.[98] Integrating computational mutation predictions with MD simulation analysis has been pivotal in pinpointing disease-causing mutations.[99] This approach has allowed for the identification of the most harmful mutations from a large pool of mutations, offering valuable insights into the molecular mechanisms underlying various diseases.[100] Computational methods are essential in providing the foundation for genetic research and enabling the understanding of the molecular basis of diseases.[101] Moreover, computational methods play a crucial role in identifying disease-causing mutations and exploring potential therapeutic strategies.[102,103] These methods also aid in the clinical assessment of genetic variants, enabling more informed and effective treatment decisions.

5. Conclusion

This investigation into the oncogenic missense mutations of *CCL2*, particularly the C59G mutation, revealed that this specific mutation may impair CCL2 activity, potentially lower the risk of cancer, and enhance the immune response. Through bioinformatics and computational analyses, we found that the C59G mutation significantly affects the stability and function of CCL2, potentially hindering its interaction with the CCR2 receptor. This mutation, one of the 83 *CCL2* missense mutations, is associated with disease causation and has implications for cancer development. MD simulations and structural analyses confirmed that these mutations induce substantial conformational changes, decrease stability, and alter the ED. Despite the increased binding affinities of mutant CCL2 to CCR2, the C59G mutation markedly affects the protein's stability and function. This study emphasizes the importance of understanding the molecular characteristics of CCL2 mutations, particularly C59G, in influencing disease processes, such as that of colorectal cancer, and highlights the potential implications for immune responses and cancer regulation.

Acknowledgments

None.

Funding

This work was supported by National Natural Science Foundation of China (32270438, 32170498, 31970388), the National Key Research and Development Program of China (2021YFF0702000, 2018YFD0900602), 1.3+.5 project for disciplines of excellence, West China Hospital, Sichuan University (ZYJC21050), the Science and Technology Department of Sichuan Province (2022YFH0116), the Priority Academic Program Development of Jiangsu Higher Education Institutions (PAPD), the National Clinical Research Center for Geriatrics, West China Hospital, and Sichuan University (Z2023JC003).

Conflict of interest

Mohammad Amjad Kamal is the Guest Editor of this special issue, but was not in any way involved in the editorial and peer-review process conducted for this paper,

directly or indirectly. Separately, other authors declared that they have no known competing financial interests or personal relationships that could have influenced the work reported in this paper.

Author contributions

Conceptualization: Shah Kamal, Cheng Deng, Shanshan Lai
Formal analysis: Shah Kamal, Amanullah Amanullah, Najeeb Ullah, Mariam Ahmed Mujtaba, Kashif Ali Khan
Investigation: Shah Kamal, Mohammad Amjad Kamal, Shanshan Lai, Cheng Dend
Methodology: Najeeb Ullah, Shah Kamal, Mariam Ahmed Mujtaba, Kashif Ali Khan
Writing–original draft: Shah Kamal, Cheng Deng, Mohammad Amjad Kamal, Shanshan Lai
Writing–review & editing: Shanshan Lai, Mohammad Amjad Kamal, Najeeb Ullah, Cheng Deng

Ethics approval and consent to participate

Not applicable.

Consent for publication

Not applicable.

Availability of data

All datasets generated for this study are available from the corresponding authors on reasonable request.

References

1. Zhu S, Liu M, Bennett S, Wang Z, Pfleger KDG, Xu J. The molecular structure and role of CCL2 (MCP-1) and C-C chemokine receptor CCR2 in skeletal biology and diseases. *J Cell Physiol*. 2021;236(10):7211-7222.

   doi: 10.1002/jcp.30375

2. Schubert M, Bleuler-Martinez S, Butschi A, *et al*. Plasticity of the β-trefoil protein fold in the recognition and control of invertebrate predators and parasites by a fungal defence system. *PLoS Pathog*. 2012;8(5):e1002706.

   doi: 10.1371/journal.ppat.1002706

3. Joshi N, Kumar D, Poluri KM. Elucidating the molecular interactions of chemokine CCL2 orthologs with flavonoid baicalin. *ACS Omega*. 2020;5(35):22637-22651.

   doi: 10.1021/acsomega.0c03428

4. Shao Z, Tan Y, Shen Q, *et al*. Molecular insights into ligand recognition and activation of chemokine receptors CCR2 and CCR3. *Cell Discov*. 2022;8(1):44.

   doi: 10.1038/s41421-022-00403-4

5. Li H, Wu M, Zhao X. Role of chemokine systems in cancer and inflammatory diseases. *MedComm* (*2020*). 2022;3(2):e147.

   doi: 10.1002/mco2.147

6. Turner MD, Nedjai B, Hurst T, Pennington DJ. Cytokines and chemokines: At the crossroads of cell signalling and inflammatory disease. *Biochim Biophys Acta*. 2014;1843(11):2563-2582.

   doi: 10.1016/j.bbamcr.2014.05.014

7. White GE, Iqbal AJ, Greaves DR. CC chemokine receptors and chronic inflammation-therapeutic opportunities and pharmacological challenges. *Pharmacol Rev*. 2013;65(1):47-89.

   doi: 10.1124/pr.111.005074

8. Dommel S, Blüher M. Does C-C motif chemokine ligand 2 (CCL2) link obesity to a pro-inflammatory state? *Int J Mol Sci*. 2021;22(3):1500.

   doi: 10.3390/ijms22031500

9. Xu M, Wang Y, Xia R, Wei Y, Wei X. Role of the CCL2-CCR2 signalling axis in cancer: Mechanisms and therapeutic targeting. *Cell Prolif*. 2021;54(10):e13115.

   doi: 10.1111/cpr.13115

10. Ben-Baruch A. Host microenvironment in breast cancer development: Inflammatory cells, cytokines and chemokines in breast cancer progression: Reciprocal tumor-microenvironment interactions. *Breast Cancer Res*. 2002;5(1):31.

    doi: 10.1186/bcr554

11. Yoshimura T, Li C, Wang Y, Matsukawa A. The chemokine monocyte chemoattractant protein-1/CCL2 is a promoter of breast cancer metastasis. *Cell Mol Immunol*. 2023;20(7):714-38.

    doi: 10.1038/s41423-023-01013-0

12. Soria G, Yaal-Hahoshen N, Azenshtein E, *et al*. Concomitant expression of the chemokines RANTES and MCP-1 in human breast cancer: A basis for tumor-promoting interactions. *Cytokine*. 2008;44(1):191-200.

    doi: 10.1016/j.cyto.2008.08.002

13. Furukawa S, Soeda S, Kiko Y, *et al*. MCP-1 promotes invasion and adhesion of human ovarian cancer cells. *Anticancer Res*. 2013;33(11):4785-4790.

14. Hefler L, Tempfer C, Heinze G, *et al*. Monocyte chemoattractant protein-1 serum levels in ovarian cancer patients. *Br J Cancer*. 1999;81(5):855-829.

    doi: 10.1038/sj.bjc.6690776

15. Bhat AA, Nisar S, Maacha S, *et al*. Cytokine-chemokine network driven metastasis in esophageal cancer; promising avenue for targeted therapy. *Mol Cancer*. 2021;20:2.

    doi: 10.1186/s12943-020-01294-3

16. Singh S, Anshita D, Ravichandiran V. MCP-1: Function, regulation, and involvement in disease. *Int*

Immunopharmacol. 2021;101(Pt B):107598.

doi: 10.1016/j.intimp.2021.107598

17. Kitadai Y. Cancer-stromal cell interaction and tumor angiogenesis in gastric cancer. *Cancer Microenviron*. 2010;3:109-116.

doi: 10.1007/s12307-009-0032-9

18. Tesch GH, Schwarting A, Kinoshita K, Lan HY, Rollins BJ, Kelley VR. Monocyte chemoattractant protein-1 promotes macrophage-mediated tubular injury, but not glomerular injury, in nephrotoxic serum nephritis. *J Clin Invest*. 1999;103(1):73-80.

doi: 10.1172/jci4876

19. Niiya M, Niiya K, Kiguchi T, *et al*. Induction of TNF-alpha, uPA, IL-8 and MCP-1 by doxorubicin in human lung carcinoma cells. *Cancer Chemother Pharmacol*. 2003;52(5):391-398.

doi: 10.1007/s00280-003-0665-1

20. Huang S, Singh RK, Xie K, *et al*. Expression of the JE/MCP-1 gene suppresses metastatic potential in murine colon carcinoma cells. *Cancer Immunol Immunother*. 1994;39(4):231-238.

doi: 10.1007/bf01525986

21. Pandurangan AP, Blundell TL. Prediction of impacts of mutations on protein structure and interactions: SDM, a statistical approach, and mCSM, using machine learning. *Protein Sci*. 2020;29(1):247-257.

doi: 10.1002/pro.3774

22. Capriotti E, Altman RB, Bromberg Y. Collective judgment predicts disease-associated single nucleotide variants. *BMC Genomics*. 2013;14 Suppl 3:S2.

doi: 10.1186/1471-2164-14-s3-s2

23. Adzhubei I, Jordan DM, Sunyaev SR. Predicting functional effect of human missense mutations using PolyPhen-2. *Curr Protoc Hum Genet*. 2013;Chapter 7:Unit7.20.

doi: 10.1002/0471142905.hg0720s76

24. López-Ferrando V, Gazzo A, de la Cruz X, Orozco M, Gelpí JL. PMut: A web-based tool for the annotation of pathological variants on proteins, 2017 update. *Nucleic Acids Res*. 2017;45(W1):W222-W228.

doi: 10.1093/nar/gkx313

25. Rogers MF, Shihab HA, Mort M, Cooper DN, Gaunt TR, Campbell C. FATHMM-XF: Accurate prediction of pathogenic point mutations via extended features. *Bioinformatics*. 2018;34(3):511-513.

doi: 10.1093/bioinformatics/btx536

26. Pires DE, Ascher DB, Blundell TL. mCSM: Predicting the effects of mutations in proteins using graph-based signatures. *Bioinformatics*. 2014;30(3):335-342.

doi: 10.1093/bioinformatics/btt691

27. Worth CL, Preissner R, Blundell TL. SDM--a server for predicting effects of mutations on protein stability and malfunction. *Nucleic Acids Res*. 2011;39(Web Server issue):W215-W222.

doi: 10.1093/nar/gkr363

28. Pires DE, Ascher DB, Blundell TL. DUET: A server for predicting effects of mutations on protein stability using an integrated computational approach. *Nucleic Acids Res*. 2014;42(Web Server issue):W314-W319.

doi: 10.1093/nar/gku411

29. Yang J, Zhang Y. I-TASSER server: New development for protein structure and function predictions. *Nucleic Acids Res*. 2015;43(W1):W174-W181.

doi: 10.1093/nar/gkv342

30. Gorai S, Junghare V, Kundu K, *et al*. Synthesis of dihydrobenzofuro[3,2-b]chromenes as potential 3CLpro inhibitors of SARS-CoV-2: A molecular docking and molecular dynamics study. *ChemMedChem*. 2022;17(8):e202100782.

doi: 10.1002/cmdc.202100782

31. Farajzadeh-Dehkordi M, Mafakher L, Harifi A, Samiee-Rad F, Rahmani B. Computational analysis of the functional and structural impact of the most deleterious missense mutations in the human Protein C. *PLoS One*. 2023;18(11):e0294417.

doi: 10.1371/journal.pone.0294417

32. Martin FJ, Amode MR, Aneja A, *et al*. Ensembl 2023. *Nucleic Acids Res*. 2023;51(D1):D933-D941.

doi: 10.1093/nar/gkac958

33. Sherry ST, Ward MH, Kholodov M, *et al*. dbSNP: The NCBI database of genetic variation. *Nucleic Acids Res*. 2001;29(1):308-311.

doi: 10.1093/nar/29.1.308

34. UniProt Consortium. UniProt: A hub for protein information. *Nucleic Acids Res*. 2015;43(Database issue):D204-D212.

doi: 10.1093/nar/gku989

35. Goodsell DS, Zardecki C, Di Costanzo L, *et al*. RCSB Protein Data Bank: Enabling biomedical research and drug discovery. *Protein Sci*. 2020;29(1):52-65.

doi: 10.1002/pro.3730

36. Hecht M, Bromberg Y, Rost B. Better prediction of functional effects for sequence variants. *BMC Genomics*. 2015;16 Suppl 8(Suppl 8):S1.

doi: 10.1186/1471-2164-16-s8-s1

37. Mi H, Lazareva-Ulitsky B, Loo R, *et al*. The PANTHER database of protein families, subfamilies, functions and pathways. *Nucleic Acids Res*. 2005;33(Database issue):D284-D288.

doi: 10.1093/nar/gki078

38. Ng PC, Henikoff S. SIFT: Predicting amino acid changes that affect protein function. *Nucleic Acids Res*. 2003;31(13):3812-3814.

doi: 10.1093/nar/gkg509

39. Bendl J, Stourac J, Salanda O, *et al*. PredictSNP: Robust and accurate consensus classifier for prediction of disease-related mutations. *PLoS Comput Biol*. 2014;10(1):e1003440.

doi: 10.1371/journal.pcbi.1003440

40. Pejaver V, Mooney SD, Radivojac P. Missense variant pathogenicity predictors generalize well across a range of function-specific prediction challenges. *Hum Mutat*. 2017;38(9):1092-108.

doi: 10.1002/humu.23258

41. Adzhubei IA, Schmidt S, Peshkin L, *et al*. A method and server for predicting damaging missense mutations. *Nat Methods*. 2010;7(4):248-249.

doi: 10.1038/nmeth0410-248

42. Vila JA. Proteins' evolution upon point mutations. *ACS Omega*. 2022;7(16):14371-14376.

doi: 10.1021/acsomega.2c01407

43. Pandurangan AP, Ochoa-Montaño B, Ascher DB, Blundell TL. SDM: A server for predicting effects of mutations on protein stability. *Nucleic Acids Res*. 2017;45(W1):W229-W235.

doi: 10.1093/nar/gkx439

44. Choudhury A, Mohammad T, Anjum F, *et al*. Comparative analysis of web-based programs for single amino acid substitutions in proteins. *PLoS One*. 2022;17(5):e0267084.

doi: 10.1371/journal.pone.0267084

45. Rodrigues CHM, Myung Y, Pires DEV, Ascher DB. mCSM-PPI2: Predicting the effects of mutations on protein-protein interactions. *Nucleic Acids Res*. 2019;47(W1):W338-W344.

doi: 10.1093/nar/gkz383

46. Rodrigues CHM, Pires DEV, Ascher DB. mmCSM-PPI: Predicting the effects of multiple point mutations on protein-protein interactions. *Nucleic Acids Res*. 2021;49(W1):W417-W424.

doi: 10.1093/nar/gkab273

47. Chen CW, Lin J, Chu YW. iStable: Off-the-shelf predictor integration for predicting protein stability changes. *BMC Bioinformatics*. 2013;14 Suppl 2(Suppl 2):S5.

doi: 10.1186/1471-2105-14-s2-s5

48. Panchal NK, Bhale A, Verma VK, Beevi SS. Computational and molecular dynamics simulation approach to analyze the impact of XPD gene mutation on protein stability and function. 2020.

doi: 10.1101/2020.07.18.209841

49. Shihab HA, Gough J, Cooper DN, Day IN, Gaunt TR. Predicting the functional consequences of cancer-associated amino acid substitutions. *Bioinformatics*. 2013;29(12):1504-1510.

doi: 10.1093/bioinformatics/btt182

50. Ashkenazy H, Abadi S, Martz E, *et al*. ConSurf 2016: An improved methodology to estimate and visualize evolutionary conservation in macromolecules. *Nucleic Acids Res*. 2016;44(W1):W344-W350.

doi: 10.1093/nar/gkw408

51. Ishimoto N, Park JH, Kawakami K, *et al*. Structural basis of CXC chemokine receptor 1 ligand binding and activation. *Nat Commun*. 2023;14(1):4107.

doi: 10.1038/s41467-023-39799-2

52. Lovell SC, Davis IW, Arendall WB 3rd, *et al*. Structure validation by Calpha geometry: phi,psi and Cbeta deviation. *Proteins*. 2003;50(3):437-50.

doi: 10.1002/prot.10286

53. Konopka BM, Nebel JC, Kotulska M. Quality assessment of protein model-structures based on structural and functional similarities. *BMC Bioinformatics*. 2012;13(1):242.

doi: 10.1186/1471-2105-13-242

54. Ravikumar A, Ramakrishnan C, Srinivasan N. Stereochemical assessment of (ϕ,ψ) outliers in protein structures using bond geometry-specific Ramachandran steric-maps. *Structure*. 2019;27:1875-1884.

doi: 10.1016/j.str.2019.09.009

55. Durrant JD, McCammon JA. Molecular dynamics simulations and drug discovery. *BMC Biol*. 2011;9(1):71.

doi: 10.1186/1741-7007-9-71

56. Hollingsworth SA, Dror RO. Molecular dynamics simulation for all. *Neuron*. 2018;99(6):1129-1143.

doi: 10.1016/j.neuron.2018.08.011

57. Muhammed MT, Aki-Yalcin E. Homology modeling in drug discovery: Overview, current applications, and future perspectives. *Chem Biol Drug Des*. 2019;93(1):12-20.

doi: 10.1111/cbdd.13388

58. Binbay FA, Rathod DC, George AAP, Imhof D. Quality assessment of selected protein structures derived from homology modeling and AlphaFold. *Pharmaceuticals* (*Basel*). 2023;16(12):1662.

doi: 10.3390/ph16121662

59. Brooks BR, Brooks CL 3rd, Mackerell AD Jr., *et al*. CHARMM: The biomolecular simulation program. *J Comput Chem*. 2009;30(10):1545-1614.

doi: 10.1002/jcc.21287

60. Vieira IHP, Botelho EB, de Souza Gomes TJ, Kist R, Caceres RA, Zanchi FB. Visual dynamics: A WEB application for molecular dynamics simulation using GROMACS. *BMC Bioinformatics*. 2023;24(1):107.

doi: 10.1186/s12859-023-05234-y

61. Bagewadi ZK, Khan TM, Gangadharappa B, Kamalapurkar A, Shamsudeen SM, Yaraguppi DM. Molecular dynamics and simulation analysis against superoxide dismutase (SOD) target of *Micrococcus luteus* with secondary metabolites from *Bacillus licheniformis* recognized by genome mining approach. *Saudi J Biol Sci*. 2023;30:103753.

doi: 10.1016/j.sjbs.2023.103753

62. Shahraki O, Zargari F, Edraki N, Khoshneviszadeh M, Firuzi O. Molecular dynamics simulation and molecular docking studies of 1,4- dihydropyridines as P-glycoprotein's allosteric inhibitors. *J Biomol Struct Dyn*. 2016;36:112-125.

doi: 10.1080/07391102.2016.1268976

63. Ferreira LG, Dos Santos RN, Oliva G, Andricopulo AD. Molecular docking and structure-based drug design strategies. *Molecules*. 2015;20(7):13384-13421.

doi: 10.3390/molecules200713384

64. Hildebrand PW, Rose AS, Tiemann JKS. Bringing molecular dynamics simulation data into view. *Trends Biochem Sci*. 2019;44(11):902-913.

doi: 10.1016/j.tibs.2019.06.004

65. Tumskiy RS, Tumskaia AV. Multistep rational molecular design and combined docking for discovery of novel classes of inhibitors of SARS-CoV-2 main protease 3CLpro. *Chem Phys Lett*. 2021;780:138894.

doi: 10.1016/j.cplett.2021.138894

66. Carter P, Andersen CA, Rost B. DSSPcont: Continuous secondary structure assignments for proteins. *Nucleic Acids Res*. 2003;31(13):3293-3295.

doi: 10.1093/nar/gkg626

67. Yan Y, Wen Z, Wang X, Huang SY. Addressing recent docking challenges: A hybrid strategy to integrate template-based and free protein-protein docking. *Proteins*. 2016;85:497-512.

doi: 10.1002/prot.25234

68. Case DA, Cheatham TE 3rd, Darden T, *et al*. The Amber biomolecular simulation programs. *J Comput Chem*. 2005;26(16):1668-1688.

doi: 10.1002/jcc.20290

69. Huang SY, Zou X. MDockPP: A hierarchical approach for protein-protein docking and its application to CAPRI rounds 15-19. *Proteins*. 2010;78(15):3096-3103.

doi: 10.1002/prot.22797

70. Huang SY, Yan C, Grinter SZ, Chang S, Jiang L, Zou X. Inclusion of the orientational entropic effect and low-resolution experimental information for protein-protein docking in Critical Assessment of PRedicted Interactions (CAPRI). *Proteins*. 2013;81(12):2183-2191.

doi: 10.1002/prot.24435

71. Martí-Renom MA, Stuart AC, Fiser A, Sánchez R, Melo F, Sali A. Comparative protein structure modeling of genes and genomes. *Annu Rev Biophys Biomol Struct*. 2000;29:291-325.

doi: 10.1146/annurev.biophys.29.1.291

72. Shah K, Amanullah A, Qingqing W, *et al*. Bioinformatics analysis of missense mutations in CXCR1 implicates altered protein stability and function. *Tumor Discov*. 2024;3:2512.

doi: 10.36922/td.2512

73. Sobitan A, Edwards W, Jalal MS, *et al*. Prediction of the effects of missense mutations on human myeloperoxidase protein stability using *in silico* saturation mutagenesis. *Genes* (*Basel*). 2022;13(8):1412.

doi: 10.3390/genes13081412

74. Yang J, Zhang Y. Protein structure and function prediction using I-TASSER. *Curr Protoc Bioinformatics*. 2015;52:5.8.1-5.8.15.

doi: 10.1002/0471250953.bi0508s52

75. Zhang Y. I-TASSER server for protein 3D structure prediction. *BMC Bioinformatics*. 2008;9:40.

doi: 10.1186/1471-2105-9-40

76. Sobolev OV, Afonine PV, Moriarty NW, *et al*. A global Ramachandran score identifies protein structures with unlikely stereochemistry. *Structure*. 2020;28(11):1249-1258.e2.

doi: 10.1016/j.str.2020.08.005

77. Yang Z, Lasker K, Schneidman-Duhovny D, *et al*. UCSF Chimera, MODELLER, and IMP: An integrated modeling system. *J Struct Biol*. 2012;179(3):269-278.

doi: 10.1016/j.jsb.2011.09.006

78. Wang L, Ding MY, Wang J, Gao JG, Liu RM, Li HT. Effects of site-directed mutagenesis of cysteine on the structure of sip proteins. *Front Microbiol*. 2022;13:805325.

doi: 10.3389/fmicb.2022.805325

79. Konrat R, Kräutler B, Weiskirchen R, Bister K. Structure of cysteine-and glycine-rich protein CRP2. Backbone dynamics reveal motional freedom and independent spatial orientation of the lim domains. *J Biol Chem.* 1998;273(36):23233-23240.

doi: 10.1074/jbc.273.36.23233

80. Qiu H, Honey DM, Kingsbury JS, *et al*. Impact of cysteine variants on the structure, activity, and stability of recombinant human α-galactosidase A. *Protein Sci*. 2015;24(9):1401-1411.

doi: 10.1002/pro.2719

81. Gerlza T, Winkler S, Atlic A, *et al*. Designing a mutant CCL2-

HSA chimera with high glycosaminoglycan-binding affinity and selectivity. *Protein Eng Des Sel*. 2015;28(8):231-240.

doi: 10.1093/protein/gzv025

82. Hao Q, Vadgama JV, Wang P. CCL2/CCR2 signaling in cancer pathogenesis. *Cell Commun Signal*. 2020;18(1):82.

doi: 10.1186/s12964-020-00589-8

83. Lim SY, Yuzhalin AE, Gordon-Weeks AN, Muschel RJ. Targeting the CCL2-CCR2 signaling axis in cancer metastasis. *Oncotarget*. 2016;7(19):28697-28710.

doi: 10.18632/oncotarget.7376

84. Kadomoto S, Izumi K, Mizokami A. Roles of CCL2-CCR2 axis in the tumor microenvironment. *Int J Mol Sci*. 2021;22(16):8530.

doi: 10.3390/ijms22168530

85. Iwamoto H, Izumi K, Mizokami A. Is the C-C motif ligand 2–C-C chemokine receptor 2 axis a promising target for cancer therapy and diagnosis? *Int J Mol Sci*. 2020;21(23):9328.

doi: 10.3390/ijms21239328

86. Anderson EM, Thomassian S, Gong J, Hendifar A, Osipov A. Advances in pancreatic ductal adenocarcinoma treatment. *Cancers* (*Basel*). 2021;13(21):5510.

doi: 10.3390/cancers13215510

87. Li X, Zhong J, Deng X, *et al*. Targeting myeloid-derived suppressor cells to enhance the antitumor efficacy of immune checkpoint blockade therapy. *Front Immunol*. 2021;12:754196.

doi: 10.3389/fimmu.2021.754196

88. Chen W, Pan X, Cui X. RCC immune microenvironment subsequent to targeted therapy: A friend or a foe? *Front Oncol*. 2020;10:573690.

doi: 10.3389/fonc.2020.573690

89. Jin J, Lin J, Xu A, *et al*. CCL2: An important mediator between tumor cells and host cells in tumor microenvironment. *Front Oncol*. 2021;11:722916.

doi: 10.3389/fonc.2021.722916

90. Toya M, Zhang N, Tsubosaka M, *et al*. CCL2 promotes osteogenesis by facilitating macrophage migration during acute inflammation. *Front Cell Dev Biol*. 2023;11:1213641.

doi: 10.3389/fcell.2023.1213641

91. Butcher MJ, Galkina EV. wRAPping up early monocyte and neutrophil recruitment in atherogenesis via Annexin A1/FPR2 signaling. *Circ Res*. 2015;116(5):774-777.

doi: 10.1161/circresaha.115.305920

92. Deshmane SL, Kremlev S, Amini S, Sawaya BE. Monocyte chemoattractant protein-1 (MCP-1): An overview. *J Interferon Cytokine Res*. 2009;29(6):313-326.

doi: 10.1089/jir.2008.0027

93. Suetomi K, Rojo D, Navarro J. Identification of a signal transduction switch in the chemokine receptor CXCR1. *J Biol Chem*. 2002;277(35):31563-31566.

doi: 10.1074/jbc.M204713200

94. Studer RA, Dessailly BH, Orengo CA. Residue mutations and their impact on protein structure and function: Detecting beneficial and pathogenic changes. *Biochem J*. 2013;449:581-594.

doi: 10.1042/BJ20121221

95. Gerasimavicius L, Livesey BJ, Marsh JA. Loss-of-function, gain-of-function and dominant-negative mutations have profoundly different effects on protein structure. *Nat Commun*. 2022;13(1):3895.

doi: 10.1038/s41467-022-31686-6

96. Arshad M, Bhatti A, John P. Identification and in silico analysis of functional SNPs of human TAGAP protein: A comprehensive study. *PLoS One*. 2018;13(1):e0188143.

doi: 10.1371/journal.pone.0188143

97. Schwaigerlehner L, Pechlaner M, Mayrhofer P, Oostenbrink C, Kunert R. Lessons learned from merging wet lab experiments with molecular simulation to improve mAb humanization. *Protein Eng Des Sel*. 2018;31(7-8):257-265.

doi: 10.1093/protein/gzy009

98. Cárdenas R, Martínez-Seoane J, Amero C. Combining experimental data and computational methods for the non-computer specialist. *Molecules*. 2020;25(20):4783.

doi: 10.3390/molecules25204783

99. Kamaraj B, Purohit R. Computational screening of disease-associated mutations in OCA2 gene. *Cell Biochem Biophys*. 2013;68:97-109.

doi: 10.1007/s12013-013-9697-2

100. Stefl S, Nishi H, Petukh M, Panchenko A, Alexov E. Molecular mechanisms of disease-causing missense mutations. *J Mol Biol*. 2013;425:3919-3936.

doi: 10.1016/j.jmb.2013.07.014

101. Peterson TA, Doughty E, Kann MG. Towards precision medicine: Advances in computational approaches for the analysis of human variants. *J Mol Biol*. 2013;425(21):4047-4063.

doi: 10.1016/j.jmb.2013.08.008

102. Mugumbate G, Nyathi B, Zindoga A, Munyuki G. Application of computational methods in understanding mutations in *Mycobacterium tuberculosis* drug resistance. *Front Mol Biosci*. 2021;8:643849.

doi: 10.3389/fmolb.2021.643849

103. Luo P, Chen B, Liao B, Wu FX. Predicting disease-associated genes: Computational methods, databases, and evaluations. *WIREs Data Min Knowl Discov*. 2020;11:e1383.

doi: 10.1002/widm.1383

ACCSCIENCE PUBLISHING

Tumor Discovery

ORIGINAL RESEARCH ARTICLE

A new immunomagnetic microfluidic device for characterizing *EGFR* mutations in circulating tumor cells from patients with non-small cell lung cancer

Nkeiruka O. Ogidi[1,2], Michael J. Lind[3], and John Greenman[1]*

[1]Centre for Biomedicine, University of Hull, Kingston upon Hull, United Kingdom

[2]Department of Medical Laboratory Sciences, College of Medicine, University of Lagos, Idi-araba, Lagos state, Nigeria

[3]Centre for Clinical Sciences, University of Hull, Kingston upon Hull, United Kingdom

(This article belongs to the *Special Issue: New Developments in Lung Cancer Research, Diagnosis, Treatment, and Prognosis*)

Abstract

Incorporating precision oncology into cancer management has begun to improve clinical outcomes. Accurate sampling techniques that detect molecular aberrations are crucial for effective implementation. Circulating tumor cells (CTCs), derived from primary or metastatic sites and present in the blood, are proposed as useful diagnostic tools, though their use has been limited due to their rarity, especially in early-stage cancers. This study presents a novel immunomagnetic microfluidic device that efficiently isolates CTCs for analyzing epidermal growth factor receptor (*EGFR*) mutations in patients with non-small cell lung cancer (NSCLC). The device was designed and laser-cut from polymethylmethacrylate. Validation experiments involved spiking PC-9 cells (an established lung cancer cell line containing GLU 746-ALA 750 deletion mutations in exon 19 of the *EGFR* gene) into media and isolating these cells. Exons 18 – 21 of *EGFR* were amplified using a polymerase chain reaction to demonstrate the device's rapid mutation detection capability. Next-generation sequencing was used to characterize these exons in a cohort of 38 NSCLC patients, successfully isolating CTCs from all. Among these patients, 30 (79%) had *EGFR* mutations, with exon 19 showing the highest mutation rate (87%) and exon 21 the highest point mutation rate (23%). Our device captured CTCs effectively in <1 h, enabling mutation detection. Further studies are needed to assess the prognostic significance of these mutations, but this technology has potential applications in various solid tumors.

Keywords: Precision oncology; CTC; NSCLC; EGFR; Microfluidics; Immunomagnetic

***Corresponding author:**
John Greenman
(j.greenman@hull.ac.uk)

Citation: Ogidi NO, Lind MJ, Greenman J. A new immunomagnetic microfluidic device for characterizing EGFR mutations in circulating tumor cells from patients with non-small cell lung cancer. *Tumor Discov.* 2024;3(4):3987. doi: 10.36922/td.3987

Received: June 19. 2024

Accepted: September 19, 2024

Published Online: November 12, 2024

1. Introduction

Presently, the management of patients with non-small cell lung cancer (NSCLC) uses knowledge of a patient's mutational profile to guide the selection of therapy that is most likely to be effective.[1] Over the past two decades, several clinical trials have reported

improved clinical outcomes, particularly progression-free survival (PFS) and overall survival (OS), in patients with exon 18 – 21 mutations in the epidermal growth factor receptor (*EGFR*) gene who were treated with tyrosine kinase inhibitors (TKIs).[2,3] These TKIs are agents that specifically bind in, or close to, the ATP cleft of EGFR.[4] Such mutations stabilize the binding of TKIs to ATP, thereby inhibiting constitutive autophosphorylation and blocking the amplified catalytic activation of the tyrosine kinase domain after ligand binding.[5]

The response of NSCLC patients with mutations in exon 18 – 21 of the *EGFR* gene to TKIs is highly varied.[6] Common mutations, such as deletions in exon 19 (LREA regions), which removes codons 746 – 750, and the codon 858 mutation on exon 21 where leucine replaces arginine, account for around 85% of *EGFR* mutations in NSCLC and have been reported to be associated with better tumor responses (longer time to progression/survival) to TKIs when compared to other *EGFR* mutations.[7,8] Similarly, several clinical studies have reported that tumors with mutations in exon 18 are responsive to TKIs, whereas deletions and insertions in exon 18 have been associated with short-lived responses to TKIs.[9-11] Exon 19 deletions around the non-LREA regions are less responsive to TKIs when compared to deletions in these regions.[12] Mutations in exon 19 are rare and account for approximately 0.5% of all *EGFR* mutations.[13] Tumors with exon 19 mutations have heterogeneous responses to TKIs, ranging from moderately responsive (L747F, E746G, and P733L) to fully resistant (D761Y and L747S).[14,15]

Around 15% of NSCLC patients with an *EGFR* mutation have either an exon 20 mutation and/or an insertion. Aberrations in exon 20 have been associated with tumors that are mostly non-responsive to TKIs.[16] The T790M mutation on codon 790 of exon 20 is the most clinically relevant mutation on this exon,[17] with around 10% of patients with advanced lung cancer having this mutation.[18] Interestingly, more than 50% of patients with an exon 19 deletion or L858R point mutation undergoing treatment with TKIs acquire the T790M mutation and thus develop resistance to first- and second-generation TKIs.[19] However, patients with the T790M mutation are responsive to third-generation TKIs (osimertinib).[20] Tumors with the C797S mutation and exon 20 insertions (D770_N771insNPG at residues 762 – 775) are also generally non-responsive to TKIs.[21] Exon 21 mutations are rare and have been associated with lower sensitivity to TKIs (L861Q, L862V, A859X, and V851X) when compared to L858R mutations.[22] Because of their scarcity, the sensitivity of tumors with many exon 21 mutations (e.g., E866K, H870Y, H825L, H870R, G863S, and P848L) to TKIs is yet to be determined.[22]

As a result of the benefits experienced by NSCLC patients with EGFR mutations, such as longer time to progression and/or survival, through tailored therapies that suit their molecular pathology along with cost reduction associated with prudent use of TKIs, means that molecular testing has been recommended by several regulatory bodies as the standard of care.[23-25] The effectiveness of such patient stratification is highly dependent on detailed and efficient capture of the genomic environment of the malignancy in real time.[26]

In the clinic, the tumor biopsy used for detecting the mutational profile of patients with malignancies, currently the gold standard may not be adequate for effective molecular testing.[27] First, around 40% of patients with NSCLC may not be eligible for surgery, because their malignancies are at an advanced stage, and they are too weak to undergo surgery.[28] Furthermore, a single lesion or segment of a tissue biopsy may not provide sufficient information on tumor heterogeneity.[29] Re-sampling to monitor mutational changes that have some influence on progression and resistance is not practicable for the patient;[30] thus, alternatives are being actively explored. Cell-free DNA (cfDNA) is one alternative that has been utilized successfully for mutational analysis. However, its widespread use has been limited because of issues with low sensitivity particularly with regard to identifying resistant clones with specific mutations.[31,32]

Circulating tumor cells (CTCs) have been explored as a prognostic indicator for PFS and OS[33,34] and as a diagnostic tool for the detection of mutations with varying degrees of success. Some researchers indicate that the CTC sample matrix may be superior to tumor biopsy as the number of mutations detected increase, with the hypothesis being that CTCs reflect cells derived from the primary malignancy and metastatic sites.[35,36] However, other studies have reported equal or fewer numbers of mutations obtained from CTCs when compared to tissue biopsy and/or cfDNA.[37,38] The implementation of CTC sampling as a diagnostic tool has been limited by their relatively low numbers in the blood, especially in the early stages of tumor development, relatively cumbersome work flows, and the high costs of the techniques. In addition, some of the approaches for isolating CTCs from the blood have reported moderate purity values of ≤60% and yield of CTCs at ≤70%.[39,40] Most approaches for isolating CTCs from the blood of patients with NSCLC for subsequent downstream detection of *EGFR* mutations have employed the principles of immune isolation and/or size disparity between CTCs and other blood cells for isolation and polymerase chain reaction (PCR) techniques to detect mutations in exons 18 – 21.[41,42] The translation of these devices to routine use

in the clinics has been hampered by challenges related to reproducibility, low throughput, and intricate work mechanisms.[43] This study aimed to describe the design and functionality of an immunomagnetic microfluidic device that isolates epithelial cell adhesion molecule (EpCAM)-positive CTCs from the blood of patients with NSCLC and to evaluate exon 18 – 21 mutations of the *EGFR* gene with the aim of providing a rapid and robust way of obtaining clinically relevant information that can aid in treatment decisions.

2. Materials and methods

2.1. Materials

HPC Laser LS3060 60W CO_2 laser cutter (HPC Laser, Halifax, UK); polymethylmethacrylate (PMMA) sheet (Vink Plastics, Manchester, UK); PC-9 cell lines (obtained from European Collection of Authenticated Cell Cultures); neodymium iron boron (NdFeB) magnets (Integrated Magnetics, California, USA); RPMI 1640 media (Lonza, Slough, UK); Dynal anti-EpCAM magnetic beads (Thermo Fischer Scientific, Loughborough, UK); 4,6-diamidino-2-phenylindole (Vector Laboratories, Newark, USA); fluorescein-conjugated pan-cytokeratin monoclonal antibody (San Diego, USA); rhodamine-conjugated mouse anti-human CD45 antibodies (BD Biosciences, Fremont, California USA); and PCR mix and primers (Stab Vida Genetics, Laboratory, Lisbon, Portugal).

2.2. Manufacture of the PMMA chip

The dimensions of the PMMA chip were first drawn using an AutoCAD DXF file and then transferred to the laser cutter software to cut the design from a 3-mm PMMA sheet. Two pieces of PMMA measuring 98 × 98 mm were cut using an HPC Laser LS3060 60W CO_2 laser cutter. Afterward, the pieces were bonded together using ethanolic treatment and then underwent ultraviolet irradiation for 25 s as described previously.[44] A single PMMA sheet measuring 57 × 66 mm was also fabricated to form the lid.

2.3. Fabrication of the electromagnetic arm of the device

The magnetic arm is made of a C-shaped polycarbonate piece (measuring 10 cm in height and 4 mm in thickness) to which the NdFeB magnets (Integrated Magnetics, USA), measuring 20 × 5 × 4 mm, are attached at the top and bottom arms (Figure 1). The movement of the magnetic arm is controlled by a high-voltage power supply that moves the arm in the x, y, and z axes. A magnetic actuator program ensures precise movement of the arm. The magnetic device and controller unit were manufactured by Micro-Lab Devices Leeds, UK.

2.4. Cell culture

A lung adenocarcinoma cell line (PC-9)[45] obtained from the European Collection of Authenticated Cell Cultures (ECACC, www.phe-culturecollections.org.uk) was cultured in RPMI-1640 media (Lonza, UK) containing 10% (v/v) fetal bovine serum (Labtech.com, USA), with a final concentration of 50 µg/mL penicillin and 250 µg/mL streptomycin (Lonza, UK). Cells were maintained in a humidified incubator at 37°C with an atmosphere of 5% CO_2 (Galaxy 170 S, New Brunswick Scientific, Stevenage, UK). Cells were used for experiments when they were 80% – 90% confluent.

2.5. Spiking experiments

PC-9 cell lines were harvested from culture media, and a cell viability count was undertaken. Cells were always at least 85% viable when used. PC-9 cells were added to 12 mL of RPMI-1640 media (Lonza, UK) at the following concentrations: 1×10^6, 2×10^5, 4×10^4, and 8×10^3 cells/mL. Thereafter, the cells were isolated using the microfluidic device. Cells isolated were thereafter subjected to PCR to validate the device's ability to process CTCs for downstream analysis and detection of mutations. A range of cell concentrations were used for spiking experiments to validate the utility of the device in isolating EpCAM-positive cell lines. Some of these concentrations reflected concentrations of EpCAM-positive CTCs reported in the blood of NSCLC patients (1 – 80,000 cells/mL).[46,47]

2.6. Patient recruitment/sample processing for CTC analysis

Fifty-nine patients aged between 47 and 81 years diagnosed with NSCLC and admitted to the Castle Hill Hospital were recruited for the study after ethical approval had been received from the North East-Newcastle and North Tyneside Local Research Ethics Committee (REC13/NE/0242). Written informed consent was obtained from all participants (Appendix A1). Patients' demographic/clinicopathological data were obtained from their medical records by Professor Michael Lind and presented in a pseudo-anonymized format.

A total of 13.5 mL of whole blood was collected into three 3.2% trisodium vacutainer sample bottles (BD, USA). Each sample bottle contained 4.5 mL of blood. Within 15 min of sample collection, the blood was transported on ice to the laboratory where processing was done in a class II biological safety cabinet (ESCO Scientific). Blood was pooled in a sterile 50-mL Falcon tube, and 2 mL of phosphate-buffered saline was added to reduce blood viscosity. The tube was mixed thoroughly by inverting the tube three times and then immediately loaded into the chip (Section 2.7).

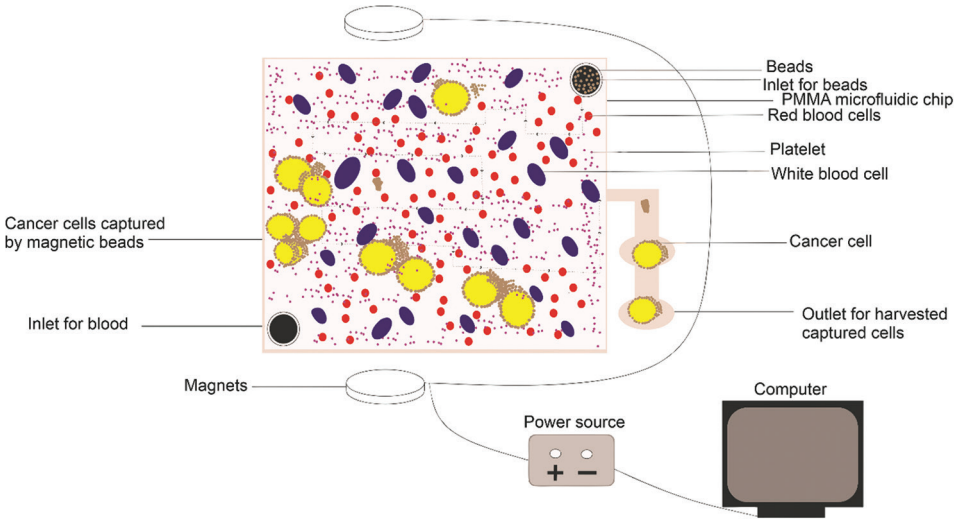

Figure 1. Schematic of the isolation of epithelial cell adhesion molecule (EpCAM)-positive cells from a heterogeneous mixture using a novel immunomagnetic microfluidic chip. The magnetic field, from the immobilized neodymium iron boron magnets positioned at the top and bottom of the polymethylmethacrylate chip, was moved across the device so that the anti-EpCAM magnetic beads (brown beads) bound to the circulating tumor cells in the blood would be collected (EpCAM-positive cancer cells in yellow). The mobility of the magnetic arm and the precision by which the arm skims across the chip are under the control of a high-voltage source and magnetic actuator app installed on the computer, respectively.

2.7. Isolation of EpCAM-positive cell line/CTCs from media/blood using the microfluidic device

Dynal magnetic beads (6 µL) coupled with an anti-EpCAM antibody (Dynabeads™ Epithelial Enrich, ThermoFisher Scientific) were placed in the bead inlet on the PMMA chip, and 13 mL of media spiked with PC-9 cells or patient blood samples were placed in the inlet for blood shown in Figure 1. EpCAM-positive cells were isolated using the immunomagnetic unit.

2.8. Immunostaining of EpCAM-positive cells

EpCAM-positive cells isolated from the device were concentrated onto microscope slides using a cytospin machine (ThermoFisher Scientific, USA). After preparation, the slides were allowed to air dry for 2 h, fixed in 100% methanol for 10 min, and finally allowed to dry for 3 h. After drying, the slides were rinsed with tap water to remove all traces of methanol. The slides were then flooded with Horse serum (blocking reagent) for 10 min (ThermoFisher Scientific, UK). Following blocking, 100 µL of fluorescein-conjugated pan-cytokeratin monoclonal antibody (Biolegend, USA) was added to the slides for 30 min to stain for cytokeratin-positive tumor cells. After incubation at room temperature, the slides were rinsed thrice in tris-buffered saline (TBS) and stained again for 30 min with 100 µL of rhodamine-conjugated mouse anti-human CD45 antibody to evaluate the presence of peripheral blood mononuclear cells. CD45, also known as leucocyte common antigen, was used to ascertain the level of any contaminating white blood cells isolated along with the CTCs. After staining, the slides were washed thrice in TBS and then rinsed in tap water before the addition of 4,6-diamidino-2-phenylindole (DAPI) (Vector Laboratories, USA) to stain the nuclei. The images were identified and evaluated using the Zeiss fluorescence microscope with Zeiss software for identifying CTCs and leucocyte contamination.

2.9. *EGFR* mutation detection in tumor biopsy samples

DNA was extracted from formalin-fixed and paraffin-embedded tissue biopsy samples using the cobas® EGFR DNA extraction kit in accordance with the manufacturer's protocol. Thereafter, extracted DNA was analyzed for selected mutations in exons 18 – 21 of the *EGFR* gene using the cobas® *EGFR* Mutation Test.

2.10. PCR experiments to identify exon 18 – 21 mutations in the *EGFR* gene of EpCAM-positive cells

PC-9 cell lines, bearing mutations in exons 18 – 21 of the *EGFR* gene, and CTCs from patients with NSCLC were used to demonstrate the device's ability to isolate CTCs for downstream analysis. Genomic DNA (gDNA) extracted from EpCAM-positive cells were isolated from a heterogeneous mixture of cells using the device as described earlier, and exons 18 – 21 of the *EGFR* gene were amplified using 0.75 µL of the following primers at a concentration of 10 pmol/µL: **exon** 18: forward (fwd) primers-GCTGAGGTGACCCTTGTCTC, reverse (rev)-TGGAGTTTCCCAAACACTCAG (300bp); **exon 19**:

fwd-GCTGGTAACATCCACCCAGA rev-TTATCTC CCCTCCCCGTATC (261 bp); exon 20: fwd-CACA CT GACGTGCCTCTCC rev-TTATCTCCCCTCCCCGTA TC (251 bp); exon 21: fwd-AGCCATAAGTCCTCG ACGTG rev-CCTGGTGTCAGGAAAATGCT (320 bp) (primer sequences were obtained from Stab Vida Genetics Laboratory, Portugal). Genomic DNA (3 µL) was added to 47 µL of standard PCR mix (provided by Stab Vida Genetics Laboratory, Portugal) Thermocycling temperatures were as follows: initial denaturing at 98 °C for 15 min, then 40 cycles of denaturation at 94 °C for 30 s, annealing at 58 °C for 1 min, and amplification at 75 °C for 1 min, with a final elongation step at 70 °C for 5 min. PCR products were evaluated using gel electrophoresis on 2% (w/v) agarose gel.

2.11. Next-generation sequencing (NGS) to determine exon 18 – 21 mutations in patient samples

Amplicon and library generation were performed according to the procedure of Nextera XT (15031942) (Illumina, USA). The amplicon generated was sequenced using an Illumina sequencer, with the data being processed using Trim galore (version 0.4.3.1) and Prinseq (version 0.20.4). After sorting, data were aligned to the reference with BWA (MEM) version 0.7.17.1. Variants were detected using the VAR direct version from 07.03.2018 (sequencing was done at Stab Vida Genetics Laboratory, Portugal).

2.12. Statistical analysis

Data were analyzed using Prism version 9.0 (Graph pad software, San Diego California USA).

3. Results

3.1. Device description and validation

The device was designed to isolate EpCAM-positive cells in blood contained within a PMMA device using a 4.5-µm diameter magnetic bead covalently bound to an anti-EpCAM antibody sweeping through the blood on a chip (Figure 1). As the magnetic bead sweeps through the blood, it binds with any EpCAM-positive cells. The movement of the magnetic beads can be attributed to the magnetic field generated by NdFeBr magnets attached to the electromagnetic arms of the unit. The arm moves across the chip in step delays of 6 s to allow sufficient time for all magnetized cells to be dragged through the fluid and kept together until they arrive at the outlet where the collected cells were easily isolated for further analysis (Figure 1). The total time taken for isolation of EpCAM-positive cells from 13 mL of fluid using the device was 50 min. Spiking experiments using the PC-9 cell line spiked into media showed that the device was able to capture EpCAM-positive cells (Figure 2). Having established the optimal parameters for collection, the CTCs from PC-9 were analyzed for mutations in 4 exons of the *EGFR* gene. Figure 3A shows the gene amplification of each exon independently using gDNA obtained from the PC-9 cell line, showing that all mutations were detectable. Figure 3B shows a multiplex PCR using the same primers on cells isolated from experiments where the PC-9 cells were spiked into media at various concentrations (1×10^6, 2×10^5, 4×10^4, and 8×10^3 cells/mL).

3.2. Isolation of EpCAM-positive cells from the blood of patients with NSCLC

CTCs isolated from the blood of patients were immunostained to identify markers of epithelial cells and ensure that the cells isolated were tumor-derived. Figure 4A shows a brightfield image of a clump of cells and beads isolated from the patient's blood. Figure 4B shows that the isolated cells were tumor-derived as the clump stained well with a pan-cytokeratin antibody (which stains for epithelial-derived cells). Figure 4C shows that only a few cells stained positive for CD45 antigen using rhodamine-conjugated mouse anti-human CD45 antibodies (a marker for hematological cells), most possibly showing a few leukocytes co-isolated with the tumor cells. Figure 4D shows that most of the cells stained positive for DNA content using DAPI. Figure 4E presents a merged image of the three fluorescence channels, clearly showing that the epithelial tumor cells are the predominant cell type isolated.

3.3. Patient characteristics

Fifty-nine patients recruited for the study were diagnosed following a tissue biopsy. Their clinicopathological characteristics are shown in Table 1, and the process of recruitment is described in Figure 5.

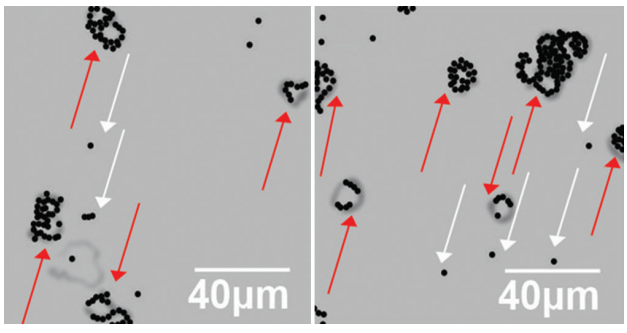

Figure 2. PC-9 cells bound to epithelial cell adhesion molecule (EpCAM)-coated beads. PC-9 cell lines (expressing relatively high levels of EpCAM) were spiked in media and isolated from media using the device. The results Panel A- show the capture of PC-9 cell lines by the device (red arrow depicts cell lines positive for EpCAM captured by beads. White arrow depicts free beads unattached to cells (scale bar: 40 µm). The same was also observed in Panel B (scale bar: 40 µm) (representative data from four repeats)

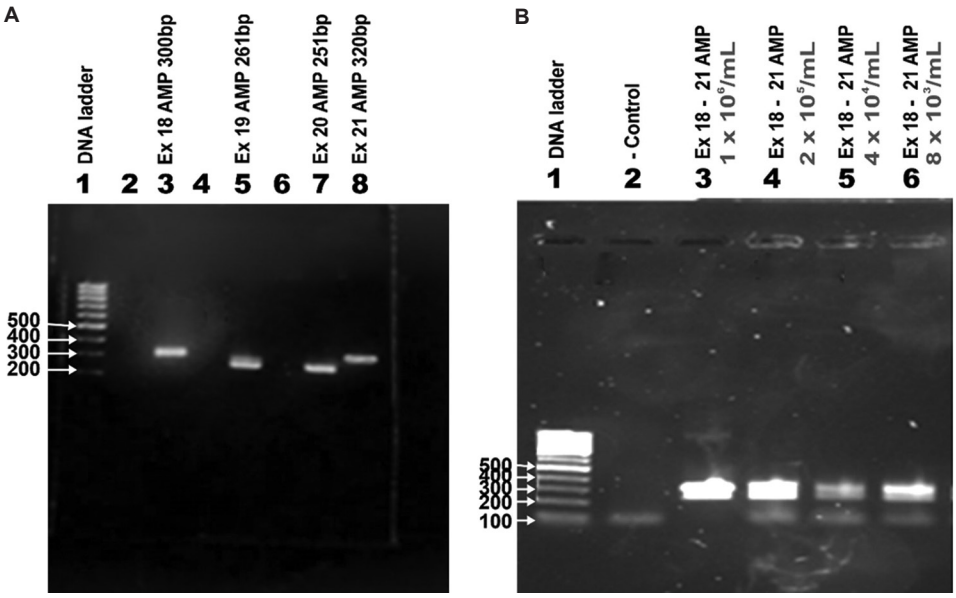

Figure 3. Validation experiments to show that isolated epithelial cell adhesion molecule-positive cells can be used for downstream polymerase chain reaction (PCR) analysis. DNA from isolated PC-9 cell lines had exons 18 – 21 of the *EGFR* gene amplified individually and then as a multiplex. (A) Lane 1, DNA ladder; lane 2, negative control; lanes 3, 5, 7, and 8 show amplification of exons 18, 19, 20, and 21 regions individually from a single sample. (B) Lane 1, DNA ladder; lane 2, negative control; lanes 3, 4, 5, and 6 show the multiplex PCR of amplification of exons 18, 19, 20, and 21 of PC-9 cell lines spiked at the following concentrations (1×10^6, 2×10^5, 4×10^4, 8×10^3 cells/mL) in media and thereafter isolated from the media using the device (representative data from 3 repeats).

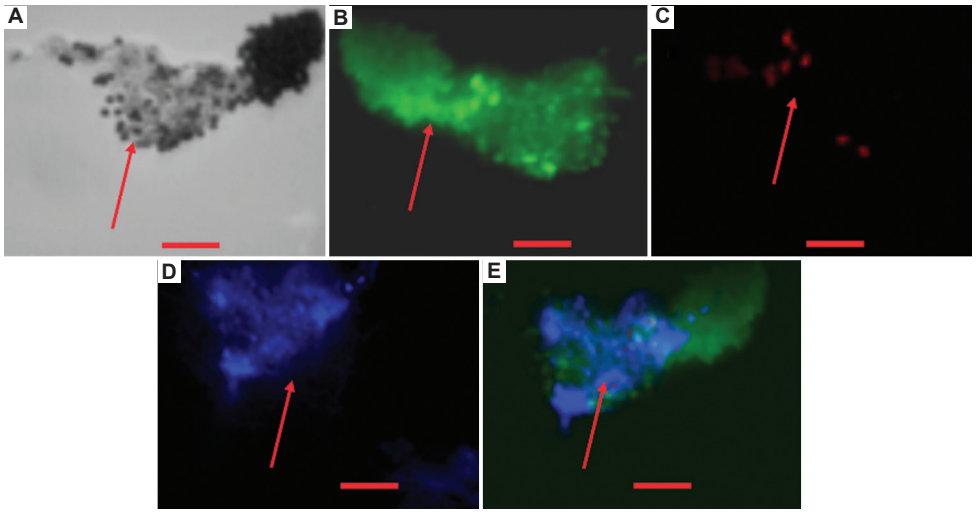

Figure 4. Immunostaining of cells isolated from the blood of patients with non-small cell lung cancer (scale bar: 40 μm for panels A-E). (A) brightfield imaging of epithelial cell adhesion molecule-positive cells surrounded by magnetic beads, isolated from blood of patients. (B) cells staining positive for a fluorescein-conjugated pan-cytokeratin monoclonal antibody (BioLegend, USA). (C) few cells staining positive with a rhodamine-conjugated anti-CD45 antibody. (D) 4,6-Diamidino-2-phenylindole-stained-nuclei of cells. (E) Merged image of the three fluorescence channels (representative data from three independent repeats).

3.4. Detection of mutations in CTCs

Among the 38 patients who had their CTC-enriched samples analyzed for *EGFR* mutations, 30 (79%) presented with a mutation. Mutated events (expressed in %) among all mutations detected ranged from 1% to 55% (Table 2). Exon 19 had the highest number of genetic variants seen in 26 patients (87%), with E746_A750 delELREA deletions being the most common variation. Exon 21 had the highest number of point mutations with 7 (23%), whereas exon 20 had the highest number of single nucleotide variants/single

Table 1. Clinicopathological characteristics of NSCLC patients who underwent CTC analysis for mutations

	N (%)
Age	
Mean age	65.4 years
Range	47 – 76 years
Sex	
Male	20 (52.6)
Female	18 (47.3)
Smoking status	
Unknown	21 (55.3)
Yes	13 (34.2)
No	4 (10.5)
Type of NSCLC	
Adenocarcinoma	36 (94.7)
Large cell	1 (2.6)
Other	1 (2.6)
Stage of cancer	
IIb	2 (5.2)
IIIA	5 (13.1)
IIIb	7 (18.4)
IV	24 (59.3)
Metastatic regions*	
Lung	10 (26.3)
Lymph nodes	2 (5.3)
Bone	9 (23.7)
Liver	1 (2.6)
Kidney	1 (2.6)
Pleura	4 (10.5)
Brain	2 (5.3)
Neck	1 (2.6)
Mediastinal	9 (23.7)
PDL1 expression ≥1%	30 (78.9)
Other mutations	
ROS1	1 (2.6)

*One tumor had metastasized to two different regions.
Abbreviations: NSCLC: Non-small cell lung cancer; CTC: Circulating tumor cell; PDL1: Programmed death ligand 1; ROS1: ROS proto-oncogene 1 receptor tyrosine kinase.

nucleotide polymorphisms at 4 (13%) (Figure 6A and B). The most frequent point mutations on exon 21 were L858R and P848L (3 occurrences, 8%) (**Figure 6B**). Among the CTC samples analyzed, 9 (31%) had mixed *EGFR* mutations. All patients with a mixed mutation had an exon 19 deletion (Table 3). This study also detected uncommon mutations of varied clinical significance (Table 4).

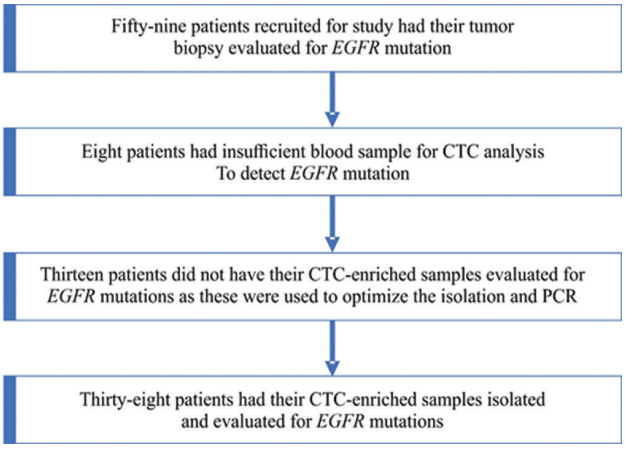

Figure 5. Flow chart for patient recruitment
Abbreviations: *EGFR*: Epidermal growth factor receptor; CTC: Circulating tumor cell.

3.5. Comparison of mutations detected using NGS in CTCs with cobas® EGFR mutation testing of matched tumor biopsies

Similarities and differences in *EGFR* mutations detected in CTCs and matched tumor biopsies were evaluated. Our results (Table 5 and Figure 7) showed that significantly more mutations were detected in the CTCs than in the matched biopsies (Fisher's exact test, $P = 0.0173$; Figure 7). *EGFR* mutations were diagnosed in 30 CTC samples, whereas only 4 matched biopsies (Patients: 17, 27, 40, and 59; Table 5) showed a mutation. The current study showed that NGS analysis of isolated CTCs had a higher likelihood ratio of detecting mutations than did the cobas® EGFR analysis of the tumor biopsy (Fisher's exact test, likelihood ratio 1.855; Figure 7). In addition, only one of the four tissue biopsy samples positive for an *EGFR* mutation had a similar mutation result obtained from its matched CTC sample (Patient 27; Table 5). The mutations obtained from the other three biopsy samples were discordant from their matched CTC samples; however, for the eight CTC samples with no *EGFR* mutation detected, the same lack of mutations was observed in the matched tumor biopsies (Table 5 and Figure 7).

4. Discussion

The present study was designed to describe the ability of a new immunomagnetic microfluidic device to isolate CTCs for downstream analysis. In addition, the clinical potential for the use of CTCs as a sample matrix for the diagnosis of *EGFR* mutations in NSCLC was also demonstrated.

The results in Table 2 show that among the 38 patients whose CTC samples were evaluated for *EGFR* mutations, 30 (79%) contained at least one mutation. This differs

Table 2. *EGFR* mutations detected in CTCs

Patient ID	Exon	Mutations	Percentage of mutations detected using NGS	No. of CTCs counted
1		WT		
3		**WT**		
8		**WT**		
9	**21**	**L858R**	**ND**	**NR**
10		**WT**		
11		**WT**		
13	**19**	**Deletion** (E746_A750delELREA)	**ND**	**NR**
14		**WT**		
15	**19**	**Deletion** (E746_A750delELREA)	**ND**	**NR**
16	**19**	**Deletion** (E746_A750delELREA)	**ND**	**NR**
17	**19**	**Deletion** (E746_A750delELREA)	**ND**	**NR**
	21	**L858R**	**ND**	**NR**
19	**19**	**Deletion** (E746_A750delELREA)	**ND**	**NR**
20	**21**	**L858R**	**ND**	**NR**
21		**WT**		
22		**WT**		
24	**19** **20**	**Deletion** (E746_A750delELREA) C.2389T > A	**2.01** **1.3**	**7**
25	**20**	**c. 2375T > C**	**0.6**	**4**
26	**19**	**Deletion** (E746_A750delELREA)	**55.39**	**402**
27	**19**	**Deletion** (E746_A750delELREA)	**6.18**	**59**
28	**19**	**Deletion** (E746_A750delELREA)	**3.4**	**3**
	19	**P733L**	**1.74**	
29	**21**	**c. 2573T > G**	**0.76**	**23**
30	**19**	**Deletion** (E746_A750delELREA)	**3.19**	**35**
	19	**P733L**	**1.13**	
	20	**c. 2318A ≥ G**	**0.58**	
31	**19**	**Deletion** (E746_A750delELREA)	**1.4**	**81**
	20	**R766H**	**1.2**	
	20	**c. 2327G > A, c. 2375T > C**	**0.75, 0.55**	
32	**19**	**Deletion** (E746_A750delELREA)	**2.4**	
	19	**P735S G696E**	**1.2**	
	18	**L703P**	**1.01**	
	21	**P848L**	**0.86**	
34	**19**	**Deletion** (E746_A750delELREA)	**0.65**	
	21,19	**c. 2573T > c, c. 2281G > A**	**0.55, 1.21**	
36	**19**	**Deletion** (E746_A750delELREA)	**2.65**	
	19	**c. 2281G ≥ A**	**1.17**	
37	**19** **18**	**Deletion** (E746_A750delELREA) c. 2123A > G	**2.65** **0.83**	**90**
38	**19**	**Deletion** (E746_A750delELREA)	**6.11**	**32**
39	**19**	**Deletion** (E746_A750delELREA)	**5.83**	**11**
	20	**T790M**	**0.83**	

(cont'd...)

Table 2. ***(Continued)***

Patient ID	Exon	Mutations	Percentage of mutations detected using NGS	No. of CTCs counted
	18	**N700D**	**0.69**	
40	**19**	**Deletion** (E746_A750delELREA) **L841P**	**19.67** **1.4**	**5**
43	**19**	**Deletion** (E746_A750delELREA)	**2.43**	**41**
	21	**V843L**	**0.53**	
53	**19**	**Deletion** (E746_A750delELREA)	**8.47**	
54	**19**	**Deletion** (E746_A750delELREA)	**1.11**	
55	**19**	**Deletion** (E746_A750delELREA)	**14.34**	
56	**19** **20**	**Deletion** (E746_A750delELREA) **R776H**	**3.26** **1.34**	**300**
57	**19**	**Deletion** (E746_A750delELREA)	**32.64**	**115**
58	**19**	**Deletion** (E746_A750delELREA)	**22.85**	**505**
59	**19**	**Deletion** (E746_A750delELREA)	**1.66**	**52**

Abbreviations: WT: Wild-type (negative for an *EGFR* mutation); ND: Not done; NR: No result; *EGFR*: Epidermal growth factor receptor; CTCs: Circulating tumor cells; NGS: Next-generation sequencing. The bold values represent mutations/deletions on exons 18-21 of the EGFR gene.

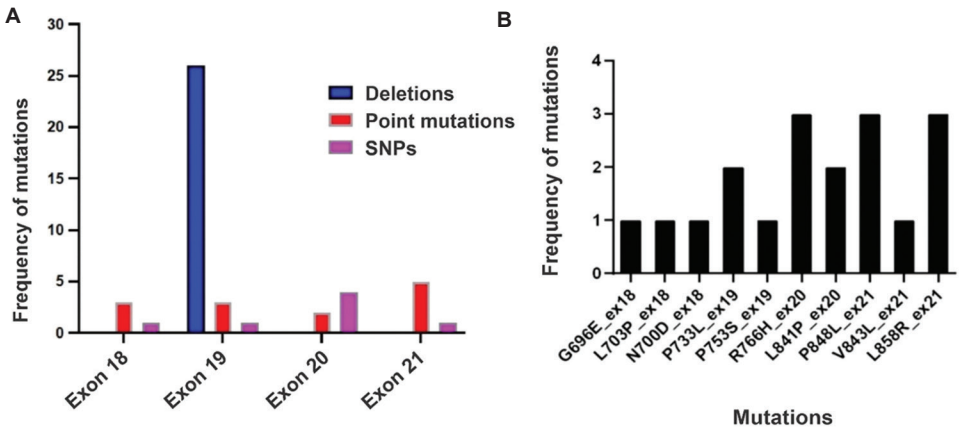

Figure 6. Number of mutations and single nucleotide polymorphism obtained in exons 18, 19, 20, and 21 of epithelial cell adhesion molecule (EpCAM)-positive circulating tumor cells (CTCs) obtained from patients with non-small cell lung cancer (NSCLC). A, frequency of aberrations on exons 18 – 21 of EpCAM-positive CTCs obtained from NSCLC patients; B, Frequency of point mutations on the exons.

from previously reported incidences of *EGFR* mutations in exons 18 – 21 among Caucasian patients with NSCLC, with most of these studies reporting an incidence between 10% and 40%.[48,49] The disparity in results may be attributed to the sample matrix used, as this study used CTCs, whereas most other studies used tissue biopsies. CTCs represent a culmination of events occurring at the initiation of the malignancy and during metastasis, whereas tissue biopsies represent molecular events only occurring at the primary site of a malignancy.[50] Second, most published works employed PCR for the analysis of mutations (e.g., amplification refractory mutation analysis, restriction fragment polymorphism mutant allele detection, and locked PCR clamping, all of which look for specific mutations).[51] Here, NGS had been used to scan the whole *EGFR* gene for mutations. Mao *et al.*[52] evaluated the frequency of *EGFR* mutations in 21,324 patients with NSCLC admitted to oncology clinics in China using PCR, Sanger sequencing, and NGS and reported that most of the mutations were detected using NGS (71%), whereas 45% and 35% of them were detected using Sanger sequencing and qPCR, respectively. The use of NGS in this Chinese study reported *EGFR* mutation rates that were very similar to those observed in the current, small-scale, cohort.

Furthermore, it has been reported that NGS has a relatively high false discovery rate of between 0.1% and 1%.[53] Overestimation of mutations by NGS has been linked to

sequence artifacts attributed, at least in part, to the low quality of DNA, the clonal amplification of DNA strands, and/or the need for a relatively high number of PCR cycles due to the low quantity of starting material, as well as chemical modifications that occur during the NGS workflow.[54] However, in this study, CTCs were analyzed for mutations at a read depth of ×10,000, which has been recommended as best practice in the literature.[55,56] Therefore, we believe this reduces the probability of methodological errors. In contrast, some studies have suggested that because CTCs comprise a very small percentage of the total tumor mass, any mutation detected with sufficient coverage should be recognized as a potentially important clinical variant.[55] The incidence of *EGFR* mutations using the CTC + NGS matrix will be investigated in further studies using a microfluidic device (designed by our group) capable of single-cell RNASeq.

Table 3. Patients with mixed *EGFR* mutations

Patient No.	Exon	Mutations
28	19	**Deletion (E746_A750delELREA), P733L**
30	19	**Deletion (E746_A750delELREA), P733L, L841P**
31	19 20	**Deletion (E746_A750delELREA)** **R776H**
32	19 21 18	**Deletion (E746_A750delELREA), P753S** **P848L** **G696E, L703P**
39	19 20 18	**Deletion (E746_A750delELREA)** **T790M** **N700D**
43	19 21	**Deletion (E746_A750delELREA)** **V843I**
17	19 21	**Deletion (E746_A750delELREA)** **L858R**
40	19 20	**Deletion (E746_A750delELREA)** **L841P, P848L**
56	20	**R766H**

Abbreviation: *EGFR*: Epidermal growth factor receptor. The bold values represent mutations/deletions on exons 18-21 of the EGFR gene.

The results from mutational profiling of the CTCs are generally consistent with the exon 18 – 21 mutational profile of patients with NSCLC using tumor biopsy. For example, 86.7% of CTC-enriched samples analyzed in this study had a deletion in exon 19 (E746_A750delELREA), which is consistent with published literature reporting that around 80% – 90% of NSCLC patients with an *EGFR* mutation have either this deletion or an exon 21 L858R mutation.[2,8,12,28] However, the frequency of mixed mutations was much higher in the current study (30%) than that in others, with Caucasian patients having reported frequencies of 5% – 7% for mixed mutations.[56-58] The difference in frequency rates may be attributed to the relatively small sample size of the present study or, as described earlier, the disparity in analysis techniques. To the best of our knowledge, the only study that has employed NGS for mutational analysis of *EGFR* mutations in CTCs obtained from NSCLC reported an incidence of 13% for mixed mutation for a cohort of 37 patients enrolled for the study,[59] which was higher than that reported in other studies using PCR-based mutation analysis on tumor biopsies but was still lower than that observed in the current study.[51,52]

The higher incidence reported in our study than in the study by Marchetti *et al.*[59] may be due to the difference in isolation technique for CTCs. The latter used CELL SEARCH for isolating CTCs, whereas the present study used a novel immunomagnetic microfluidic device. CELL SEARCH technique has been associated with a CTC yield of ≤60% and a purity of around 50%.[40] Perhaps the CTCs isolated were not totally representative of the molecular events in the malignant environment, which may have resulted in an under reporting of mutations present. Preliminary validation studies on the yield and purity of the device in this study using cell lines expressing varying levels of EpCAM spiked in media and blood have shown that the device isolates EpCAM-positive cells with a yield of ≥65% and purity of ≥95% (unpublished data from our laboratory). The yield and purity of CTCs isolated using the device may have contributed to the increased mixed mutation incidence reported in the current study.

Table 4. Rare *EGFR* single nucleotide variants identified in patient CTC-enriched samples using NGS

Patient ID	Nomenclature (SNV)	Exon	RS no.	Amino acid	Comments
31,34	**c. 2375T>C**	**20**	**132563568**	**L792P**	Pathogenic mutation of somatic origin[10,31,60]
24	**c. 2389T>A**	**20**	**1057519861**	**C797S**	Pathogenic mutation of somatic origin associated with drug resistance[10,31,62]
31	**c. 2327G>A**	**20**	**483352806**	**R509H**	Germline origin of uncertain significance[31,60,62]
30	**c. 2318A>G**	**20**	**121913432**	**H506R**	Somatic likely pathogenic[60]
37	**c. 2123A>G**	**18**	**144932466**	**K708R**	Somatic likely pathogenic[63,65]
34	**c. 2281G>A**	**19**	**121913418**	**D761N**	Somatic likely pathogenic[57,62-64]
29	**c. 2573T>G**	**21**	**121434568**	**L591R**	Somatic associated with a drug response[31,60,61]

Abbreviations: CTC: Circulating tumor cell; *EGFR*: Epidermal growth factor receptor; NGS: Next-generation sequencing. The bold values represent mutations/deletions on exons 18-21 of the EGFR gene.

Table 5. Comparison of mutations detected in CTCs and tumor biopsies

Patient ID	Exon EGFR CTC	*EGFR* mutation in CTCs	Percentage of mutations detected using NGS	Exon *EGFR* biopsy	*EGFR* mutation tumor biopsy	Matched (Yes or No)
1		**WT**			**WT**	Yes
3		**WT**			**WT**	Yes
8		**WT**			**WT**	Yes
9	**21**	**L858R**			**WT**	No
10		**WT**			**WT**	Yes
11		**WT**			**WT**	Yes
13	**19**	**Deletion** (E746_A750delELREA)			**WT**	No
14		**WT**			**WT**	Yes
15	**19**	**Deletion** (E746_A750delELREA)			**WT**	No
16	**19**	**Deletion** (E746_A750delELREA)			**WT**	No
17	**19**	**Deletion** (E746_A750delELREA)		20	**Exon 20 insertion**	No
	21	**L858R**				
19	**19**	**Deletion** (E746_A750delELREA)			**WT**	No
20	**21**	**L858R**			**WT**	No
21		**WT**			**WT**	Yes
22		**WT**			**WT**	Yes
24	**19** **20**	**Deletion** (E746_A750delELREA), c. 2389T>A	**2.01** **1.3**		**WT**	No
25	**20**	**c. 2375T>C**	**0.6**		**WT**	No
26	**19**	**Deletion** (E746_A750delELREA)	**55.39**		**WT**	No
27	**19**	**Deletion** (E746_A750delELREA)	**6.18**	19	**Exon 19 del**	Yes
28	**19**	**Deletion** (E746_A750delELREA)	**3.4**		**WT**	No
	19	**P733L**	**1.74**			
29	**21**	**c. 2573T>c**	**0.76**		**WT**	No
30	**19**	**Deletion** (E746_A750delELREA)	**3.19**		**WT**	No
	19	**P733L**	**1.13**			
	20	**c2318A≥G**	**0.58**			
31	**19** **20**	**Deletion** (E746_A750delELREA) c. 2375T>c, c. 2327>G	**1.4** **0.55, 0.75**		**WT**	No
	20	**R766H**	**1.2**			
	20	**c2441T≥A**	**0.75**			
32	**19**	**Deletion** (E746_A750delELREA)	**2.4**		**WT**	No
	19	**P735S**	**1.2**			
	18	**L703P**	**1.01**			
	21	**P848L**	**0.86**			
34	**19** **19**	**Deletion** (E746_A750delELREA) c. 2281G>A	**0.65** **0.58**		**WT**	No
	21	**c2573T≥c**	**0.55**			
36	**19**	**Deletion** (E746_A750delELREA)	**2.65**		**WT**	No
	19	**c2281G≥A**	**1.17**			
37	**19** **18**	**Deletion** (E746_A750delELREA) c. 2123A>G	**2.65** **0.83**		**WT**	No
38	**19**	**Deletion** (E746_A750delELREA)	**6.11**		**WT**	No

(cont'd...)

Table 5. ***(Continued)***

Patient ID	Exon EGFR CTC	*EGFR* mutation in CTCs	Percentage of mutations detected using NGS	Exon *EGFR* biopsy	EGFR mutation tumor biopsy	Matched (Yes or No)
39	**19**	**Deletion** (E746_A750delELREA)	**5.83**		**WT**	No
	20	**T790M**	**0.83**			
	18	**N700D**	**0.69**			
40	**19** **20**	**Deletion** (E746_A750delELREA) L841P	**19.67** **1.4**	21	**L858R**	No
43	**19**	**Deletion** (E746_A750delELREA)	**2.43**		**WT**	No
	21	**V843L**	**0.53**			
53	**19**	**Deletion** (E746_A750delELREA)	**8.47**		**WT**	No
54	**19**	**Deletion** (E746_A750delELREA)	**1.11**		**WT**	No
55	**19**	**Deletion** (E746_A750delELREA)	**14.34**		**WT**	No
56	**19** **20**	**Deletion** (E746_A750delELREA) R766H	**3.26** **0.92**		**WT**	No
57	**19**	**Deletion** (E746_A750delELREA)	**32.64**		**WT**	No
58	**19**	**Deletion** (E746_A750delELREA)	**22.85**		**WT**	No
59	**19**	**Deletion** (E746_A750delELREA)	**1.66**	21	**L858R**	No

Abbreviations: WT: Wild-type (no mutation detected); CTCs: Circulating tumor cells; *EGFR*: Epidermal growth factor receptor; NGS: Next-generation sequencing. The bold values represent mutations/deletions on exons 18-21 of the EGFR gene.

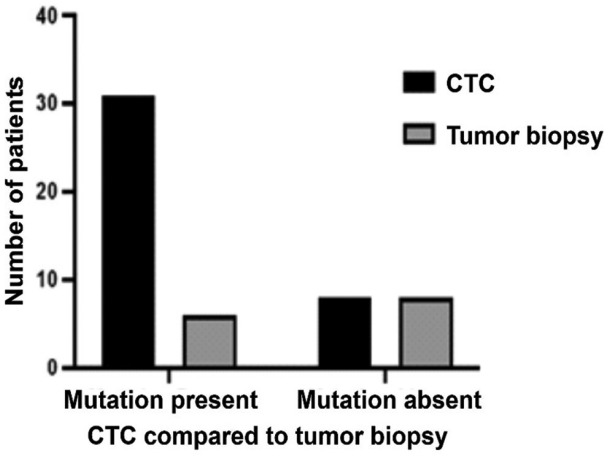

Figure 7. Epidermal growth factor receptor (*EGFR*) mutations present and/or absent in matched circulating tumor cells (CTCs) and tumor biopsy samples. Statistical analysis from Fisher's exact test showing that the CTC + next-generation sequencing (NGS) sampling technique detected significantly more mutations ($P = 0.0173$) than cobas® EGFR mutation analysis of the matched tumor biopsy. In addition, the likelihood of detecting mutations in *EGFR* from the CTC + NGS matrix was 1.855 (Fisher's exact test).

Rare mutations detected in the present study (e.g., L792P, C797S, H506R, and L591R) have been reported previously in NSCLC with clinical correlations. L591R has been associated with drug response to gefitinib,[31,60-63] and C795S mutation has been linked to resistance to osimertinib.[31,62] D761N mutation has been reported in biopsies of NSCLC and colon and prostate cancers, and has also been associated with partial response to erlotinib.[57,62-64] A K708R mutation has been reported in ovarian cancers where it has been associated with abnormal phosphorylation of AKT and ERK.[62] It has also been reported once in a Chinese study[65] but never in Caucasian populations; thus, the response of this mutation to TKIs is not clear. These patient-specific point mutations will potentially offer new insights into treatment responses and should be analyzed in a large cohort.

The marked disparity in the number of mutations detected in CTCs (78.95%) when compared to matched tumor biopsies (13.3%) reported in the current study differs from that published in other studies. Most of these studies report a similarity in the number of mutations in matched CTC and tumor biopsy samples,[38,39,46] whereas some studies have reported a lower number of mutations in CTC samples than in matched tumor biopsy samples.[37,66,67] However, both groups of studies highlighted above only analyzed CTCs for *EGFR* mutations in patients whose tumor biopsy samples were positive for a mutation. Conversely, the current study analyzed samples "blindly," i.e., CTC samples were analyzed for mutations from all patients before the mutational status of the biopsy was known, rather than only focusing on patients with a biopsy containing mutations.

The discordance in the type of mutations observed in three of the four patients who had a mutation detected in both CTCs and biopsies was similar to that observed in

the two previous studies.[66,67] Both these studies proposed that the discordance in mutations between CTCs and tumor biopsies may be due to the heterogeneity of tumors as discussed above. The apparent discordance in mutations observed in CTCs and tumor biopsies will need to be further investigated using approaches for CTC isolation and downstream analysis that properly define mutations derived from single cells or multiple cell clones.

5. Conclusion

The results obtained from this study suggest that the new microfluidic device described can be used to isolate CTCs for downstream mutational analysis of *EGFR* mutations. The device was able to isolate EpCAM-expressing PC-9 cell lines and EpCAM-positive CTCs from media and blood, respectively, with the isolated EpCAM-positive cells having been successfully analyzed for mutations in the *EGFR* gene. The mutational profile obtained from CTCs for the recruited patients has positive clinical implications as it indicates that a single blood draw may be able to provide a snapshot of molecular events in a malignancy from initiation to metastasis. However, the current study is limited by the sample size. Hence, it is our intention to carry out further studies in a larger cohort to better evaluate the utility of this technology and make the necessary modifications for translation into clinical practice. Furthermore, we intend to analyze different methods for the genomic analysis of CTCs to define mutations in single cells.

Acknowledgments

The authors are grateful to colleagues at the STAB VIDA, Portugal for help with next-generation sequencing, Dr. Alex Iles (Department of Chemistry, University of Hull) for chip design and manufacture, and Dr. Emmanuel Nna of Biosystem Laboratories, Bedford, United Kingdom for help with bioinformatics analysis.

Funding

The travel and consumable costs related to this work were supported by the EU/Marie Curie Lung Card project (No. 734790) and Yorkshire Cancer Research (H395).

Conflict of interest

The authors declare that they have no competing interests.

Author contributions

Conceptualization: John Greenman, Micheal J. Lind
Formal analysis: Nkeiruka O. Ogidi, John Greenman
Investigation: Nkeiruka O. Ogidi
Methodology: Nkeiruka O. Ogidi, John Greenman
Writing – original draft: Nkeiruka O. Ogidi
Writing – review & editing: Micheal J. Lind, John Greenman

Ethics approval and consent to participate

The study adhered to the REMARK guidelines. It was conducted at the Queens Centre for Oncology and Hematology, Castle Hill Hospital, Hull, in collaboration with the Centres for Biomedicine and Clinical Sciences at the University of Hull, United Kingdom. The North East-Newcastle & North Tyneside Local Research Ethics Committee approved this study (REC13/NE/0242). In accordance with the Declaration of Helsinki, informed consent was obtained in written form from all participants.

Consent for publication

Consent in written form was obtained from participants in the study to publish their data.

Availability of data

The data from this study can be obtained on request from the senior author, Prof J. Greenman.

References

1. Rajadurai P, Yap NY, Mohamed Yousoof SB, Cheah YK. Mutational profiling of lung cancer using next generation sequencing: A Malaysian real-world clinical diagnostic experience. *J Mol Pathol*. 2023;4(1):31-43.

   doi: 10.3390/jmp4010004

2. Petrelli F, Borgonovo K, Cabiddu M, Barni S. Efficacy of EGFR tyrosine kinase inhibitors in patients with EGFR-mutated non-small-cell lung cancer: A meta-analysis of 13 randomized trials. *Clin Lung Cancer*. 2012;13(2):107-114.

   doi: 10.1016/j.cllc.2011.08.005

3. Petrella F, Rizzo S, Attili I, *et al*. Stage III non-small-cell lung cancer: An overview of treatment options. *Curr Oncol*. 2023;30(3):3160-3175.

   doi: 10.3390/curroncol30030239

4. Robichaux JP, Le X, Vijayan RSK, *et al*. Structure-based classification predicts drug response in EGFR-mutant NSCLC. *Nature*. 2021;597(7878):732-737.

   doi: 10.1038/s41586-021-03898-1

5. Sasaki A, Fujimoto Y., Inada T, *et al*. Efficacy of tyrosine kinase inhibitors in patients with non-small-cell lung cancer with performance status 4: A case series and review of the literature. *J Med Case Rep*. 202;17(1):410.

   doi: 10.1186/s13256-023-04145-z

6. Russo A, Franchina T, Ricciardi G, Picciotto M, Adamo V. Heterogeneous responses to epidermal growth factor receptor (EGFR) tyrosine kinase inhibitors (TKIs) in

patients with uncommon EGFR mutations: New insights and future perspectives in this complex clinical scenario. *Int J Mol Sci*. 2019;20:1431.

doi: 10.3390/ijms20061431

7. Janne P, Wang X, Sociniski M, *et al*. Randomized phase II trial of erlotinib alone or with carboplatin and paclitaxel in patients who were never or light former smokers with advanced lung adenocarcinoma. CALGB30406 trial. *J Clin Oncol*. 2012;30(17):2063-2069.

doi: 10.1200/JCO.2011.40.1315

8. Wu YL, Zhou C, Liam CK, *et al*. First-line erlotinib versus gemcitabine/cisplatin in patients with advanced EGFR mutation-positive non-small-cell lung cancer: Analyses from the phase III, randomized, open-label, ENSURE study. *Ann Oncol*. 2015;26:1883-1889.

doi: 10.1093/annonc/mdv270

9. Yang JC, Wu YL, Schuler M, *et al*. Afatinib versus cisplatin-based chemotherapy for EGFR mutation-positive lung adenocarcinoma (LUX-Lung 3 and LUX-Lung 6): Analysis of overall survival data from two randomized, phase 3 trials. *Lancet Oncol*. 2015;16(2):141-151.

doi: 10.1016/S1470-2045(14)71173-8

10. Costa DB. Kinase inhibitor-responsive genotypes in EGFR mutated lung adenocarcinomas: Moving past common point mutations or indels into uncommon kinase domain duplications and rearrangements. *Transl Lung Cancer Res*. 2016;5:331-337.

doi: 10.21037/tlcr.2016.06.04

11. Xu H, Yang G, Li W, *et al*. EGFR exon 18 mutations in advanced non-small cell lung cancer: A real-world study on diverse treatment patterns and clinical outcomes. *Front Oncol*. 2021;11:713483.

doi: 10.3389/fonc.2021.713483

12. Rossi S, D'Argento E, Basso M, *et al*. Different EGFR gene mutations in exon 18, 19 and 21 as prognostic and predictive markers in NSCLC: A single institution analysis. *Mol Diagn Ther*. 2016;20(1):55-63.

doi: 10.1007/s40291-015-0176-x

13. Klughammer B, Brugger W, Cappuzzo F, *et al*. Examining treatment outcomes with erlotinib in patients with advanced non-small cell lung cancer whose tumors harbor uncommon EGFR mutations. *J Thorac Oncol*. 2016;11:545-555.

doi: 10.1016/j.jtho.2015.12.107

14. Zhang T, Wan B, Zhao Y, *et al*. Treatment of uncommon EGFR mutations in non-small cell lung cancer: New evidence and treatment. *Transl Lung Cancer Res*. 2019;8(3):302-316.

doi: 10.21037/tlcr.2019.04.12

15. Brindel A, Althakafi W, Barritault M, *et al*. Uncommon EGFR mutations in lung adenocarcinoma: Features and response to tyrosine kinase inhibitors. *Transl Lung Cancer Res*. 2020;12(9):4643-4650.

doi: 10.21037/jtd-19-3790

16. Byeon S, Kim Y, Lim SW, *et al*. Clinical outcomes of EGFR exon 20 insertion mutations in advanced non-small cell lung cancer in Korea. *Cancer Res Treat*. 2019;51(2):623-631.

doi: 10.4143/crt.2018.151

17. Ou SI, Lin HM, Hong JL, *et al*. Real-world response and outcomes in patients with NSCLC with *EGFR* exon 20 insertion mutations. *JTO Clin Res Rep*. 2023;4(10):100558.

doi: 10.1016/j.jtocrr.2023.100558

18. Vaclova T, Grazini U, Ward L, *et al*. Clinical impact of subclonal EGFR T790M mutations in advanced-stage EGFR-mutant non-small-cell lung cancers. *Nat Commun*. 2021;12:1780.

doi: 10.1038/s41467-021-22057-8

19. Bencze E, Bogos K, Kohánka A, *et al*. EGFR T790M mutation detection in patients with non-small cell lung cancer after first line EGFR TKI therapy: Summary of results in a three-year period and a comparison of commercially available detection kits. *Pathol Oncol Res*. 2022;28:1610607.

doi: 10.3389/pore.2022.1610607

20. Zhao Z, Li L, Wang Z, Duan J, Bai H, Wang J. The status of the EGFR T790M mutation is associated with the clinical benefits of osimertinib treatment in non-small cell lung cancer patients: A meta-analysis. *J Cancer*. 2020;11(11):3106-3113.

doi: 10.7150/jca.38411

21. Araki T, Kanda S, Horinouchi H, Ohe Y. Current treatment strategies for *EGFR*-mutated non-small cell lung cancer: From first line to beyond osimertinib resistance. *Jpn J Clin Oncol*. 2023;53(7):547-561.

doi: 10.1093/jjco/hyad052

22. Attili I, Passaro A, Pisapia P, Malapelle U, de Marinis F. Uncommon EGFR compound mutations in non-small cell lung cancer (NSCLC): A systematic review of available evidence. *Curr Oncol*. 2022;29(1):255-266.

doi: 10.3390/curroncol29010024

23. Kalemkerian GP, Narula N, Kennedy EB, *et al*. Molecular testing guideline for the selection of patients with lung cancer for treatment with targeted tyrosine kinase inhibitors: American Society of Clinical Oncology Endorsement of the College of American Pathologists/International Association for the Study of Lung Cancer/Association for Molecular Pathology Clinical Practice Guideline Update. *J Clin Oncol*. 2018;36:911-919.

doi: 10.1200/JCO.2017.76.7293

24. Ettinger DS, Aisner DL, Wood DE, *et al*. NCCN guidelines® insights: Non-small cell lung cancer. *J Natl Compr Canc Netw*. 2023;21(4):340-350.

doi: 10.6004/jnccn.2023.0020

25. Lindeman NI, Cagle PT, Aisner DL, *et al*. Updated molecular testing guideline for the selection of lung cancer patients for treatment with targeted tyrosine kinase inhibitors: Guideline from the College of American Pathologists, the International Association for the Study of Lung Cancer, and the Association for Molecular Pathology. *Arch Pathol Lab Med*. 2018;142:321-346.

doi: 10.5858/arpa.2017-0388-CP

26. Martins I, Ribeiro IP, Jorge J, *et al*. Liquid biopsies: Applications for cancer diagnosis and monitoring. *Genes* (*Basel*). 2021;12(3):349.

doi: 10.3390/genes12030349

27. Kim MH, Kim SH, Lee MK, Eom JS. Recent advances in adjuvant therapy for non-small-cell lung cancer. *Tuberc Respir Dis* (*Seoul*). 2024;87(1):31-39.

doi: 10.4046/trd.2023.0085

28. Malapelle U, Muscarella LA, Pisapia P, Rossi A. Targeting emerging molecular alterations in the treatment of non-small cell lung cancer: Current challenges and the way forward. *Expert Opin Investig Drugs*. 2020;29(4):363-372.

doi: 10.1080/13543784.2020.1732922

29. Jamal-Hanjani M, Wilson GA, McGranahan N, *et al*. Tracking the evolution of non-small-cell lung cancer. *N Engl J Med*. 2017;376(22):2109-2121.

doi: 10.1056/NEJMoa1616288

30. Tan AC, Tan DSW. Targeted therapies for lung cancer patients with oncogenic driver molecular alterations. *J Clin Oncol*. 2022;40(6):611-625.

doi: 10.1200/JCO.21.01626

31. Thress KS, Brant R, Carr TH, *et al.* EGFR mutation detection in ctDNA from NSCLC patient plasma: A cross-platform comparison of leading technologies to support the clinical development of AZD9291. *Lung Cancer*. 2015;90(3):509-515.

doi: 10.1016/j.lungcan.2015.10.004

32. Roldan Ruiz J, Fuentes Gago MG, Chinchilla Tabora LM, *et al.* The impact of liquid biopsies positive for EGFR mutations on overall survival in non-small cell lung cancer patients. *Diagnostics* (*Basel*). 2023;13(14):2347.

doi: 10.3390/diagnostics13142347

33. Rossi E, Aieta M, Tartarone A, *et al*. A fully automated assay to detect the expression of pan-cytokeratins and of EML4-ALK fusion protein in circulating tumour cells (CTCs) predicts outcome of non-small cell lung cancer (NSCLC) patients. *Transl Lung Cancer Res*. 2021;10(1):80-92.

doi: 10.21037/tlcr-20-855

34. Nguyen TNA, Huang PS, Chu PY, Hseih CH, Wu MH. Recent progress in enhanced cancer diagnosis, prognosis, and monitoring using a combined analysis of the number of Circulating Tumor Cells (CTCs) and other clinical parameters. *Cancers* (*Basel*). 2023;15(22):5372.

doi: 10.3390/cancers15225372

35. Lawrence R, Watters M, Davies CR, Pantel K, Lu YJ. Circulating tumour cells for early detection of clinically relevant cancer. *Nat Rev Clin Oncol*. 2023;20(7):487-500.

doi: 10.1038/s41571-023-00781-y

36. Auwal A, Matakabbir Hassan M, Haque Prony TU, *et al*. Clinical significance of genomic sequencing of Circulating Tumour Cells (CTCs) in cancer. *J Liq Biopsy*. 2024;3:100135.

doi: 10.1016/j.jlb;2023.100135

37. Punnoose E, Atwal S, Liu W, *et al*. Evaluation of circulating tumor cells and circulating tumor DNA in non-small cell lung cancer: Association with clinical endpoints in a phase II clinical trial of pertuzumab and erlotinib. *Clin Cancer Res*. 2012;18(8):2391-2401.

doi: 10.1158/1078-0432.CCR-11-3148

38. Sunderesan TK, Sequist LV, Haymach JV, *et al*. Detection of T790M, the acquired resistance EGFR mutation, by tumor biopsy versus noninvasive blood-based analyses. *Clin Cancer Res*. 2016;22(5):1103-1110.

doi: 10.1158/1078-0432ccr-15-1031

39. Keup C, Kimmig, R,Kasimir-Bauer S. Multimodality in liquid biopsy: Does a combination uncover insights undetectable in individual blood analytes? *J Lab Med*. 2022;46(4):255-264.

doi: 10.1515/labmed-2022-0009

40. Nagrath S, Sequist L, Maheswaran S, *et al*. Isolation of rare circulating tumour cells in cancer patients by microchip technology. *Nature*. 2007;450(7173):1235-1239.

doi: 10.1038/nature06385

41. Rushton A, Nteliopoulos G, Shaw J, Coombes RS. A review of circulating tumour cell enrichment technologies. *Cancers* (*Basel*). 2021;13(5):970.

doi: 10.3390/cancers13050970

42. Habili Z, Al chama W, Saab R, Kadara H, Kharaiche ML. Circulatory tumour cell detection technologies and clinical utility: Challenges and opportunities. *Cancers* (*Basel*). 2020;12(7):1930.

doi: 10.3390/cancers12071930

43. Ring A, Nguyen-Sträuli BD, Wicki A, Aceto N. Biology, vulnerabilities and clinical applications of circulating tumour cells. *Nat Rev Cancer*. 2023;23:95-111.

doi: 10.1038/s41568-022-00536-4

44. Tran HH, Wu W, Lee NY. Ethanol and UV-assisted instantaneous bonding of PMMA assemblies and tuning in bonding reversibility. *Sens Actuators B Chem*. 2013;181:955-962.

doi: 10.1016/j.snb.2012.11.060

45. Tsuji K, Hayata Y. *Riken Cell Bank*; 1989. Available from: https://www.cellbank.brc@rike.jp/rcb4455.pc9 [Last accessed on 2024 May 22].

46. Maheswaran S, Sequist LV, Nagrath S, *et al*. Detection of mutations in EGFR in circulating lung-cancer cells. *N Engl J Med*. 2008;359(4):366-377.

doi: 10.1056/NEJMoa0800668

47. Ju S, Chen C, Zhang J, *et al*. Detection of circulating tumor cells: Opportunities and challenges. *Biomark Res*. 2022;10(1):58.

doi: 10.1186/s40364-022-00403-2

48. Zhang YL, Yuan JQ, Wang KF, *et al*. The prevalence of EGFR mutation in patients with non-small cell lung cancer: A systematic review and meta-analysis. *Oncotarget*. 2016;7(48):78985-78993.

doi: 10.18632/oncotarget.12587

49. Graham RP, Treece AL, Lindeman NI, *et al*. Worldwide frequency of commonly detected EGFR mutations. *Arch Pathol Lab Med*. 2018;142(2):163-167.

doi: 10.5858/arpa.2016-0579-cp

50. Alix-Panabières C, Pantel K. Liquid biopsy: From discovery to clinical implementation. *Mol Oncol*. 2021;15(6):1617-1621.

doi: 10.1002/1878-0261.12997

51. Midha A, Dearden S, McCormack R. EGFR mutation incidence in non-small-cell lung cancer of adenocarcinoma histology: A systematic review and global map by ethnicity (mutMapII). *Am J Cancer Res*. 2015;5(9):2892-2911.

52. Mao L, Zhao W, Li X, *et al*. Mutation spectrum of EGFR from 21,324 Chinese patients with non-small cell lung cancer (NSCLC) successfully tested by multiple methods in a CAP-accredited laboratory. *Pathol Oncol Res*. 2021;27:602726.

doi: 10.3389/pore.2021.602726

53. Petrackova A, Vasinek M, Sedlarikova L, *et al*. Standardization of sequencing coverage depth in NGS: Recommendation for detection of clonal and subclonal mutations in cancer diagnostics. *Front Oncol*. 2019;9:851.

doi: 10.3389/fonc.2019.00851

54. Singh RR. Next-generation sequencing in high-sensitive detection of mutations in tumours: Challenges, advances, and applications. *J Mol Diagn*. 2020;22(8):994-1007.

doi: 10.1016/j.jmoldx.2020.04.213

55. Jennings LJ, Arcila ME, Corless C, *et al*. Guidelines for validation of next-generation sequencing-based oncology panels: A joint consensus recommendation of the association for molecular pathology and college of American Pathologist. *J Mol Diagn*. 2017;19(3):341-365.

doi: 10.1016/j.jmoldx.2017.01.011

56. Heitzer E, Auer M, Gasch C, *et al*. Complex tumor genomes inferred from single circulating tumor cells by array-CGH and next-generation sequencing. *Cancer Res*. 2013;73(10):2965-2975.

doi: 10.1158/0008-5472.CAN-12-4140

57. Evans M, O'Sullivan B, Smith M, *et al*. Large-scale EGFR mutation testing in clinical practice: Analysis of a series of 18,920 Non-small cell lung cancer cases. *Pathol Oncol Res*. 2019;25(4):1401-1409.

doi: 10.1007/s12253-018-0460-2

58. Martin J, Lehmann A, Klauschen F, *et al*. Clinical impact of rare and compound mutations of epidermal growth factor receptor in patients with non-small-cell lung cancer. *Clin Lung Cancer*. 2019;20(5):350-362.e4.

doi: 10.1016/j.cllc.2019.04.012

59. Marchetti A, Del Grammastro M, Felicioni L, *et al*. Assessment of EGFR mutations in circulating tumor cell preparations from NSCLC patients by next generation sequencing: Toward a real-time liquid biopsy for treatment. *PLoS One*. 2014;9(8):e103883.

doi: 10.1371/journal.pone.0103883

60. Lynch TJ, Bell DW, Sordella R, *et al*. Activating mutations in the epidermal growth factor receptor underlying responsiveness of non-small-cell lung cancer to gefitinib. *N Engl J Med*. 2004;350(21):2129-2139.

doi: 10.1056/NEJMoa040938

61. Tsao MS, Sakurada A, Cutz JC, *et al*. Erlotinib in lung cancer - molecular and clinical predictors of outcome. *N Engl J Med*. 2005;353(2):133-144.

doi: 10.1056/NEJMoa050736

62. González Manzano R, Martínez Navarro E, Eugenieva E, Fernandez Morejon FJ, Farre J, Brugaralos A. A novel EGFR nonsense mutation in a non-small-cell lung cancer (NSCLC) patient who did not derive any clinical benefit with combination chemotherapy and erlotinib. *Clin Transl Oncol*. 2008;10(7):442-444.

doi: 10.1007/s12094-008-0229-2

63. Fu M, Zhang W, Shan L, *et al*. Mutation status of somatic EGFR and KRAS genes in Chinese patients with prostate cancer (PCa). *Virchows Arch*. 2014;464(5):575-581.

doi: 10.1007/s00428-014-1566-x

64. Kim H, Kim BH, Lee D, Shin E. Genomic alterations in signet ring and mucinous patterned colorectal carcinoma. *Pathol Res Pract*. 2019;215(10):152566.

doi: 10.1016/j.prp.2019.152566

65. Tanaka Y, Terai Y, Tanabe A, *et al*. Prognostic effect of epidermal growth factor receptor gene mutations and the aberrant phosphorylation of Akt and ERK in ovarian cancer. *Cancer Biol Ther*. 2011;11(1):50-57.

doi: 10.4161/cbt.11.1.13877

66. Zhang Q, Nong J, Wang J, *et al*. Isolation of circulatory tumour cells and detection of EGFR mutations in patients with non-small-cell lung cancer. *Oncol Lett*. 2019;17(4):3799-3807.

doi: 10.3892/ol.2019.10016

67. Ntzifa A, Kotsakis A, Georgoulias V, Lianidou E. Detection of EGFR mutations in plasma cfDNA and paired CTCs of NSCLC patients before and after osimertinib therapy using crystal digital PCR. *Cancers* (*Basel*). 2021;13(11):2736.

doi: 10.3390/cancers 13112736

Appendix

Appendix A1. Consent Form

Title: Developing an evidence-based system to facilitate the predictive assessment and optimization of older adults under investigation

Hull and East Yorkshire Hospitals NHS
NHS Trust

UNIVERSITY OF Hull

PATIENT CONSENT FORM

Peripheral blood detection of EGFR status in lung cancer patients

Name of Researcher: <insert name>

Chief Investigator: Professor M. J. Lind

Patient Study Number:

Please INITIAL boxes; do not tick

1. I confirm that I have read and understood the information sheet (Version 1.2 15/03/2017) for the above study. ☐
2. I confirm that I have had the opportunity to consider the information, ask questions and have had these answered satisfactorily. ☐
3. I understand that my participation is voluntary and that I am free to withdraw from the study at any time without giving any reason, and without my medical care or legal rights being affected. ☐
4. I give permission for a 10 ml blood sample to be taken for research purposes. ☐

   For selected individuals only:
   a. I give permission for an additional 5 ml blood sample to be taken for research purposes. ☐
5. I give permission, if I am given the tablet treatment, for a further 10 ml blood sample to be taken if the treatment stops working. ☐
6. I agree to my sample being sent to the University of Hull for the analysis to be performed. ☐
7. I agree to my medical records being looked at for research purposes by an authorised member of the research team to record my EGFR status results. ☐

(cont'd...)

Appendix A1. (*Continued*)

8. I understand that to enable the study to be properly monitored and regulated, relevant sections of my medical records and data collected during the study may be looked at by members of the research team, and individuals from the Sponsor (Hull and East Yorkshire Hospitals NHS Trust) or possibly from regulatory authorities. I give permission for these individuals to have access to my medical records to view sections that are relevant to my taking part in this study. ☐

9. I understand that the information will be used for medical research only and that I will not be identified in any way in the analysis and reporting of the results. ☐

10. I understand that the information collected about me will be used to support other research in the future, and may be shared anonymously with other researchers. ☐

11. I agree to my General Practitioner being informed of my participation in the study. ☐

12. I agree to take part in the above research study. ☐

.....	.....	.....
Name of patient (BLOCK CAPITALS)	Signature	Date

.....	.....	.....
Name of person taking consent (if different from researcher) (BLOCK CAPITALS)	Signature	Date

.....	.....	.....
Name of researcher (BLOCK CAPITALS)	Signature	Date

When completed: 1 copy for patient, 1 copy to be kept in medical notes, 1 original for researcher site file.

ACCSCIENCE PUBLISHING

Tumor Discovery

ORIGINAL RESEARCH ARTICLE

A 12-year analysis of presentation, histopathological features, high-risk factors, and survival in retinoblastoma patients undergoing primary enucleation at a tertiary eye care center in Bangladesh

Soma Rani Roy[1]*, Rahat Anjum[2], and Sujit Kumar Biswas[3]

[1]Department of Oculoplasty and Ocular Oncology, Chittagong Eye Infirmary, Chattogram, Bangladesh

[2]Department of Histopathology and Cytopathology, Apollo Imperial Hospitals, Chattogram, Bangladesh

[3]Department of Cornea, Chittagong Eye Infirmary, Chattogram, Bangladesh

Abstract

Retinoblastoma is the most common primary intraocular malignancy in children, with approximately 100% survival rates in higher-income countries. The outcomes of retinoblastoma depend on factors such as disease presentation, treatment access, histopathological high-risk factors, and national income level. This retrospective study analyzed 12-year data (2012 – 2023), including presentation, histopathological features, histopathological high-risk factors, and survival outcomes, of 78 retinoblastoma patients who had undergone primary enucleation at a tertiary eye center in Bangladesh. The overall median age was 33 months, with a slightly older median age among females (35 months) and a mild male predominance. The mean symptom duration was 5.68 ± 3.56 months, with earlier presentation in male patients. The most common presenting sign was leukocoria (70.5%), followed by red eye (20.5%). Combined endophytic and exophytic tumor growth (36%) and poor differentiation (44.9%) were prevalent. High-risk factors were present in 84.6% of patients, with massive choroidal invasion (41%) and retrolaminar optic nerve invasion (38.5%) being the most frequent. Approximately 57.7% of patients solely underwent enucleation, and 27% of children died, yielding an overall survival rate of 69.23%. The findings of this study suggest that multiple high-risk factors are often present in advanced tumors, posing challenges in management and increasing the risk for metastasis. Efforts to improve outcomes should focus on raising awareness, promoting early presentation, enhancing histopathological reporting, and developing specialized human resources.

Keywords: Primary enucleation; Delayed presentation; Advanced tumor; Histopathological high-risk factor; Massive choroidal invasion; Retrolaminar invasion

***Corresponding author:**
Soma Rani Roy
(soma@ctgeyeinfirmary.info)

Citation: Roy SR, Anjum R, Biswas SK. A 12-year analysis of presentation, histopathological features, high-risk factors, and survival in retinoblastoma patients undergoing primary enucleation at a tertiary eye care center in Bangladesh. *Tumor Discov*. 2024;3(4):4336.
doi: 10.36922/td.4336

Received: July 26, 2024

Accepted: October 12, 2024

Published Online: November 21, 2024

1. Introduction

Retinoblastoma (RB) is the most common primary intraocular malignancy in children, accounting for approximately 11% of cancers diagnosed in the first year of life globally.[1]

The incidence rate is 1 in 16,000 – 18,000 live births,[1] with approximately 9,000 new cases added each year worldwide.[2] In the United States, the number of new cases detected annually has remained steady at 200 – 300 over the past 40 years. In contrast, higher incidence rates have been reported in Europe.[3,4] The median age at diagnosis is 18 months globally, although it is 14 months in high-income countries and 30.5 months in low-income countries.[5] In unilateral retinoblastoma, the median age of diagnosis was 35 and 19.7 months in low- and high-income countries, respectively, where's 22.9 and 8.1 months, respectively, in bilateral cases.[5]

RB presentation and outcomes vary by age at diagnosis and national income level. Leukocoria is the most common presenting sign, followed by strabismus; these early presentations are more typical in high-income countries. In contrast, advanced presentations, such as proptosis, orbital cellulitis, and red eye, are more frequent in low-income countries.[5]

The tumor is typically confined to the globe at early stages, supporting both ocular salvage and higher survival rates. Treatment modalities include enucleation, chemotherapy (various routes), radiotherapy, and local therapy. A multidisciplinary team approach, involving ophthalmologists (ocular oncologists, retina specialists, pediatric ophthalmologists, and/or oculoplastic surgeons), pediatric oncologists, radiation oncologists, anesthesiologists, histopathologists, ocularists, counselors, and social support groups, is the current standard for RB treatment. In early cases, treatment may be limited to local therapy and chemotherapy. However, in delayed cases, treatment options include enucleation or neoadjuvant chemotherapy, followed by secondary enucleation of the worse eye, with or without radiotherapy. Some patients may require adjuvant chemotherapy with or without radiotherapy following primary enucleation. For all enucleated cases, histopathology plays a crucial role in guiding the management plan, making histopathological examination of enucleated eyes mandatory. The presence of histopathological high-risk factors (HRFs) can provide early indications of local recurrence, distant metastases, tumor progression, and overall prognosis. Key HRFs associated with metastases include invasion of the choroid, sclera, extrascleral space, and optic nerve (beyond the lamina cribrosa, total optic nerve, or cut end).[6] Expert histopathologists are thus integral to the multidisciplinary management team for RB.

In high-income and upper-middle–income countries, the 3-year survival rates are approximately 99% and 91%, respectively, with high ocular salvage rates and fewer reported HRFs.[7,8] In contrast, lower-middle-income and low-income countries report survival rates of 77% and 40%, respectively, with significantly higher rates of mortality and metastasis.[7] Most of these low- and lower-middle-income countries are underdeveloped or developing countries in Asia and Africa, where delayed presentation complicates the management of RB cases. Factors such as delayed presentation, inadequate treatment facilities, lack of trained ocular oncologists and histopathologists, and financial challenges contribute to higher child mortality rates in these regions.

This study aimed to describe the pattern of HRFs following primary enucleation in patients with RB as well as the presentation, histopathological features, and survival outcomes of these patients in a lower-middle-income country in Southeast Asia.

2. Methods

2.1. Study design

This hospital-based retrospective study analyzed patients with RB who had undergone primary enucleation. Data were collected from the Orbit, Oculoplasty, and Ocular Oncology Department of Chittagong Eye Infirmary, a tertiary eye care and retinoblastoma center in Bangladesh. Data from January 2012 to December 2023 were included, covering a 12-year period. A total of 96 children with RB who had undergone primary enucleation were classified as Groups D and E. Among these, 78 patients were included in the study.

2.2. Tumor grading, staging, and HRFs

Tumors were classified according to the International Intraocular Retinoblastoma Classification (IIRC) for intraocular tumors and the International Retinoblastoma Staging System (IRSS) for extraocular tumors based on data obtained from medical records, evaluation under anesthesia (EUA), imaging, and histopathology reports.[9,10] The IIRC categorizes tumors as follows:

- Group A: Tumor ≤3 mm, ≥3 mm from the fovea, and ≥1.5 mm from the optic disc, with no seeding.
- Group B: Tumor of any size or location (except Group A criteria), without vitreous or subretinal seeding, and with subretinal fluid ≤5 mm from the tumor margin.
- Group C: Discrete tumor of any size or site with focal vitreous or subretinal seeding and subretinal fluid up to one quadrant.
- Group D: Diffuse vitreous or subretinal seeding and/or extensive endophytic (tumor spread toward vitreous cavity) or exophytic disease (subretinal tumor spread), with seeding exceeding Group C criteria and retinal detachment of more than one quadrant.

- Group E: Massive tumor causing anatomical or functional eye destruction, with neovascular glaucoma, intraocular tumor (Figure 1), aseptic orbital cellulitis, tumor touching the lens, tumor anterior to the anterior vitreous face, diffuse infiltrating tumor, and phthisis or pre-phthisis.

The IRSS categorizes patients with RB into five stages (Stages 0 – IV). Stage 0 includes patients treated conservatively, whereas Stage I includes cases with enucleated eyes in which resection is histologically complete. Stage II indicates a microscopic residual tumor in an enucleated eye. Stage III includes regional extension, subdivided into overt orbital disease and pre-auricular or cervical lymph node involvement. Stage IV involves distant metastatic disease and is further divided into two subgroups: (a) Hematogenous metastasis, with a single lesion or multiple lesions, and (b) central nervous system (CNS) extension, with pre-chiasmatic lesions, CNS mass, or leptomeningeal disease.

Data were collected about age, sex, laterality of the tumor, presenting symptoms, duration of symptoms, tumor grading and staging, tumor growth pattern, tumor differentiation, histopathological HRFs, adjuvant treatments received, follow-up period, and survival. Of the 96 patients, data from 78 patients were completed and included in the study. Patients who had undergone secondary enucleation or had incomplete data were excluded from the study.

The criteria for histopathological HRFs were selected based on various global studies conducted to identify and evaluate HRFs, including anterior chamber, iris, trabecular meshwork, Schlemm's canal, ciliary body, choroid (massive, defined as >3 mm choroidal invasion in thickness or width),

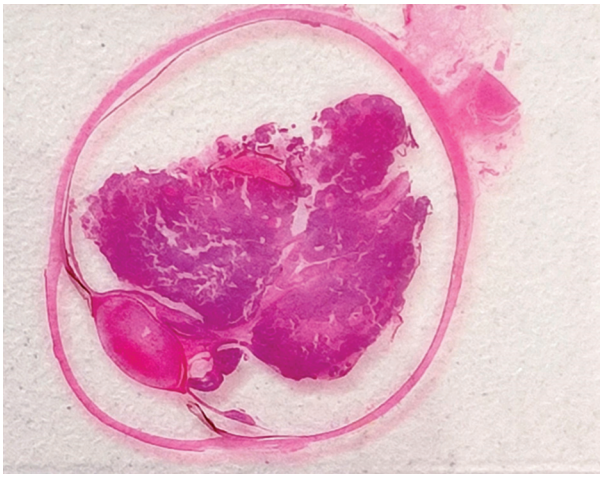

Figure 1. Cross-sectional view of the eyeball through pupil-optic nerve section, showing intraocular retinoblastoma stained with eosin and hematoxylin (H&E) stain, occupying >50% of the globe

sclera, extraocular structures, and retrolaminar optic nerve (including the cut end).[11,12] Tumor differentiation was classified according to rosette formation into well-differentiated (presence of Homer–Wright, Flexner–Wintersteiner, and/or fleurettes), moderately differentiated (presence of Homer–Wright and/or Flexner–Wintersteiner rosettes), poorly differentiated (presence of only Homer–Wright rosettes), and undifferentiated (absence of rosettes/fleurettes).[13]

This retrospective study posed no risk to individual patient identification; therefore, institutional review board (IRB) approval was obtained. The study was approved by the local IRB and conducted in accordance with the principles of the 2013 Declaration of Helsinki.

2.3. Statistical analysis

Statistical analyses were conducted using SPSS 16, with a $P < 0.05$ considered statistically significant. Differences between the male and female symptom duration were analyzed using an independent t-test. Survival rates were calculated using Kaplan–Meier survival analysis.

3. Results

3.1. Demographic profile

The mean age of the patients was 34.56 ± 19.90 months, ranging from 3 months to 90 months. Males had a mean age of 35.90 ± 20.95 months, whereas females had a mean age of 32.91 ± 19.68 months. The overall median age was 33 months (30 months for males and 35 months for females). The lowest and highest presenting ages in males were 3 months and 90 months, respectively, whereas those in females were 4 months and 84 months, respectively. Approximately 62% of the children were older than 24 months, with 31% aged 13–24 months and 8% being younger than 12 months. The most frequent presenting age was 24 months.

Male patients accounted for 55.1% (n = 43) of the included patients, whereas females accounted for 44.9% (n = 35) of the total patients, yielding a male-to-female ratio of 1.4:1 (Table 1). Approximately 90% of cases were unilateral RB. Among bilaterally presenting cases (10.3%, n = 8), only one child underwent bilateral enucleation (1.3%). Left-eye involvement was more common (53.6%). Only 2.6% (n = 2) had a family history of RB, presenting as unilateral cases.

3.2. Lag time with clinical presentation

The mean duration from symptom onset to diagnosis was 5.89 ± 4.30 months (5.68 ± 3.56 months for males and 5.94 ± 5.09 months for females), with a p-value of 0.9, indicating no statistical significance (Table 2). Symptom durations

Table 1. Demographic profile of patients (*n*=78)

Characteristics	Number of patients (n, %)
Age	Months
Median	33
Mean	34.56±19.90
Range	3–90
Male median age	30
Male mean age	35.90±20.95
Female median age	35
Female mean age	32.91±19.68
Presentation (months)	Number
0 – 12	06 (7.69%)
13 – 24	24 (30.77%)
>24	48 (61.54%)
Most frequent presenting age	24 months
Gender	
Male	43 (55.1%)
Female	35 (44.9%)
Laterality of presentation (*n*=78)	
Unilateral	70 (89.7%)
Bilateral	08 (10.25%)
Enucleation (*n*=78, eye=79)	
Right	36 (46.2%)
Left	41 (52.6%)
Both	01 (1.3%)
Positive family history	
Yes	02 (2.6%)
No	76 (97.4%)

Table 2. Presentation of the patients

Clinical feature[a]	Number
Leukocoria	55 (70.5%)
Red eye	16 (20.5%)
Squint	10 (12.8%)
Proptosis	05 (6.4%)
Painful blind eye	03 (3.8%)
Decreased vision	03 (3.8%)
Phthisis bulbi	01 (1.3%)
Duration of the symptom	**Months**
Range of duration	0.5 – 24
Mean	5.89±4.30
Mean duration for males	5.68±3.56
Mean duration for females	5.94±5.09
P value	0.966
IIRC underwent enucleation (*n*=78; eye=79)	
Group D	06 (7.7%)
Group E	73 (93.6%)

[a]A single child may present with multiple signs. One patient required bilateral enucleation, initially presenting with Group E in one eye and Group C in the other. After the first enucleation, the patient was lost to follow-up and later returned with recurrence.

ranged from 15 days to 14 months in males and 30 days to 24 months in females. The most common presenting symptom was leukocoria (70.5%, n = 55), followed by red eye (20.5%, n = 16) and squint (12.8%, n = 10; Table 2). One patient (1.3%) presented with phthisis bulbi, an atypical presentation.

Most cases of primary enucleation were classified as Group E RB (93.6%), with 8% as Group D RB (Table 2). Among the eight bilateral cases, six were classified as Groups E and B, and two cases as Groups D and C. The distribution of stages was as follows: 58% (n = 45) in Stage I, 33% (n = 26) in Stage II, and 5% (n = 4) in Stage III.

3.3. Histopathological features and HRFs

Most patients (36%, n = 28) exhibited both endophytic and exophytic growth patterns, followed by exophytic growth patterns (30.8%, n = 24). Approximately 26% (n = 20) of cases were endophytic tumors, while diffuse infiltrating patterns were the least common at 7.7% (n = 6). Poor differentiation (44.9%, n = 35) was the most prevalent tumor differentiation. Well-differentiated tumors were observed in approximately 26% (n = 20) of cases, followed by moderately differentiated tumors in 24% (n = 19) of cases (Figure 2). Undifferentiated tumors were the least frequent, occurring in only 5% (n = 4; Table 3). Among 78 patients, 84.6% (n = 66) were HRF-positive, while 15.4% (n = 12) had tumors confined to the retina. Tumor invasion was more prevalent in the posterior segment than in the anterior segment. In cases of anterior segment invasion, the anterior chamber was the most commonly infiltrated (19.2%, n = 15), followed by the ciliary body (16.7%, n = 13) and iris (15.4%, n = 12). Both the trabecular meshwork and Schlemm's canal were infiltrated in 11.5% (n = 9) of cases each. Regarding posterior segment involvement, massive choroidal invasion occurred in 41% (n = 32) of cases, which was higher than optic nerve invasion at 38.5% (n = 30), and 26.9% (n = 21) of cases showed retrolaminar invasion without optic nerve transection. Choroidal (focal) and optic nerve (pre-laminar and laminar) invasion were observed in 20.6% (n = 16) of cases. Among cases with scleral invasion (15.4%, n = 12), 10.2% (n = 8) showed inner-third invasion, while 5.1% (n = 4) had a full-thickness invasion. Beyond intraocular invasion, extrascleral invasion was found in 6.4% (n = 5) of cases, and orbital invasion was identified in 3.8% (n = 3; Table 3).

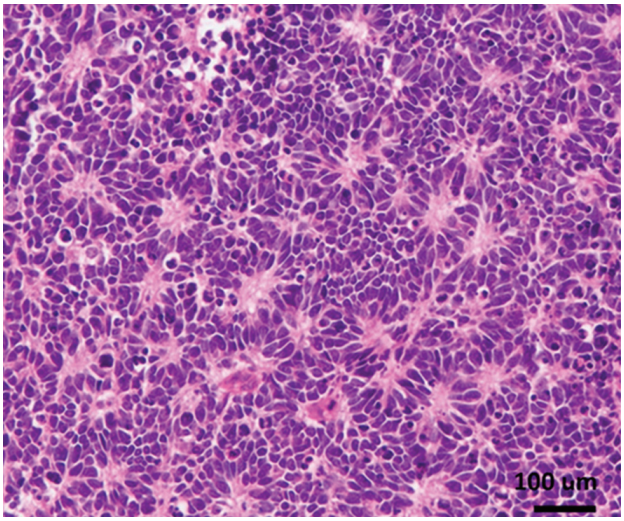

Figure 2. Slide of well-differentiated retinoblastoma showing rosettes in eosin and hematoxylin (H&E) at 20× magnification. Scale bar: 100 µm

Table 3. Histopathological characteristics

	Number (%)
Growth pattern (*n*=78)	
Endophytic	20 (25.6)
Exophytic	24 (30.8)
Both	28 (36)
Diffuse infiltrating	06 (7.7)
Tumor differentiation (*n*=78)	
Well-differentiated	20 (25.6)
Moderate differentiated	19 (24.4)
Poorly differentiated	35 (44.9)
Undifferentiated	04 (5.1)
Histopathological high-risk factor present (*n*=78, HRF=66)	
Anterior chamber infiltration	15 (19.2)
Iris infiltration	12 (15.4)
Trabecular meshwork	09 (11.5)
Schlemm's canal	09 (11.5)
Ciliary body	13 (16.7)
Choroid (massive)	32 (41)
Optic nerve (retrolaminar)	
Post-laminar optic nerve invasion (PLONI)	21 (26.9)
Transection of the optic nerve	09 (11.5)
Combined choroid (focal) and optic nerve (pre-laminar and laminar)	16 (20.6)
Sclera	12 (15.4)
Extra scleral	05 (6.4)
Orbital	03 (3.9)

Note: More than one histopathological feature was present in one enucleated eye.

3.4. Treatment and outcomes

In addition to primary enucleation, 33.3% (n = 26) of patients received adjuvant chemotherapy only and 5.1% (n = 4) received both adjuvant chemotherapy and external beam radiotherapy (EBRT). A total of 57.7% (n = 45) of patients underwent primary enucleation without additional chemotherapy due to the absence of histopathological HRFs and 3.8% (n = 3) refused further treatment. Approximately 27% (n = 21) of children died and 3.8% (n = 3) were lost to follow-up (presumed deceased). Approximately 23.07% (n = 18) of patients died due to metastasis and 3.8% (n = 3) died suddenly of unknown causes. The overall survival rate was 69.23%. The follow-up period after enucleation ranged from 6 months to 12 years.

4. Discussion

RB is a rare but deadly malignant tumor, accounting for 2%–3% of all childhood cancers.[14] Intraocular malignant tumors are most commonly malignant melanomas, with RB as the second most prevalent tumor. Approximately 200 years ago, this tumor was recognized as a distinct disease from fungal infection by James Wardrop of Scotland in 1809.[1] Since then, various diagnostic methods and treatments have been developed. Recently, a multidisciplinary team management approach has been initiated in several centers to treat this tumor and ensure comprehensive care under one umbrella. Due to advancements in diagnosis and management in higher-income countries, survival and globe salvage rates are nearly 100%.[7] Prognoses and survival rates are less favorable in low- and middle-income countries.

Literature indicates that approximately 90% of RB cases are from underdeveloped countries, where patients typically present with advanced intraocular RB or even more severe disease.[15] In these cases, life-saving measures often take priority over globe-salvaging treatments. Many institutions lack the resources and trained personnel required for chemotherapy, radiotherapy, and imaging. In addition, families of patients with RB may lack access to information, face financial challenges, and hold traditional beliefs that complicate timely treatment, leading to high rates of enucleation. A global study by the Retinoblastoma Outcome Study Group, which included 260 centers from 149 countries, reported that enucleation was the only available treatment in all centers, with intravenous chemotherapy available in 254 centers, while low-income countries had access to intra-arterial chemotherapy.[7]

In the present study, the median age of presentation was 33 months, with female patients presenting at an older age than male patients (35 vs. 30 months). According to

the Global Retinoblastoma Presentation Study, the median age of presentation in unilateral cases was 27.1 months, whereas that in bilateral cases was 12.3 months.[5] The median age of unilateral RB presentation in lower-middle-income countries in the same study was 29.1 months. Our country, a lower-middle-income country in Southeast Asia, demonstrated a higher median age of presentation than that mentioned in the above study. The age of presentation may vary based on geographical location.[5] A recent study on RB presentation across Asia reported a median age of 25 months, although it did not differentiate between unilateral and bilateral cases.[16] This study also found that the mean age was higher in South Asian countries than in other Asian regions. In the present study, the mean age of presentation was 34.56 ± 19.90 months, whereas in Southeast Asia, the median age was 30 months.[17] A study from India showed a mean age range of 29 to 33 months,[18] whereas two separate studies from Pakistan reported means of 36 ± 28 months and 42 ± 20 months. In the present study, 8% of children were under 1 year of age, 30% were between 1 and 2 years, and 61% were above 2 years; this distribution was similar to an Indian study where 38% of children were under 2 years and 62% were above 2 years of age.[19]

Leukocoria was the most common presenting symptom in our study (70.5%), followed by red eye (20.5%). However, global studies and most other studies have reported squint as the second most common presentation.[5,15] In a Chinese study, leukocoria was reported in 67% of cases, followed by red eye in 13%.[17] An Eastern Indian study noted proptosis as the second most common sign after leukocoria, whereas squint was most frequent in other parts of India.[15,20] In the present study, late-stage symptoms, such as proptosis, were observed in 6.4% of cases, and a painful blind eye was observed in 3.8% of cases. High-income countries, such as the United States and South Korea, have much lower rates of proptosis (0.5% and 1.4%, respectively), whereas this rate is significantly higher in lower-middle-income countries, such as Nigeria (44.2%), Pakistan (52.8%), and Thailand (26.7%).[18]

Our study observed a male predominance in sex distribution (55.1% male, n = 43; 44.9% female, n = 35), with a male-to-female ratio of 1.4:1,[1]; this finding was in line with the 1.52:1 ratio observed in India and 1.8:1 noted in Asian children by the Global Retinoblastoma Study Group.[21]

In this study, 10.25% (n = 8) of patients presented with bilateral RB, with only 2.6% (n = 2) of patients reporting a family history. While heritable RB often presents bilaterally, approximately 12%–15% of unilateral cases may also have a heritable basis and can later manifest bilaterally.[1] One of our patients required bilateral enucleation after initially presenting unilaterally, subsequently returning after a year with advanced RB in the previously healthy eye. The family refused neoadjuvant chemotherapy, and enucleation was performed to save the child's life.

The time from symptom onset to diagnosis is critical for RB outcomes. A symptom duration of 6 months or more correlates with poorer outcomes. In the present study, the mean symptom duration was 5.89 ± 4.30 months. A recent study reported an average lag time of 5 months for Asian children, 8 months in Southeast Asia, and 15 months in Central Asia.[16] In sub-Saharan Africa, this period is 8.5 months.[22] A prolonged lag time results in more advanced tumors, increasing enucleation rates.[16] Lag time exceeding 1 year is associated with a higher risk of extraocular invasion and increased mortality.[23] Factors contributing to longer lag times include poverty, reliance on traditional medicine, limited awareness of treatment options, lack of awareness among local pediatricians and physicians, and geographic distance from treatment facilities. In our study, we identified poverty, belief in traditional medicine, and lack of treatment facilities and physician awareness as the main factors causing delays.

In the present study, 93.7% (n = 73) of patients presented with advanced RB in Group E whereas only 7% presented with advanced RB in Group D. A review of 2,697 Indian patients with RB showed that 73 – 78% presented with advanced RB (Groups D and E).[19,20,24] Another study on 700 Chinese children undergoing primary enucleation showed that 60% of patients in Group E and 32% in Group D presented with advanced RB.[17] Among 78 study patients, 58% were in Stage I, 33% in Stage II, and 5% in Stage III. Accurate diagnosis and treatment planning for RB necessitate grouping and staging, which requires EUA before initiating treatment. Although RB is primarily diagnosed clinically, additional imaging such as ultrasonography (B-scan), computed tomography (CT), and magnetic resonance (MRI) may be necessary for unclear cases and to assess tumor extension. In this study, all patients underwent EUA and B-scans; most had CT scans, while only a few had MRIs, primarily due to constraints. As CT scans present a risk of radiation exposure, which is particularly concerning for hereditary RB cases, MRI is generally preferred. However, the high cost of MRI made it inaccessible for most of our patients. The Global Retinoblastoma Presentation Study demonstrated a preference for imaging based on income level: lower-income countries performed CT scans in 69% of cases, MRIs in 16.5%, and both modalities in 17.1%. In contrast, high-income countries performed CT scans in only 0.6% of cases, MRIs in 34.7%, and both imaging types in 64.7%.[7]

For unilateral RB, enucleation is often the preferred treatment in many underdeveloped and developing countries across Africa, Asia, and Latin America, where alternative treatment options are limited. According to the Global Retinoblastoma Outcome Study, enucleation rates are high, with 73.6% in low-income countries and 67.1% in lower-middle-income countries.[7] This study also indicated that this rate in higher-income countries is 59.7%. Reddy *et al.*[25] reported that in Southeast Asia, enucleation is the primary treatment for Group D and E unilateral RB. Following enucleation, it is essential to send the enucleated eye for histopathological evaluation, and the optic nerve length should be >10 mm. Research suggests that a 10 – 15-mm long section of the optic nerve is curative in 85 – 90% of non-heritable unilateral cases without extraocular involvement.[26]

Histopathological analysis plays a crucial role in identifying HRFs, as the subsequent treatment plan, metastasis risk, and survival outcomes depend on HRF presence. Older presentation age (>24 months) is associated with HRFs.[8,26,27] In the present study, the median age at presentation was 33 months, with 62% (n = 48) of patients above 24 months. Among 78 patients who underwent primary enucleation, 84.61% (n = 66) patients were HRF-positive, supporting findings from previous studies.[8,26,27] In the present study, a mixed endophytic and exophytic growth pattern was observed in 36% of cases, followed by an exophytic pattern in 30%. Tumor differentiation revealed a higher prevalence of poorly differentiated tumors (44.9%, n = 35). Asian studies also indicate a trend toward poorly differentiated tumors in older patients (over 24 months).[8,28]

Delayed presentation contributed to multiple HRFs in 37.6% (n = 27) of our patients, aligning with rates reported by Kaliki *et al.* (38%) and Yaqoob *et al.* (35.2%).[8,29] Most patients had massive choroidal invasion (41%, n = 32; Figure 3), which is documented in the literature with prevalence ranging from 15.2% to 62%.[26] Recent studies have suggested that focal choroidal invasion if associated with optic nerve invasion (pre-laminar and laminar), is also a risk factor. Cases involving both choroidal and optic nerve invasion have a poorer prognosis and higher recurrence risk, necessitating careful adjuvant therapy.[30] In our study, 20.6% (n = 16) of patients exhibited both focal choroidal and pre-laminar or laminar optic nerve invasion.

Survival and metastasis risk are significantly impacted by optic nerve invasion, especially post-laminar optic nerve invasion (PLONI) and optic nerve transection involvement. Metastasis rates for PLONI range from 12% to 42% and those for optic nerve transection involvement range from 41% to 78%.[31,32] In this study, retrolaminar optic nerve invasion (38.4%, n = 30) was the second most common HRF (Figure 4A and B). PLONI without transection occurred in 26.9% (n = 21) of cases, and PLONI with transection occurred in 11.5% (n = 9). Higher rates than ours have been reported in middle-income countries, ranging from 39.6% to 49%.[8,33]

A comparative study of 331 Indian and 193 American children showed that Indian children had a five-fold greater risk of optic nerve invasion and a three-fold greater risk of massive choroidal invasion

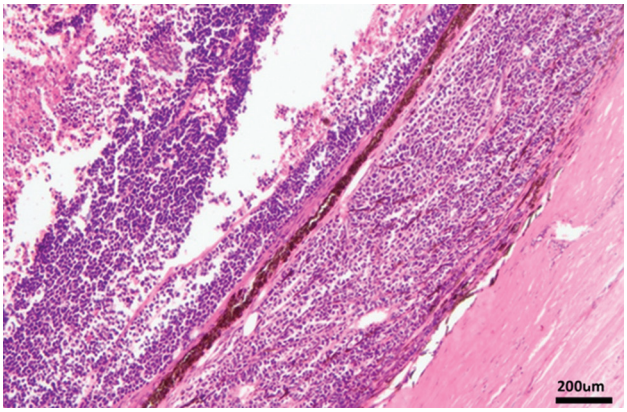

Figure 3. Massive choroidal invasion >3 mm, observed in eosin and hematoxylin (H&E) stain at 20× magnification. Scale bar: 200 µm

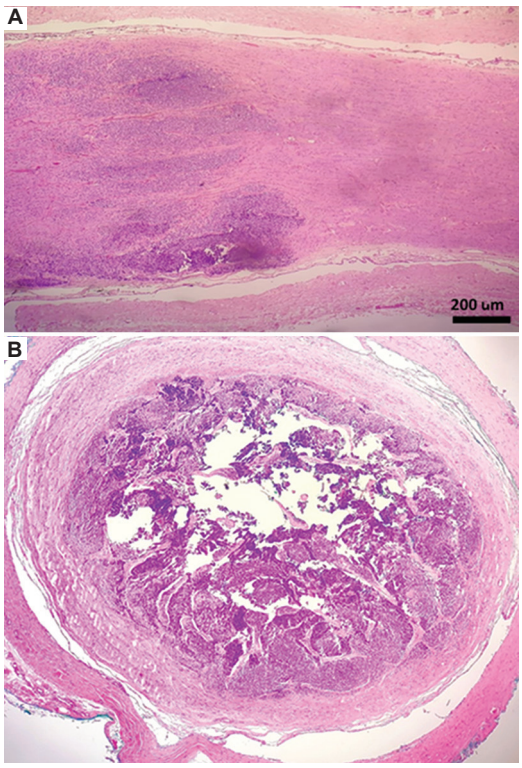

Figure 4. Optic nerve invasion by tumor. (A) Post-laminar invasion, Scale bar: 200 µm; (B) Optic nerve transection involved with tumor

than American children.[31] In the present study, HRFs of the anterior segment included the involvement of the anterior chamber (19.2%), iris (15.4%), trabecular meshwork (11.5%), Schlemm's canal (11.5%), and ciliary body (16.7%). Ciliary body and iris involvement in our study was higher than that reported by Kaliki *et al.* and Yaqoob *et al.* (3.7% each and 4.7% each, respectively) but lower than the rates observed by Yahaya *et al.* (28% and 21.5%).[8,33,34] These studies did not mention about the invasion of the anterior chamber, trabecular meshwork, or Schlemm's canal. In addition, we observed scleral invasion in 15.4% of cases, extrascleral invasion in 6.4%, and orbital invasion in 3.9%. Studies from the Indian subcontinent reported scleral invasion rates between 4.9% and 14% and extrascleral invasion from 1.6% to 11.8%, whereas a study from Uganda found a scleral invasion rate of 22.7%.[8,35] In comparison studies with American and Indian RB patients, these rates were 1% and 2%, respectively.[31] Of the 78 patients, 38.4% (n = 30) received adjuvant treatment; approximately 33% received vincristine, etoposide, and carboplatin chemotherapy, and 5.1% received both chemotherapy and external beam radiotherapy (EBRT). In 3.8% of cases, the parents refused any treatment.

A significant global burden (43%) of RB cases exists in six Asia-Pacific countries: China, India, Indonesia, Pakistan, Philippines, and Bangladesh.[15] Mortality rates for this cancer vary by continent: the highest rates are observed in Africa (70%) and Asia (40%) compared with North America (3%) and Europe (5%).[23] Increased mortality in Africa and Asia is attributed to factors such as economic challenges, illiteracy, lack of awareness, shortages of trained medical personnel, limited treatment facilities, and cultural beliefs. Survival rates also correlate with a country's income level, as socioeconomic conditions affect the likelihood of seeking medical attention. Early presentation and improved treatment facilities have notably increased survival rates in higher-income countries. For example, a 2002 study reported a 5-year survival rate of 87% in the United States, and a 2021 study found a 4- – 8-year survival rate of 99%. In Europe, the 5-year survival rate was 95% in a 2002 study and 100% in a 2017 study, while Japan reported a 10-year survival rate of 95%.[7] These high rates apply to only 10% of patients with RB worldwide, primarily those in high-income countries. However, 80% of patients with RB worldwide live in low- and middle-income countries in Asia, Africa, and Latin America.[5] In Asia, 5-year survival rates vary by income level: 89% in Taiwan (high income), 86% in China (upper-middle-income), and 37% in Indonesia (middle-income). Lower-middle-income Asian countries have similarly variable rates, with Uzbekistan at 66.6%, India at 48%, and Nepal (10-year survival) at 24%.[7,23] In Africa, 5-year survival rates are 60% in Uganda (low-income), 53% in Senegal (lower-middle-income), and 46% in Namibia (upper-middle-income).[7,23] The overall survival rate in our study was 69.23%, based on a follow-up period of 6 months to 12 years. According to the Global Retinoblastoma Outcome Study, the survival rate in low-income countries is 40% compared with 77% in lower-middleincome and 79% in upper-middle-income countries.[7]

Bangladesh, a lower-middle-income country, has a survival rate of 69.3%, which is below the estimated rate of 77% for similar-income countries. Approximately 27% of study children died, with 23% due to metastasis, possibly linked to delayed presentation, multiple HRFs, and treatment refusal. The Global Retinoblastoma Outcome Study reported metastasis rates by economic status: 24% in low-income, 51.4% in lower-middle-income, 16.9% in upper-middle–income, and 2.1% in high-income countries. Authors attributed lower metastasis rates in low-income countries to underreporting and higher rates in lower-middle-income countries to delayed presentation and numerous histopathological HRFs.[8] In this study, the mortality rate due to RB alone was 23.07%, with additional deaths (3.8%) due to other causes. In a 3-year study of RB outcomes, mortality rates were reported as 29.7% in low-income, 52.3% in lower-middle-income, 16.9% in upper-middle–income, and only 1.1% in high-income countries.[8]

In this retrospective analysis, 21 patients died, 3 were lost to follow-up, and the remaining patients were either in regular or irregular follow-up, with periods ranging from 6 months to 12 years. Counseling on the disease's nature proved effective for tumor recurrence detection, initiating prompt treatment, sibling screening, and raising awareness among patients' families and neighbors.

This study was conducted at a tertiary eye care center in Bangladesh, which is a lower-middle-income country with a high population density. Limited healthcare infrastructure and personnel hinder the availability of ophthalmic services nationwide. Complete RB treatment is available at only two tertiary eye care centers, with some secondary hospitals offering only enucleation services. Most healthcare centers lack trained personnel for histopathological assessment and RB treatment, potentially contributing to the underreporting of metastasis and survival rates. This study mainly focused on the presence of a high HRF (84.6%), underscoring the need for early case detection and lag time reduction. Recently, multidisciplinary management for RB has been recommended to preserve life and vision, although such a model is challenging in low- and lower-

middle-income countries. In such contexts, awareness programs, training of specialized ophthalmologists through fellowships, professional collaboration, and effective referrals can promote early detection and reduce the advanced presentation of RB.

This retrospective study may have biases in some data, and it only reports the overall survival rate.

5. Conclusion

Enucleation marks the beginning, not the end, of treatment in advanced RB cases. Detailed histopathology reports specifying HRFs are crucial for further management. Delayed presentation complicates treatment and is a poor prognostic factor due to higher metastasis risks. To improve outcomes, we should prioritize awareness, early presentation, accurate histopathological reporting, and human resource development alongside appropriate treatment.

Acknowledgments

None.

Funding

None.

Conflict of interest

The authors declare they have no competing interests.

Author contributions

Conceptualization: Soma Rani Roy
Formal analysis: Sujit Kumar Biswas
Investigation: Rahat Anjum
Methodology: Soma Rani Roy
Writing – original draft: Soma Rani Roy
Writing – review & editing: Sujit Kumar Biswas

Ethics approval and consent to participate

This study was approved by the local IRB of the Chittagong Eye Infirmary and Institute of Community Ophthalmology. Informed consent written and verbally were obtained from the parents or legal guardians of the patients before their participation.

Consent for publication

Consent was taken from the parents or legal guardians of the patients to use their data and images in this study.

Availability of data

Not applicable.

References

1. Roy SR, Kaliki S. Retinoblastoma: A major review. *Mymensingh Med J*. 2021;30(3):881-895.
2. Zhang Y, Wang Y, Zhi T, Jin M, Huang D, Ma X. Clinical characteristics, treatment and prognosis of infants with retinoblastoma: A multicenter, 10-year retrospective analysis. *BMC Pediatr*. 2023;23(1):229.
   doi: 10.1186/s12887-023-03984-5
3. Stacey AW, Bowman R, Foster A, *et al.* Incidence of retinoblastoma has increased: Results from 40 European countries. *Ophthalmology*. 2021;128(9):1369-1371.
   doi: 10.1016/j.ophtha.2021.01.024
4. Fernandes AG, Pollock BD, Rabito FA. Retinoblastoma in the United States: A 40-year incidence and survival analysis. *J Pediatr Ophthalmol Strabismus*. 2018;55(3):182-188.
   doi: 10.3928/01913913-20171116-03
5. Global Retinoblastoma Study Group, Fabian ID, Abdallah E, *et al.* Global retinoblastoma presentation and analysis by national income level. *JAMA Oncol*. 2020;6(5):685-695.
   doi: 10.1001/jamaoncol.2019.6716. Erratum in: *JAMA Oncol.* 2020;6(11):1815.
   doi: 10.1001/jamaoncol.2020.5133
6. Chevez-Barrios P, Eagle RC, Marback EF. Histopathologic features & prognostic factors. In: *Clinical Ophthalmic Oncology*. Berlin: Springer; 2019. p. 221-237.
   doi: 10.12669/pjms.38.ICON-2022.5787
7. Global Retinoblastoma Study Group. The Global Retinoblastoma Outcome Study: A prospective, cluster-based analysis of 4064 patients from 149 countries. *Lancet Glob Health*. 2022;10(8):e1128-e1140.
   doi: 10.1016/S2214-109X(22)00250-9
8. Yaqoob N, Mansoor S, Aftab K, Kaleem B, Hamid A, Jamal S. High risk histopathological factors in retinoblastoma in upfront enucleated eyes: An experience from a tertiary care centre of Pakistan. *Pak J Med Sci*. 2022;38(2):369-374.
   doi: 10.12669/pjms.38.ICON-2022.5787
9. Shields CL, Mashayekhi A, Demirci H, Meadows AT, Shields JA. Practical approach to management of retinoblastoma. *Arch Ophthalmol.* 2004;122(5):729-735.
   doi: 10.1001/archopht.122.5.729
10. Chantada G, Doz F, Antoneli CB, *et al.* A proposal for an international retinoblastoma staging system. *Pediatr Blood Cancer*. 2006;47(6):801-805.
    doi: 10.1002/pbc.20606
11. Thaung C, Karaa EK. Standard reporting of high-risk histopathology features in retinoblastoma. *Community Eye Health*. 2018;31(101):31-33.

12. Alsharif H, Helmi H, Maktabi A. Histopathological characteristics and classification for prognostic indicators. In: Manaa Alkatan H, editor. *Retinoblastoma-Past, Present and Future*. London, UK: IntechOpen; 2019.

doi: 10.5772/intechopen.89410

13. Mendoza PR, Specht CS, Hubbard GB, *et al.* Histopathologic grading of anaplasia in retinoblastoma. *Am J Ophthalmol*. 2015;159(4):764-776.

doi: 10.1016/j.ajo.2014.12.014

14. Alkatan HM, Al Marek F, Elkhamary S. Demographics of pediatric orbital lesions: A tertiary eye center experience in Saudi Arabia. *J Epidemiol Glob Health*. 2019;9(1):3-10.

doi: 10.2991/jegh.k.181224.001

15. Jain M, Rojanaporn D, Chawla B, Sundar G, Gopal L, Khetan V. Retinoblastoma in Asia. *Eye (Lond)*. 2019;33(1):87-96.

doi: 10.1038/s41433-018-0244-7

16. Kaliki S, Vempuluru VS, Mohamed A, *et al.* Retinoblastoma in Asia: Clinical presentation and treatment outcomes in 2112 patients from 33 countries. *Ophthalmology*. 2024;131(4):468-477.

doi: 10.1016/j.ophtha.2023.10.015

17. Zhao J, Feng Z, Leung G, Gallie BL. Retinoblastoma survival following primary enucleation by AJCC staging. *Cancers* (*Basel*). 2021;13(24):6240.

doi: 10.3390/cancers13246240

18. Roy SR, Nuruddin M, Asgar A. Scenario of retinoblastoma among Bangladeshi children – a single center experience of 10 years. *BOHR Int J Curr Res Optometry Ophthalmol*. 2022;1(1):62-66.

doi: 10.54646/bijcroo.017

19. Gupta N, Pandey A, Dimri K, Prinja S. Epidemiological profile of retinoblastoma in North India: Implications for primary care and family physicians. *J Family Med Prim Care*. 2020;9(6):2843-2848.

doi: 10.4103/jfmpc.jfmpc_265_20

20. Ali MS, Sinha R, Bhaskar G, Kumari N, Sinha B. Demographic and clinical characteristics of retinoblastoma cases at a tertiary care center in Eastern India. *Cureus*. 2024;16(7):e64659.

doi: 10.7759/cureus.64659

21. Fabian ID, Khetan V, Stacey AW, *et al.* Sex, gender, and retinoblastoma: Analysis of 4351 patients from 153 countries. *Eye* (*Lond*). 2022;36(8):1571-1577.

doi: 10.1038/s41433-021-01675-y

22. Lukamba RM, Yao JA, Kabesha TA, *et al.* Retinoblastoma in Sub-Saharan Africa: Case studies of the republic of côte d'ivoire and the democratic republic of the Congo. *J Glob Oncol*. 2018;4:1-8.

doi: 10.1200/JGO.17.00056

23. Utomo PT, Respatika D, Ardianto B, *et al.* Lag time, high-risk histopathological features, metastasis, and survival interrelation in retinoblastoma: A perspective from lower-middle income country. *Int J Ophthalmol*. 2022;15(12):1994-2000.

doi: 10.18240/ijo.2022.12.15

24. Tan RJ, Umerez DC, Alindayu JI, Conjares MJ, Go DA, Paulino RG. Retinoblastoma in South Asia: A scoping review. *Asian Pac J Cancer Care*. 2021;6(4):493-500.

doi: 10.31557/APJCC.2021.6.4.493

25. Reddy SC, Anusya S. Clinical presentation of retinoblastoma in Malaysia: A review of 64 patients. *Int J Ophthalmol*. 2010;3(1):64-8.

doi: 10.3980/j.issn.2222-3959.2010.01.15.

26. Cruz-Gálvez CC, Ordaz-Favila JC, Villar-Calvo VM, Cancino-Marentes ME, Bosch-Canto V. Retinoblastoma: Review and new insights. Front Oncol. 2022 Nov 2;12:963780.

doi: 10.3389/fonc.2022.963780

27. Kashyap S, Sethi S, Meel R, *et al.* A histopathologic analysis of eyes primarily enucleated for advanced intraocular retinoblastoma from a developing country. *Arch Pathol Lab Med*. 2012;136(2):190-193.

doi: 10.5858/arpa.2010-0759-OA

28. Gupta R, Vemuganti GK, Reddy VA, Honavar SG. Histopathologic risk factors in retinoblastoma in India. *Arch Pathol Lab Med*. 2009;133(8):1210-1214.

doi: 10.5858/133.8.1210

29. Sari NM, Hadiputri R, Kuntorini MS, Agustina H, Mardianty F. High-risk histopathologic features of retinoblastoma treated at a tertiary hospital in West Java, Indonesia. *Ocul Oncol Pathol*. 2021;7(5):353-360.

doi: 10.1159/000517100

30. Kaliki S, Gupta S, Ramappa G, Mohamed A, Mishra DK. High-risk retinoblastoma based on age at primary enucleation: A study of 616 eyes. *Eye* (*Lond*). 2020;34(8):1441-1448.

doi: 10.1038/s41433-019-0698-2

31. Chévez-Barrios P, Eagle RC Jr., Krailo M, *et al.* Study of unilateral retinoblastoma with and without histopathologic high-risk features and the role of adjuvant chemotherapy: A children's oncology group study. *J Clin Oncol*. 2019;37(31):2883-2891.

doi: 10.1200/JCO.18.01808

32. Kaliki S, Shields CL, Eagle RC Jr., Iram S, Shields JA. High-risk intraocular retinoblastoma: Comparison between Asian Indians and Americans from two major referral centers. *Retina*. 2018;38(10):2023-2029.

doi: 10.1097/IAE.0000000000001816

33. Honavar SG, Singh AD, Shields CL, *et al.* Postenucleation adjuvant therapy in high-risk retinoblastoma. *Arch Ophthalmol*. 2002;120(7):923-931.

doi: 10.1001/Archopht.120.7.923

34. Kaliki S, Srinivasan V, Gupta A, Mishra DK, Naik MN. Clinical features predictive of high-risk retinoblastoma in 403 Asian Indian patients: A case-control study. *Ophthalmology*. 2015;122(6):1165-1172.

doi: 10.1016/J.Ophtha.2015.01.018

35. Yahaya JJ, Rugwizangoga B, Mremi A, Munema A. Clinicopathological findings of retinoblastoma: A 10-year experience from a tertiary hospital in Kampala, Uganda. *J Ophthalmol*. 2019;2019:5829284.

doi: 10.1155/2019/5829284.

ACCSCIENCE PUBLISHING

Tumor Discovery

ORIGINAL RESEARCH ARTICLE

Deregulation of Casein Kinase-2 in non-small-cell lung cancer: A subunit-specific analysis

George V. Pérez[1,2], Chen Li[3], Chenyi Deng[4], Ying Yi[5], Qiang Zhao[4], Zhiwei Zhang[3], Wen Li[5]*, Silvio E. Perea[1]*, and Yasser Perera[1,5]*

[1]Department of Pharmaceuticals, Biomedical Research Division, Center for Genetic Engineering and Biotechnology, Havana, Cuba

[2]Department of Biochemistry and Molecular Biology, Complutense, Madrid, Spain

[3]Key Laboratory of Cancer Cellular and Molecular Pathology, Cancer Research Institute of Hengyang Medical School, University of South China, Hengyang, Hunan, People's Republic of China

[4]Department of Pathology, The First Affiliated Hospital of University of South China, Hengyang, Hunan, People's Republic of China

[5]China-Cuba Biotechnology Joint Innovation Center, Yongzhou Development and Construction Investment Co., Ltd., Yongzhou, Hunan, People's Republic of China

(This article belongs to the *Special Issue: New Developments in Lung Cancer Research, Diagnosis, Treatment, and Prognosis*)

Abstract

Casein kinase-2 (CK2) is a constitutively active kinase that supports neoplastic properties. Although there is an extensive body of preclinical research on CK2, translational and clinical information remains limited and sparse. In this study, we interrogated clinical multiomics databases to examine CK2 deregulation across various cancers. Specifically, we analyzed the mutational frequency, copy-number alterations (CNA), and mRNA expression of CK2 catalytic (*CSNK2A1* and *CSNK2A2)* and regulatory (*CSNK2B)* subunits across two major cancer genomic repositories (The Cancer Genome Atlas/International Cancer Genome Consortium). These genomic and transcriptomic analyses were further focused on lung cancer and complemented by *in situ* assessments of CK2 protein subunits and enzymatic activity in biopsies from non-small-cell lung cancer (NSCLC). Our findings indicate that gene mutations and CNA do not account for the elevated mRNA levels and enzymatic activity of CK2 subunits in lung adenocarcinoma (LUAD) and lung squamous cell carcinoma (LUSC). Particularly, the upregulation of *CSNK2A1* and *CSNK2B* mRNA was associated with a worse prognosis and showed a direct correlation with the infiltration of myeloid-derived suppressor cells in LUAD. At the protein levels, all CK2 subunits and enzymatic activity were markedly elevated in LUAD (n = 103) and LUSC (n = 31) biopsies; however, only *CSNK2A1* expression correlated positively with tumor size and disease stage. Finally, CSNK2A1 appeared to be more tumor-specific than CSNK2A2, suggesting that targeted therapies against this catalytic subunit or its homotetramer may offer a more favorable therapeutic window in NSCLC.

Keywords: Casein Kinase-2; Casein kinase-2 regulation; Lung cancer; Translational study; Oncology target

***Corresponding authors:**
Yasser Perera
(ypereranegrin@ccbjic.com)
Silvio E. Perea
(silvio.perea@cigb.edu.cu)
Wen Li
(liwen@ccbjic.com)

Citation: Pérez GV, Li C, Deng C, *et al*. Deregulation of Casein Kinase-2 in non-small-cell lung cancer: A subunit-specific analysis. *Tumor Discov.* 2024;3(4):4571. doi: 10.36922/td.4571

Received: August 19, 2024

Accepted: October 17, 2024

Published Online: November 29, 2024

1. Introduction

Casein kinase-2 (CK2) is a constitutively active Ser/Thr-protein kinase frequently deregulated in cancer, with broad tumor-supporting roles classified as "non-oncogene addiction".[1] The CK2 holoenzyme comprises two catalytic subunits (CSNK2A1 and CSNK2A2) and two regulatory subunits (CSNK2B), which assemble as either homotetramers ($CSNK2A1_2$/$CSNK2B_2$ or $CSNK2A2_2$/$CSNK2B_2$) or heterotetramers (CSNK2A1/CSNK2A2/$CSNK2B_2$).[2] In addition, CK2's supramolecular structures, spatiotemporal subunit associations, and functional specialization introduce further regulatory intricacies in both health and disease.[3] Notably, CK2 participates in multiple tumor-related signaling cascades, promoting aberrant cell proliferation, survival, and metastasis.[4] However, CK2's unique biochemical features, vast range of substrates, and multifaceted impact on signaling cascades have sparked debates about its viability as an oncology target.[5,6] These discussions include inquiries about CK2's essentiality in cancer versus non-neoplastic tissues, as well as concerns regarding the specificity of current CK2 inhibitors.[7,8]

A myriad of natural and synthetic compounds with diverse CK2 inhibition mechanisms has been described.[9] Recent compounds exhibit ATP-competitive or dual inhibition mechanisms, targeting the ATP-binding site and an allosteric pocket unique to CK2.[7,10] However, only two distinct CK2 inhibitors have reached clinical application: the synthetic peptide CIGB-300 and the small molecule CX-4945.[11,12] Despite extensive pre-clinical research, translational and clinical data on CK2 remain limited and sparse, and its role as a validated oncology target is yet to be established.[13]

In this study, we interrogated multiomics cancer databases to investigate CK2 gene mutations and deregulated expression in clinical samples. We performed meta-analyses to explore potential associations between CK2 subunit expression and overall survival (OS) of non-small-cell lung cancer (NSCLC) patients. Our analysis centers on individual CK2 subunits, assuming subunit-specific functions across cancers, with a particular focus on two major NSCLC types: lung adenocarcinoma (LUAD) and lung squamous cell carcinoma (LUSC). CK2 protein subunit levels were measured by performing immunohistochemistry (IHC) in LUAD and LUSC patient samples and correlated with selected clinicopathological features. Finally, by measuring two canonical CK2 substrates as indicators of *in situ* CK2 enzymatic activity, we demonstrated that CK2 upregulation in LUAD and LUSC corresponds with increased CK2 enzymatic activity in these NSCLC subtypes.

2. Materials and methods

2.1. *CSNK2* gene mutational burden in cancer cohorts

The cBioPortal for Cancer Genomics (https://www.cbioportal.org/) was used to retrieve data on the mutational burden – specifically, the total frequency and types of alterations – of the *CSNK2A1*, *CSNK2A2*, and *CSNK2B* subunits. This data were sourced from the Pan-Cancer Analysis of Whole Genomes Consortium of the International Cancer Genome Consortium and The Cancer Genome Atlas (TCGA) (Nature 2020).[14,15] Samples with mutations and copy-number alterations (CNA) data were selected across 38 tumor types, comprising 2683 samples from 2565 patients.

For a more detailed analysis within NSCLC cohorts, cBioPortal was further queried for genetic alterations specific to *CSNK2A1*, *CSNK2A2*, and *CSNK2B* subunits in LUAD and LUSC. The select genomic profiles included mutations, putative CNA from the Genome Identification of Significant Targets in Cancer, and mRNA expression *z*-scores relative to normal samples (log RNA Seq V2 RSEM). For LUAD, the TCGA PanCancer Atlas cohort (n = 566 samples) was interrogated, while for LUSC, the TCGA PanCancer Atlas cohort (n = 487 samples) was used.

Driver feature prediction, based on the mutational frequency, distribution, and functional impact of individual mutations, was performed through the IntOgene platform, which interrogates 66 cancer types across 221 studies (n = 28,076 samples; https://www.intogen.org/search).[16] Cancer driver annotations were obtained from OncoKB™MSK's Precision Oncology Knowledge Base (OncoKB) (https://www.oncokb.org/).[17]

2.2. *CSNK2* gene expression in cancer

Expression levels of *CSNK2* genes across pan-cancer studies were interrogated using data from the TCGA available through the University of Alabama at Birmingham database (UALCAN) (https://ualcan.path.uab.edu).[18] Tumor and non-tumor samples are represented in red and blue, respectively. Box-and-whisker plots display gene expression levels, including maximum, upper quartile, median, lower quartile, and minimum values. Statistical comparisons were conducted using the Student's *t*-test with unequal variances. The following TCGA tumor subtypes were included: Bladder urothelial carcinoma, breast invasive carcinoma, cervical squamous cell carcinoma, cholangiocarcinoma, colon adenocarcinoma, esophageal carcinoma, glioblastoma multiforme, head-and-neck squamous cell carcinoma, kidney chromophobe, kidney renal clear cell carcinoma, kidney renal papillary cell

carcinoma, liver hepatocellular carcinoma, LUAD, LUSC, pancreatic adenocarcinoma, prostate adenocarcinoma, pheochromocytoma and paraganglioma, rectal adenocarcinoma, sarcoma, skin cutaneous melanoma, thyroid carcinoma, thymoma, stomach adenocarcinoma, and uterine corpus endometrial carcinoma.

2.3. Survival meta-analysis of *CSNK2* genes in NSCLC

A survival meta-analysis for each *CSNK2* gene was interrogated using the LUAD or LUSC subtype explorer database (https://lce.biohpc.swmed.edu/lungcancer/index.php#about).[19] Output values were displayed based on all curated studies available.

2.4. Metastasis potential of *CSNK2* genes in NSCLC

Differential expression analysis of *CSNK2* genes in tumor, normal, and metastatic tissues was carried out using the TNMplot database (https://tnmplot.com/analysis/).[20] The statistical method was set automatically to the Kruskal–Wallis one-way non-parametric test.

2.5. Correlation of *CSNK2* genes with immune infiltration

The gene module from the TIMER2.0 web server (http://timer.cistrome.org)[21] was used to select genes of interest (*CSNK2* subunits) and visualize the correlation between their expression levels and the immune and stromal cell populations infiltrating tumor samples from TCGA.[22] Immune infiltrate abundances were estimated using multiple immune deconvolution methods, including Tumor Immune Dysfunction and Exclusion (TIDE), Microenvironment Cell Populations-counter (MCPCounter), Estimating the Proportion of Immune and Cancer cells (EPIC), and xCell. The generated heatmap shows purity-adjusted Spearman's rho correlations across various cancer types.

2.6. Immunohistochemical analysis of LUAD and LUSC specimens

A total of 134 pairs of wax blocks were prepared from primary tumor specimens (LUAD = 103; LUSC = 31) and corresponding para-neoplastic tissue (>5 cm from the tumor) collected from patients initially diagnosed at the First Affiliated Hospital of South China University (Hunan, China) since December 2021. This study was approved by the Medical Ethics Committee of Nanhua University Affiliated First Hospital, Issuance, Review Batch Number: 2021LL0115001, Meeting Date: January 15, 2021. Reviewed materials included the Research Plan Version YJFA20210114 and the Informed Consent Form Version ZQTY20210114. Clinical and pathological records provided data on patient age, sex, histological grade, tumor size, invasion depth (T stage), and lymph node metastasis. At the time of specimen collection, patients had not undergone radiotherapy and displayed no other systemic primary tumors besides NSCLC. Post-operative hematoxylin and eosin sections confirmed diagnoses of LUAD or LUSC.

IHC analysis was performed using primary antibodies against CSNK2A1 (Ab76040, Abcam, USA), CSNK2A2 (#PA5-109601, Invitrogen, USA), CSNK2B (Ab#76025, Abcam, USA), AKT (CST#4691, Cell Signaling Technology, USA), AKTs129 (#BS-5188R, Bioss, USA), NPM1 (ab52644, Abcam, USA), NPM1s125 (ab109546, Abcam, USA), and Ki67 (RMA-0542 WWW, Fuzhou Maishin Biotechnology, China), following the immunohistochemical SP method with the Fuzhou Maishin Ultrasensitive SP (Mouse/Rabbit) IHC Kit (Fuzhou Maishin Biotechnology, China). A combined immunoreactivity score (CIS) was calculated based on signal intensity (scored from "0" for non-stained to "3" for strong brown staining) and the frequency of positive cells (from <5% = 0 points to >75% = 4 points) in tumor samples. Each section analyzed was selected randomly from the upper, lower, left, right, and central regions of a magnified field (×400) to ensure representative interpretation. The combined scores (A×B) were classified as follows:

- Score 1 – 3: – (negative)
- Score 4 – 5: + (weak positive)
- Score 6 – 7: ++ (positive)
- Score ≥8: +++ (strong positive)

2.7. Statistical analysis

Statistical analysis of IHC experiments was performed using the Statistical Package for the Social Sciences 27.0. Chi-squared tests and Fisher's exact tests were used to analyze correlations. A two-sided $P < 0.05$ was considered statistically significant for all calculations.

3. Results

3.1. Mutational burden of *CSNK2* subunits across cancer cohorts

Deregulation of CK2 in cancer is regarded as an example of non-oncogene addition. To explore genetic alterations in *CSNK2* genes that may contribute to aberrant kinase activity, we analyzed available cancer genomics databases. Figure 1A illustrates that the genetic alteration rates for *CSNK2A1, CSNK2A2*, and *CSNK2B* in a pan-cancer cohort were 7%, 1.8%, and 6%, respectively. Most alterations were CNA, while missense, splice site, and truncating mutations were below 0.3%. Notably, these uncommon mutations did not exhibit oncogenic potential based on their frequency, distribution, and functional impact, as determined by

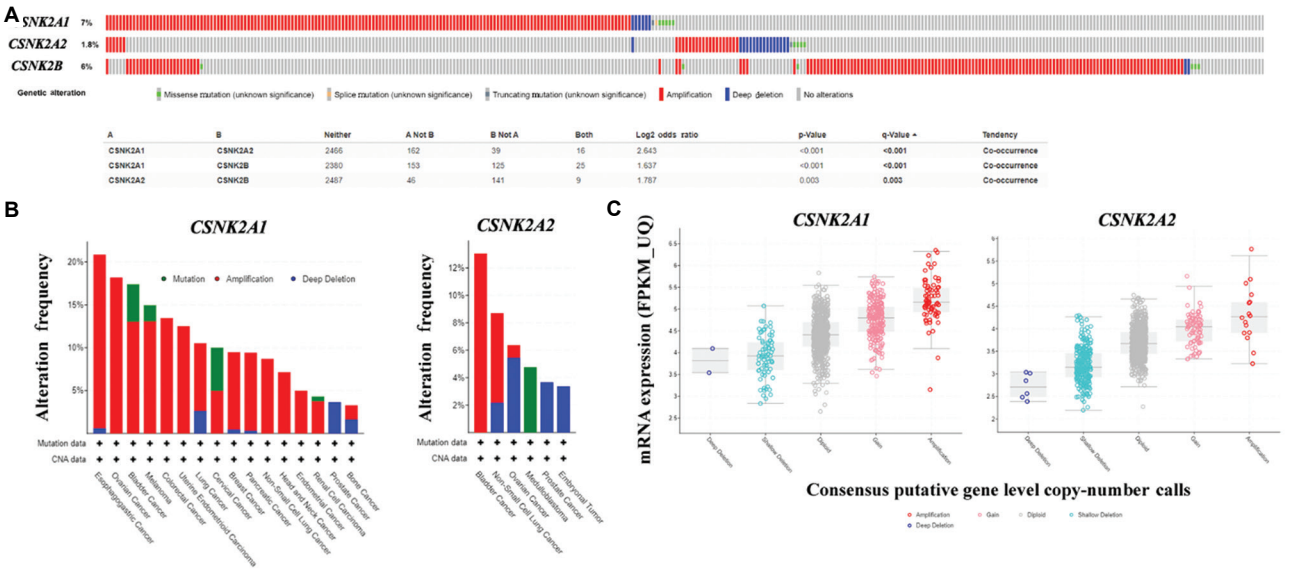

Figure 1. Oncoprint analysis of genetic alterations in pan-cancer cohorts (International Cancer Genome Consortium/The Cancer Genome Atlas, Nature 2020) for catalytic (CSNK2A1/CSNK2A2) and regulatory subunits (CSNK2B). (A) Oncoprint and co-occurrence analysis, including only samples with mutation and CNA information (92% of the cohort, n = 2,683 samples). (B) Cumulative alterations in selected *CSNK2* subunits, displaying only tumors with an alteration frequency of 3% or higher for the target gene. (C) Correlation between CNA (consensus putative gene-level copy-number call) and gene expression (mRNA expression, FPKM_UQ) across the database. In this database, "lung cancer" (n = 38) and "NSCLC" (n = 46) encompass data from LUAD-US (n = 35 plus 3 additional unknown samples) and the LUSC-US study (n = 46), respectively. All annotations and analyses were obtained from cBioPortal, as described in the Materials and Methods section.
Abbreviation: CNA: Copy-number alterations.

IntOgene and annotations from the Precision OncoKB. Overall, genetic alterations in *CSNK2A1*, *CSNK2A2*, and *CSNK2B* frequently co-occurred, both when analyzing CNAs and mutations together (Figure 1A) and when analyzing CNAs alone (data not shown). For *CSNK2A2*, copy-number amplifications and deletions were identified in five tumor types, while *CSNK2A1* and *CSNK2B* amplifications predominated across 14 out of 16 tumor locations, using a 3% threshold for *CSNK2* gene alterations (Figures 1B and S1B).

In addition, cumulative gene alteration frequencies on *CSNK2* subunits exceeded 10% in 15 different tumors (Figure S1A). The highest alteration rates were reported in melanoma and bladder cancer (>30%), with LUAD (denoted as "lung cancer" in Figure 1) and LUSC (denoted as "NSCLC" in Figure 1) being the fifth and sixth most altered cancer types concerning CSNK2 subunits (18.4%), respectively (Figure S1A). In the LUSC cohort, all *CSNK2A1* alterations were amplifications (4/46 cases [9%]), while *CSNK2A2* and CSNK2B exhibited amplifications (3/46 cases [7%] and 2/46 cases [4%], respectively) or deletions (1/46 cases [2%] and 2/46 cases [4%], respectively) (Figures 1B and S1B). In this pan-cancer cohort, CNAs were consistent with mRNA expression levels for the three CSNK2 subunits (Figures 1C and S1C). Furthermore, CSNK2A1 mRNA expression showed a positive correlation with CSNK2A2 mRNA expression (Spearman: 0.24; P = 2.10e-14), while an inverse correlation was found between CSNK2A1 and CSNK2B mRNA expression (Spearman: −0.15; P = 2.91e-6). No correlation was found between CSNK2A2 and CSNK2B mRNA expression in this data cohort (Figure S1D-F).

3.2. Genomic and transcriptomic alterations of *CSNK2* subunits in major types of NSCLC

Given the limited NSCLC data in the pan-cancer cohort,[23] we interrogated more comprehensive datasets for LUAD (n = 566) and LUSC (n = 487). We prioritized samples with complete mutations, CAN, and RNA sequencing data (LUAD = 503; LUSC = 466) (Figure 2A). In cases where full datasets were unavailable, we included samples with mutation and CNA data (LUAD = 507; LUSC = 469) to ensure consistency with the analysis in Figure 1 (Figure 2B and C).

CSNK2A1 exhibited very few mutations in LUAD and LUSC samples (six mutations), and *CSNK2A2* mutations were found only in LUAD (two mutations). No mutations were detected in the regulatory subunit gene *CSNK2B* across the 976 NSCLC samples tested (Figure 2B and C). Overall, these results confirm that mutations in *CSNK2* subunits *CSNK2A1*, *CSNK2A2*, and *CSNK2B* are rare, with a cumulative mutation

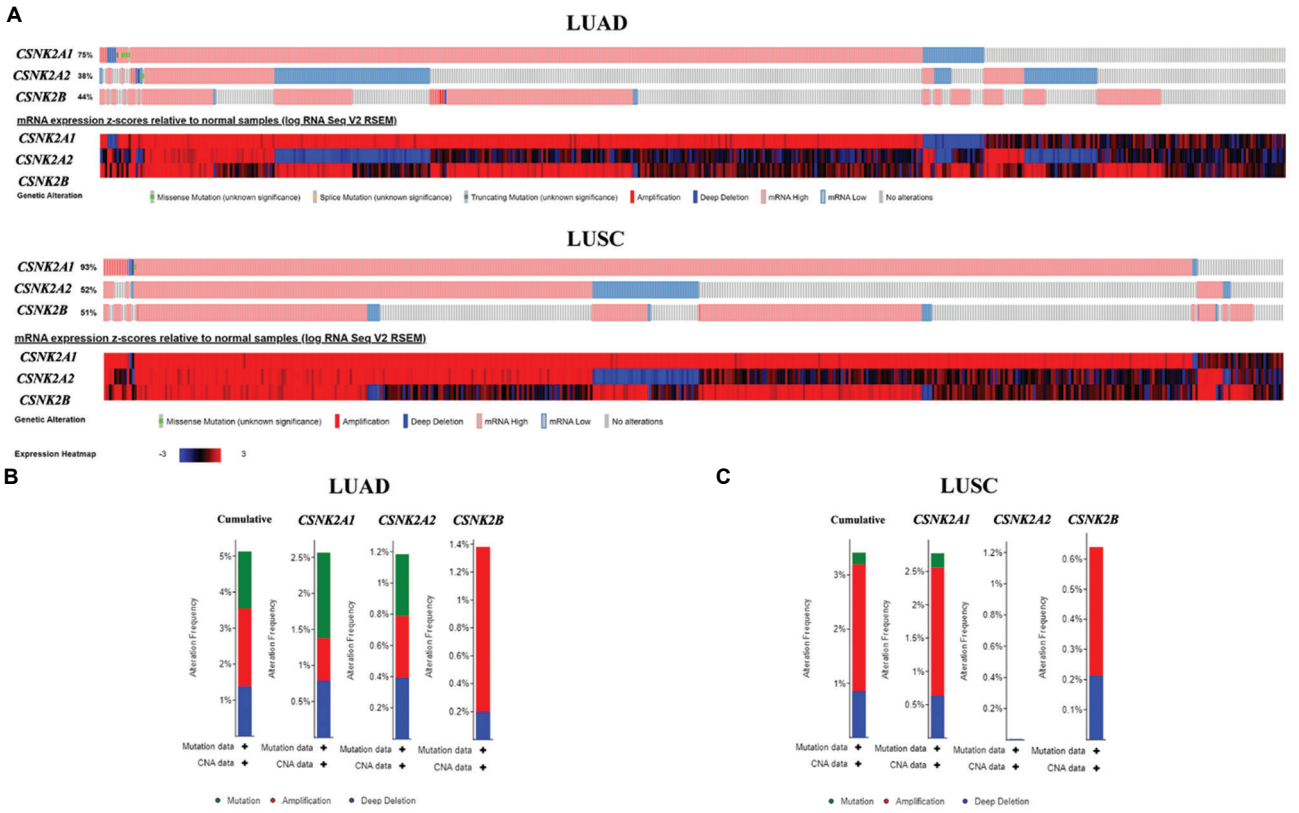

Figure 2. Oncoprint analysis of genetic alterations contained in LUAD and LUSC cohorts. (A) Only samples with mutations, CNA, and mRNA expression data were included (LUAD = 503; LUSC = 466); (B) LUAD samples with mutations and CNA data only (n = 507); (C) LUSC samples with mutations and CNA data only (n = 469). All annotations and analyses were obtained from cBioPortal, as described in the materials and methods section.
Abbreviations: LUSC: Lung squamous cell carcinoma; LUAD: Lung adenocarcinoma; CAN: Copy-number alterations.

frequency of <1.5% across the cohort. In addition, CNA events were uncommon, with amplifications and deletions found in only 3 – 4% of samples (Figure 2B and C). As in the pan-cancer cohort, these CNAs corresponded roughly with target gene expression (Figure S2).

Despite the limited impact of mutations and CNAs on individual *CSNK2* subunits, mRNA overexpression was prevalent across analyzed LUAD and LUSC cohorts (Figure 2A). Particularly, *CSNK2A1* mRNA deregulation was found in over 90% of LUSC samples and 70% of LUAD samples. Overall, catalytic subunit deregulation was more prominent in LUSC than LUAD. While *CSNK2A1* consistently showed overexpression, *CSNK2A2* mRNA levels varied, with both elevated and reduced expression relative to normal-matched tissues. For *CSNK2B*, overexpression was much more common than downregulation, with over 40% of LUAD and LUSC samples displaying higher mRNA levels compared to normal-matched tissues (Figure 2A).

As in the pan-cancer cohorts, *CSNK2A1* mRNA expression showed a weak positive correlation with *CSNK2A2* mRNA expression in both LUAD (Spearman: 0.14; P = 1.214e-3) and LUSC (Spearman: 0.24; P = 1.39e-7). However, no significant correlations were found between the catalytic subunits (*CSNK2A1*/*CSNK2A2*) and regulatory subunit *CSNK2B* at the mRNA expression level in these NSCLC subtypes (data not shown).

To investigate potential regulatory mechanisms, we analyzed methylation data for putative correlations between *CSNK2A1*-TSS200, *CSNK2A2*-TSS1500/1rstExon, and *CSNK2B*-TSS1500/1stExon/5'UTR methylation and mRNA expression levels of *CSNK2* subunits. n LUAD, we found weak negative correlations for *CSNK2A2*-TSS1500 (Spearman: −0.15; P = 8.658e-4) and *CSNK2B*-TSS1500/1stExon/5'UTR (Spearman: −0.14; P = 1.528e-3) (Figure S3A). Similarly, methylation of *CSNK2A2* and *CSNK2B* on promoter regions, but not CSNK2A1, correlated with mRNA expression in LUSC samples, with significant signals observed for *CSNK2A2*-TSS1500 (Spearman: −0.09; P = 0.0443), *CSNK2A2*-1rstExon (Spearman: −0.10; P = 0.0368), and

CSNK2B-TSS1500/1stExon/5'UTR (Spearman: −0.26; P = 9.54e-9) (Figure S3B).

3.3. Prognostic impact of *CSNK2A1* and *CSNK2B* overexpression in LUAD

We investigated whether the overexpression of *CSNK2* subunits correlates with reduced OS in clinical cohorts of NSCLC. Initially, we confirmed that *CSNK2* mRNA levels were consistently overexpressed across various tumor types, including NSCLC, except for *CSNK2A2* in LUAD (Figure S4). Particularly, *CSNK2A1* upregulation was substantially higher than that of *CSNK2A2* in LUAD (fold change: 1.40 vs. 0.95) and LUSC (fold change: 2.13 vs. 1.23) (Figure S4A and B), while *CSNK2B* displayed comparable expression levels in both LUAD and LUSC (LUAD: 1.35 vs. LUSC:1.40) (Figure S4C). In alignment with *CSNK2A1* and *CSNK2B* overexpression, a meta-analysis of mRNA expression versus OS indicated that elevated of both subunits correlated with a poorer prognosis in LUAD but not LUSC patients (*CSNK2A1*: LUAD hazard ratio [HR] = 1.17, P < 0.01; LUSC HR = 1.07, P = 0.72; *CSNK2B*: LUAD HR = 1.11, P < 0.01; LUSC HR = 0.93, P = 0.16) (Figure 3). Conversely, *CSNK2A2* overexpression in LUAD was associated with improved OS (HR = 0.92, P = 0.01) (Figure S5).

It is worth noting that, although data on metastatic samples are limited and not stratified by NSCLC subtypes, preliminary findings suggest that *CSNK2A1* (P = 1.28e-5) and *CSNK2B* (P = 1.33e-6), but not *CSNK2A2* (P = 0.52), could be linked to lung metastasis (Figure S6).

3.4. Correlation of *CSNK2* subunit expression with tumor infiltration by specific cell populations

The oncogenic potential of CK2 has been linked to both tumor-intrinsic and tumor-extrinsic factors.[24] Using various metrics to quantify the infiltration of immune and stromal cells in tumors, we found that elevated *CSNK2A1* mRNA expression levels were correlated with increased infiltration of cancer-associated fibroblasts (CAF) and myeloid-derived suppressor cells (MDSC) across multiple tumor subtypes (Figure 4A).

Tumor infiltration by CAFs showed a positive correlation with *CSNK2A1* mRNA overexpression according to three out of four metrics in both LUAD (CAF_TIDE, Rho = 0.185) and LUSC (CAF_TIDE, Rho = 0.164). MDSC infiltration showed a stronger correlation with *CSNK2A1* in LUAD (MDSC_TIDE, Rho = 0.283) compared to LUSC (MDSC_TIDE, Rho = 0.212) (Figure 4B and C). In contrast, weaker correlations were observed for *CSNK2A2* in both LUAD and LUSC (Figure S7A-C). In addition, *CSNK2B* expression levels correlated with MDSC infiltration in both NSCLC subtypes, with a relatively high correlation in LUAD (Rho = 0.43) (Figure S7D-F). Overall, the strongest and most significant correlations were observed between *CSNK2A1* and MDSC infiltration (Rho = 0.283, P = 1.49e-10) and between *CSNK2B* and MDSC infiltration (Rho = 0.43, P = 1.20e-23) in LUAD specimens.

3.5. Heightened CK-2 protein subunit levels and enzymatic activity in LUAD and lung squamous carcinoma specimens

To assess CK2 protein subunit levels and enzymatic activity in NSCLC, we carried out IHC analysis on primary LUAD and LUSC specimens from treatment-naive patients. CK2 subunit staining frequency and intensity varied across examined tissues but were consistently higher than in tumor-matched para-neoplastic tissues (Figures 5 and S8). CK2 subunits localized to both the nuclear and cytosolic compartments, while the Ki67 proliferation marker predominantly appeared in the nuclear region (Figure 5A).

To quantify protein levels of CSNK2A1, CSNK2A2, and CSNK2B in NSCLC tumors and corresponding para-neoplastic tissues, we applied a CIS incorporating frequency and signal intensity (Table 1). CIS results for Ki67 corroborated the aberrant growth of these tumors.

The CIS analysis demonstrated that all CK2 protein subunits were significantly elevated in NSCLC tumors compared to para-neoplastic tissues (Table 1). To further assess tumor specificity, we calculated CIS ratios (R) by dividing tumor (T) score by para-neoplastic (PN) score, as shown in Equation I:

$$R = T/PN \quad (1)$$

The ratio served as an indicator for tumor-specific marker association. The CSNK2A1 subunit exhibited nearly two-fold higher tumor specificity (R = 3.9) than CSNK2B (R = 2.1) and CSNK2A2 (R = 1.7) (Figure 6A). This specificity was further reinforced by analyzing samples with positive-to-strong positive (++/+++) staining, where CSNK2A1 showed a significantly higher tumor specificity (R = 18.3) than CSNK2A2 and CSNK2B (R = 3.1 – 3.2) (Figure 6A).

Subsequently, we correlated the CIS values for each CK2 subunit with selected pathophysiological features in NSCLC patients (Tables S1 and S2). Protein levels of the CSNK2A1 subunit showed a positive correlation with smoking habit, tumor histology, tumor size, and clinical stage (Table S1). In contrast, elevated levels of the CSNK2A2 subunit correlated only with tumor histology (Table S2). Notably, the catalytic CK2 subunits, CSNK2A1 and CSNK2A2, were more highly expressed in LUSC than LUAD samples (Figure 6B; Tables S1 and S2).

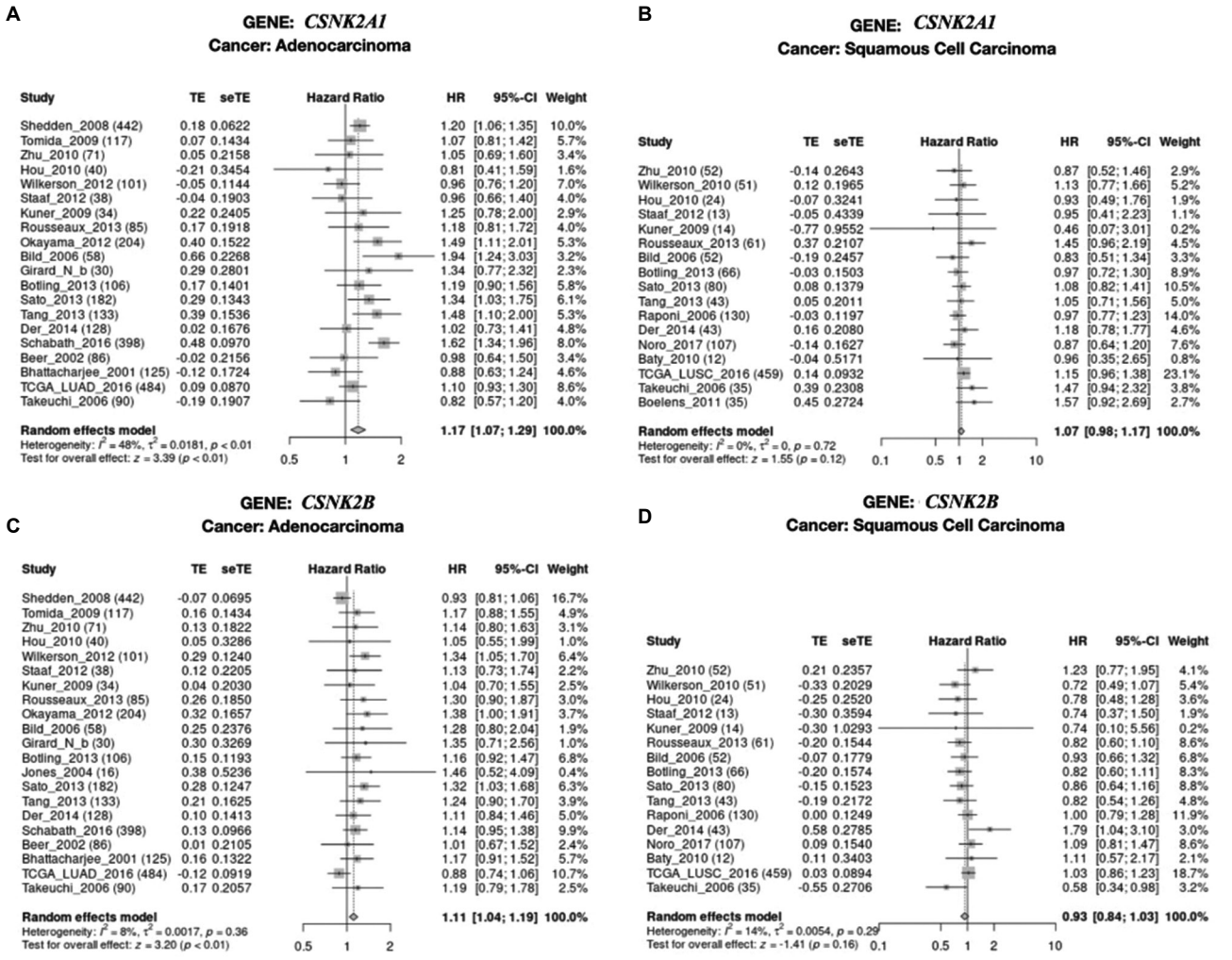

Figure 3. Meta-analysis of *CSNK2* mRNA expression versus overall survival, encompassing 20 independent LUAD and LUSC tumor data cohorts. Hazard ratios for each *CSNK2* gene were independently assessed across studies. Summary statistics and the global score are displayed at the bottom left and right corners of the charts, respectively. Hazard profiles for *CSNK2A1* and *CSNK2B* are shown for (A and C) LUAD and (B and D) LUSC.
Abbreviations: LUSC: Lung squamous cell carcinoma; LUAD: Lung adenocarcinoma.

To quantify AKTs129 phosphorylation as an indicator for CK2 enzymatic activity *in situ*, we performed IHC analysis using a phosphosite-specific antibody on a subset of LUAD (n = 76) and LUSC (n = 36) samples from the same patient cohort (Tables S3 and S4). Both total protein levels (tAKT) and phosphorylated AKTs129 protein (pAKT) were significantly elevated in LUAD and LUSC samples compared to para-neoplastic tissues, with the highest levels observed in LUSC (Figure 6C). Notably, pAKT levels did not correlate with CK2 subunit levels in either LUAD or LUSC specimens (Figure 6D). Finally, CSNK2A1 and CSNK2A2 showed strong correlations with each other in both LUAD (R = 0.504) and LUSC (R = 0.661) samples, whereas CSNK2B positively correlated only with CSNK2A1 in LUAD (R = 0.398) (Figure 6D; Table S5).

Further IHC analysis was conducted on a subset of LUAD (n = 66) and LUSC (n = 16) samples to quantify NPM1s125 phosphorylation as a second *in situ* indicator of CK2 enzymatic activity (Figure S9). Both total NPM1 protein and phosphorylated NPM1s125 protein (pNPM1) were elevated in tumor samples compared to para-neoplastic tissues (Figure S9A and B). Almost all tumor specimens (95%) showed positive-to-strong positive pNPM1 staining, with an R>2 over para-neoplastic tissues (para-LUAD = 45%; para-LUSC = 44%) (Figure S9B). Interestingly, pNPM1 phosphorylation levels correlated with CSNK2A2, but not with CSNK2A1 in LUAD; in contrast, in LUSC, pNPM1 levels correlated with both catalytic subunits, CSNK2A1 and CSNK2A2 (Figure S9C; Table S6). Finally, CK2 catalytic subunits showed strong

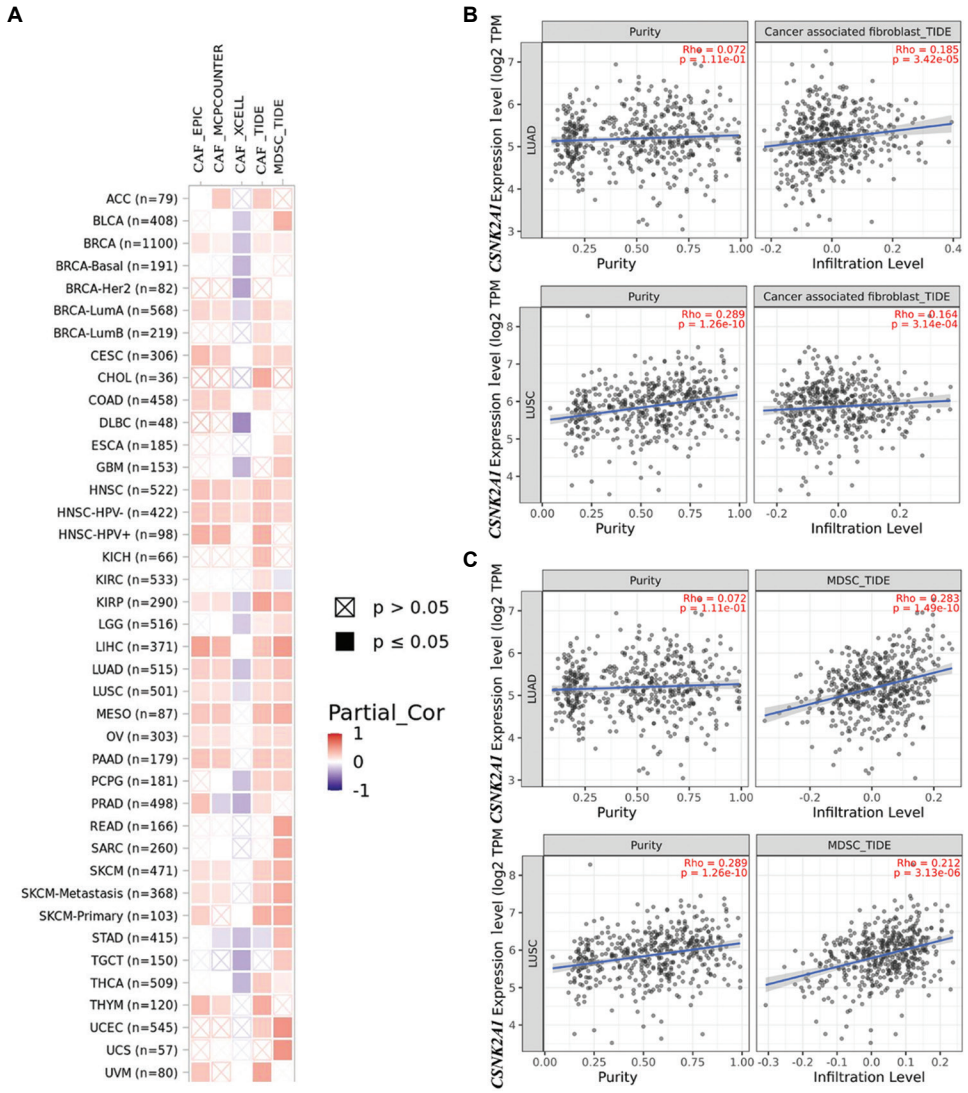

Figure 4. Correlation of CSNK2A1 gene expression levels with infiltrating cell populations in the tumor microenvironment, as analyzed using the TIMER2.0 database. (A) Correlations were assessed using four metrics for cancer-associated fibroblasts (CAFs) (CAF_EPIC, CAF_MCPCOUNTER, CAF_XCELL, CAF_TIDE) and one for myeloid-derived suppressor cells (MDCS) (MDSC_TIDE) across TCGA tumor types; "n" denotes the numbers of clinical samples within each cohort; (B) Detailed correlation analysis of CAF infiltration (CAF_TIDE metric) with CSNK2A1 expression level (Log2- TPM) in LUAD and LUSC; (C) Detailed analysis of MDSC infiltration (MDSC_TIDE metric) with CSNK2A1 expression level (Log2-TPM) in LUAD and LUSC. Each analysis was normalized for sample purity, with significant correlations indicated by color-filled boxes in the heatmap, where color intensity reflects correlation strength. Abbreviations: CAF: Cancer-associated fibroblasts; TPM: transcripts per million; LUAD: lung adenocarcinoma; LUSC: lung squamous carcinoma.

correlations with each other, particularly in LUSC samples (R = 0.683), whereas CSNK2B positively correlated only with CSNK2A1 in LUAD (R = 0.372) (Table S6).

4. Discussion

The deregulation of CK2 and its potential role in neoplastic processes have been revisited in recent studies.[24] CK2 enzyme biochemistry, aberrant expression, phosphorylation cascades, and the enzyme's tumor-supportive activities – both intrinsic and extrinsic – have been extensively investigated in preclinical models.[13,25] In parallel, several CK2 inhibitors have been developed and tested for antineoplastic effects in both *in vitro* and *in vivo*.[9] Despite this wealth of information and the availability of therapeutic compounds targeting CK2, only two CK2 inhibitors have advanced to clinical trials.[11,12]

Notably, translational and clinical data on CK2 remain relatively limited and sparse.[13] In a pioneering study, Ortega *et al.*[26] analyzed *CSNK2* transcript expression in seven tumor types, including lung cancers, using the Oncomine database. *CSNK2A1*, *CSNK2A2*, and *CSNKB* mRNA transcripts were overexpressed in 14/14,

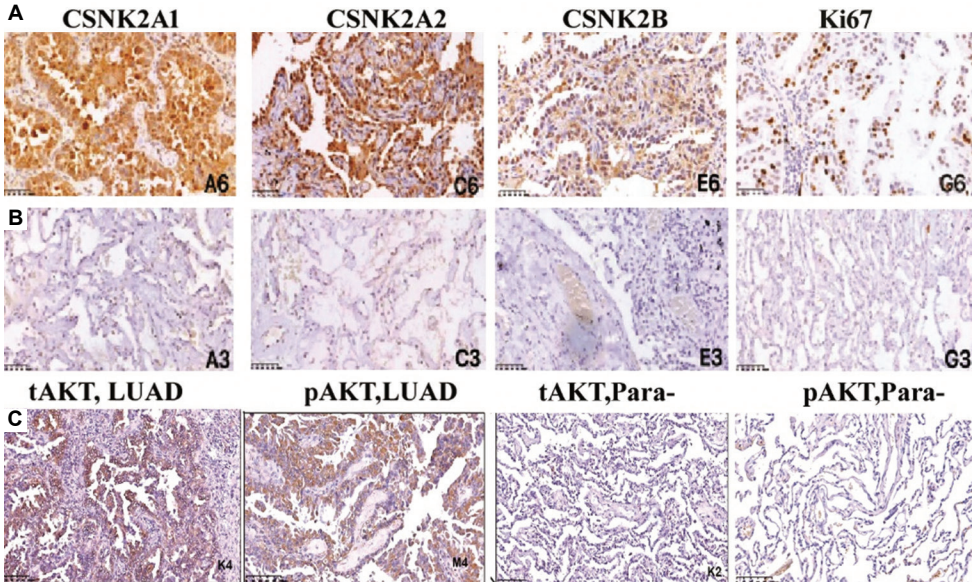

Figure 5. Immunohistochemical detection of CK2 subunits and CK2 substrate phosphorylation (AKT) in LUAD specimens and para-neoplastic tissues. Representative staining results for each CK2 subunit are shown: (A) in tumor and (B) in para-neoplastic tissues as a brown color; (C) Total AKT and phosphorylated AKTs129 (pAKT) protein levels were measured in tumor (LUAD) and para-neoplastic (Para-) tissues as an indicator of CK2 enzymatic activity in situ. Images were captured at 200× magnification. Scale bars: 100 μm.
Abbreviations: LUAD: Lung adenocarcinoma; CK2: Casein kinase-2.

Table 1. Immunohistochemical detection and quantification using a combined immunoreactivity score for independent CK2 subunits in primary tumor specimens of NSCLC and para-neoplastic tissues

Groups	Sample size	Score				Positive rate	z-score	*P*-value
		–	+	++	+++			
CK2A1								
NSCLC	134	30	50	27	27	77.6	−9.864	0.000
Para-neoplastic	134	107	24	2	1	20.1		0.000
CK2A2								
NSCLC	134	16	55	41	21	88.1	−7.248	0.000
Para-neoplastic	134	65	49	16	4	51.5		0.000
CK2B								
NSCLC	134	13	48	35	38	90.3	−8.538	0.000
Para-neoplastic	134	76	35	18	5	43.3		0.000
Ki-67								
NSCLC	134	58	32	20	24	56.7	−9.722	0.000
Para-neoplastic	134	131	3	0	0	2.2		0.000

Notes: Score 1 – 3: – (negative); Score 4 – 5: + (weak positive); Score 6 – 7: ++ (positive); Score ≥8: +++ (strong positive); Two-sided $P<0.05$ was considered statistically significant for all calculations.
Abbreviation: NSCLC: Non-small-cell lung cancer.

2/2, and 3/3 significant unique analyses, respectively, involving lung cancer specimens. In addition, Kaplan–Meier analysis revealed a significant correlation between *CSNK2B* overexpression and reduced OS, while *CSNK2A2* overexpression was unexpectedly associated with improved OS in LUAD.[26] A follow-up analysis analyzing 16 additional tumor types indicated cancer-type-specific up- or downregulation of *CSNK2* transcripts, as well as direct and inverse correlations between *CSNK2* transcripts and OS.[27] Overall, the prevailing notion is that CK2's aberrant expression levels or activity are instrumental to malignant transformation and promotion; however, the

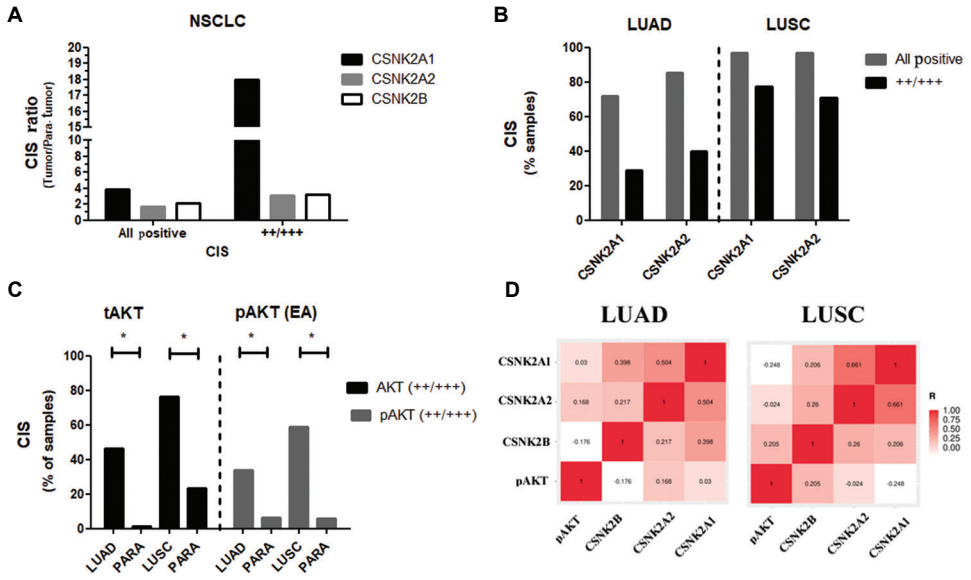

Figure 6. Quantification of IHC results in LUAD and LUSC samples using the combined IHC score. (A) Ratio (R) of tumor (T)/para-neoplastic (PN) positive staining (R = T/PN) as an indicator for tumor-specific association. The analysis included all positive (+/++/+++) or positive-to-strong positive intensity samples (++/+++); (B) Percentage of all positive or positive-to-strong positive staining in LUAD or LUSC samples; (C) IHC results for total AKT protein and phosphorylated AKTs129 protein (pAKT) in LUAD and LUSC samples; (D) Visualization of correlations between CSNK2A1/CSNK2A2/CSNKB protein subunit levels and phosphorylated AKTs129. Statistical analysis is detailed in Tables S3 and S4.
Abbreviations: IHC: Immunohistochemistry; LUAD: Lung adenocarcinoma; LUSC: Lung squamous carcinoma.

efficacy of CK2 inhibition as an anticancer strategy may be context-dependent.[13]

Despite the availability of clinical multiomics databases, there is no comprehensive analysis encompassing CK2 mutational burden, gene/protein expression, and, importantly, CK2 enzymatic activity deregulation in cancer. CK2 subunit-specific contributions to certain tumor phenotypes highlight the necessity for analyzing each subunit's regulatory patterns and functional implications individually.[28-30] Such analyses may provide fresh insights for the CK2 research community, which continues to debate whether CK2 is an actionable and safe target for cancer intervention.[6,8]

In this study, we used cBioPortal to analyze a pan-cancer dataset and two NSCLC cohorts from the TCGA PanCancer Atlas. Our results indicate that mutational events, such as single base insertions, substitutions, deletions, and/or can, are rare within *CSNK2* subunit genes and, when present, do not appear to confer oncogenic potential. These findings align with CK2's roles in the concept of "non-oncogene addiction".[1]

The *CSNK2* gene promoters display characteristics typical of housekeeping genes, including a CpG island near exon 1, which can be methylated.[31] Therefore, we investigated promoter/1stExon/5'UTR methylation and its correlations with *CSNK2* gene expression in LUSC and LUAD cohorts. Promoter/1stExon methylation showed a weak (<−0.30) negative correlation with *CSNK2A2* and *CSNK2B* mRNA levels. Interestingly, *CSNK2A1* mRNA overexpression was nearly twice as common as that of *CSNK2A2* and *CSNK2B*, with higher median expression values, particularly in LUSC samples. However, differential methylation alone does not fully explain the extensive deregulation of *CSNK2* mRNA observed in NSCLC, suggesting that more complex transcriptional and post-transcriptional regulatory mechanisms are involved.[3]

A meta-analysis of 20 LUAD and 17 LUSC clinical studies corroborated that *CSNK2A1* and *CSNK2B* mRNA overexpression correlates with poorer prognosis in LUAD, whereas *CSNK2A2* overexpression is associated with better outcomes. This trend for *CSNK2B* and *CSNK2A2* was previously observed in a microarray-based study.[26] Overall, we found that *CSNK2A1* and *CSNK2B* mRNA levels were particularly elevated in primary LUAD and LUSC samples, as well as in a limited set of metastatic NSCLC clinical samples. In addition, we identified direct correlations between *CSNK2* subunit mRNA levels and tumor infiltration by MDSC/CAF. In LUAD, the strongest correlations were observed between *CSNK2A1* and MDSC infiltration, as well as between *CSNK2B* and MDSC infiltration. These cell populations, known for their array of tumor-supportive functions, rely on secreted molecules and mediators, including CK2 substrates, for their

accumulation within the tumor microenvironment.[32-36] In summary, based on mRNA expression data, we consistently observed *CSNK2A1* and *CSNK2B* overexpression, associations with survival and metastasis, and stronger correlations with tumor-infiltrating MDSC, particularly in LUAD samples. Although internal correlations among *CSNK2* subunits may pose some analysis bias, we did not detect significant internal correlations between *CSNK2A1* and *CSNK2B*. Furthermore, correlations between the catalytic subunits were weaker in LUAD (S = 0.14) than in LUSC (S = 0.24) across analyzed cohorts.

On the other hand, protein information concerning CK2 subunits and enzymatic activity in human lung specimens is limited. Strum *et al.*[13] reviewed four studies measuring overall CK2 levels or activity in LUAD and/or LUSC samples.[37-40] In one of these studies, Liu *et al.*[39] analyzed *CSNK2A2* subunit expression in 160 NSCLC patients, finding it upregulated in both LUAD and LUSC and marginally associated with reduced OS. In our studies, we observed elevated protein levels for all three CK2 subunits in LUAD and LUSC specimens. More importantly, we demonstrate that this upregulation correlates with increased enzymatic activity *in situ*, as indicated by CK2 substrates predominantly localized in the cytoplasm (AKT) or nucleus (NPM1) of the cell. Notably, the catalytic subunits CSNK2A1 and CSNK2A2, and their purported enzymatic activity (as suggested by pAKT levels), were higher in LUSC than in LUAD specimens. We consider the canonical AKTs129 (pAKT) phosphorylation site a more reliable surrogate marker for CK2 *in situ* activity in tumors compared to NPM1s125 (pNPM1).[13] The differing extents of AKT and NPM1 phosphorylation could be explained by variations in phosphorylation turnover for each substrate and phosphorylation site within CK2 signaling, potentially faster for AKT.[41] Finally, *CSNK2A1* and *CSNK2A2* expression correlated strongly and positively with NPM1 (but not AKT), underscoring the complex interplay among kinase-phosphatase activities, CK2 substrates, and subcellular compartments.[41]

Importantly, CSNK2A1 (but not CSNK2A2) protein overexpression correlates with tumor size, stage, and proliferation score in the NSCLC tumors analyzed. This subunit-specific association is evident despite positive internal correlations between both catalytic subunits at the protein (R≈0.5) and mRNA levels (R≈0.2) across independent cohorts. Notably, at the protein level, context-dependent regulatory crosstalk occurs among CK2 subunits, reflecting overlapping activities and, in some instances, isoforms-specific functions.[3] Therefore, our findings suggest that CSNK2A1 may play a distinctive role in NSCLC. Supporting this notion, our IHC studies indicate that CSNK2A1 protein is more tumor-specific than CSNK2A2. Interestingly, a preliminary *in vitro* assessment of dependency scores from knocking out (CRISPR-Chronos) individual *CSNK2* genes in 98 NSCLC cell lines suggests that *CSNK2A1*-KO is approximately 10-fold more "essential" than *CSNK2A2*-KO in these lung cancer models (https://depmap.org/portal/).[42]

5. Conclusion

Our data suggest that transcriptional regulatory mechanisms, rather than mutational and CNA events, drive the increased mRNA expression of CK2 subunits in NSCLC samples. Correspondingly, CK2 subunits and enzymatic activity are significantly upregulated in NSCLC, particularly in LUSC. Correlative studies at both mRNA and protein levels indicate that CSNK2A1, and potentially its homotetramer ($CSNK2A1_2/CSNK2B_2$), may exert specific tumor-supportive functions in LUAD. These compelling yet correlative findings highlight the potential need for isoform-specific CK2-targeted therapies and may further elucidate CK2's role in NSCLC on the development of tailored drugs against specific CSNK2 isoforms or homotetramers.

Acknowledgments

The results published here are partly based on data generated by the TCGA Research Network (https://www.cancer.gov/tcga). We also thank assistant researchers and technicians from the First Affiliated Hospital of the University of South China.

Funding

This research was supported by the National Key R&D Program of China (2021YFE0192100).

Conflict of interest

The authors declare that they have no competing interests.

Author contributions

Conceptualization: George V. Pérez, Yasser Perera
Investigation: All authors
Methodology: George V. Pérez, Qiang Zhao, Zhiwei Zhang, Yasser Perera
Writing – original draft: Yasser Perera
Writing – review & editing: George V. Pérez

Ethics approval and consent to participate

Studies involving human specimens were conducted in accordance with ethical principles from the Helsinki Declaration (2013), the Regulations on Biomedical Ethics Review Involving Humans (2016), the Regulations on

Clinical Research Ethics Review in Traditional Chinese Medicine, and the International Ethical Guidelines for Biomedical Research Involving Human Subjects. This project, titled "Research on Novel Peptide Drugs Targeting CK2-Mediated Phosphorylation for the Treatment of Non-Small-Cell Lung Cancer (NSCLC)" was reviewed and approved by the Nanhua University Affiliated First Hospital Medical Ethics Review Committee. Review information is as follows: Review Batch Number: 2021LL0115001; Meeting Date: January 15, 2021. Reviewed Materials: Research Plan Version: YJFA20210114; Informed Consent Form Version: ZQTY20210114. Signature by Medical Ethics Committee of Nanhua University Affiliated First Hospital Issuance Date: January 15, 2021.

Consent for publication

Written informed consent forms were obtained for the participation and subsequent publication of human data masking or concealing any identifying information of the patients.

Availability of data

The original contributions presented in the study are included in the article/supplementary material; further inquiries can be directed to the corresponding author/s.

Further disclosure

Part of the analysis/data has been uploaded to or deposited as preliminary findings in a preprint server BioRxiv doi: https://doi.org/10.1101/2023.08.04.551954.

References

1. Ruzzene M, Pinna LA. Addiction to protein kinase CK2: A common denominator of diverse cancer cells? *Biochim Biophys Acta*. 2010;1804(3):499-504.

   doi: 10.1016/j.bbapap.2009.07.018

2. Borgo C, Franchin C, Cesaro L, *et al.* A Proteomics analysis of CK2β$^{(-/-)}$ C_2C_{12} Cells provides novel insights into the biological functions of the non-catalytic β subunit. *FEBS J*. 2019;286(8):1561-1575.

   doi: 10.1111/febs.14799

3. Roffey SE, Litchfield DW. CK_2 regulation: Perspectives in 2021. *Biomedicines*. 2021;9(10):1361.

   doi: 10.3390/biomedicines9101361

4. Trembley JH, Kren BT, Afzal M, Scaria GA, Klein MA, Ahmed K. Protein kinase CK_2- diverse roles in cancer cell biology and therapeutic promise. *Mol Cell Biochem*. 2023;478(4):899-926.

   doi: 10.1007/s11010-022-04558-2

5. Borgo C, D'Amore C, Cesaro L, *et al.* How can a traffic light properly work if it is always green? The paradox of CK_2 signaling. *Crit Rev Biochem Mol Biol.* 2021;56(4):321-359.

   doi: 10.1080/10409238.2021.1908951

6. Salvi M, Borgo C, Pinna LA, Ruzzene M. Targeting CK_2 in cancer: A valuable strategy or a waste of time? *Cell Death Discov.* 2021;7(1):325.

   doi: 10.1038/s41420-021-00717-4

7. Wells CI, Drewry DH, Pickett JE, *et al.* Development of a potent and selective chemical probe for the pleiotropic kinase CK_2. *Cell Chem Biol.* 2021;28(4):546-558.e10.

   doi: 10.1016/j.chembiol.2020.12.013

8. Licciardello MP, Workman P. A New chemical probe challenges the broad cancer essentiality of CK_2. *Trends Pharmacol Sci.* 2021;42(5):313-315.

   doi: 10.1016/j.tips.2021.02.002

9. Cozza G. The development of CK_2 inhibitors: From traditional pharmacology to *in silico* rational drug design. *Pharmaceuticals* (*Basel*). 2017;10(1):26.

   doi: 10.3390/ph10010026

10. Bancet A, Frem R, Jeanneret F, *et al.* AB668, a novel highly selective protein kinase CK_2 inhibitor with a distinct anti-tumor mechanism as compared to CX-4945 and SGC-CK2-1. bioRxiv [Preprint]. 2022.

    doi: 10.1101/2022.12.16.520736

11. Solares AM, Santana A, Baladrón I, *et al.* Safety and preliminary efficacy data of a novel casein kinase 2 (CK_2) peptide inhibitor administered intralesionally at four dose levels in patients with cervical malignancies. *BMC Cancer*. 2009;9:146.

    doi: 10.1186/1471-2407-9-146

12. Pierre F, Chua PC, O'Brien SE, *et al.* Discovery and SAR of 5-(3-chlorophenylamino)benzo[c][2,6]naphthyridine-8-carboxylic acid (CX-4945), the first clinical stage inhibitor of protein kinase CK2 for the treatment of cancer. *J Med Chem*. 2011;54(2):635-654.

    doi: 10.1021/jm101251q

13. Strum SW, Gyenis L, Litchfield DW. CSNK2 in cancer: Pathophysiology and translational applications. *Br J Cancer.* 2022;126(7):994-1003.

    doi: 10.1038/s41416-021-01616-2

14. Cerami E, Gao J, Dogrusoz U, *et al.* The CBio cancer genomics portal: An open platform for exploring multidimensional cancer genomics data. *Cancer Discov*. 2012;2(5):401-404.

    doi: 10.1158/2159-8290.CD-12-0095

15. Gao J, Aksoy BA, Dogrusoz U, *et al.* Integrative analysis of complex cancer genomics and clinical profiles using the CBioPortal. *Sci Signal*. 2013;6(269):pl1.

doi: 10.1126/scisignal.2004088

16. Martínez-Jiménez F, Muiños F, Sentís I, *et al.* A compendium of mutational cancer driver genes. *Nat Rev Cancer.* 2020;20(10):555-572.

doi: 10.1038/s41568-020-0290-x

17. Chakravarty D, Gao J, Phillips SM, *et al.* OncoKB: A precision oncology knowledge base. *JCO Precis Oncol.* 2017;1:1-16.

doi: 10.1200/PO.17.00011

18. Chandrashekar DS, Bashel B, Balasubramanya SAH, *et al.* UALCAN: A portal for facilitating tumor subgroup gene expression and survival analyses. *Neoplasia.* 2017;19(8): 649-658.

doi: 10.1016/j.neo.2017.05.002

19. Cai L, Lin S, Girard L, *et al.* LCE: An open web portal to explore gene expression and clinical associations in lung cancer. *Oncogene.* 2019;38(14):2551-2564.

doi: 10.1038/s41388-018-0588-2

20. Bartha Á, Győrffy B. TNMplot.Com: A web tool for the comparison of gene expression in normal, tumor and metastatic tissues. *Int J Mol Sci.* 2021;22(5):2622.

doi: 10.3390/ijms22052622

21. Li T, Fu J, Zeng Z, *et al.* TIMER2.0 for analysis of tumor-infiltrating immune cells. *Nucleic Acids Res.* 2020;48(W1):W509-W514.

doi: 10.1093/nar/gkaa407

22. TCGA Research Network. Available from: https://www.cancer.gov/tcga [Last accessed on 2024 Nov 27].

23. ICGC/TCGA Pan-Cancer Analysis of Whole Genomes Consortium. Pan-cancer analysis of whole genomes. *Nature.* 2020;578(7793):82-93.

doi: 10.1038/s41586-020-1969-6

24. Firnau MB, Brieger A. CK_2 and the hallmarks of cancer. *Biomedicines.* 2022;10(8):1987.

doi: 10.3390/biomedicines10081987

25. Chua MMJ, Ortega CE, Sheikh A, *et al.* CK_2 in cancer: Cellular and biochemical mechanisms and potential therapeutic target. *Pharmaceuticals* (*Basel*). 2017;10(1):18.

doi: 10.3390/ph10010018

26. Ortega CE, Seidner Y, Dominguez I. Mining CK_2 in cancer. *PLoS One.* 2014;9(12):e115609.

doi: 10.1371/journal.pone.0115609

27. Chua MMJ, Lee M, Dominguez I. Cancer-type dependent expression of CK_2 transcripts. *PLoS One.* 2017;12(12):e0188854.

doi: 10.1371/journal.pone.0188854

28. Filhol O, Giacosa S, Wallez Y, Cochet C. Protein kinase CK_2 in breast cancer: The CK2β regulatory subunit takes center stage in epithelial plasticity. *Cell Mol Life Sci.* 2015;72(17):3305-3322.

doi: 10.1007/s00018-015-1929-8

29. Litchfield DW, Bosc DG, Canton DA, Saulnier RB, Vilk G, Zhang C. Functional specialization of CK_2 isoforms and characterization of isoform-specific binding partners. *Mol Cell Biochem.* 2001;227(12):21-29.

30. Zonta F, Borgo C, Quezada Meza CP, *et al.* Contribution of the CK_2 catalytic isoforms α and α' to the glycolytic phenotype of tumor cells. *Cells.* 2021;10(1):181.

doi: 10.3390/cells10010181

31. Ackermann K, Neidhart T, Gerber J, Waxmann A, Pyerin W. The catalytic subunit alpha' gene of human protein kinase CK_2 ($CSNK_2A_2$): Genomic organization, promoter identification and determination of Ets1 as a key regulator. *Mol Cell Biochem.* 2005;274(1-2):91-101.

doi: 10.1007/s11010-005-3076-2

32. Sheida F, Razi S, Keshavarz-Fathi M, Rezaei N. The role of myeloid-derived suppressor cells in lung cancer and targeted immunotherapies. *Expert Rev Anticancer Ther.* 2022;22(1):65-81.

doi: 10.1080/14737140.2022.2011224

33. Chen C, Hou J, Yu S, *et al.* Role of cancer-associated fibroblasts in the resistance to antitumor therapy, and their potential therapeutic mechanisms in non-small cell lung cancer. *Oncol Lett.* 2021;21(5):413.

doi: 10.3892/ol.2021.12674

34. Wu F, Yang J, Liu J, *et al.* Signaling pathways in cancer-associated fibroblasts and targeted therapy for cancer. *Signal Transduct Target Ther.* 2021;6(1):218.

doi: 10.1038/s41392-021-00641-0

35. Glabman RA, Choyke PL, Sato N. Cancer-associated fibroblasts: Tumorigenicity and targeting for cancer therapy. *Cancers* (*Basel*). 2022;14(16):3906.

doi: 10.3390/cancers14163906

36. Umansky V, Blattner C, Gebhardt C, Utikal J. The role of myeloid-derived suppressor cells (MDSC) in cancer progression. *Vaccines* (*Basel*). 2016;4(4):36.

doi: 10.3390/vaccines4040036

37. Daya-Makin M, Sanghera JS, Mogentale TL, *et al.* Activation of a tumor-associated protein kinase (P40TAK) and casein kinase 2 in human squamous cell carcinomas and adenocarcinomas of the lung. *Cancer Res.* 1994;54(8): 2262-2268.

38. Yaylim I, Isbir T. Enhanced casein kinase II (CK II) activity in human lung tumours. *Anticancer Res.* 2002;22(1A): 215-218.

39. Liu Y, Amin EB, Mayo MW, *et al.* CK2α' drives lung cancer metastasis by targeting BRMS1 nuclear export and degradation. *Cancer Res.* 2016;76(9):2675-2686.

doi: 10.1158/0008-5472.CAN-15-2888

40. Xie ZC, Tang RX, Gao X, *et al.* A meta-analysis and bioinformatics exploration of the diagnostic value and molecular mechanism of mir-193a-5p in lung cancer. *Oncol Lett*. 2018;16(4):4114-4128.

doi: 10.3892/ol.2018.9174

41. Cesaro L, Zuliani AM, Travain VB, Salvi M. Exploring protein kinase CK_2 substrate recognition and the dynamic response of substrate phosphorylation to kinase modulation. *Kinases Phosphatases*. 2023;1(4):251-264.

doi: 10.3390/kinasesphosphatases1040015

42. Tsherniak A, Vazquez F, Montgomery PG, *et al.* Defining a cancer dependency map. *Cell*. 2017;170(3):564-576.e16.

doi: 10.1016/j.cell.2017.06.010

ACCSCIENCE PUBLISHING

Tumor Discovery

CASE REPORT

Signet ring cell carcinoma of the urinary bladder presenting with carcinocythemia and skeletal metastasis: A case report

Emma Rullo[1]*, Piergianni Biondi[2], Chiara Nicolazzo[3], Walter Gianni[2], Luciano Colangelo[2], Mirella Cilli[2], Paola Gazzaniga[3], Mara Riminucci[1], Alessandro Corsi[1], and Salvatore Minisola[2]

[1]Department of Molecular Medicine, Sapienza University, and Section of Pathology, Policlinico Umberto I, Rome, Italy

[2]Department of Clinical, Internal, Anesthesiologic and Cardiovascular Sciences, Sapienza University, and Mineral Metabolism Section, Policlinico Umberto I, Rome, Italy

[3]Department of Molecular Medicine, Sapienza University, and Cancer Liquid Biopsy Unit, Policlinico Umberto I, Rome, Italy

Abstract

Cancer of unknown primary accounts for approximately 3 – 5% of all malignancies and is typically associated with a dismal prognosis. We describe a 65-year-old man who presented with skeletal metastasis and circulating tumor cells exhibiting signet ring (SR) morphology. The patient was diagnosed with SR cell carcinoma (SRCC) through a bone marrow biopsy. This case report aimed to emphasize the importance of clinicians' awareness of SRCC of the urinary bladder. The primary site of tumor origin was not identified as *antemortem*. The patient died 2 months after being admitted for pulmonary embolism. At autopsy, the urinary bladder was determined to be the primary site of the tumor. Primary SRCC of the urinary bladder is extremely rare. There are currently no established consensus guidelines for its management. Surgery continues to be the primary treatment option when the condition is localized.

Keywords: Cancer of unknown primary; Signet ring cell carcinoma; Urinary bladder carcinoma; Carcinocythemia

***Corresponding author:**
Emma Rullo
(emma.rullo@uniroma1.it)

Citation: Rullo E, Biondi P, Nicolazzo C, *et al*. Signet ring cell carcinoma of the urinary bladder presenting with carcinocythemia and skeletal metastasis: A case report. *Tumor Discov*. 2024;3(4):3736. doi: 10.36922/td.3736

Received: May 22, 2024

Accepted: August 7, 2024

Published Online: October 8, 2024

1. Introduction

Cancer of unknown primary (CUP) is defined by the European Society of Medical Oncology as a "carcinoma or undifferentiated neoplasm for which a standardized diagnostic workup fails to identify the primary tumor responsible for metastatic seeding."[1] It constitutes <5% of all cancers and its incidence is higher in men and increases with age.[1-4] Histologically, approximately 80% of the tumors are adenocarcinomas or undifferentiated carcinomas.[1-6] Typically, patients exhibit metastases in various organs, with the liver being the most frequently affected site.[1-4]

In the urinary bladder, primary adenocarcinomas account for <2% of all primary malignant tumors.[7] Pure signet ring cell carcinoma (SRCC) is one of the rarest histological subtypes and is associated with the worst prognosis because of its presentation at an advanced stage and possible intrinsic aggressive biological features.[7-10]

Adenocarcinomas are the most prevalent histologic type that manifests as CUP. SRCC, a poorly differentiated aggressive subtype of adenocarcinoma, has been rarely reported to manifest as metastatic SRCC of unknown primary origin.[11] This case report describes a patient who presented with skeletal metastasis and circulating tumor cells (CTCs) exhibiting signet ring (SR) morphology. The diagnosis of SRCC was confirmed through bone marrow biopsy results. Despite an in-depth diagnostic workup, we were unable to establish the primary site of the tumor. The patient died 2 months after hospitalization. At autopsy, the urinary bladder was established as the primary site of the tumor.

2. Case presentation

A 65-year-old man was admitted for severe asthenia and low-grade fever. He reported having previously undergone mandibular surgery for ameloblastoma. Blood tests revealed severe anemia (Hemoglobin = 3.8 g/dL), thrombocytopenia (34.000/mm^3), high ferritin (2100 ng/mL) and lactate dehydrogenase levels (777 U/L), hypokalemia (1.61 mEq/L), hypoproteinemia, and normal liver enzymes and tumor markers. Serum alkaline phosphatase levels were elevated (1102 U/L, n.v. 34 – 102 U/L). Tc-99m-methylene-diphosphonate scintigraphy revealed a super-scan pattern (i.e., there was a concentration of the radiotracer in the skeleton with minimal or no activity in the soft tissues or urinary tract) with multiple foci of increased tracer uptake throughout the skeleton (Figure 1A). Whole-body computed tomography (CT) revealed mixed (lytic and sclerotic) vertebral lesions (Figure 1B), indicating metastatic skeletal disease. The free/total prostate-specific antigen (PSA) ratio was 9.41. The FDA-approved CellSearch® system (Menarini Silicon Biosystems, Castel Maggiore, Bo, Italy) detected 387 solitary and 9 clustered (2 – 3 cells) cytokeratin (CK)-positive CTCs with SR morphology (Figure 2A), as previously described.[12] Briefly, 7.5 mL of whole blood was processed using the CellSearch® CTC kit. After EpCAM-based immunomagnetic capture, the cells were stained with antibodies anti-CK8,18,19-fluorescein isothiocyanate and anti-CD45-allophycocyanin and with 4′,6-diamidino-2-phenylindole for detecting the nucleus. Immunofluorescence images were eventually analyzed using CellSearch® Analyzer II. SRCC metastasis was diagnosed on the iliac crest and vertebral biopsies (Figure 2B and C). The neoplastic cells tested negative for CK7, CK20, TTF1, and PSA. Because SRCC is known to originate more frequently from the gastrointestinal tract, esophagogastroduodenoscopy, colonoscopy, small-intestine contrast ultrasonography, and CT enterography revealed negative results. Transrectal ultrasonography and urinary cytology also revealed

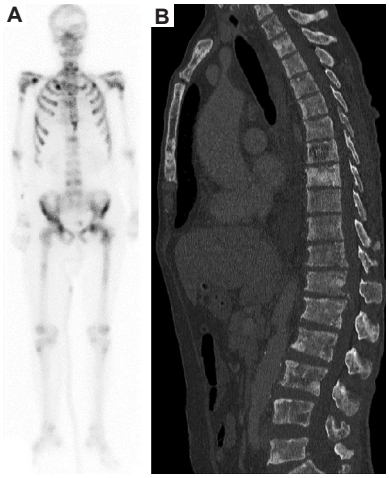

Figure 1. Findings of skeletal involvement (A) Tc-99m-methylene-diphosphonate scintigraphy revealing a super-scan pattern with multiple foci of increased tracer uptake throughout the skeleton, with little or no activity in the soft tissues or urinary tract. (B) Computed tomography (sagittal plane) image revealing mixed (lytic and sclerotic) lesions in the vertebral bodies.

negative results. Two peripheral lesions indeterminate for malignancy were identified during multiparametric prostate-magnetic resonance imaging, which was conducted in response to the low free/total PSA ratio and the negative results of the immunohistochemical staining for CK7 and CK20.[1,3-6] Prostatic biopsy was planned but not performed because of the rapid deterioration of the patient's general conditions (Eastern Cooperative Oncology Group/World Health Organization Performance Status 4). Androgen deprivation therapy and zoledronate were initiated, but the patient died suddenly. An autopsy revealed pulmonary embolism as the cause of death. The entire prostate was processed for histological examination due to the clinical suspicion of prostate cancer; however, it was revealed to be malignancy-free. The urinary bladder was devoid of any intraluminal mass. Histological examination revealed diffuse SRCC cell infiltration within the entire thickness of the lamina propria (Figure 2D and E). Rare cells were immunoreactive for CK7 and CK20. Neoplastic lymphatic invasion within the urinary bladder wall was significant. Mesenteric lymph nodes had metastases along the vertebrae.

3. Discussion

The case reported here represents a typical example of CUP, in which an extensive diagnostic workup failed to establish the tumor's primary origin. CUP, a well-established oncologic condition, is associated with a dismal outcome and a median survival duration of 8 – 11 months.[1-4] Its diagnosis is always based on the histopathologic examination of the biopsy specimen

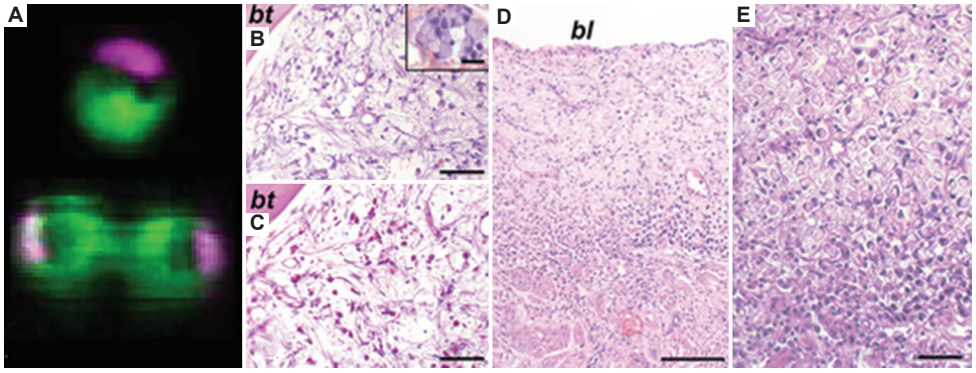

Figure 2. Representative images of a single (top) circulating tumor cell (CTC) and a cluster of two (bottom) CTCs exhibiting small signet ring (SR) morphology (cytokeratin/4′,6-diamidino-2-phenylindole) are shown in panel (A). (B and C) Consecutive sections of the bone marrow biopsy stained with hematoxylin–eosin and periodic acid–Schiff are shown in panels (B) and (C), respectively. The insert in B shows a cluster of SR cells. These cells are promptly recognizable for the eccentrically located nucleus and the abundant amount of mucin within the cytoplasm. Representative low- and high-power magnification of the urinary bladder wall stained with hematoxylin–eosin are shown in panels (D) and (E), respectively. The whole thickness of the lamina propria is diffusely infiltrated by neoplastic cells with SR morphology.
Abbreviations: *bt* (in B and C) is for bone trabecula and *bl*, *lp*, and *mp* (in D) are for urinary bladder lumen, lamina propria, and muscularis propria, respectively. Magnification for A: 10 ×. Scale bars: 100 mm for B-D and 80 mm for E.

from a metastatic site.[3] Immunostaining for CK7 and CK20 is typically performed when adenocarcinoma is detected histopathologically, providing physicians with indications of the tumor's primary site. CK7 is widely expressed in the breast, lung, pancreas, biliary tract, and transitional carcinomas, whereas CK20 is expressed in the gastrointestinal tract (especially colon and rectum) and transitional carcinomas.[1,3-6] In our patient, results for the CKs, TTF1, and PSA were negative on sections from the bone marrow biopsy specimen.

Despite extensive clinical workup, a primary tumor is identified in <20% of patients with CUP. *Antemortem* and autopsy studies have reported that 70% of cases remain undiagnosed.[4] Autopsy enabled us to identify the urinary bladder as the primary site of the tumor's origin. The urinary bladder is not among the most frequently encountered sites of the primary tumor, which typically include the pancreas (20 – 26%), lungs (17 – 23%), colon/rectum (4 – 10%), liver (3 – 11%), stomach (3 – 8%), kidneys (4 – 6%), ovaries (3 – 4%), prostate (3 – 4%), and breast (2%).[3,4] In our case, the issue was further complicated by the histological type of the diagnosed tumor. SRCC most commonly originates in the gastrointestinal tract and, in the genitourinary system, it rarely occurs in the prostate[7] and urinary bladder, where it accounts for no more than 0.6% of all primary malignant tumors.[8-10] Recent reviews on primary SRCC of the urinary bladder have indicated that approximately 300 cases have been reported in the English literature.[8-10] The carcinoma commonly arises in men in their seventh decade of life, typically at an advanced tumor stage, and exhibits an aggressive clinical course with a high frequency of metastasis and an ominous prognosis.[8-10] Its clinical presentation is comparable to that of the more common urothelial carcinoma of the urinary bladder, and hematuria is its most prevalent presenting symptom.[8-10] Imaging features are not specific, and SRCCs have been identified in only urine samples rarely.[13] Notably, the manifestation of SRCC as CUP has been rarely reported.[11] In our patient, SRCC manifested with skeletal metastasis and carcinocythemia (i.e., blood circulating cells from solid epithelial tumors), which indicated an advanced tumor stage, and the tumor's site of origin was determined during autopsy. Carcinocythemia, first described by Carey *et al.*,[14] is a rare finding that is reportedly becoming more common.[15] To the best of our knowledge, carcinocythemia has never been associated with primary urinary bladder SRCC.

In cases such as the one reported here, a comprehensive diagnostic workup is necessary to identify the primary site of malignancy and determine the best therapeutic options to improve the prognosis. However, due to the rarity of primary urinary bladder SRCC, there are no established consensus guidelines for its management.[8-10] The localized form is treated primarily with surgery, and the prognosis is favorable when the tumor is detected early and removed through radical resection.[10] Diverse treatment approaches involving surgery, radiotherapy, chemotherapy, and their combinations for both localized and metastatic urinary bladder SRCC have been recently reviewed.[8] As indicated by Lendorf *et al.*,[8] exploring the role of immune checkpoint inhibitors may represent a valuable area for future clinicopathological research in the context of primary urinary bladder SRCC. However, because modern therapeutic approaches tend to be limited

to the primary site of origin of a malignant tumor[2] and molecular approaches that could be useful to this goal are not always accessible,[16,17] the application of deep-learning-based algorithms on whole-slide histological images[18] is a promising tool for identifying the primary site of origin of a CUP.

4. Conclusion

Primary SRCC is a variant of adenocarcinoma that rarely develops primarily in the urinary bladder. It may manifest as a CUP, as evidenced by the case described here. The prognosis of this carcinoma is typically dismal as it is an aggressive tumor, and the diagnosis is generally made at an advanced stage of the disease. The urinary bladder should be considered as a site of origin of SRCC when the most common sites of origin (i.e., the gastrointestinal tract) have been excluded, even in the absence of an endoluminal mass and with negative urinary cytology results, as observed in the case reported here. We believe that our case may have significant implications in clinical practice. It is imperative that clinicians are aware of the possibility of a metastatic SRCC originating from the urinary bladder.

Acknowledgments

None.

Funding

None.

Conflict of interest

The authors declare that they have no competing interests.

Author contributions

Conceptualization: Emma Rullo, Mara Riminucci, Alessandro Corsi, Salvatore Minisola

Formal analysis: Emma Rullo, Piergianni Biondi, Chiara Nicolazzo, Walter Gianni, Luciano Colangelo, Mirella Cilli, Paola Gazzaniga, Mara Riminucci, Alessandro Corsi

Methodology: Emma Rullo, Chiara Nicolazzo, Paola Gazzaniga, Mara Riminucci, Alessandro Corsi

Investigation: Emma Rullo, Chiara Nicolazzo, Paola Gazzaniga, Mara Riminucci, Alessandro Corsi, Salvatore Minisola

Writing–original draft: Emma Rullo

Writing–review & editing: Emma Rullo, Mara Riminucci, Alessandro Corsi, Salvatore Minisola

Ethics approval and consent to participate

Ethical approval is not required as this is a case report. All the clinical and pathologic investigations detailed in the manuscript have been conducted in accordance with the Declaration of Helsinki and its later amendments.

Consent for publication

Informed consent for the publication of data and images was obtained from the next-of-kin as the subject had passed away.

Availability of data

All data generated or analyzed during this study are included in the submitted article.

References

1. Krämer A, Bochtler T, Pauli C, *et al*. Cancer of unknown primary: ESMO Clinical Practice Guideline for diagnosis, treatment and follow-up. *Ann Oncol*. 2023;34(3):228-246.

   doi: 10.1016/j.annonc.2022.11.013

2. Levi F, Te VC, Erler G, Randimbison L, La Vecchia C. Epidemiology of unknown primary tumours. *Eur J Cancer*. 2002;38(13):1810-1812.

   doi: 10.1016/s0959-8049(02)00135-1

3. Massard C, Loriot Y, Fizazi K. Carcinomas of an unknown primary origin--diagnosis and treatment. *Nat Rev Clin Oncol*. 2011;8(12):701-710.

   doi: 10.1038/nrclinonc.2011.158

4. Pavlidis N, Fizazi K. Carcinoma of unknown primary (CUP). *Crit Rev Oncol Hematol*. 2009;69(3):271-278.

   doi: 10.1016/j.critrevonc.2008.09.005

5. Oien KA. Pathologic evaluation of unknown primary cancer. *Semin Oncol*. 2009;36(1):8-37.

   doi: 10.1053/j.seminoncol.2008.10.009

6. Beauchamp K, Moran B, O'Brien T, *et al*. Carcinoma of unknown primary (CUP): An update for histopathologists. *Cancer Metastasis Rev*. 2023;42:1189-1200.

   doi: 10.1007/s10555-023-10101-6

7. Celik O, Budak S, Ekin G, Akarken I, Ilbey YO. A case with primary signet ring cell adenocarcinoma of the prostate and review of the literature. *Arch Ital Urol Androl*. 2014;86(2):148-149.

   doi: 10.4081/aiua.2014.2.148

8. Lendorf ME, Dohn LH, Dunga BA, Loya AC, Pappot H. An updated review on primary signet-ring cell carcinoma of the urinary bladder and report of a case. *Scand J Urol*. 2018;52(2):87-93.

   doi: 10.1080/21681805.2017.1418020

9. Benerjee N, Parmar K, Vaiphei K. Primary signet-ring cell carcinoma of the urinary bladder. *Autops Case Rep*. 2021;11:e2021264.

doi: 10.4322/acr.2021.264

10. Ivanov A, Antonov P, Zapryanov M, Uchikov P, Belovezhdov V. Primary signet-ring cell adenocarcinoma of the bladder-A case report and review of literature. *Urol Case Rep*. 2022;42:102022.

    doi: 10.1016/j.eucr.2022.102022

11. Bagaporo Larrazabal R Jr., Cheng PVC, David-Wang A, Requiso D. Signet-ring cell adenocarcinoma of unknown primary presenting with superior vena cava (SVC) syndrome: Rare type of cancer. *BMJ Case Rep*. 2019;12(12):e232269.

    doi: 10.1136/bcr-2019-232269

12. Nicolazzo C, Raimondi C, Gradilone A, *et al*. Circulating tumor cells in right- and left-sided colorectal cancer. *Cancers* (*Basel*). 2019;11(8):1042.

    doi: 10.3390/cancers11081042

13. DeMay RM, Grathwohl MA. Signet-ring-cell (colloid) carcinoma of the urinary bladder. Cytologic, histologic and ultrastructural findings in one case. *Acta Cytol*. 1985;29(2):132-136.

14. Carey RW, Taft PD, Bennett JM, Kaufman S. Carcinocythemia (carcinoma cell leukemia). An acute leukemia-like picture due to metastatic carcinoma cells. *Am J Med*. 1976;60(2):273-278.

    doi: 10.1016/0002-9343(76)90437-x

15. Ronen S, Kroft SH, Olteanu H, Hosking PR, Harrington AM. Carcinocythemia: A rare entity becoming more common? A 3-year, single institution series of seven cases and literature review. *Int J Lab Hematol*. 2019;41(1):69-79.

    doi: 10.1111/ijlh.12924

16. Krawczyk P, Jassem J, Wojas-Krawczyk K, Krzakowski M, Dziadziuszko R, Olszewski W. New genetic technologies in diagnosis and treatment of cancer of unknown primary. *Cancers* (*Basel*). 2022;14(14):3429.

    doi: 10.3390/cancers14143429

17. Hayashi H, Takiguchi Y, Minami H, *et al*. Site-specific and targeted therapy based on molecular profiling by next-generation sequencing for cancer of unknown primary site: A nonrandomized phase 2 clinical trial. *JAMA Oncol*. 2020;6(12):1931-1938.

    doi: 10.1001/jamaoncol.2020.4643

18. Lu MY, Chen TY, Williamson DFK, *et al*. AI-based pathology predicts origins for cancers of unknown primary. *Nature*. 2021;594(7861):106-110.

    doi: 10.1038/s41586-021-03512-4

ACCSCIENCE PUBLISHING

Tumor Discovery

CASE REPORT

Sarcomatoid mesothelioma presenting as a mediastinal mass: A case report

Elizabeth Chiang[1]*, Neda Zarrin-Khameh[2], and Alec B. Rezigh[3]

[1]Department of Medicine, School of Medicine, Baylor College of Medicine, Houston, Texas, United States of America

[2]Department of Pathology and Immunology, Baylor College of Medicine and Ben Taub Hospital, Houston, Texas, United States of America

[3]Department of Medicine, Baylor College of Medicine, Houston, Texas, United States of America

(This article belongs to the *Special Issue: New Developments in Lung Cancer Research, Diagnosis, Treatment, and Prognosis*)

Abstract

Sarcomatoid mesothelioma (SM) is a subtype of mesothelioma, a deadly cancer strongly related to asbestos exposure. Herein, we present the case of a 50-year-old female who presented with back pain and non-specific symptoms for approximately 9 months. The diagnostic investigation revealed a large, centrally necrotic mass in the thorax that appeared to arise from the mediastinum and surrounded vital structures, including the superior vena cava. A biopsy of the thoracic mass revealed SM. The patient developed hematemesis, and emergent endoscopy revealed a gastric ulcer composed of malignant SM cells, a rare finding in pleural mesothelioma. Her disease was too advanced for surgical resection and conventional therapy. She tragically died weeks after diagnosis. The findings of this report highlight the varied presentation of SM to underscore the importance of early diagnosis and treatment of patients in improving overall survival.

Keywords: Mediastinal mass; Dyspnea; Back pain; Sarcomatoid mesothelioma; Lung cancer

***Corresponding author:**
Elizabeth Chiang
(elizabeth.chiang@bcm.edu)

Citation: Chiang E, Zarrin-Khameh N, Rezigh AB. Sarcomatoid mesothelioma presenting as a mediastinal mass: A case report. *Tumor Discov.* 2024;3(4):4420. doi: 10.36922/td.4420

Received: August 2, 2024

Accepted: September 25, 2024

Published Online: October 10, 2024

1. Introduction

Sarcomatoid mesothelioma (SM) is a subtype of mesothelioma, a rare cancer arising from mesothelial surfaces of tissues – most commonly the pleura – and is directly related to asbestos exposure.[1] Asbestos-related diseases have long latency periods, so consequences of exposure tend to be detectable approximately 40 years after initial contact. Due to this, many patients first present in their fifth or sixth decades of life with late-stage disease, often with signs of progressing respiratory failure, making treatment challenging.[2,3] Mesothelioma is classified into three main subtypes based on histology: epithelioid, sarcomatoid, and biphasic. SM is the least common but most aggressive of these classes, with the lowest median survival time of approximately 3.5 – 7.4 months.[2,4,5] Herein, we report a case of advanced SM with an atypical presentation due to a heavy burden of locally invasive disease and extrathoracic metastases. This case report aims to highlight the importance of early diagnosis and treatment in patients with SM with the aim of improving their overall survival.

2. Case presentation

A 50-year-old female with diabetes presented with acute-on-chronic right-sided upper back pain. Nine months before presentation, the patient experienced intermittent right-sided back pain without an identifiable trigger. Subsequently, non-productive cough and dyspnea on exertion developed 4 months before presentation. Her symptoms progressed, and she developed progressively worsening anorexia and nausea, as well as experiencing 20 pounds of unintentional weight loss over 2 weeks, all of which prompted her to seek medical consultation and her admission to the hospital. Fevers, chills, and chest pain were absent. She was a non-smoker with no history of secondhand smoke exposure. According to her, multiple family members had succumbed to an unknown lung cancer.

Physical examination revealed tachycardia and decreased breath sounds over the middle and lower lobes of the right lung. Routine hematology was notable for mild neutrophilic leukocytosis and thrombocytosis. Additional metabolic and infectious testing was unrevealing. A chest radiograph showed a large right-sided pleural effusion with compressive atelectasis. Computed tomography (CT) of the chest redemonstrated the effusion and revealed a 14.5 × 6.9 cm centrally necrotic right hemithorax mass arising from the mediastinum with invasion into the adjacent anterior chest wall and compression of the superior vena cava and right interlobar and upper lobe bronchi (Figure 1).

The patient developed hypoxemia. Subsequently, a chest tube was placed, and cytologic examination revealed an exudative pleural effusion with reactive mesothelial cells. Bacterial, fungal, and acid-fast bacilli cultures were negative. A biopsy of the mediastinal mass showed a spindle cell neoplasm composed of large, highly atypical pleomorphic spindle cells with irregular hyperchromatic nuclei. Immunohistochemical tests showed that the biopsied mass was positive for D2-40, calretinin, and WT-1, revealing SM. On further investigation of environmental exposures, the patient and her family reported prior residence next to a large asbestos plant in Central America with frequent exposure to friends and family employed at the plant, often with asbestos fibers on their clothing.

Given the proximity of the mass to key thoracic structures, it was deemed unresectable, and the patient was to start chemotherapy at discharge. However, she suddenly developed large-volume hematemesis and an emergent endoscopy was immediately conducted, revealing a malignant gastric ulcer, which was confirmed on biopsy to be metastatic SM (Figure 2). Shortly thereafter, she developed a pulmonary embolism with right heart strain and respiratory failure. Her condition progressed rapidly to obstructive shock, ultimately causing her death.

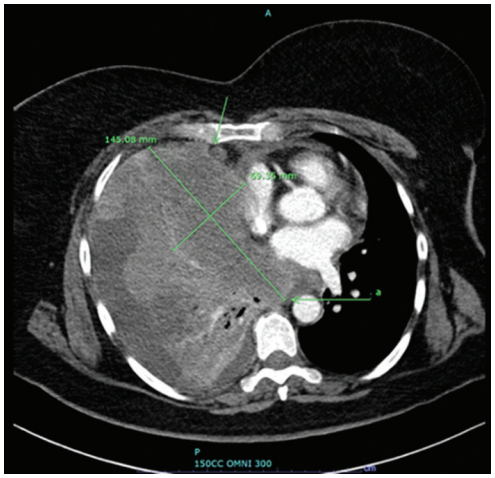

Figure 1. Computed tomography of the thorax in the axial plane shows a 14.5 × 6.9 cm mass arising from the mediastinum, which invades the anterior chest wall and causes significant superior vena cava stenosis.

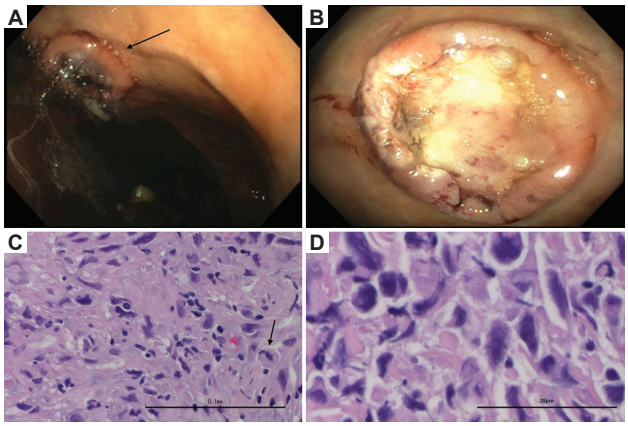

Figure 2. Pleural mesothelioma is complicated by a metastatic gastric ulcer. (A) Gastric body ulcer visualized endoscopically (black arrow). (B) Enhanced view of the ulcer. (C) Hematoxylin-eosin (H&E) staining of biopsied gastric cancer specimens shows cells with pleomorphism with the absence of normal gastric parenchyma. Mitotic figures are seen (black arrow). Scale bar: 0.1 mm (×10 magnification). (D) Higher-magnification view of H&E-stained malignant cells with enlarged irregular nuclei. Malignant cells are positive for pancytokeratin, D2-40, WT1 (in a subset of cells), CAM5.2, CK5&6 (rare cells), and calretinin (in a small subset of cells), but they are negative for P63, S100, beta-catenin, desmin, EMA, MOC31, and CD34. The histology and immunostaining pattern are consistent with the histopathologic features of metastatic mesothelioma. Scale bar: 0.025 mm (×40 magnification).

3. Discussion

Globally, the incidence rate of mesothelioma has declined over the last few decades following nationwide bans on asbestos in many countries, including the United States and most European countries.[1,6] However, asbestos production

and commercialization still occur widely in Asia and many Central and South American countries.[7-9] In a highly globalized world with accessible travel, it is critical for physicians to recognize and manage mesothelioma, even if asbestos production is limited in their home nation.

Initial symptoms of SM are often non-specific, most commonly cough and dyspnea. Many patients are incidentally found to have pleural effusions on imaging. Chest wall or back pain are less commonly described in SM, though they were presenting features in our case.[3,10] Much of the morbidity and mortality associated with SM is due to local disease progression and invasion of critical structures in the mediastinum.[2] Previously believed to be rare, tumor dissemination in extrapleural and extrathoracic sites is common, occurring in 87.7% and 55.4% of patients, respectively.[11] In lung cancer, however, metastasis to the gastrointestinal tract is exceptionally uncommon, noted in only ~0.5% of cases.[12] In pleural mesothelioma specifically, metastasis to the gastrointestinal lumen in the absence of peritoneal disease is rare, with <20 cases reported in the literature thus far. Most of these cases were caused by epithelioid mesothelioma, and three resulted from SM. Only one case reported gastric ulcers from metastatic SM,[13] similar to our case.

Challenges in diagnosing SM include difficulty in differentiating it from other spindle cell neoplasms and inconsistent expression of the common tumor markers used in immunohistochemistry.[13,14] On biopsy, SM is characterized by spindle-shaped cells and a lack of the typical glandular structures seen in other types of mesothelioma.[15] However, SM may mimic other neoplasms depending on the anatomic site involved, namely sarcomatoid carcinoma and intraabdominal synovial sarcoma, which share a similar histomorphology.[13] Common mesothelial markers for immunohistochemical studies include calretinin, D2-40, WT-1, and cytokeratin. For SM specifically, staining is typically positive for cytokeratin and calretinin, but there have been rare cases with negative calretinin expression, making diagnosis additionally challenging.[14,16]

Management of SM centers around surgical resection of the tumor and chemotherapy. For resectable tumors, surgery lessens the tumor burden, relieving dyspnea and reducing the occurrence of pleural effusions.[14] Neoadjuvant or adjuvant chemotherapy with cisplatin and pemetrexed is the only Food and Drug Administration-approved combination for the treatment of pleural mesothelioma and remains the sole treatment modality for patients in the United States who are either not candidates for surgery or have unresectable disease.[2,14] Globally, immune checkpoint inhibitors, such as nivolumab, and anti-angiogenic drugs, such as bevacizumab, have shown efficacy against malignant pleural mesothelioma.[17] Unfortunately, Mansfield *et al.*[18] found that compared to patients with other subtypes, fewer patients with SM have complete and partial responses to treatment, with response rates recorded at 13.9% and 21.9%, respectively. Novel research into alternative treatment modalities, including trimodal therapy with surgery, chemotherapy, and adjuvant radiotherapy, as well as molecular targeted therapy, is needed to improve outcomes for patients with SM.[14]

4. Conclusion

SM is the rarest main form of mesothelioma, a disease that has remained unknown to the public for a long time due to international governmental policies limiting asbestos production and use. The long latency period since exposure, non-specific symptom manifestation, and challenges in diagnostics lead to the majority of patients presenting with late-stage disease upon diagnosis. During the terminal stage of the disease, local invasion of the tumor has typically become too extensive for surgical resection, and conventional chemotherapy options have proven unsuccessful in managing SM. Therefore, clinicians must have high diagnostic suspicion for mesothelioma, particularly SM, when encountering patients originating from asbestos-producing regions to ensure prompt diagnosis and treatment and to optimize patient outcomes.

Acknowledgments

None.

Funding

None.

Conflict of interest

The authors declare no conflicts of interest.

Author contributions

Conceptualization: Elizabeth Chiang, Alec B. Rezigh
Investigation: Elizabeth Chiang, Alec B. Rezigh
Methodology: Elizabeth Chiang
Writing – original draft: Elizabeth Chiang
Writing – review & editing: All authors

Ethics approval and consent to participate

The manuscript and patient data were written and collected in accordance with the declaration of Helsinki and our institutional ethics guidelines.

Consent for publication

We have obtained informed verbal consent from the patient for the publication of this report. The authors have

obtained permission to reprint any figures or tables that were initially printed elsewhere, should they be required.

Availability of data

Data are available from the corresponding author upon reasonable request.

References

1. Alpert N, van Gerwen M, Taioli E. Epidemiology of mesothelioma in the 21st century in Europe and the United States, 40 years after restricted/banned asbestos use. *Transl Lung Cancer Res*. 2020;9(Suppl 1):S28-S38.

   doi: 10.21037/tlcr.2019.11.11

2. Billè A, Okiror L, Harling L, *et al.* Analysis of survival of patients with metastatic malignant pleural mesothelioma. *Tumori*. 2021;107(2):110-118.

   doi: 10.1177/0300891620926239

3. Mott FE. Mesothelioma: A review. *Ochsner J*. 2012;12(1):70-79.

4. Klebe S, Brownlee NA, Mahar A, *et al.* Sarcomatoid mesothelioma: A clinical-pathologic correlation of 326 cases. *Modern Pathol*. 2010;23(3):470-479.

   doi: 10.1038/modpathol.2009.180

5. Leigh J, Rogers AJ, Ferguson DA, *et al.* Lung asbestos fiber content and mesothelioma cell type, site, and survival. *Cancer*. 1991;68(1):135-141.

   doi: 10.1002/1097-0142(19910701)68:1<135:AID-CNCR2820680125>3.0.CO;2-S

6. Huang J, Chan SC, Pang WS, *et al.* Global incidence, risk factors, and temporal trends of mesothelioma: A population-based study. *J Thorac Oncol*. 2023;18(6):792-802.

   doi: 10.1016/j.jtho.2023.01.095

7. Hernández-Blanquisett A, Álvarez-Londoño A, Martinez-Avila MC, *et al.* Asbestos and cancer in Latin America and the Caribbean: We may have won some battles, but definitely not the war. *J Public Health Res*. 2021;11(2):2549.

   doi: 10.4081/jphr.2021.2549

8. Singh R, Frank AL. Analysis of the Indian Government's position on the use of asbestos and its health effects. *Public Health Action*. 2023;13(2):50-52.

   doi: 10.5588/pha.23.0013

9. Li X, Ding D, Xie W, *et al.* Risk assessment and source analysis of heavy metals in soil around an asbestos mine in an arid plateau region, China. *Sci Rep.* 2024;14(1):7552.

   doi: 10.1038/s41598-024-58117-4

10. Mann S, Khawar S, Moran C, *et al.* Revisiting localized malignant mesothelioma. *Ann Diagn Pathol*. 2019;39:74-77.

    doi: 10.1016/j.anndiagpath.2019.02.014

11. Finn RS, Brims FJH, Gandhi A, *et al.* Postmortem findings of malignant pleural mesothelioma: A two-center study of 318 patients. *Chest*. 2012;142(5):1267-1273.

    doi: 10.1378/chest.11-3204

12. Pezzuto A, Mariotta S, Fioretti F, *et al.* Metastasis to the colon from lung cancer presenting with severe hyponatremia and dyspnea in a young male: A case report and review of the literature. *Oncol Lett.* 2013;5(5):1477-1480.

    doi: 10.3892/ol.2013.1208

13. Agaimy A, Wünsch PH. Epithelioid and sarcomatoid malignant pleural mesothelioma in endoscopic gastric biopsies: A diagnostic pitfall. *Pathol Res Pract*. 2006;202(8):617-622.

    doi: 10.1016/j.prp.2006.05.002

14. Clopton B, Long W, Santos M, Asarian A, Genato R, Xiao P. Sarcomatoid mesothelioma: Unusual findings and literature review. *J Surg Case Rep.* 2022;2022(11):rjac512.

    doi: 10.1093/jscr/rjac512

15. Mehta K, Mehta S, Joshi M, Bharadwaj HR, Ardeshana G, Tenkorang PO. Challenging diagnosis of sarcomatoid hepatic mesothelioma: A case report with review of literature. *Ann Med Surg* (*Lond*). 2023;85(10):5123-5126.

    doi: 10.1097/MS9.0000000000001148

16. Amatya VJ, Kushitani K, Mawas AS, *et al.* MUC4, a novel immunohistochemical marker identified by gene expression profiling, differentiates pleural sarcomatoid mesothelioma from lung sarcomatoid carcinoma. *Mod Pathol*. 2017;30(5):672-681.

    doi: 10.1038/modpathol.2016.181

17. Assié JB, Crépin F, Grolleau E, *et al.* Immune-checkpoint inhibitors for malignant pleural mesothelioma: A French, multicenter, retrospective real-world study. *Cancers* (*Basel*). 2022;14(6):1498.

    doi: 10.3390/cancers14061498

18. Mansfield AS, Symanowski JT, Peikert T. Systematic review of response rates of sarcomatoid malignant pleural mesotheliomas in clinical trials. *Lung Cancer*. 2014;86(2):133-136.

    doi: 10.1016/j.lungcan.2014.08.017

Our Journals

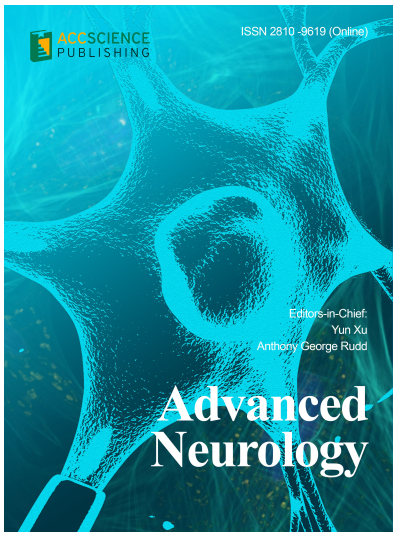

Advanced Neurology is a peer-reviewed and open-access journal that aims to publish and disseminate novel research in the breadth of neurology and neuroscience. The journal aims to advance our understanding in the nervous system and provide a platform to neuroscientists and physicians to showcase their findings in original fundamental and clinical research as well as to present new ideas that highlight the changes in the neurological clinical practice.

Advanced Neurology covers subject areas, including but not limited to the following:

- Neurological disorders
- Neurodegenerative disease
- Cerebrovascular disease
- Epilepsy and movement disorders
- Neuroimmune disease
- Neurological infections
- Muscle disease
- Molecular and cellular neuroscience
- Systems neuroscience
- Cognitive neuroscience
- Computational modeling of nervous system

Global Translational Medicine is a quarterly journal that focuses on medicine, biological sciences, and biomaterials engineering. The goal of *Global Translational Medicine* is to provide a platform to researchers for showcasing their latest research works in translational medicine so as to advance the field towards the betterment of human health. Despite the advancement of omics and new technologies, the process of transforming these technologies and scientific research results into effective therapies and putting them into clinical use still has a long way to go. *Global Translational Medicine* provides a platform to fill the gaps in preclinical and inter-disciplinary research, to promote clinical translation of scientific research results, and to contribute to the conception of new and improved preventive measures as well as diagnostic and therapeutic techniques of diseases.

Global Translational Medicine covers the following themes: cardiovascular disease, metabolism/diabetes/obesity, neuroscience/neurology, cancer, biomaterials and their applications in medicine, proteomics/metabolomics, pharmacogenomics, biomarkers, bioinformatics and data mining, animal and clinical research, and medical methods arising from interdisciplinary crossover.

Start a new journal

Write to us via email if you are interested to start a new journal with AccScience Publishing. Please attach your CV, professional profile page and a brief pitch proposal in your email. We shall inform you of our decision whether we are interested to collaborate in starting a new journal.

Contact: info@accscience.com

https://accscience.com/journal/TD

Contact

www.accscience.com

8 Burn Road, #15-03 Trivex, Singapore 369977

Email: editorial@accscience.com

Phone: +65 8182 1586